UNIVERSITY OF CALIFORNIA,
IRVINE

Quantum Trajectory Surface Hopping: Theory and its Inner Workings

DISSERTATION

submitted in partial satisfaction of the requirements
for the degree of

DOCTOR OF PHILOSOPHY

in Chemistry

by

Miaoyu Dorothy Huang

Dissertation Committee:
Professor Craig C. Martens, Chair
Professor Vladimir Mandelshtam
Professor Filipp Furche

2024

DEDICATION

To my nephews, Edgar and Everest,
my nieces, Lauren and Ashley,
and my Godson, Aaron.

You remind me of all that is good and beautiful in the world.

TABLE OF CONTENTS

Page

LIST OF FIGURES **vi**

LIST OF TABLES **xvi**

ACKNOWLEDGMENTS **xvii**

VITA **xix**

ABSTRACT OF THE DISSERTATION **xx**

1 Introduction to the Dissertation **1**
- 1.1 Modeling Non-Adiabatic Molecular Dynamics . . . 2
  - 1.1.1 Trajectory Surface Hopping . . . 2
- 1.2 Diabatic and Adiabatic Representations . . . 5
- 1.3 Quantum-Classical Limit of Quantum Mechanics . . . 9
- 1.4 Electronic Nuclear Dynamics . . . 12
  - 1.4.1 Quantum-Classical Liouville Equation . . . 12
- 1.5 Quantum Trajectory Surface Hopping (QTSH) . . . 15
  - 1.5.1 Time Evolution of Electronic State . . . 15
  - 1.5.2 Time Evolution of Nuclear Motion . . . 20
- 1.6 Modified Tully 1D Systems . . . 26
  - 1.6.1 Chemical Relevance . . . 31
- 1.7 Dissertation Outline . . . 32

2 Role of Quantum Forces in QTSH **34**
- 2.1 Introduction . . . 34
- 2.2 Derivation of FSSH Momentum Jumps . . . 36
  - 2.2.1 Frustrated Hops . . . 50
  - 2.2.2 Energy Conservation & Quantum Backreaction . . . 52
- 2.3 Methods . . . 54
  - 2.3.1 Systems . . . 54
  - 2.3.2 Simulation Details . . . 57
- 2.4 Results & Discussion . . . 59
  - 2.4.1 Wigner Distribution Dynamics . . . 59
  - 2.4.2 Feedback between Nuclear and Electronic Degrees of Freedom . . . 63

2.5 Conclusions . . . 73

3 An Investigation of the Representation Invariance of QTSH 75
3.1 Introduction . . . 75
3.2 Transformation Theory in the Quantum-Classical Limit . . . 77
3.2.1 Wigner Distribution . . . 77
3.2.2 Forces . . . 84
3.3 Computational Details . . . 95
3.4 Results & Discussion . . . 95
3.4.1 Wigner Distribution . . . 95
3.4.2 Forces . . . 116
3.5 Conclusions . . . 130
3.6 Future Work . . . 131

4 Classical and Non-classical Effects of Forces and Representation 133
4.1 Introduction . . . 133
4.2 Simple Derivation of Adiabatic Forces . . . 135
4.2.1 Classical Force in the Adiabatic Representation . . . 135
4.2.2 Quantum Force in the Adiabatic Representation . . . 136
4.2.3 Application to Tully's 1D Systems [1] . . . 137
4.3 Computational Details . . . 151
4.4 Results & Discussion . . . 152
4.4.1 Classical and Non-classical Forces . . . 152
4.4.2 Exploiting Representation Invariance . . . 163
4.5 Conclusions . . . 174

5 Chemical Work, Gibbs Free Energy Change, and Spontaneity in Introductory Chemistry - Chemical Education 175
5.1 Motivation . . . 175
5.2 Theoretical Background . . . 177
5.2.1 Pressure-Volume Expansion and 'Useful' Non-expansion Work . . . 177
5.2.2 Chemical Work, Spontaneity and the Sign Convention for Work . . . 180
5.2.3 Molecular View of Chemical Potential: Current Approach . . . 183
5.3 Chemical Work: A Molecular Mechanics Perspective . . . 184
5.3.1 Suggestions for the Classroom . . . 185
5.4 Connecting Spontaneity and Sign Conventions for Work in Chemistry . . . 190
5.5 Chemical Potential and the Standard Molar Gibbs Free Energy . . . 192
5.6 Conclusions . . . 193

Bibliography 194

Appendix A Approximate Diabatic Density Matrix for Dual Avoided Crossing Model 203

Appendix B Details of the Wigner-Moyal Transformation 206

Appendix C Adiabatic Forces on Trajectory in Dual Avoided Crossing System **209**

LIST OF FIGURES

Page

1.1 The grey shaded region spans the region of strong adiabatic coupling. The inset image shows an enlarged image of the grey shaded region. The dotted, dashed, and dashdotted lines in the inset images correspond to the diabatic coupling constants of $C = 0.0005$, $C = 0.001$, and $C = 0.002$, respectively. **(a)** Adiabatic potential energy surfaces (PESs) for the modified Tully's simple avoided crossing model. The upper surface is labeled $V_+(q)$ and the lower surface is labeled $V_-(\boldsymbol{q})$. The parameter $\hbar\omega(\boldsymbol{q}_{\boldsymbol{d}_{\text{peak}}})$ shows the size of the energy gap where the adiabatic coupling is strongest. The inset shows the the energy gap increases with the strength of the diabatic coupling. **(b)** Non-adiabatic coupling $\boldsymbol{d}(\boldsymbol{q})$ for the modified Tully's simple avoided crossing model. The parameter $\boldsymbol{d}_{\text{peak}}$ indicates the maximum strength of the adiabatic coupling, and $w_{0.5,\text{peak}}$ indicates the width of the adiabatic coupling at half maximum. 28

1.2 The grey shaded region spans the two regions of strong adiabatic coupling. The inset image shows an enlarged image of the grey shaded region. The dotted, dashed, and dashdotted lines in the inset images correspond to the diabatic coupling constants of $C = 0.0015$, $C = 0.003$, and $C = 0.006$, respectively. **(a)** Adiabatic potential energy surfaces (PESs) for the modified Tully's dual avoided crossing model. The upper surface is labeled $V_+(\boldsymbol{q})$ and the lower surface is labeled $V_-(\boldsymbol{q})$. The parameters $\hbar\omega(\boldsymbol{q}_{\boldsymbol{d}_{\text{peak1}}})$ and $\hbar\omega(\boldsymbol{q}_{\boldsymbol{d}_{\text{peak2}}})$ show the size of the energy gap where the adiabatic couplings are strongest. The inset shows that the energy gaps increase with increasing diabatic coupling strength. **(b)** Non-adiabatic coupling $\boldsymbol{d}(\boldsymbol{q})$ for the modified Tully's dual avoided crossing model. The parameters $\boldsymbol{d}_{\text{peak1}}$ and $\boldsymbol{d}_{\text{peak2}}$ indicate the maximum strengths of the non-adiabatic coupling, and $w_{0.5,\text{peak1}}$ and $w_{0.5,\text{peak2}}$ indicate the width of each region of strong adiabatic coupling at half maximum. 30

1.3 Schematic depiction of the potential energy curves as a function of a one-dimensional reactive coordinate for the (a) Tully simple avoided crossing model, and the (b) Tully dual avoided crossing model, and the time traces of the potential energies for trajectory surface hopping for Ibele-Curchod molecular models for (c) ethene that corresponds to the simple avoided crossing model, and (d) 4-N,N-Dimethylaminobenzonitrile (DMABN). The path described by the one-dimensional particle (circle and arrow) exemplifies a possible outcome of the dynamics probed by each model. Lower panel: Time traces of the potential energies along a trajectory surface hopping trajectory for ethylene (d), DMABN (e), and fulvene (f). The excited-state dynamics for each molecular Tully model mimics the particle dynamics of the corresponding one-dimensional Tully models depicted in the upper panel. Reproduced from L. M. Ibele and B. F. E. Curchod, *Phys. Chem. Chem. Phys.*, 2020, **22**, 15183 **DOI:** 10.1039/D0CP01353F (Ref [2]), with permission from the PCCP Owner Societies. 31

2.1 Self-consistency between the classical nuclear and quantum electronic subsystems as a result of the quantum backreaction that occurs following an electronic transition. Reprinted from John C. Tully; Perspective: non-adiabatic dynamics theory. *J. Chem. Phys.* 14 December 2012; 137 (22): 22A301. (Ref [3]), with the permission of AIP Publishing. 35

2.2 Schematic representation of a localized quantum state/trajectory undergoing a non-adiabatic transition from the upper to the lower adiabatic state at the avoided crossing. Diabatic potentials for the simple avoided crossing system are given in Eqns 1.83-1.84. 39

2.3 Schematic representation of a localized quantum state/trajectory traveling along the diabatic potential $V_1(q)$, corresponding to the process in Fig 2.2. Diabatic potentials for the simple avoided crossing system are given in Eqns 1.83-1.84. 39

2.4 Schematic representation of a localized quantum state/trajectory undergoing a non-adiabatic transition from the lower to the upper adiabatic state at the avoided crossing. Diabatic potentials for the simple avoided crossing system are given in Eqns 1.83-1.84. 40

2.5 Schematic representation of a localized quantum state/trajectory traveling along the diabatic potential $V_2(\boldsymbol{q})$, corresponding to the process in Fig 2.4. Diabatic potentials for the simple avoided crossing system are given in Eqns 1.83-1.84. 40

2.6 (a) The non-adiabatic mixing angle $\phi(\boldsymbol{q})$, (b) the non-adiabatic coupling vector $\boldsymbol{d}(\boldsymbol{q})$, (c) the real part of the coherence $\alpha(\boldsymbol{q})$, and (d) the quantum force $F_{\text{quant}}(\boldsymbol{q})$ for the process shown in Fig 2.2, as described in text. The dotted, dashed, and dashdotted lines represent the models where $C = 0.0005$, $C = 0.001$, and $C = 0.002$, respectively. 41

2.7 (a) The real part of the coherence $\alpha(q)$, and (b) the quantum force $F_{\text{quant}}(\boldsymbol{q})$ for the process shown in Fig 2.4, as described in text. The dotted, dashed, and dashdotted lines represent the models where $C = 0.0005$, $C = 0.001$, and $C = 0.002$, respectively. 42
2.8 Schematic representation of a localized quantum state/trajectory undergoing a non-adiabatic transition from the lower to the upper adiabatic state at the avoided crossing, traveling on the upper adiabatic surface, and finally undergoing another non-adiabatic transition from the upper to the lower adiabatic state. Diabatic potentials for the dual avoided crossing system are given in Eqns 1.86-1.87. 56
2.9 Schematic representation of a localized quantum state/trajectory traveling along the diabatic potential $V_2(\boldsymbol{q})$, corresponding to the process in Fig 2.8. Diabatic potentials for the dual avoided crossing system are given in Eqns 1.86-1.87. 56
2.10 Comparison of the phase space averaged populations on the upper adiabatic PES $\langle\rho_{++}(t)\rangle$ and the lower adiabatic PES $\langle\rho_{--}(t)\rangle$, and the real and imaginary parts of the coherence, $\langle\alpha(t)\rangle$ and $\langle\beta(t)\rangle$, respectively, obtained from QTSH with exact quantum results for the modified Tully's simple avoided crossing system with a starting population on the upper adiabatic state at an initial average momentum $\hbar k_0 = 15$ a.u., and $C = 0.0005, 0.001$ and 0.002. . 61
2.11 Comparison of the phase space averaged populations on the upper adiabatic PES $\langle\rho_{++}(t)\rangle$ and the lower adiabatic PES $\langle\rho_{--}(t)\rangle$, and the real and imaginary parts of the coherence, $\langle\alpha(t)\rangle$ and $\langle\beta(t)\rangle$, respectively, obtained from QTSH with exact quantum results for the modified Tully's simple avoided crossing system with a starting population on the lower adiabatic state at an initial average momentum $\hbar k_0 = 15$ a.u., and $C = 0.0005, 0.001$ and 0.002. . 61
2.12 Comparison of the phase space averaged populations on the upper adiabatic PES $\langle\rho_{++}(t)\rangle$ and the lower adiabatic PES $\langle\rho_{--}(t)\rangle$, and the real and imaginary parts of the coherence, $\langle\alpha(t)\rangle$ and $\langle\beta(t)\rangle$, respectively, obtained from QTSH with exact quantum results for the modified Tully's dual avoided crossing system with a starting population on the lower adiabatic state at an initial average momentum $\hbar k_0 = 40.3$ a.u., and $C = 0.0015, 0.003$ and 0.006. 62
2.13 QTSH results for the phase space averaged work done by the electronic degrees of freedom on the nuclear degrees of freedom $\langle W_{\text{e}\to\text{n}}(t)\rangle$ and the work done by the nuclear degrees of freedom on the electronic degrees of freedom calculated with $\dot{a}_{++}(t)$, $\langle W^a_{\text{n}\to\text{e}}(t)\rangle$, and its sum $\langle W_{\text{e}\to\text{n}}(t)\rangle + \langle W^a_{\text{n}\to\text{e}}(t)\rangle$ for the modified Tully's simple avoided crossing system at an initial average momentum $\hbar k_0 = 15$, with the initial population on the upper surface. 67
2.14 QTSH results for the phase space averaged work done by the electronic degrees of freedom on the nuclear degrees of freedom $\langle W_{\text{e}\to\text{n}}(t)\rangle$ and the work done by the nuclear degrees of freedom on the electronic degrees of freedom calculated with $\dot{a}_{++}(t)$, $\langle W^a_{\text{n}\to\text{e}}(t)\rangle$, and its sum $\langle W_{\text{e}\to\text{n}}(t)\rangle + \langle W^a_{\text{n}\to\text{e}}(t)\rangle$ for the modified Tully's simple avoided crossing system at an initial average momentum $\hbar k_0 = 15$, with the initial population on the lower surface. 67

2.15 QTSH results for the phase space averaged work done by the electronic degrees of freedom on the nuclear degrees of freedom $\langle W_{\mathrm{e}\to\mathrm{n}}(t)\rangle$ and the work done by the nuclear degrees of freedom on the electronic degrees of freedom calculated with $\dot{a}_{++}(t)$, $\langle W^{a}_{\mathrm{n}\to\mathrm{e}}(t)\rangle$, and its sum $\langle W_{\mathrm{e}\to\mathrm{n}}(t)\rangle + \langle W^{a}_{\mathrm{n}\to\mathrm{e}}(t)\rangle$ for the modified Tully's dual avoided crossing system at an initial average momentum $\hbar k_0 = 40.3$, with the initial population on the lower surface. 68
2.16 QTSH results for the phase space averaged (a) work done by the electronic degrees of freedom on the nuclear degrees of freedom $\langle W_{\mathrm{e}\to\mathrm{n}}(t)\rangle$ and the work done by the nuclear degrees of freedom on the electronic degrees of freedom calculated with $\Delta\sigma(t)$, $\langle W^{\sigma}_{\mathrm{n}\to\mathrm{e}}(t)\rangle$, its sum $\langle W_{\mathrm{e}\to\mathrm{n}}(t)\rangle + \langle W^{\sigma}_{\mathrm{n}\to\mathrm{e}}(t)\rangle$, and (b) population on the upper adiabatic PES $\langle \rho_{++}(t)\rangle$, proxy population on the upper adiabatic PES $\langle a_{++}(t)\rangle$, and the surface hopping consistency $\langle \rho_{++}(t)\rangle - \langle a_{++}(t)\rangle$ for the modified Tully's simple avoided crossing system at an initial average momentum $\hbar k_0 = 15$, with the initial population on the upper adiabatic surface. The inset shows a magnified portion of the plot for the time interval between $t = 10$ fs and $t = 40$ fs 69
2.17 QTSH results for the phase space averaged (a) work done by the electronic degrees of freedom on the nuclear degrees of freedom $\langle W_{\mathrm{e}\to\mathrm{n}}(t)\rangle$ and the work done by the nuclear degrees of freedom on the electronic degrees of freedom calculated with $\Delta\sigma(t)$, $\langle W^{\sigma}_{\mathrm{n}\to\mathrm{e}}(t)\rangle$, its sum $\langle W_{\mathrm{e}\to\mathrm{n}}(t)\rangle + \langle W^{\sigma}_{\mathrm{n}\to\mathrm{e}}(t)\rangle$, and (b) population on the upper adiabatic PES $\langle \rho_{++}(t)\rangle$, proxy population on the upper adiabatic PES $\langle a_{++}(t)\rangle$, and the surface hopping consistency $\langle \rho_{++}(t)\rangle - \langle a_{++}(t)\rangle$ for the modified Tully's simple avoided crossing system at an initial average momentum $\hbar k_0 = 15$, with the initial population on the lower adiabatic surface. The inset shows a magnified portion of the plot for the time interval between $t = 10$ fs and $t = 40$ fs 70
2.18 QTSH results for the phase space averaged (a) work done by the electronic degrees of freedom on the nuclear degrees of freedom $\langle W_{\mathrm{e}\to\mathrm{n}}(t)\rangle$ and the work done by the nuclear degrees of freedom on the electronic degrees of freedom calculated with $\Delta\sigma(t)$, $\langle W^{\sigma}_{\mathrm{n}\to\mathrm{e}}(t)\rangle$, its sum $\langle W_{\mathrm{e}\to\mathrm{n}}(t)\rangle + \langle W^{\sigma}_{\mathrm{n}\to\mathrm{e}}(t)\rangle$, and (b) population on the upper adiabatic PES $\langle \rho_{++}(t)\rangle$, proxy population on the upper adiabatic PES $\langle a_{++}(t)\rangle$, and the surface hopping consistency $\langle \rho_{++}(t)\rangle - \langle a_{++}(t)\rangle$ for the modified Tully's dual avoided crossing system at an initial average momentum $\hbar k_0 = 40.3$, with the initial population on the lower adiabatic surface. The inset shows a magnified portion of the plot for the time interval between $t = 7.5$ fs and $t = 17.5$ fs 71

3.1 Two sets of data can be obtained to test the representation invariance of Quantum Trajectory Surface Hopping (QTSH). Running QTSH in the adiabatic representation and converting the results to the diabatic representation (a2d QTSH), and running QTSH in the diabatic representation and converting the results to the adiabatic representation (d2a QTSH). 76

3.2 Comparison of exact quantum result for (a) the phase space average population $\langle\rho_{++}(t)\rangle$ with the adiabatic QTSH result and the transformed d2a QTSH result, and (b) the phase space average population $\langle\rho_{11}(t)\rangle$ with the diabatic QTSH result, and the transformed a2d QTSH result, for the for the processes described in Figs 2.2 and 2.3 for the simple avoided crossing system described by the diabatic potentials given by Eqns 1.83-1.84. The inset shows the magnified plot between $t = 10$ fs and $t = 40$ fs. 98
3.3 Comparison of exact quantum result for (a) the phase space average population $\langle\rho_{++}(t)\rangle$ with the adiabatic QTSH result and the transformed d2a QTSH result, and (b) the phase space average population $\langle\rho_{11}(t)\rangle$ with the diabatic QTSH result, and the transformed a2d QTSH result, for the for the processes described in Figs 2.4 and 2.5 for the simple avoided crossing system described by the diabatic potentials given by Eqns 1.83-1.84. The inset shows the magnified plot between $t = 10$ fs and $t = 40$ fs. 99
3.4 Comparison of exact quantum result for (a) the phase space average population $\langle\rho_{++}(t)\rangle$ with the adiabatic QTSH result and the transformed d2a QTSH result, and (b) the phase space average population $\langle\rho_{11}(t)\rangle$ with the diabatic QTSH result, and the transformed a2d QTSH result, for the for the processes described in Figs 2.8 and 2.9 for the dual avoided crossing system described by the diabatic potentials given by Eqns 1.86-1.87. The inset shows the magnified plot between $t = 7.5$ fs and $t = 17.5$ fs. 100
3.5 Comparison of exact quantum result for (a) the phase space averaged real part of the coherence $\left\langle\alpha^{\mathrm{A}}(t)\right\rangle$ with the adiabatic QTSH result and the transformed d2a QTSH result, and (b) the phase space averaged real part of the coherence $\left\langle\alpha^{\mathrm{D}}(t)\right\rangle$ with the diabatic QTSH result, and the transformed a2d QTSH result, for the for the processes described in Figs 2.2 and 2.3 for the simple avoided crossing system described by the diabatic potentials given by Eqns 1.83-1.84. The inset shows the magnified plot between $t = 10$ fs and $t = 40$ fs. 106
3.6 Comparison of exact quantum result for (a) the phase space averaged real part of the coherence $\left\langle\alpha^{\mathrm{A}}(t)\right\rangle$ with the adiabatic QTSH result and the transformed d2a QTSH result, and (b) the phase space averaged real part of the coherence $\left\langle\alpha^{\mathrm{D}}(t)\right\rangle$ with the diabatic QTSH result, and the transformed a2d QTSH result, for the for the processes described in Figs 2.4 and 2.5 for the simple avoided crossing system described by the diabatic potentials given by Eqns 1.83-1.84. The inset shows the magnified plot between $t = 10$ fs and $t = 40$ fs. 107
3.7 Comparison of exact quantum result for (a) the phase space averaged real part of the coherence $\left\langle\alpha^{\mathrm{A}}(t)\right\rangle$ with the adiabatic QTSH result and the transformed d2a QTSH result, and (b) the phase space averaged real part of the coherence $\left\langle\alpha^{\mathrm{D}}(t)\right\rangle$ with the diabatic QTSH result, and the transformed a2d QTSH result, for the for the processes described in Figs 2.8 and 2.9 for the dual avoided crossing system described by the diabatic potentials given by Eqns 1.86-1.87. The black box highlights the plot between $t = 7.5$ fs and $t = 17.5$ fs. 108

3.8 Comparison of exact quantum result for (a) the phase space averaged imaginary part of the coherence $\langle \beta^{A}(t) \rangle$ with the adiabatic QTSH result and the transformed d2a QTSH result, and (b) the phase space averaged imaginary part of the coherence $\langle \beta^{D}(t) \rangle$ with the diabatic QTSH result, and the transformed a2d QTSH result, for the for the processes described in Figs 2.2 and 2.3 for the simple avoided crossing system described by the diabatic potentials given by Eqns 1.83-1.84. The inset shows the magnified plot between $t = 10$ fs and $t = 40$ fs. 112
3.9 Comparison of exact quantum result for (a) the phase space averaged imaginary part of the coherence $\langle \beta^{A}(t) \rangle$ with the adiabatic QTSH result and the transformed d2a QTSH result, and (b) the phase space averaged imaginary part of the coherence $\langle \beta^{D}(t) \rangle$ with the diabatic QTSH result, and the transformed a2d QTSH result, for the for the processes described in Figs 2.4 and 2.5 for the simple avoided crossing system described by the diabatic potentials given by Eqns 1.83-1.84. The inset shows the magnified plot between $t = 10$ fs and $t = 40$ fs. 113
3.10 Comparison of exact quantum result for (a) the phase space averaged imaginary part of the coherence $\langle \beta^{A}(t) \rangle$ with the adiabatic QTSH result and the transformed d2a QTSH result, and (b) the phase space averaged imaginary part of the coherence $\langle \beta^{D}(t) \rangle$ with the diabatic QTSH result, and the transformed a2d QTSH result, for the for the processes described in Figs 2.8 and 2.9 for the dual avoided crossing system described by the diabatic potentials given by Eqns 1.86-1.87. The black box highlights the plot between $t = 7.5$ fs and $t = 17.5$ fs. 114
3.11 QTSH results for the phase space averaged total force in the diabatic and adiabatic representation, $\langle \boldsymbol{F}^{D}_{total} \rangle$ and $\langle \boldsymbol{F}^{A}_{total} \rangle$ for the processes described in Figs 2.2 and 2.3 for the simple avoided crossing system described by the diabatic potentials given by Eqns 1.83-1.84. 118
3.12 QTSH results for the phase space averaged total force in the diabatic and adiabatic representation, $\langle \boldsymbol{F}^{D}_{total} \rangle$ and $\langle \boldsymbol{F}^{A}_{total} \rangle$ for the processes described in Figs 2.4 and 2.5 for the simple avoided crossing system described by the diabatic potentials given by Eqns 1.83-1.84. 118
3.13 QTSH results for the phase space averaged total force in the diabatic and adiabatic representation, $\langle \boldsymbol{F}^{D}_{total} \rangle$ and $\langle \boldsymbol{F}^{A}_{total} \rangle$ for the processes described in Figs 2.8 and 2.9 for the dual avoided crossing system described by the diabatic potentials given by Eqns 1.86-1.87. The black box highlights the plot in the time interval $t = 7.5$ fs and $t = 17.5$ fs. 119
3.14 Comparison of the adiabatic QTSH and d2a QTSH results for the system phase space averaged classical force $\langle \boldsymbol{F}^{A}_{class}(t) \rangle$, quantum force $\langle \boldsymbol{F}^{A}_{quant}(t) \rangle$, and total force $\langle \boldsymbol{F}^{A}_{total}(t) \rangle$ in the adiabatic representation for the non-adiabatic process in the simple avoided crossing system depicted by Fig 2.2, with the diabatic coupling constants (a) $C = 0.0005$, and (b) $C = 0.002$. The inset shows a magnified view of the plot in the time interval $t = 10$ fs and $t = 40$ fs. 122

3.15 Comparison of the adiabatic QTSH and d2a QTSH results for the system phase space averaged classical force $\left\langle \boldsymbol{F}^{\mathrm{A}}_{\mathrm{class}}(t)\right\rangle$, quantum force $\left\langle \boldsymbol{F}^{\mathrm{A}}_{\mathrm{quant}}(t)\right\rangle$, and total force $\left\langle \boldsymbol{F}^{\mathrm{A}}_{\mathrm{total}}(t)\right\rangle$ in the adiabatic representation for the non-adiabatic process in the simple avoided crossing system depicted by Fig 2.4, with the diabatic coupling constants (a) $C = 0.0005$, and (b) $C = 0.002$. The inset shows a magnified view of the plot in the time interval $t = 10$ fs and $t = 40$ fs. 123
3.16 Comparison of the adiabatic QTSH and d2a QTSH results for the system phase space averaged classical force $\left\langle \boldsymbol{F}^{\mathrm{A}}_{\mathrm{class}}(t)\right\rangle$, quantum force $\left\langle \boldsymbol{F}^{\mathrm{A}}_{\mathrm{quant}}(t)\right\rangle$, and total force $\left\langle \boldsymbol{F}^{\mathrm{A}}_{\mathrm{total}}(t)\right\rangle$ in the diabatic representation for the non-adiabatic process in the dual avoided crossing system depicted by Fig 2.8, with the diabatic coupling constants (a) $C = 0.0015$, and (b) $C = 0.006$. The inset shows a magnified view of the plot in the time interval $t = 7.5$ fs and $t = 17.5$ fs. 124
3.17 Comparison of the diabatic QTSH and a2d QTSH results for the system phase space averaged classical force $\left\langle \boldsymbol{F}^{\mathrm{D}}_{\mathrm{class}}(t)\right\rangle$, quantum force $\left\langle \boldsymbol{F}^{\mathrm{D}}_{\mathrm{quant}}(t)\right\rangle$, and total force $\left\langle \boldsymbol{F}^{\mathrm{D}}_{\mathrm{total}}(t)\right\rangle$ in the diabatic representation for the non-adiabatic process in the simple avoided crossing system depicted by Fig 2.3, with the diabatic coupling constants (a) $C = 0.0005$, and (b) $C = 0.002$. The inset shows a magnified view of the plot in the time interval $t = 10$ fs and $t = 40$ fs. 127
3.18 Comparison of the diabatic QTSH and a2d QTSH results for the system phase space averaged classical force $\left\langle \boldsymbol{F}^{\mathrm{D}}_{\mathrm{class}}(t)\right\rangle$, quantum force $\left\langle \boldsymbol{F}^{\mathrm{D}}_{\mathrm{quant}}(t)\right\rangle$, and total force $\left\langle \boldsymbol{F}^{\mathrm{D}}_{\mathrm{total}}(t)\right\rangle$ in the diabatic representation for the non-adiabatic process in the simple avoided crossing system depicted by Fig 2.5, with the diabatic coupling constants (a) $C = 0.0005$, and (b) $C = 0.002$. The inset shows a magnified view of the plot in the time interval $t = 10$ fs and $t = 40$ fs. 128
3.19 Comparison of the diabatic QTSH and a2d QTSH results for the system phase space averaged classical force $\left\langle \boldsymbol{F}^{\mathrm{D}}_{\mathrm{class}}(t)\right\rangle$, quantum force $\left\langle \boldsymbol{F}^{\mathrm{D}}_{\mathrm{quant}}(t)\right\rangle$, and total force $\left\langle \boldsymbol{F}^{\mathrm{D}}_{\mathrm{total}}(t)\right\rangle$ in the diabatic representation for the non-adiabatic process in the dual avoided crossing system depicted by Fig 2.9, with the diabatic coupling constants (a) $C = 0.0015$, and (b) $C = 0.006$. The inset shows a magnified view of the plot in the time interval $t = 7.5$ fs and $t = 17.5$ fs. . . . 129

4.1 Nonadiabatic mixing angle for the simple avoided crossing system given by the diabatic potentials in Eqns 1.83-1.84, where the diabatic coupling constant $C \to 0$. The blue marker marks $\phi(0) = \frac{\pi}{2}$, $\phi(q)$ at the nuclear coordinate where the transition takes place at $q^* = 0$. The orange markers mark $\phi(q(t^* - \epsilon)) = 0$ and $\phi(q(t^* - \epsilon)) = \pi$, the nuclear coordinates the instant ϵ right before and right after the transition, $q(t^* - \epsilon)$ and $q(t^* + \epsilon)$, respectively. 140
4.2 (a) The non-adiabatic mixing angle $\phi(q)$, (b) the non-adiabatic coupling vector $\boldsymbol{d}(\boldsymbol{q})$, (c) the real part of the coherence $\alpha(q)$, and (d) the quantum force $F_{\mathrm{quant}}(q)$ for the process shown in Fig 2.8, as described in text. The dotted, dashed, and dashdotted lines represent the models where $C = 0.0015, 0.003,$ and 0.006, respectively. 149

4.3 Nonadiabatic mixing angle for the simple avoided crossing system given by the diabatic potentials in Eqns 1.86-1.87, where the diabatic coupling constant $C \to 0$. The blue marker marks $\phi(-1.57) = \frac{\pi}{2}$ and $\phi(1.57) = \frac{\pi}{2}$, where a complete and localized transition from the lower to the upper adiabatic state takes place at $\boldsymbol{q}_1^* = -1.57$, and from the upper to the lower adiabatic state at $\boldsymbol{q}_2^* = 1.57$ in the adiabatic representation given by Fig 2.8. 150
4.4 (a) Classical and quantum force components that make up the total force in the adiabatic representation for the process in Fig 2.2. (b) Classical and quantum force components that make up the total force in the diabatic representation for the process in Fig 2.3. Diabatic potentials for the simple avoided crossing system [1] are given in Eqns 1.83-1.84, with the diabatic potential coupling constant $C = 0.0005$. 157
4.5 (a) Classical and quantum force components that make up the total force in the adiabatic representation for the process in Fig 2.4. (b) Classical and quantum force components that make up the total force in the diabatic representation for the process in Fig 2.5. Diabatic potentials for the simple avoided crossing system [1] are given in Eqns 1.83-1.84, with the diabatic potential coupling constant $C = 0.0005$. 158
4.6 (a) Classical and quantum force components that make up the total force in the adiabatic representation for the process in Fig 2.8. (b) Classical and quantum force components that make up the total force in the diabatic representation for the process in Fig 2.9. Diabatic potentials for the simple avoided crossing system are given in Eqns 1.86-1.87, with the diabatic potential coupling constant $C = 0.0015$. 159
4.7 Phase space averaged classical diabatic force associated with the localized quantum states/trajectories traveling along the single diabatic potential energy surface $V_1(\boldsymbol{q})$, and the phase space averaged total adiabatic force corresponding to the process in Fig 2.2. Diabatic potentials for the simple avoided crossing system are given in Eqns 1.83-1.84, with the diabatic coupling constant $C = 0.0005$. 161
4.8 Phase space averaged classical diabatic force associated with the localized quantum states/trajectories traveling along the single diabatic potential energy surface $V_2(\boldsymbol{q})$, and the phase space averaged total adiabatic force corresponding to the process in Fig 2.4. Diabatic potentials for the simple avoided crossing system [1] are given in Eqns 1.83-1.84, with the diabatic coupling constant $C = 0.0005$. 161
4.9 Phase space averaged classical diabatic force associated with the localized quantum states/trajectories traveling along the single diabatic potential energy surface $V_2(\boldsymbol{q})$, and the phase space averaged total adiabatic force corresponding to the process in Fig 2.8. Diabatic potentials for the dual avoided crossing system are given in Eqns 1.86-1.87, with the diabatic coupling constant $C = 0.0015$. 162

4.10 Comparison of QTSH against quantum wavepacket results (a) for $\langle\rho_{--}(t)\rangle$ in the adiabatic representation, for the process in the simple avoided crossing system with the initial population on the lower adiabatic surface, (b) and for $\langle\rho_{22}(t)\rangle$ in the diabatic representation, for the corresponding process in the diabatic representation. The trajectories had an average starting momentum of $\hbar k_0 = 8.0$, with the diabatic potential coupling constant $C = 0.001$. 165
4.11 (a) Classical and quantum force components that make up the total force in the adiabatic representation for the process in the simple avoided crossing system with the initial population on the lower adiabatic surface. (b) Classical and quantum force components that make up the total force in the corresponding process in the diabatic representation. The trajectories had an average starting momentum of $\hbar k_0 = 8.0$, with the diabatic potential coupling constant $C = 0.001$. 166
4.12 Comparison of QTSH, and the QTSH diabatic to adiabatic transformed (QTSH d2a) results against exact quantum results for $\langle\rho_{--}(t)\rangle$, for the simple avoided crossing system with the initial population on the lower adiabatic surface. The trajectories had an average starting momentum of $\hbar k_0 = 8.0$, with the diabatic potential coupling constant $C = 0.001$. 167
4.13 Comparison of QTSH against quantum wavepacket results (a) for $\langle\rho_{--}(t)\rangle$ in the adiabatic representation, for the process in the dual avoided crossing system with the initial population on the lower adiabatic surface, (b) and for $\langle\rho_{22}(t)\rangle$ in the diabatic representation, for the corresponding process in the diabatic representation. The trajectories had an average starting momentum of $\hbar k_0 = 77.2$ a.u., with the diabatic potential coupling constant $C = 0.0015$. 170
4.14 (a) Classical and quantum force components that make up the total force in the adiabatic representation for the process in the dual avoided crossing system with the initial population on the lower adiabatic surface. (b) Classical and quantum force components that make up the total force in the corresponding process in the diabatic representation. Diabatic potentials for the dual avoided crossing system are given in Eqns 1.86-1.87, with the diabatic potential coupling constant $C = 0.0015$. 171
4.15 Comparison of QTSH, and the QTSH diabatic to adiabatic transformed (QTSH d2a) results against exact quantum results for $\langle\rho_{--}(t)\rangle$, for the dual avoided crossing system with the initial population on the lower adiabatic surface. The trajectories had an average starting momentum of $\hbar k_0 = 77.2$ a.u., with the diabatic potential coupling constant $C = 0.0015$. 172

5.1 Potential energy associated with intramolecular interactions associated with (a) bond stretching, (b) angle bending, and (c) bond twisting. (d) Changes in potential energy associated with changes in intermolecular interactions such as hydrogen bonding, as a result of the rearrangement of molecules. 186

5.2 Molecular modes of motion that contribute the the chemical potentials of the reactants, H_2 and O_2 include the bond stretching modes and rotational modes of H_2 molecules and O_2 molecules. Molecular modes of motion that contribute the the chemical potential of the product, H_2O include the bond stretching modes, rotational modes, and angle bending modes of H_2O molecules (not all bond stretching modes are displayed.). Depending on the extent of the reaction ξ, different intermolecular forces of attraction contribute the the chemical potentials, as summarized in the table. 187
5.3 stretch, ... 189
5.4 The vaporization of water occurs when liquid water $H_2O(l)$ is placed at a temperature and pressure that lies along the vaporization curve (orange line) or within the gas region (shaded orange region). When along the vaporization curve, the chemical potential of liquid water and water vapour are equal. . . 190

LIST OF TABLES

Page

1.1 Summary of the parameters maximum strength of the adiabatic coupling $\boldsymbol{d}_{\text{peak}}$, the width of the non-adiabatic coupling at half maximum $w_{0.5,\text{peak}}$, the position of strongest non-adiabatic coupling $\boldsymbol{q}_{\boldsymbol{d}_{\text{peak}}}$, and the size of the energy gap where non-adiabatic coupling is strongest $\hbar\omega(\boldsymbol{q}_{\boldsymbol{d}_{\text{peak}}})$ for the simple avoided crossing system [1] for the values of the diabatic coupling constants $C = 0.0005, 0.001$ and 0.002. 27

1.2 Summary of the parameters maximum strength of the adiabatic coupling $\boldsymbol{d}_{\text{peak1}}$, the width of the non-adiabatic coupling at half maximum $w_{0.5,\text{peak1}}$, the position of strongest non-adiabatic coupling $\boldsymbol{q}_{\boldsymbol{d}_{\text{peak1}}}$, and the size of the energy gap where non-adiabatic coupling is strongest $\hbar\omega(\boldsymbol{q}_{\boldsymbol{d}_{\text{peak1}}})$ for the dual avoided crossing system [1] for the values of the diabatic coupling constants $C = 0.0015, 0.003$ and 0.006. 29

1.3 Summary of the parameters maximum strength of the adiabatic coupling $\boldsymbol{d}_{\text{peak2}}$, the width of the non-adiabatic coupling at half maximum $w_{0.5,\text{peak2}}$, the position of strongest non-adiabatic coupling $\boldsymbol{q}_{\boldsymbol{d}_{\text{peak2}}}$, and the size of the energy gap where non-adiabatic coupling is strongest $\hbar\omega(\boldsymbol{q}_{\boldsymbol{d}_{\text{peak2}}})$ for the dual avoided crossing system [1] for the values of the diabatic coupling constants $C = 0.0015, 0.003$ and 0.006. 29

ACKNOWLEDGMENTS

I would like to thank my advisor, Prof. Craig Martens, and my former advisor, Prof. Shaul Mukamel for the opportunities and help they have given me, and for the lessons they have taught me. To my thesis committee members, Prof. Kieron Burke and Prof. Filipp Furche, thank you for the advice you have given me.

I am also thankful for the help that I received from Prof. Ramesh Arasasingham, Prof. Joe Patterson, and Prof. Alan Heyduk while I was a teaching assistant and an instructor-of-record.

To my current labmate in the Martens group, Austin Green, and our collaborator, Leonardo Araujo, thank you for the interesting conversations we have shared.

I would also like to acknowledge the help and encouragement that I have received from Cynthia Dennis and Morgan Sibley in the UCI Chemistry department. Their help has made all the difference.

I would also like to thank my graduate school friends at UCI for the pleasant memories that we have shared. Johanna Rinnaman, Marcus Marracci, Jenn Campos, Gabriel Phun, Elianna Frank, Justin Chen, and Shane Flynn have made my time at UCI much brighter.

To my former postdoc friends in the Mukamel lab, Stefano Cavaletto, Daniel Keefer, and Bing Gu, thank you for making my early graduate school days such a joy and for providing me with much needed moral support. The office we shared was very much a home away from home for us foreigners.

From my undergraduate institution, National University of Singapore, I would like to thank Prof. Zhang Chun, Prof. Kang Hway Chuan, and Dr. Quek Ser Hwee. Prof. Zhang Chun showed me what it meant to be a scientist. He is my favourite scientist, and I aspire to pass on the lessons that he has taught me. Prof. Kang Hway Chuan taught me to find my own solutions as my honours thesis advisor. It was a valuable skill in obtaining this degree, and will continue to be along my journey to becoming an independent thinker. Dr. Quek Ser Hwee has been my mentor since I was an undergraduate. While she's most certainly a Historian, her wise words have got me through difficult times.

I would also like to thank my friends, Thida and Thida, at Cafe Espresso. My ability to speak Khmer has vastly improved because of our friendly exchanges.

To my church family, Pastor Matt, Cristina, Sharon and Josie, thank you for helping me to retain my humanity, and for reminding me that there is more to life than the pursuit of achievements.

To the friends that are close to my heart, Tomoko Louie, Gaynor Choo, and Shawn Tan. Thank you for keeping in touch through the years. They see me for who I am, and remind me of it when I forget. My life is richer because of them. I hope that we will continue to be

friends for many years to come.

To Masafumi Karita, who so generously shared everything he knew with me while he was my supervisor in the Colloidal Science lab at Proctor and Gamble. He never withheld anything from me. I still remember much of what he taught me, and I admire him for his incredible fighting spirit.

Last but not least, I would like to thank members of my family.

To my siblings, Daniel Huang and Deborah Huang, and my sibling-in-laws, Audrey Lin and Ivan Gian, thank you for holding the family together and for relieving me of many familial responsibilities while I have been away. To my "little" cousins Blaise Ferguson and Keira Ferguson, thank you for teaching me that being older and "in-charge" meant having to be responsible and accountable. I treasure our childhood memories very much.

I would also like to thank my favourite people, my nephews, Edgar Huang and Everest Huang, my nieces, Lauren Gian and Ashley Gian, and my Godson, Aaron. According to Nietzsche, "He who has a why to live for can bear almost any how." They give me reason to overcome every obstacle that life throws my way, as I strive to be a better role model for them everyday. They give me hope that the world can be a better place for future generations.

Portions of Chapter 2 of this dissertation are reproduced from Dorothy Miaoyu Huang, Austin T. Green, Craig C. Martens; A first principles derivation of energy-conserving momentum jumps in surface hopping simulations. *J. Chem. Phys.* **2023**; 159 (21): 214108., with the permission of AIP Publishing. The coauthors listed in this publication are Austin T. Green and Craig C. Martens. Craig C. Martens directed and supervised research which forms the basis for the dissertation.

I thank AIP Publishing, for allowing me to include copyrighted figures, and excerpts as part of my thesis. I also thank the PCCP Owner Societies for allowing me to include a figure as part of my thesis.

Financial support was provided by the National Science Foundation under Grant No. CHE-1764209.

VITA

Miaoyu Dorothy Huang

EDUCATION

Doctor of Philosophy in Chemistry **2024**
University of California, Irvine *Irvine, CA*

Master of Science in Chemistry **2020**
University of California, Irvine *Irvine, CA*

Bachelors of Science (Second Upper Hons) in Chemistry **2015**
National University of Singapore *Singapore, Singapore*

University Scholars Programme **2015**
National University of Singapore *Singapore, Singapore*

RESEARCH EXPERIENCE

Graduate Research Assistant **2019–2024**
University of California, Irvine *Irvine, California*

TEACHING EXPERIENCE

Instructor-of-Record **2023**
University of California, Irvine *Irvine, California*

Teaching Assistant **2018–2024**
University of California, Irvine *Irvine, California*

REFEREED JOURNAL PUBLICATIONS

Dorothy Miaoyu Huang, Austin T. Green, Craig C. Martens; A first principles derivation of energy-conserving momentum jumps in surface hopping simulations. *J. Chem. Phys.* 7 December 2023; 159 (21): 214108.

ABSTRACT OF THE DISSERTATION

Quantum Trajectory Surface Hopping: Theory and its Inner Workings

By

Miaoyu Dorothy Huang

Doctor of Philosophy in Chemistry

University of California, Irvine, 2024

Professor Craig C. Martens, Chair

Quantum trajectory surface hopping (QTSH) is a trajectory surface hopping method that is rigorously derived from the quantum-classical Liouville equation, developed to study non-adiabatic molecular dynamics of multistate systems. This work explores the unique features of QTSH - energy conservation on the ensemble level without the imposition of ad hoc momentum rescaling, and its rigorous derivation in both the diabatic and adiabatic representations - that distinguish it from the widely used fewest switches trajectory surface hopping method (FSSH). We show that in the limit of complete and localized population transfer in the adiabatic representation, the work done by the quantum force that characterizes QTSH is akin to the strict classical energy conserving momentum 'jumps' of FSSH. Our numerical results show that the feedback between nuclear and electronic degrees of freedom, mediated by the quantum forces that work to conserve the quantum-classical energy on average, is well-incorporated in QTSH. By transforming the QTSH results for the elements of the Wigner distribution and forces from one representation to another, we conclude that QTSH is representation invariant. By analyzing the classical and quantum forces for non-adiabatic processes in both the diabatic and adiabatic representations, we found that highly non-classical processes in the adiabatic representation are, conversely, highly classical in the diabatic representation. Since errors due to inconsistencies in surface hopping are larger when significant population transfers occur, it allows us to conclude that QTSH results

for the highly non-classical processes in the adiabatic representation are less accurate than for the corresponding more classical processes in the diabatic representation. We exploit the representation invariance of QTSH to obtain more accurate results for the population dynamics in the adiabatic representation.

Chapter 1

Introduction to the Dissertation

A complete quantum mechanical description of molecular dynamics can only be obtained by solving the time-dependent Schrödinger equation with all nuclear and electronic degrees of freedom. Solving the problem exactly has, however, proven to be an intractable problem due to its high computational cost [4].

A fundamental approximation that has greatly reduced the complexity of the problem is the Born-Oppenheimer approximation [5, 6] - also known as the adiabatic approximation. Within the framework of the adiabatic approximation, the fast electronic degrees of freedom are assumed to depend only parametrically on the slow nuclear degrees of freedom [7], and the electronic and nuclear states are not coupled. However, in regions where the energy gap between many-body electronic potential energy surfaces (PESs) approaches the scale of the inverse of the time scale of nuclear motion [8, 9], non-adiabatic processes that involve the coupling of the nuclear and electronic degrees of freedom occur [9], resulting in the breakdown of the adiabatic approximation.

Many chemical applications involve chemical processes that require electronic transitions between electronic states. Some of these processes include light emission [10–14], charge

separation [15–18], non-radiative relaxation [19–21], intersystem crossing [22–24], and photoisomerization [25–28]. Non-adiabatic molecular dynamics (NAMD) is involved in the study of these processes.

Modeling NAMD involves two important aspects. The first, an electronic structure method that allows for the calculation of the ground state and excited state electronic potential energy surfaces (PESs) to reasonable chemical accuracy. The second, a molecular dynamics algorithm that accounts for non-adiabatic occurrences while propagating trajectories.

As quantum trajectory surface hopping (QTSH) - the focus of this dissertation - is a molecular dynamics algorithm used in modeling NAMD, we will now provide a brief account of the molecular dynamics algorithms used to model NAMD. In particular, those that utilize classical trajectories for computational tractability.

1.1 Modeling Non-Adiabatic Molecular Dynamics

The development of NAMD algorithms that utilize classical trajectories fall under two broad categories - semiclassical, and mixed quantum-classical methods. Some approaches are trajectory surface hopping [1, 29, 30], mapping Hamiltonians [31–34], ring polymer methods [35], symmetrical windowing of quasiclassical trajectories [36, 37], and quantum-classical Wigner function-based approaches [38–47]. These computationally feasible methods reproduce the key quantum features of complex systems within the framework of classical mechanics.

1.1.1 Trajectory Surface Hopping

Owing to its simple implementation and fast convergence [8], the most popular mixed quantum-classical NAMD algorithm, where the nuclear degrees of freedom are treated clas-

sically, and the electronic degrees of freedom are treated quantum mechanically [4, 48], is a trajectory surface hopping method [1, 49] called the fewest switches surface hopping (FSSH) method [1].

In trajectory surface hopping, the nuclear wavepacket is represented by swarms of independent classical trajectories that evolve on single electronic PESs, where non-adiabatic transitions are represented by hops between electronic PESs. Although each trajectory in phase space is analogous to a localized wavepacket, the actual non-locality of nuclear dynamics in electronic and phase space is accounted for by running an ensemble of trajectories [1, 8].

In FSSH, the trajectories evolve in nuclear phase space according to Newton's classical equations of motion [50], with each trajectory experiencing the force of the single PES that it is evolving on, interrupted only by *instantaneous* hops from one PES to another [1].

An approximate time-dependent Schrödinger equation is also solved for each trajectory, with each trajectory possessing a 'proxy' density matrix and finite hopping probabilities from one PES to another.

The FSSH [1] probability of each trajectory hopping from PES L to K utilizes the populations and coherences obtained from the 'proxy' density matrix of each trajectory. The hopping probability for each trajectory calculated using the fewest switches algorithm [1] is given by the ratio of the population increment on PES K due to the flux from PES L during the timestep to the population on PES L [50].

A stochastic algorithm that utilizes the hopping probability of each trajectory is then used to determine whether, and to which state a trajectory hops. When a hop occurs, motivated by the Pechukas force [51], the momentum is rescaled in the direction of the non-adiabatic coupling vector $\boldsymbol{d}(\boldsymbol{q})$ [50, 51] to allow for strict conservation of energy on the *trajectory* level, with the sign of the momentum 'jumps' assigned by physical arguments [29, 30]. These

momentum 'jumps' are *ad hoc* in nature and reflect strict classical energy conservation that fail to account for the non-locality of electronic transitions in phase space.

When a trajectory 'hop' dictated by the stochastic algorithm does not occur due to the trajectory possessing insufficient kinetic energy, the 'hop' is aborted and considered frustrated. These frustrated hops contribute to the breakdown of surface hopping consistency in FSSH that is defined as the agreement between the state occupancy statistics of the converged trajectory ensemble and the average populations of the proxy density matrix [50].

As important quantum effects that arise from the *interdependence* of members of the trajectory ensemble [39–41, 52–58], the treatment of trajectories as *independent* from other members of the trajectory ensemble gives rise to the well-documented lack of decoherence in FSSH that contributes to the lack of internal consistency in FSSH [59].

The question of whether FSSH in the adiabatic representation, in which FSSH was derived [1] can be transformed to the diabatic representation [60, 61], has been a longstanding one, with no straightforward answers. A rigorous trajectory surface hopping method should be representation invariant.

In quantum trajectory surface hopping (QTSH) [62, 63], the quantum-classical description of systems are derived rigorously from quantum-classical limit of the multistate Liouville equation [38–40, 64], in the context of the *independent* trajectory approximation, QTSH can be derived rigorously, and performed in both the diabatic and adiabatic representations.

Before introducing the quantum-classical Liouville equation (QCLE) [38–40] that underpins the QTSH method, and the QTSH formalism [62, 63], we introduce the local diabatic [65] and adiabatic representations and the unitary transformation between them. For berevity, we will refer to the local diabatic representation [65] as the diabatic representation for the rest of this dissertation.

1.2 Diabatic and Adiabatic Representations

Systems in the diabatic and adiabatic representation are related by a unitary transformation.

The unitary transformation of an $n \times n$ unitary matrix of operators of an n-state system in the diabatic representation $\hat{\mathbf{A}}^{\mathrm{D}}$ gives the corresponding operator of an n-state system in the adiabatic representation $\hat{\mathbf{A}}^{\mathrm{A}}$ given by the expression

$$\hat{\mathbf{A}}^{\mathrm{A}} = \mathbf{U}^{\dagger}(\boldsymbol{q})\hat{\mathbf{A}}^{\mathrm{D}}\mathbf{U}(\boldsymbol{q}), \tag{1.1}$$

and the inverse unitary transformation of $\hat{\mathbf{A}}^{\mathrm{A}}$ gives $\hat{\mathbf{A}}^{\mathrm{D}}$ given by the expression

$$\hat{\mathbf{A}}^{\mathrm{D}} = \mathbf{U}(\boldsymbol{q})\hat{\mathbf{A}}^{\mathrm{A}}\mathbf{U}^{\dagger}(\boldsymbol{q}), \tag{1.2}$$

where $\mathbf{U}(\boldsymbol{q})$ represents the $n \times n$ unitary matrix, of an n-state system.

We now present the unitary transformation of the 2×2 Hamiltonian of a two-state system from the diabatic representation to the adiabatic representation.

The Hamiltonian of the a multielectronic state system $\hat{\mathbf{H}}$ is given by the sum of the nuclear kinetic energy $\hat{\mathbf{T}}$, and the electronic potential $\hat{\mathbf{V}}$,

$$\hat{\mathbf{H}} = \hat{\mathbf{T}} + \hat{\mathbf{V}}. \tag{1.3}$$

In the diabatic representation, the Hamiltonian of a two-state system $\hat{\mathbf{H}}^{\mathrm{D}}$ is given by a 2×2 matrix that consists of a kinetic energy operator $\hat{\mathbf{T}}^{\mathrm{D}}$ and electronic potential energy operator $\hat{\mathbf{V}}^{\mathrm{D}}$.

The kinetic energy operator is given by

$$\hat{\mathbf{T}}^{\mathrm{D}} = \begin{pmatrix} \frac{\hat{\mathbf{p}}^2}{2m} & 0 \\ 0 & \frac{\hat{\mathbf{p}}^2}{2m}, \end{pmatrix} \tag{1.4}$$

where $\hat{\mathbf{p}} = -i\hbar\nabla_{\boldsymbol{q}}$. The kinetic energy operator is diagonal since any nuclear momentum coupling terms vanishes in the diabatic representation [66, 67].

The potential energy operator is given by

$$\hat{\mathbf{V}}^{\mathrm{D}} = \begin{pmatrix} \hat{\mathrm{V}}_{11} & \hat{\mathrm{V}}_{12} \\ \hat{\mathrm{V}}_{21} & \hat{\mathrm{V}}_{22}, \end{pmatrix} \tag{1.5}$$

where $\hat{\mathrm{V}}_{11} = V_1(\boldsymbol{q})$, $\hat{\mathrm{V}}_{22} = V_2(\boldsymbol{q})$, and $\hat{\mathrm{V}}_{12} = \hat{\mathrm{V}}_{21} = V_{12}(\boldsymbol{q})$. Note that $V_{12}(\boldsymbol{q}) \in \mathbb{R}$.

In the diabatic representation, the off-diagonal terms in the Hamiltonian are present in the potential energy operator $\hat{\mathbf{V}}^{\mathrm{D}}$ in the form of the coupling potential $V_{12}(\boldsymbol{q})$ that couples the electronic states in the diabatic representation, $|1\rangle$ and $|2\rangle$.

Applying the unitary transformation given by Eqn 1.1 to the the Hamiltonian of the two-state system in the diabatic representation $\hat{\mathbf{H}}^{\mathrm{D}}$ gives the corresponding Hamiltonian in the adiabatic representation $\hat{\mathbf{H}}^{\mathrm{A}}$.

The 2×2 unitary matrix that relates the diabatic representation of a two-state system to its corresponding system in the adiabatic representation is given by

$$\mathbf{U}(\boldsymbol{q}) = \begin{pmatrix} \cos\frac{\phi(\boldsymbol{q})}{2} & -\sin\frac{\phi(\boldsymbol{q})}{2} \\ \sin\frac{\phi(\boldsymbol{q})}{2} & \cos\frac{\phi(\boldsymbol{q})}{2} \end{pmatrix}, \tag{1.6}$$

where $\phi(\boldsymbol{q})$ is the transformation angle between the diabatic and adiabatic representation.

The transformation angle $\phi(\boldsymbol{q})$ in terms of the diagonal diabatic potentials $V_1(\boldsymbol{q})$ and $V_2(\boldsymbol{q})$, and the off-diagonal diabatic potential $V_{12}(\boldsymbol{q})$, is given by the following relations

$$\tan\phi(\boldsymbol{q}) = \frac{2V_{12}(\boldsymbol{q})}{V_1(\boldsymbol{q}) - V_2(\boldsymbol{q})}, \tag{1.7}$$

where

$$\sin\phi(\boldsymbol{q}) = \frac{2V_{12}(\boldsymbol{q})}{\sqrt{\big(V_1(\boldsymbol{q}) - V_2(\boldsymbol{q})\big)^2 + 4V_{12}(\boldsymbol{q})^2}}, \tag{1.8}$$

and

$$\cos\phi(\boldsymbol{q}) = \frac{V_1(\boldsymbol{q}) - V_2(\boldsymbol{q})}{\sqrt{\big(V_1(\boldsymbol{q}) - V_2(\boldsymbol{q})\big)^2 + 4V_{12}(\boldsymbol{q})^2}}. \tag{1.9}$$

Applying the unitary transformation given in Eqn 1.1 on $\hat{\mathrm{T}}^{\mathrm{D}}$ (Eqn 1.4) and $\hat{\mathrm{V}}^{\mathrm{D}}$ (Eqn 1.5), separately, we obtain the kinetic energy and potential energy operators in the adiabatic representation.

The kinetic energy operator in the adiabatic representation is given by

$$\hat{\mathbf{T}}^{\mathrm{A}} = \begin{pmatrix} \frac{\hat{\mathbf{p}}^2}{2m} + \frac{\hbar^2 \boldsymbol{d}(\boldsymbol{q})^2}{2m} & -i\frac{\hbar}{2m}\big(\hat{\mathbf{p}}\cdot\boldsymbol{d}(\boldsymbol{q}) + \boldsymbol{d}(\boldsymbol{q})\cdot\hat{\mathbf{p}}\big) \\ i\frac{\hbar}{2m}\big(\hat{\mathbf{p}}\cdot\boldsymbol{d}(\boldsymbol{q}) + \boldsymbol{d}(\boldsymbol{q})\cdot\hat{\mathbf{p}}\big) & \frac{\hat{\mathbf{p}}^2}{2m} + \frac{\hbar^2 \boldsymbol{d}(\boldsymbol{q})^2}{2m} \end{pmatrix}, \tag{1.10}$$

where $\boldsymbol{d}(\boldsymbol{q})$ represents the non-adiabatic coupling vector.

The off-diagonal terms in the Hamiltonian in the adiabatic representation are present in the kinetic energy operator $\hat{\mathbf{T}}^{\mathrm{A}}$ (Eqn 1.10). These terms arise because the nuclear momentum operator $\hat{\mathbf{p}} = -i\hbar\nabla_{\boldsymbol{q}}$ acts on the electronic states that parametrically depend on the nuclear coordinate $\boldsymbol{q}$ in the adiabatic representation, $|+\rangle$ and $|-\rangle$.

This couples the nuclear and electronic degrees of freedom in the form of the non-adiabatic coupling vector $\boldsymbol{d}(\boldsymbol{q}) = \langle + | \nabla_{\boldsymbol{q}} | - \rangle$. In terms of the $\phi(\boldsymbol{q})$, $\boldsymbol{d}(\boldsymbol{q}) = -\frac{\nabla_{\boldsymbol{q}}\phi(\boldsymbol{q})}{2}$.

The potential energy operator in the adiabatic representation is given by

$$\hat{\mathbf{V}}^{\mathrm{A}} = \begin{pmatrix} \hat{\mathrm{V}}_{++} & 0 \\ 0 & \hat{\mathrm{V}}_{--} \end{pmatrix}, \tag{1.11}$$

where the $\hat{\mathrm{V}}_{++} = V_{+}(\boldsymbol{q})$ and $\hat{\mathrm{V}}_{--} = V_{-}(\boldsymbol{q})$.

The adiabatic potentials for a two-state system $V_{\pm}(\boldsymbol{q})$ can be expressed in terms of the diabatic diagonal potentials $V_{1/2}(\boldsymbol{q})$, and the diabatic off-diagonal potential $V_{12}(\boldsymbol{q})$ as

$$V_{\pm}(\boldsymbol{q}) = \frac{V_1(\boldsymbol{q}) + V_2(\boldsymbol{q})}{2} \pm \frac{\sqrt{\big(V_1(\boldsymbol{q}) - V_2(\boldsymbol{q})\big)^2 + 4V_{12}(\boldsymbol{q})^2}}{2}. \tag{1.12}$$

In the diabatic representation, the density matrix of a two-state system $\hat{\boldsymbol{\rho}}^{\mathrm{D}}$ is given by a 2×2 matrix that is given by

$$\hat{\boldsymbol{\rho}}^{\mathrm{D}} = \begin{pmatrix} \hat{\rho}_{11} & \hat{\rho}_{12} \\ \hat{\rho}_{21} & \hat{\rho}_{22} \end{pmatrix}, \tag{1.13}$$

where the diagonal $\hat{\rho}_{11}$ and $\hat{\rho}_{22}$ operators represent the electronic populations, and the off-diagonal $\hat{\rho}_{12}$ and $\hat{\rho}_{12}$ operators represent the coherences.

In the adiabatic representation, the corresponding density matrix of a two-state system $\hat{\boldsymbol{\rho}}^{\mathrm{A}}$ is given by a 2×2 matrix that is given by

$$\hat{\boldsymbol{\rho}}^{\mathrm{A}} = \begin{pmatrix} \hat{\rho}_{++} & \hat{\rho}_{+-} \\ \hat{\rho}_{-+} & \hat{\rho}_{--} \end{pmatrix}, \tag{1.14}$$

where the diagonal $\hat{\rho}_{++}$ and $\hat{\rho}_{--}$ operators represent the electronic populations, and the off-diagonal $\hat{\rho}_{+-}$ and $\hat{\rho}_{-+}$ operators represent the coherences.

The coherence is a quantum feature that arises due to the correlation of electronic states as a result of quantum superposition [68].

As QTSH [62, 63], was derived from the quantum-classical Liouville equation (QCLE) [38], the quantum-classical limit of the Liouville-Von Neumann equation [69, 70], we will now introduce the quantum-classical limit of quantum mechanics.

1.3 Quantum-Classical Limit of Quantum Mechanics

In the quantum-classical limit, a quantum mechanical operator $\hat{\mathrm{A}}$ can be expressed as the Weyl function [71, 72]

$$A(\boldsymbol{q},\boldsymbol{p}) = \int \left\langle \boldsymbol{q} + \frac{\boldsymbol{y}}{2} \right| \hat{\mathrm{A}} \left| \boldsymbol{q} - \frac{\boldsymbol{y}}{2} \right\rangle \mathrm{e}^{-i\frac{\boldsymbol{p}\cdot\boldsymbol{y}}{\hbar}} \mathrm{d}\boldsymbol{y}. \tag{1.15}$$

The QTSH method was derived in the quantum-classical limit, where the quantum operators are represented by Weyl functions given by Eqn 1.15.

The product of quantum mechanical operators $\hat{\mathrm{A}}\hat{\mathrm{B}}$ in the quantum-classical limit can be expressed as the Moyal/star product [73] that is represented by the $\star$ symbol

$$A(\boldsymbol{q},\boldsymbol{p}) \star B(\boldsymbol{q},\boldsymbol{p}) = A(\boldsymbol{q},\boldsymbol{p})\mathrm{e}^{\frac{i\hbar}{2}\overleftrightarrow{\Lambda}} B(\boldsymbol{q},\boldsymbol{p}), \tag{1.16}$$

where $\star \equiv \mathrm{e}^{\frac{i\hbar}{2}\overleftrightarrow{\Lambda}}$ and $\overleftrightarrow{\Lambda} = \overleftarrow{\nabla}_{\boldsymbol{q}}\overrightarrow{\nabla}_{\boldsymbol{p}} - \overleftarrow{\nabla}_{\boldsymbol{p}}\overrightarrow{\nabla}_{\boldsymbol{q}}$.

The Taylor expansion of $\mathrm{e}^{\frac{i\hbar}{2}\overleftrightarrow{\Lambda}}$ can be expressed as

$$\mathrm{e}^{\frac{i\hbar}{2}\overleftrightarrow{\Lambda}} = \sum_n \left(\frac{i\hbar}{2}\overleftrightarrow{\Lambda}\right)^n = \sum_n \left(\frac{i\hbar}{2}\right)^n \overleftrightarrow{\Lambda}^n. \tag{1.17}$$

The time-dependent density operator $\hat{\boldsymbol{\rho}}(t)$ that represents the state of the system is expressed as the Wigner distribution $\boldsymbol{\rho}(\boldsymbol{q},\boldsymbol{p},t)$ [73, 74] - a quasiprobability distribution in phase space - in the quantum-classical limit, obtained by performing a partial Wigner transformation [74, 75] only on the nuclear degrees of freedom, given by Eqn 1.18.

The Wigner distribution [74] that represents an n-dimensional system that is described by the density matrix $\hat{\boldsymbol{\rho}}$ is given by

$$\boldsymbol{\rho}(\boldsymbol{q},\boldsymbol{p},t) = \frac{1}{(2\pi\hbar)^n}\int \left\langle \boldsymbol{q}+\frac{\boldsymbol{y}}{2}\right| \hat{\boldsymbol{\rho}}(t) \left|\boldsymbol{q}-\frac{\boldsymbol{y}}{2}\right\rangle \mathrm{e}^{-i\frac{\boldsymbol{p}\cdot\boldsymbol{y}}{\hbar}}\mathrm{d}\boldsymbol{y}. \tag{1.18}$$

For a two-state system, the Wigner distribution in the diabatic representation is given by

$$\boldsymbol{\rho}^{\mathrm{D}}(\boldsymbol{q},\boldsymbol{p},t) = \begin{pmatrix} \rho^{\mathrm{D}}_{11}(\boldsymbol{q},\boldsymbol{p},t) & \rho^{\mathrm{D}}_{12}(\boldsymbol{q},\boldsymbol{p},t) \\ \rho^{\mathrm{D}}_{21}(\boldsymbol{q},\boldsymbol{p},t) & \rho^{\mathrm{D}}_{22}(\boldsymbol{q},\boldsymbol{p},t) \end{pmatrix}, \tag{1.19}$$

where $\mathrm{Re}\left(\rho^{\mathrm{D}}_{12}(\boldsymbol{q},\boldsymbol{p},t)\right) = \mathrm{Re}\left(\rho^{\mathrm{D}}_{21}(\boldsymbol{q},\boldsymbol{p},t)\right) = \alpha^{\mathrm{D}}(\boldsymbol{q},\boldsymbol{p},t)$, and
$\mathrm{Im}\left(\rho^{\mathrm{D}}_{12}(\boldsymbol{q},\boldsymbol{p},t)\right) = -\mathrm{Im}\left(\rho^{\mathrm{D}}_{21}(\boldsymbol{q},\boldsymbol{p},t)\right) = \beta^{\mathrm{D}}(\boldsymbol{q},\boldsymbol{p},t)$, and the Wigner distribution in the adiabatic representation is given by

$$\boldsymbol{\rho}^{\mathrm{A}}(\boldsymbol{q},\boldsymbol{p},t) = \begin{pmatrix} \rho^{\mathrm{A}}_{++}(\boldsymbol{q},\boldsymbol{p},t) & \rho^{\mathrm{A}}_{+-}(\boldsymbol{q},\boldsymbol{p},t) \\ \rho^{\mathrm{A}}_{-+}(\boldsymbol{q},\boldsymbol{p},t) & \rho^{\mathrm{A}}_{--}(\boldsymbol{q},\boldsymbol{p},t) \end{pmatrix}, \tag{1.20}$$

where $\mathrm{Re}\left(\rho^{\mathrm{A}}_{+-}(\boldsymbol{q},\boldsymbol{p},t)\right) = \mathrm{Re}\left(\rho^{\mathrm{A}}_{-+}(\boldsymbol{q},\boldsymbol{p},t)\right) = \alpha^{\mathrm{A}}(\boldsymbol{q},\boldsymbol{p},t)$, and
$\mathrm{Im}\left(\rho^{\mathrm{A}}_{+-}(\boldsymbol{q},\boldsymbol{p},t)\right) = -\mathrm{Im}\left(\rho^{\mathrm{A}}_{-+}(\boldsymbol{q},\boldsymbol{p},t)\right) = \beta^{\mathrm{A}}(\boldsymbol{q},\boldsymbol{p},t)$.

The relationship between the Wigner distribution in the diabatic and adiabatic representation is non-trivial and is reported in Ref [76].

A more exact relationship can be obtained by applying the Moyal/star product as given in Eqn 1.16 in place of a matrix product. This will be presented in Chapter 3 of this dissertation.

The elements of the Wigner distribution [74] in the adiabatic representation in terms of that in the diabatic representation, for the two-state system as reported in Ref [76] are

$$\begin{aligned}\rho^{\mathrm{A}}_{++}(\boldsymbol{q},\boldsymbol{p},t) &= \frac{\rho^{\mathrm{D}}_{11}(\boldsymbol{q},\boldsymbol{p},t)+\rho^{\mathrm{D}}_{22}(\boldsymbol{q},\boldsymbol{p},t)}{2}+\frac{\rho^{\mathrm{D}}_{11}(\boldsymbol{q},\boldsymbol{p},t)-\rho^{\mathrm{D}}_{22}(\boldsymbol{q},\boldsymbol{p},t)}{2}\cos\phi(\boldsymbol{q}) \\ &\quad +\alpha^{\mathrm{D}}(\boldsymbol{q},\boldsymbol{p},t)\sin\phi(\boldsymbol{q}), \qquad (1.21)\end{aligned}$$

$$\begin{aligned}\rho^{\mathrm{A}}_{--}(\boldsymbol{q},\boldsymbol{p},t) &= \frac{\rho^{\mathrm{D}}_{11}(\boldsymbol{q},\boldsymbol{p},t)+\rho^{\mathrm{D}}_{22}(\boldsymbol{q},\boldsymbol{p},t)}{2}-\frac{\rho^{\mathrm{D}}_{11}(\boldsymbol{q},\boldsymbol{p},t)+\rho^{\mathrm{D}}_{22}(\boldsymbol{q},\boldsymbol{p},t)}{2}\cos\phi(\boldsymbol{q}) \\ &\quad -\alpha^{\mathrm{D}}(\boldsymbol{q},\boldsymbol{p},t)\sin\phi(\boldsymbol{q}), \qquad (1.22)\end{aligned}$$

$$\alpha^{\mathrm{A}}(\boldsymbol{q},\boldsymbol{p},t) = -\frac{\rho^{\mathrm{D}}_{11}(\boldsymbol{q},\boldsymbol{p},t)-\rho^{\mathrm{D}}_{22}(\boldsymbol{q},\boldsymbol{p},t)}{2}\sin\phi(\boldsymbol{q})+\alpha^{\mathrm{D}}(\boldsymbol{q},\boldsymbol{p},t)\cos\phi(\boldsymbol{q}), \qquad (1.23)$$

$$\beta^{\mathrm{A}}(\boldsymbol{q},\boldsymbol{p},t) = \beta^{\mathrm{D}}(\boldsymbol{q},\boldsymbol{p},t), \qquad (1.24)$$

equivalent to dropping any $\mathcal{O}(\hbar)$ or higher terms in the Moyal/star product that will be presented in Chapter 3.

We will now introduce the time evolution of the state of the system represented by the density matrix $\hat{\boldsymbol{\rho}}(t)$ in the Schrödinger picture, and the quantum-classical Liouville equation (QCLE) [38].

1.4 Electronic Nuclear Dynamics

The time evolution of the density matrix that describes the coupled electronic-nuclear dynamics of a multi-electronic state system is described by the Liouville-von Neumann equation [69, 70] given by

$$i\hbar\frac{\mathrm{d}\hat{\boldsymbol{\rho}}^{\mathrm{D}}(t)}{\mathrm{d}t} = \left[\hat{\mathbf{H}}^{\mathrm{D}}, \hat{\boldsymbol{\rho}}^{\mathrm{D}}(t)\right] \tag{1.25}$$

in the diabatic representation, and given by

$$i\hbar\frac{\mathrm{d}\hat{\boldsymbol{\rho}}^{\mathrm{A}}}{\mathrm{d}t} = \left[\hat{\mathbf{H}}^{\mathrm{A}}, \hat{\boldsymbol{\rho}}^{\mathrm{A}}\right], \tag{1.26}$$

in the adiabatic representation.

1.4.1 Quantum-Classical Liouville Equation

Expressing the nuclear degrees of freedom in the Wigner-Moyal representation [74, 75, 77] and taking the semi-classical limit, where the approximation involves neglecting the $\mathcal{O}(\hbar^2)$ or higher terms in the Taylor expansion of Moyal product ($\star$) [73] as given in Eqn 1.17, the quantum-classical Liouville equation (QCLE) [38] - the quantum-classical analog to the Liouville-von Neumann equation (Eqns 1.25-1.26) - for the two-state system can be expressed as follows.

In the diabatic representation, the QCLE [38] for the two-state system is

$$\begin{aligned}
\frac{\partial \rho_{11}^{\mathrm{D}}(\boldsymbol{q},\boldsymbol{p},t)}{\partial t} &= \left\{H_{11}^{\mathrm{D}}(\boldsymbol{q},\boldsymbol{p}),\rho_{11}^{\mathrm{D}}(\boldsymbol{q},\boldsymbol{p},t)\right\} + \left\{V_{12}(\boldsymbol{q}),\alpha^{\mathrm{D}}(\boldsymbol{q},\boldsymbol{p},t)\right\} \\
&\quad -\frac{2V_{12}(\boldsymbol{q})}{\hbar}\beta^{\mathrm{D}}(\boldsymbol{q},\boldsymbol{p},t), \qquad (1.27)\\
\frac{\partial \rho_{22}^{\mathrm{D}}(\boldsymbol{q},\boldsymbol{p},t)}{\partial t} &= \left\{H_{22}^{\mathrm{D}}(\boldsymbol{q},\boldsymbol{p}),\rho_{22}^{\mathrm{D}}(\boldsymbol{q},\boldsymbol{p},t)\right\} + \left\{V_{12}(\boldsymbol{q}),\alpha^{\mathrm{D}}(\boldsymbol{q},\boldsymbol{p},t)\right\} \\
&\quad +\frac{2V_{12}(\boldsymbol{q})}{\hbar}\beta^{\mathrm{D}}(\boldsymbol{q},\boldsymbol{p},t), \qquad (1.28)\\
\frac{\partial \alpha^{\mathrm{D}}(\boldsymbol{q},\boldsymbol{p},t)}{\partial t} &= \left\{\frac{H_{11}^{\mathrm{D}}(\boldsymbol{q},\boldsymbol{p})+H_{22}^{\mathrm{D}}(\boldsymbol{q},\boldsymbol{p})}{2},\alpha^{\mathrm{D}}(\boldsymbol{q},\boldsymbol{p},t)\right\} + \omega^{\mathrm{D}}(\boldsymbol{q})\beta^{\mathrm{D}}(\boldsymbol{q},\boldsymbol{p},t) \\
&\quad +\frac{1}{2}\left\{V_{12}(\boldsymbol{q}),\rho_{11}^{\mathrm{D}}(\boldsymbol{q},\boldsymbol{p},t)+\rho_{22}^{\mathrm{D}}(\boldsymbol{q},\boldsymbol{p},t)\right\}, \qquad (1.29)\\
\frac{\partial \beta^{\mathrm{D}}(\boldsymbol{q},\boldsymbol{p},t)}{\partial t} &= \left\{\frac{H_{11}^{\mathrm{D}}(\boldsymbol{q},\boldsymbol{p})+H_{22}^{\mathrm{D}}(\boldsymbol{q},\boldsymbol{p})}{2},\beta^{\mathrm{D}}(\boldsymbol{q},\boldsymbol{p},t)\right\} - \omega^{\mathrm{D}}(\boldsymbol{q})\alpha^{\mathrm{D}}(\boldsymbol{q},\boldsymbol{p},t) \\
&\quad +\frac{V_{12}(\boldsymbol{q})}{\hbar}\left(\rho_{11}^{\mathrm{D}}(\boldsymbol{q},\boldsymbol{p},t)-\rho_{22}^{\mathrm{D}}(\boldsymbol{q},\boldsymbol{p},t)\right), \qquad (1.30)
\end{aligned}$$

where $\omega^{\mathrm{D}}(\boldsymbol{q}) = \frac{V_1(\boldsymbol{q})-V_2(\boldsymbol{q})}{\hbar}$, $\mathrm{Re}\{\rho_{12}\}(\boldsymbol{q},\boldsymbol{p},t) = \mathrm{Re}\{\rho_{21}\}(\boldsymbol{q},\boldsymbol{p},t) = \alpha^{\mathrm{D}}(\boldsymbol{q},\boldsymbol{p},t)$, and $\mathrm{Im}\{\rho_{12}\}(\boldsymbol{q},\boldsymbol{p},t) = -\mathrm{Im}\{\rho_{21}\}(\boldsymbol{q},\boldsymbol{p},t) = \beta^{\mathrm{D}}(\boldsymbol{q},\boldsymbol{p},t)$. Since the higher order terms in $\hbar$ have been dropped, only the most essential non-classical corrections [78] are captured in the above equations.

In the adiabatic representation, the QCLE [38] for the two-state system is

$$\begin{aligned}
\frac{\partial \rho^{\mathrm{A}}_{++}(\boldsymbol{q},\boldsymbol{p},t)}{\partial t} &= \left\{H^{\mathrm{A}}_{++}(\boldsymbol{q},\boldsymbol{p}),\rho^{\mathrm{A}}_{++}(\boldsymbol{q},\boldsymbol{p},t)\right\} - \hbar\left\{\boldsymbol{d}(\boldsymbol{q})\cdot\boldsymbol{v},\beta^{\mathrm{A}}(\boldsymbol{q},\boldsymbol{p},t)\right\} \\
&\quad -2\boldsymbol{d}(\boldsymbol{q})\cdot\boldsymbol{v}\alpha^{\mathrm{A}}(\boldsymbol{q},\boldsymbol{p},t), \qquad (1.31)\\
\frac{\partial \rho^{\mathrm{A}}_{--}(\boldsymbol{q},\boldsymbol{p},t)}{\partial t} &= \left\{H^{\mathrm{A}}_{--}(\boldsymbol{q},\boldsymbol{p}),\rho^{\mathrm{A}}_{--}(\boldsymbol{q},\boldsymbol{p},t)\right\} - \hbar\left\{\boldsymbol{d}(\boldsymbol{q})\cdot\boldsymbol{v},\beta^{\mathrm{A}}(\boldsymbol{q},\boldsymbol{p},t)\right\} \\
&\quad +2\boldsymbol{d}(\boldsymbol{q})\cdot\boldsymbol{v}\alpha^{\mathrm{A}}(\boldsymbol{q},\boldsymbol{p},t), \qquad (1.32)\\
\frac{\partial \alpha^{\mathrm{A}}(\boldsymbol{q},\boldsymbol{p},t)}{\partial t} &= \left\{\frac{H^{\mathrm{A}}_{++}(\boldsymbol{q},\boldsymbol{p})+H^{\mathrm{A}}_{--}(\boldsymbol{q},\boldsymbol{p})}{2},\alpha^{\mathrm{A}}(\boldsymbol{q},\boldsymbol{p},t)\right\} + \omega^{\mathrm{A}}(\boldsymbol{q})\beta^{\mathrm{A}}(\boldsymbol{q},\boldsymbol{p},t) \\
&\quad +\boldsymbol{d}(\boldsymbol{q})\cdot\boldsymbol{v}\left(\rho^{\mathrm{A}}_{++}(\boldsymbol{q},\boldsymbol{p},t)-\rho^{\mathrm{A}}_{--}(\boldsymbol{q},\boldsymbol{p},t)\right), \qquad (1.33)\\
\frac{\partial \beta^{\mathrm{A}}(\boldsymbol{q},\boldsymbol{p},t)}{\partial t} &= \left\{\frac{H^{\mathrm{A}}_{++}(\boldsymbol{q},\boldsymbol{p})+H^{\mathrm{A}}_{--}(\boldsymbol{q},\boldsymbol{p})}{2},\beta^{\mathrm{A}}(\boldsymbol{q},\boldsymbol{p},t)\right\} - \omega^{\mathrm{A}}(\boldsymbol{q})\alpha^{\mathrm{A}}(\boldsymbol{q},\boldsymbol{p},t) \\
&\quad -\frac{\hbar}{2}\left\{\boldsymbol{d}(\boldsymbol{q})\cdot\boldsymbol{v},\rho^{\mathrm{A}}_{++}(\boldsymbol{q},\boldsymbol{p},t)+\rho^{\mathrm{A}}_{--}(\boldsymbol{q},\boldsymbol{p},t)\right\}, \qquad (1.34)
\end{aligned}$$

where $\omega^{\mathrm{A}}(\boldsymbol{q}) = \frac{V_+(\boldsymbol{q})-V_-(\boldsymbol{q})}{\hbar}$, $\mathrm{Re}\{\rho_{+-}\}(\boldsymbol{q},\boldsymbol{p},t) = \mathrm{Re}\{\rho_{-+}\}(\boldsymbol{q},\boldsymbol{p},t) = \alpha^{\mathrm{A}}(\boldsymbol{q},\boldsymbol{p},t)$, and $\mathrm{Im}\{\rho_{+-}\}(\boldsymbol{q},\boldsymbol{p},t) = -\,\mathrm{Im}\{\rho_{-+}\}(\boldsymbol{q},\boldsymbol{p},t) = \beta^{\mathrm{A}}(\boldsymbol{q},\boldsymbol{p},t)$.

The nuclear velocity is represented by $\boldsymbol{v} = \dot{\boldsymbol{q}}$. It is important to note that in the adiabatic representation, the kinematic momentum $\boldsymbol{p}_{\mathrm{kin}} = m\dot{\boldsymbol{q}}$, not the canonical momentum $\boldsymbol{p}$. While the canonical momentum appears in the diagonal kinetic energy, the velocity appears in the non-adiabatic coupling terms, which differs from the equations present in the previously published papers that first introduced quantum trajectory surface hopping (QTSH) [62, 63].

Note that the QCLE in the adiabatic representation that is presented here was derived by performing the Wigner transformation as given in Eqn 1.18 after the unitary transformation of the Hamiltonian and density operators in the diabatic representation to the adiabatic representation [38]. Another approach that involves performing the Wigner transformation on the diabatic density operator before the unitary transformation to the adiabatic representation has also been reported [64].

Having provided the requisite background, we now provide a brief overview of the quantum trajectory surface hopping (QTSH) [62, 63] method - the focus of this dissertation - and provide insight on the unique and distinguishing features that set it apart from the FSSH method [1] that was discussed in Section 1.1.1.

1.5 Quantum Trajectory Surface Hopping (QTSH)

Here we give a brief overview of the quantum trajectory surface hopping (QTSH) [62, 63], the method that is the focus of this dissertation. The full formalism of QTSH can be found in Ref [62].

In QTSH [62, 63], the quantum-classical description of multistate systems are derived rigorously from the QCLE [38–40], in the context of the *independent* trajectory approximation. As such, QTSH can be derived rigorously, and performed in both the diabatic and adiabatic representations. This is in contrast to FSSH [1] that was derived by solving the approximate time-dependent Schrödinger equation in the adiabatic representation.

We now introduce the framework of *independent* trajectories that the QTSH method utilizes to make the method computationally tractable [62, 63, 76]. A trajectory j represents a localized wavepacket in phase space, represented by the delta function $\delta\big(\boldsymbol{q} - \boldsymbol{q}_j(t)\big)\delta\big(\boldsymbol{p} - \boldsymbol{p}_j(t)\big)$. Just as in FSSH, the non-locality of nuclear dynamics in electronic and phase space is accounted for in QTSH by running an ensemble of trajectories [1, 8].

1.5.1 Time Evolution of Electronic State

The propagation of the elements of the Wigner distributions of a two-state system in both the diabatic and adiabatic representations in the QTSH [62, 63] involves solving the QCLE [38]

given by Eqns 1.27-1.30 in the diabatic representation, and Eqns 1.31-1.34 in the adiabatic representation using an ensemble of *independent* trajectories.

Similar to FSSH [1], a 'proxy' density matrix $a_{mn,j}$ that represents the approximate electronic state of the system [62, 63] is computed for each trajectory j. The fewest switches algorithm [1] was also used to compute the hopping probabilities and to decide whether, and to which state the trajectory j hops.

Under the framework of independent trajectories, the elements of the Wigner distributions [74] for each trajectory j in the diabatic representation are

$$\rho^{\mathrm{D}}_{11,j}(\boldsymbol{q},\boldsymbol{p},t) = \sigma^{\mathrm{D}}_{j}(t)\delta\big(\boldsymbol{q}-\boldsymbol{q}_j(t)\big)\delta\big(\boldsymbol{p}-\boldsymbol{p}_j(t)\big) \tag{1.35}$$

$$\alpha^{\mathrm{D}}_{j}(\boldsymbol{q},\boldsymbol{p},t) = \alpha^{\mathrm{D}}_{j}(t)\delta\big(\boldsymbol{q}-\boldsymbol{q}_j(t)\big)\delta\big(\boldsymbol{p}-\boldsymbol{p}_j(t)\big) \tag{1.36}$$

$$\beta^{\mathrm{D}}_{j}(\boldsymbol{q},\boldsymbol{p},t) = \beta^{\mathrm{D}}_{j}(t)\delta\big(\boldsymbol{q}-\boldsymbol{q}_j(t)\big)\delta\big(\boldsymbol{p}-\boldsymbol{p}_j(t)\big) \tag{1.37}$$

$$\rho^{\mathrm{D}}_{22,j}(\boldsymbol{q},\boldsymbol{p},t) = \big(1-\sigma^{\mathrm{D}}_{j}(t)\big)\delta\big(\boldsymbol{q}-\boldsymbol{q}_j(t)\big)\delta\big(\boldsymbol{p}-\boldsymbol{p}_j(t)\big), \tag{1.38}$$

and the elements in the adiabatic representation are

$$\rho^{\mathrm{A}}_{++,j}(\boldsymbol{q},\boldsymbol{p},t) = \sigma^{\mathrm{A}}_{j}(t)\delta\big(\boldsymbol{q}-\boldsymbol{q}_j(t)\big)\delta\big(\boldsymbol{p}-\boldsymbol{p}_j(t)\big) \tag{1.39}$$

$$\alpha^{\mathrm{A}}_{j}(\boldsymbol{q},\boldsymbol{p},t) = \alpha^{\mathrm{A}}_{j}(t)\delta\big(\boldsymbol{q}-\boldsymbol{q}_j(t)\big)\delta\big(\boldsymbol{p}-\boldsymbol{p}_j(t)\big) \tag{1.40}$$

$$\beta^{\mathrm{A}}_{j}(\boldsymbol{q},\boldsymbol{p},t) = \beta^{\mathrm{A}}_{j}(t)\delta\big(\boldsymbol{q}-\boldsymbol{q}_j(t)\big)\delta\big(\boldsymbol{p}-\boldsymbol{p}_j(t)\big) \tag{1.41}$$

$$\rho^{\mathrm{A}}_{--,j}(\boldsymbol{q},\boldsymbol{p},t) = \big(1-\sigma^{\mathrm{A}}_{j}(t)\big)\delta\big(\boldsymbol{q}-\boldsymbol{q}_j(t)\big)\delta\big(\boldsymbol{p}-\boldsymbol{p}_j(t)\big), \tag{1.42}$$

where the binary integer parameters $\sigma^{\mathrm{D}}_{j}(t) = \{0,1\}$, and $\sigma^{\mathrm{A}}_{j}(t) = \{0,1\}$.

In the diabatic representation, $\sigma_j^{\rm D}(t) = 1$ indicates that the trajectory j is on the diabatic surface $V_1(\boldsymbol{q})$, and $\sigma_j^{\rm D}(t) = 0$ indicates that the trajectory j is on the diabatic surface $V_2(\boldsymbol{q})$.

In the adiabatic representation, $\sigma_j^{\rm A}(t) = 1$ indicates that the trajectory j is on the upper adiabatic surface $V_+(\boldsymbol{q})$, and $\sigma_j^{\rm A}(t) = 0$ indicates that the trajectory j is on the lower adiabatic surface $V_-(\boldsymbol{q})$.

The elements of the Wigner distribution for the two-state represented by the ensemble of *independent* trajectories are then represented as

$$\rho_{11}^{\rm D}(\boldsymbol{q},\boldsymbol{p},t) = \frac{1}{N}\sum_j \sigma_j^{\rm D}(t)\delta\big(\boldsymbol{q}-\boldsymbol{q}_j(t)\big)\delta\big(\boldsymbol{p}-\boldsymbol{p}_j(t)\big), \tag{1.43}$$

$$\alpha^{\rm D}(\boldsymbol{q},\boldsymbol{p},t) = \frac{1}{N}\sum_j \alpha_j^{\rm D}(t)\delta\big(\boldsymbol{q}-\boldsymbol{q}_j(t)\big)\delta\big(\boldsymbol{p}-\boldsymbol{p}_j(t)\big), \tag{1.44}$$

$$\beta^{\rm D}(\boldsymbol{q},\boldsymbol{p},t) = \frac{1}{N}\sum_j \beta_j^{\rm D}(t)\delta\big(\boldsymbol{q}-\boldsymbol{q}_j(t)\big)\delta\big(\boldsymbol{p}-\boldsymbol{p}_j(t)\big), \tag{1.45}$$

$$\rho_{22}^{\rm D}(\boldsymbol{q},\boldsymbol{p},t) = \frac{1}{N}\sum_j \big(1-\sigma_j^{\rm D}(t)\big)\delta\big(\boldsymbol{q}-\boldsymbol{q}_j(t)\big)\delta\big(\boldsymbol{p}-\boldsymbol{p}_j(t)\big), \tag{1.46}$$

in the diabatic representation, and

$$\rho_{++}^{\rm A}(\boldsymbol{q},\boldsymbol{p},t) = \frac{1}{N}\sum_j \sigma_j^{\rm A}(t)\delta\big(\boldsymbol{q}-\boldsymbol{q}_j(t)\big)\delta\big(\boldsymbol{p}-\boldsymbol{p}_j(t)\big), \tag{1.47}$$

$$\alpha^{\rm A}(\boldsymbol{q},\boldsymbol{p},t) = \frac{1}{N}\sum_j \alpha_j^{\rm A}(t)\delta\big(\boldsymbol{q}-\boldsymbol{q}_j(t)\big)\delta\big(\boldsymbol{p}-\boldsymbol{p}_j(t)\big), \tag{1.48}$$

$$\beta^{\rm A}(\boldsymbol{q},\boldsymbol{p},t) = \frac{1}{N}\sum_j \beta_j^{\rm A}(t)\delta\big(\boldsymbol{q}-\boldsymbol{q}_j(t)\big)\delta\big(\boldsymbol{p}-\boldsymbol{p}_j(t)\big), \tag{1.49}$$

$$\rho_{--}^{\rm A}(\boldsymbol{q},\boldsymbol{p},t) = \frac{1}{N}\sum_j \big(1-\sigma_j^{\rm A}(t)\big)\delta\big(\boldsymbol{q}-\boldsymbol{q}_j(t)\big)\delta\big(\boldsymbol{p}-\boldsymbol{p}_j(t)\big), \tag{1.50}$$

in the adiabatic representation.

The time evolution of the elements of the 'proxy' density matrix $a_{ik}(t)$ for the two-state system that represent the quantum electronic state of each trajectory j, are given by [62, 63]

$$\dot{a}^{\mathrm{D}}_{11,j}(t) = -\frac{2V_{12}(\boldsymbol{q}_j)}{\hbar}\beta^{\mathrm{D}}_j(t), \tag{1.51}$$

$$\dot{a}^{\mathrm{D}}_{22,j}(t) = \frac{2V_{12}(\boldsymbol{q}_j)}{\hbar}\beta^{\mathrm{D}}_j(t), \tag{1.52}$$

$$\dot{\alpha}^{\mathrm{D}}_j(t) = \omega^{\mathrm{D}}(\boldsymbol{q}_j)\beta^{\mathrm{D}}_j(t), \tag{1.53}$$

$$\dot{\beta}^{\mathrm{D}}_j(t) = -\omega^{\mathrm{D}}(\boldsymbol{q}_j)\alpha^{\mathrm{D}}_j(t) + \frac{V_{12}(\boldsymbol{q}_j)}{\hbar}\left(a^{\mathrm{D}}_{11,j}(t) - a^{\mathrm{D}}_{22,j}(t)\right), \tag{1.54}$$

in the diabatic representation, where $\alpha^{\mathrm{D}}_j(t) = \mathrm{Re}(a^{\mathrm{D}}_{12,j}(t)) = \mathrm{Re}(a^{\mathrm{D}}_{12,j}(t))$,
and $\beta^{\mathrm{D}}_j(t) = \mathrm{Im}(a^{\mathrm{D}}_{12,j}(t)) = -\mathrm{Im}(a^{\mathrm{D}}_{21,j}(t))$, and

$$\dot{a}^{\mathrm{A}}_{++,j}(t) = -2\boldsymbol{d}(\boldsymbol{q}_j)\cdot\boldsymbol{v}_j(t)\alpha^{\mathrm{A}}_j(t), \tag{1.55}$$

$$\dot{a}^{\mathrm{A}}_{--,j}(t) = 2\boldsymbol{d}(\boldsymbol{q}_j)\cdot\boldsymbol{v}_j(t)\alpha^{\mathrm{A}}_j(t), \tag{1.56}$$

$$\dot{\alpha}^{\mathrm{A}}_j(t) = \omega^{\mathrm{A}}(\boldsymbol{q}_j)\beta^{\mathrm{D}}_j(t) + \boldsymbol{d}(\boldsymbol{q}_j)\cdot\boldsymbol{v}_j(t)\left(a^{\mathrm{A}}_{11,j}(t) - a^{\mathrm{A}}_{22,j}(t)\right), \tag{1.57}$$

$$\dot{\beta}^{\mathrm{A}}_j(t) = -\omega^{\mathrm{A}}(\boldsymbol{q}_j)\alpha^{\mathrm{D}}_j(t) \tag{1.58}$$

in the adiabatic representation, where $\alpha^{\mathrm{A}}_j(t) = \mathrm{Re}(a^{\mathrm{A}}_{+-,j}(t)) = \mathrm{Re}(a^{\mathrm{A}}_{-+,j}(t))$,
and $\beta^{\mathrm{A}}_j(t) = \mathrm{Im}(a^{\mathrm{A}}_{+-,j}(t)) = -\mathrm{Im}(a^{\mathrm{A}}_{-+,j}(t))$.

We note that equations representing the elements of the 'proxy' density matrix for the two-state system in QTSH [62, 63] in the adiabatic representation are identical to that of FSSH [1].

The continuous populations represented by $a^{\mathrm{D}}_{11,j}(t)$ in the diabatic representation, and $a^{\mathrm{A}}_{++,j}(t)$ in the adiabatic representation are related to the average of the stochastic occupation integers $\left\langle \sigma^{\mathrm{D}}_j(t) \right\rangle$ in the diabatic representation and $\left\langle \sigma^{\mathrm{A}}_j(t) \right\rangle$ in the adiabatic representation at the point $(\boldsymbol{q}_j, \boldsymbol{p}_j)$ in phase space when trajectories in the ensemble *interact* with each other as in the consensus surface hopping reported in Ref [79].

The relations that describe the consistency of surface hopping are given by

$$a^{\mathrm{D}}_{11,j}(t) = \left\langle \sigma^{\mathrm{D}}_j(t) \right\rangle , \tag{1.59}$$

and

$$a^{\mathrm{A}}_{++,j}(t) = \left\langle \sigma^{\mathrm{A}}_j(t) \right\rangle , \tag{1.60}$$

in consensus surface hopping [79].

In the limit of *independent* trajectories where the trajectories *do not interact* the surface hopping consistency condition can be rewritten as the ensemble averages [50]

$$\left\langle a^{\mathrm{D}}_{11}(t) \right\rangle = \left\langle \sigma^{\mathrm{D}}(t) \right\rangle \tag{1.61}$$

and

$$\left\langle a^{\mathrm{A}}_{++}(t) \right\rangle = \left\langle \sigma^{\mathrm{A}}(t) \right\rangle . \tag{1.62}$$

While the electronic state of the system in QTSH [62, 63] is propagated similarly to FSSH [1], the classical motion of the nuclei in QTSH [62, 63] varies greatly from FSSH [1].

1.5.2 Time Evolution of Nuclear Motion

Each trajectory j that can be mathematically described by the delta function $\delta\big(\boldsymbol{q}-\boldsymbol{q}_j(t)\big)\delta\big(\boldsymbol{p}-\boldsymbol{p}_j(t)\big)$ that represents a localized nuclear wavepacket in phase space $(\boldsymbol{q}_j(t),\boldsymbol{p}_j(t))$. The motion of the ensemble of independent trajectories in phase space describes the nuclear dynamics of the system. The QTSH trajectory phase space equations of motion were obtained by ensuring that the phase space partial differential equations evolve in accordance to the QCLE [38] for the total nuclear density $\rho^{\mathrm{D}}(\boldsymbol{q},\boldsymbol{p},t)$ in the diabatic representation,

$$\begin{aligned}\frac{\partial\rho^{\mathrm{D}}(\boldsymbol{q},\boldsymbol{p},t)}{\partial t} &= \frac{\partial\rho^{\mathrm{D}}_{11}(\boldsymbol{q},\boldsymbol{p},t)}{\partial t}+\frac{\partial\rho^{\mathrm{D}}_{22}(\boldsymbol{q},\boldsymbol{p},t)}{\partial t}\\ &= \overbrace{\left\{H^{\mathrm{D}}_{11}(\boldsymbol{q},\boldsymbol{p}),\rho^{\mathrm{D}}_{11}(\boldsymbol{q},\boldsymbol{p},t)\right\}+\left\{H^{\mathrm{D}}_{22}(\boldsymbol{q},\boldsymbol{p}),\rho^{\mathrm{D}}_{22}(\boldsymbol{q},\boldsymbol{p},t)\right\}}^{\text{classical evolution}}\\ &\quad+\underbrace{2\left\{V_{12}(\boldsymbol{q}),\alpha^{\mathrm{D}}(\boldsymbol{q},\boldsymbol{p},t)\right\}}_{\text{quantum evolution}}\end{aligned}\tag{1.63}$$

and the QCLE [38] for the total nuclear density $\rho^{\mathrm{D}}(\boldsymbol{q},\boldsymbol{p},t)$ in the adiabatic representation

$$\begin{aligned}\frac{\partial\rho^{\mathrm{A}}(\boldsymbol{q},\boldsymbol{p},t)}{\partial t} &= \frac{\partial\rho^{\mathrm{A}}_{++}(\boldsymbol{q},\boldsymbol{p},t)}{\partial t}+\frac{\partial\rho^{\mathrm{A}}_{--}(\boldsymbol{q},\boldsymbol{p},t)}{\partial t}\\ &= \overbrace{\left\{H^{\mathrm{A}}_{++}(\boldsymbol{q},\boldsymbol{p}),\rho^{\mathrm{A}}_{++}(\boldsymbol{q},\boldsymbol{p},t)\right\}+\left\{H^{\mathrm{A}}_{--}(\boldsymbol{q},\boldsymbol{p}),\rho^{\mathrm{A}}_{--}(\boldsymbol{q},\boldsymbol{p},t)\right\}}^{\text{classical evolution}}\\ &\quad\underbrace{-2\hbar\left\{\boldsymbol{d}(\boldsymbol{q})\cdot\boldsymbol{v},\beta^{\mathrm{A}}(\boldsymbol{q},\boldsymbol{p},t)\right\}}_{\text{quantum evolution}}.\end{aligned}\tag{1.64}$$

With reference Eqns 1.63 and 1.64, we find terms that resemble the classical Liouville equation [80] for the ensembles on each state and an additional quantum component in the diabatic and adiabatic representations.

By solving Eqns 1.63 and 1.64 within the framework of independent trajectories, we obtain the QTSH equations of motion for the phase space variables for each trajectory j in the diabatic and adiabatic representations.

In the diabatic representation, the equations of motions [62] are

$$\dot{\boldsymbol{q}}_j(t) = \frac{\boldsymbol{p}_j}{m}, \tag{1.65}$$

$$\dot{\boldsymbol{p}}_j(t) = \underbrace{-\sigma_j^{\mathrm{D}}(t)\nabla_{\boldsymbol{q}_j}V_1(\boldsymbol{q}_j) - \big(1-\sigma_j^{\mathrm{D}}(t)\big)\nabla_{\boldsymbol{q}_j}V_2(\boldsymbol{q}_j)}_{\text{classical force}} \overbrace{-2\nabla_{\boldsymbol{q}_j}V_{12}(\boldsymbol{q}_j)\alpha_j^{\mathrm{D}}(t)}^{\text{quantum force}}, \tag{1.66}$$

and in the adiabatic representation, the equations of motions [62, 81] are

$$\dot{\boldsymbol{q}}_j(t) = \frac{\overbrace{\boldsymbol{p}_j - 2\hbar\beta_j^{\mathrm{A}}(t)\boldsymbol{d}(\boldsymbol{q}_j)}^{\text{kinematic momentum } \boldsymbol{p}_{\mathrm{kin},j}}}{m}, \tag{1.67}$$

$$\dot{\boldsymbol{p}}_j(t) = -\sigma_j^{\mathrm{A}}(t)\nabla_{\boldsymbol{q}_j}V_+(\boldsymbol{q}_j) - \big(1-\sigma_j^{\mathrm{A}}(t)\big)\nabla_{\boldsymbol{q}_j}V_-(\boldsymbol{q}_j) + \frac{2\hbar}{m}\beta^{\mathrm{A}}(t)\left(\boldsymbol{p}_j\cdot\nabla_{\boldsymbol{q}_j}\right)\boldsymbol{d}(\boldsymbol{q}_j), \tag{1.68}$$

$$\dot{\boldsymbol{p}}_{\mathrm{kin},j}(t) = \underbrace{-\sigma_j^{\mathrm{A}}(t)\nabla_{\boldsymbol{q}_j}V_{++}(\boldsymbol{q}_j) - \big(1-\sigma_j^{\mathrm{A}}(t)\big)\nabla_{\boldsymbol{q}_j}V_{--}(\boldsymbol{q}_j)}_{\text{classical force}} + \overbrace{2\hbar\alpha_j^{\mathrm{D}}(t)\boldsymbol{d}(\boldsymbol{q}_j)}^{\text{quantum force}}. \tag{1.69}$$

On closer examination of the equations of motion for the generalized position $\dot{\boldsymbol{q}}_j(t)$ in the diabatic (Eqn 1.66) and the adiabatic representation (Eqn 1.68), we find that while the canonical momentum $\boldsymbol{p}_j$ is equal to the kinematic momentum $\boldsymbol{p}_{\mathrm{kin},j}(t) = m\dot{\boldsymbol{q}}_j(t)$ [37] in the diabatic representation, the kinematic momentum

$$\boldsymbol{p}_{\mathrm{kin},j}(t) = m\dot{\boldsymbol{q}}_j(t) = \boldsymbol{p}_j - 2\hbar\beta_j^{\mathrm{A}}(t)\boldsymbol{d}(\boldsymbol{q}_j), \tag{1.70}$$

in the adiabatic representation differs from the canonical momentum $\boldsymbol{p}_j$.

We have reported the equation of motion of the kinematic momentum $\dot{\boldsymbol{p}}_{\mathrm{kin},j}(t)$ in Eqn 1.69 without derivation. The derivation can be found in Ref [81].

The QTSH momentum equations of motion with which *independent* trajectories are propagated in the diabatic representation and in the adiabatic representation are, Eqn 1.66 and Eqn 1.69, respectively. In contrast to FSSH where only the classical force component is present, we find that a quantum force component that depends on the off-diagonal terms of the Hamiltonian is also present in the QTSH momentum equations of motion [62, 63] for both the diabatic and adiabatic representations.

In the diabatic representation, the quantum force acting on the trajectory j was

$$\boldsymbol{F}^{\mathrm{D}}_{\mathrm{quant}}(\boldsymbol{q}_j) = -2\nabla_{\boldsymbol{q}_j} V_{12}(\boldsymbol{q}_j)\alpha^{\mathrm{D}}_j(t), \tag{1.71}$$

making contributions when the off-diagonal diabatic potential $V_{12}(\boldsymbol{q}_j)$ and the real part of the coherence $\alpha^{\mathrm{D}}_j(t)$ are present. The off-diagonal coupling and coherence are manifestly non-classical in nature.

In the adiabatic representation, the quantum force acting on the trajectory j was

$$\boldsymbol{F}^{\mathrm{A}}_{\mathrm{quant}}(\boldsymbol{q}_j) = 2\hbar\omega^{\mathrm{A}}(\boldsymbol{q}_j)\alpha^{\mathrm{A}}_j(t)\boldsymbol{d}(\boldsymbol{q}_j), \tag{1.72}$$

making contributions when the non-adiabatic coupling vector $\boldsymbol{d}(\boldsymbol{q}_j)$, which couples the electronic and nuclear motion, and the real part of the coherence $\alpha^{\mathrm{A}}_j(t)$ are present. The quantum force in the adiabatic representation resembles the off-diagonal Hellman-Feynman force [82, 83].

While strict energy conservation is imposed on each trajectory in FSSH [1], by means of *ad hoc* momentum 'jumps' that take place when the trajectory hops, these strict classical energy conservation rules are relaxed in QTSH [62, 63]. In QTSH, the quantum-classical energy is conserved on the independent trajectory ensemble *average* level [62, 63], reflecting a more probabilistic 'quantum' picture of reality.

The system phase space average total energy is given by the trace of the product of the Weyl function [71] of the Hamiltonian and the Wigner distribution [74, 75] that in terms of the ensemble of independent trajectories is given by

$$\langle E_{\mathrm{tot}}(t)\rangle = \frac{1}{N}\sum_{j}^{N} E_{\mathrm{tot},j}. \tag{1.73}$$

In the diabatic representation, the total energy of a trajectory j, $E^{\mathrm{D}}_{\mathrm{tot},j}$ computed in QTSH is

$$E^{\mathrm{D}}_{\mathrm{tot},j}(t) = \overbrace{\frac{\boldsymbol{p}_j^2}{2m} + \sigma_j^{\mathrm{D}}(t)V_1(\boldsymbol{q}_j) + \big(1-\sigma_j^{\mathrm{D}}(t)\big)V_2(\boldsymbol{q}_j)}^{\text{classical energy}} + \underbrace{2V_{12}(\boldsymbol{q}_j)\alpha_j^{\mathrm{D}}(t)}_{\text{non-classical/quantum energy}} . \tag{1.74}$$

In the adiabatic representation, the total energy of a trajectory j, $E^{\mathrm{A}}_{\mathrm{tot},j}$ computed in QTSH, neglecting the diagonal Born-Oppenheimer term $\frac{\hbar^2\boldsymbol{d}^2(\boldsymbol{q}_j)}{2m}$ is

$$E^{\mathrm{A}}_{\mathrm{tot},j}(t) = \overbrace{\frac{\boldsymbol{p}_j^2}{2m} + \sigma_j^{\mathrm{A}}(t)V_+(\boldsymbol{q}_j) + \big(1-\sigma_j^{\mathrm{A}}(t)\big)V_-(\boldsymbol{q}_j)}^{\text{classical energy}} \underbrace{-2\hbar\beta_j^{\mathrm{A}}\boldsymbol{d}(\boldsymbol{q}_j)\cdot\frac{\boldsymbol{p}_{\mathrm{kin},j}}{m}}_{\text{non-classical/quantum energy}} . \tag{1.75}$$

The non-classical/quantum energy present in QTSH is not present in FSSH, and arises from the off-diagonal terms in the Hamiltonian and the coherence of the Wigner distribution.

Since the off-diagonal terms of the Hamiltonian are potential energy terms in the diabatic representation, we combine the non-classical/quantum energy component with the classical potential energy to give the phase space averaged potential energy

$$\left\langle V^{\mathrm{D}}(t)\right\rangle = \frac{1}{N}\sum_{j}^{N}\sigma_j^{\mathrm{D}}(t)V_1(\boldsymbol{q}_j) + \left(1-\sigma_j^{\mathrm{D}}(t)\right)V_2(\boldsymbol{q}_j) + 2V_{12}(\boldsymbol{q}_j)\alpha_j^{\mathrm{D}}(t). \tag{1.76}$$

The phase space averaged kinetic energy $\left\langle T^{\mathrm{D}}(t)\right\rangle$ in the diabatic representation is simply the classical kinetic energy given by

$$\left\langle T^{\mathrm{D}}(t)\right\rangle = \frac{1}{N}\sum_{j}^{N}\frac{\boldsymbol{p}_j^2}{2m}. \tag{1.77}$$

The phase space averaged potential energy $\left\langle V^{\mathrm{A}}(t)\right\rangle$ in the adiabatic representation is simply the classical potential energy given by

$$\left\langle V^{\mathrm{A}}(t)\right\rangle = \frac{1}{N}\sum_{j}^{N}\sigma_j^{\mathrm{A}}(t)V_+(\boldsymbol{q}_j) + \left(1-\sigma_j^{\mathrm{A}}(t)\right)V_-(\boldsymbol{q}_j). \tag{1.78}$$

In contrast, to the diabatic representation, the off-diagonal terms of the Hamiltonian in the adiabatic representation are kinetic energy terms. As such, we combine the non-classical/quantum energy component with the classical kinetic energy to give the phase space averaged kinetic energy

$$\left\langle T^{\mathrm{A}}(t)\right\rangle = \frac{1}{N}\sum_{j}^{N}\frac{\boldsymbol{p}_j^2}{2m} - 2\hbar\beta_j^{\mathrm{A}}\boldsymbol{d}(\boldsymbol{q}_j)\cdot\frac{\boldsymbol{p}_{\mathrm{kin},j}}{m} \approx \frac{\boldsymbol{p}_{\mathrm{kin},j}^2}{2m}, \tag{1.79}$$

where the approximation to $\frac{\boldsymbol{p}_{\mathrm{kin},j}^2}{2m}$ involves neglecting a term that is proportional to $\hbar^2{\beta_j^{\mathrm{A}}}^2\boldsymbol{d}^2(\boldsymbol{q}_j)$. This ensures consistency since the neglected term is of the same order as the neglected $\mathcal{O}(\hbar^2)$ diagonal Born-Oppenheimer term.

If the consistency of surface hopping is assumed in the framework of independent trajectories in QTSH, where

$$\dot{\sigma}_j^{\mathrm{D}} \approx \dot{a}_{11,j} \tag{1.80}$$

in the diabatic representation, and

$$\dot{\sigma}_j^{\mathrm{A}} \approx \dot{a}_{++,j} \tag{1.81}$$

in the adiabatic representation, is assumed and substituted into the R.H.S. of time derivative of Eqn 1.73, we find that the system phase space averaged total energy is zero in both the diabatic and adiabatic representations. The procedure is given in Ref [62].

This shows that QTSH conserves the quantum-classical energy on *average* [62, 63], without imposing the *ad hoc* momentum jumps of FSSH. The quantum forces that arise naturally from the derivation of QTSH [62, 63] from the QCLE [38], related to the off-diagonal terms of the Hamiltonian and coherences incorporates feedback between the electronic degrees of freedom and the nuclear degrees of freedom [3]. If the feedback between the classically treated nuclear degrees of freedom and the quantum mechanically treated electronic degrees of freedom is properly incorporated in QTSH, the action of the quantum force would necessarily act to conserve energy on *average*.

Having presented the QTSH method [62, 63], and how it is different from FSSH [1], we will now introduce the modified Tully 1D model systems [1] that will be used in this dissertation. We will also explain the chemical relevance of these model systems.

1.6 Modified Tully 1D Systems

The Tully one-dimensional systems [1] have long been used as a benchmark for testing non-adiabatic molecular dynamics.

In this dissertation we will modify Tully's simple avoided crossing and dual crossing systems [1] to investigate the inner workings of QTSH. The potential energy surfaces as a function of the reaction coordinate for each model are illustrated in Figs 1.3 (a) and (b), respectively.

The diabatic potentials for Tully's original simple avoided crossing system [1] are

$$V_1(\boldsymbol{q}) = A[1 - \mathrm{e}^{B\boldsymbol{q}}]\Theta(-\boldsymbol{q}) - A[1 - \mathrm{e}^{-B\boldsymbol{q}}]\Theta(\boldsymbol{q}), \tag{1.82}$$

$$V_2(\boldsymbol{q}) = -A[1 - \mathrm{e}^{B\boldsymbol{q}}]\Theta(-\boldsymbol{q}) + A[1 - \mathrm{e}^{-B\boldsymbol{q}}]\Theta(\boldsymbol{q}), \tag{1.83}$$

$$V_{12}(\boldsymbol{q}) = C\mathrm{e}^{-D\boldsymbol{q}^2}, \tag{1.84}$$

where the numerical values of the potential parameters, in atomic units, are $A = 0.01$, $B = 1.6$, $C = 0.005$, and $D = 1.0$. The mass is $m = 2000$ a.u.

The size of the diabatic potential coupling will be changed by varying the constant $C = 0.0005,\ 0.001$ and 0.002 in Eqn 1.84 for the modified simple avoided crossing systems [1].

With reference to Figure 1.1, as the diabatic coupling constant C is increased, the maximum adiabatic coupling $\boldsymbol{d}_{\mathrm{peak}}$ becomes stronger, with a more negative value, and more localized with a smaller width at half height $w_{0.5}$. The energy gap where the non-adiabatic coupling is strongest $\hbar\omega(q_{d_{\mathrm{peak}}})$ also gets larger as C increases. The values of these parameters are summarized for the modified simple avoided crossing models are summarized in table 1.1.

The diabatic potentials for Tully's original dual avoided crossing system [1] are

$$V_1(\boldsymbol{q}) = -A\mathrm{e}^{-B\boldsymbol{q}^2} + E_0, \tag{1.85}$$

$$V_2(\boldsymbol{q}) = 0, \tag{1.86}$$

$$V_{12}(\boldsymbol{q}) = C\mathrm{e}^{-D\boldsymbol{q}^2}, \tag{1.87}$$

where the numerical values of the potential parameters, in atomic units, are $A = 0.10$, $B = 0.28$, $C = 0.015$, $D = 0.06$, and $E_0 = 0.05$. The mass is $m = 2000$ a.u.

The size of the diabatic potential coupling will be changed by varying the constant $C = 0.0015,\ 0.003$ and 0.006 in Eqn 1.87 for the modified dual avoided crossing systems [1].

With reference to Figure 1.2(b), the maximum adiabatic couplings in the two regions of strong non-adiabatic coupling $\boldsymbol{d}_{\mathrm{peak1}}$ and $\boldsymbol{d}_{\mathrm{peak2}}$ becomes stronger, with a larger magnitude, and more localized with a smaller widths at half height $w_{0.5,\mathrm{peak1}}$ and $w_{0.5,\mathrm{peak2}}$. With reference to Figure 1.2(a), the energy gap where the adiabatic couplings are strongest, $\hbar\omega(\boldsymbol{q}_{\boldsymbol{d}_{\mathrm{peak1}}})$ and $\hbar\omega(\boldsymbol{q}_{\boldsymbol{d}_{\mathrm{peak1}}})$ increase as C increases. The values of these parameters are summarized for Tully's modified dual avoided crossing models are summarized in Tables 1.2 and 1.3.

Table 1.1: Summary of the parameters maximum strength of the adiabatic coupling $\boldsymbol{d}_{\mathrm{peak}}$, the width of the non-adiabatic coupling at half maximum $w_{0.5,\mathrm{peak}}$, the position of strongest non-adiabatic coupling $\boldsymbol{q}_{\boldsymbol{d}_{\mathrm{peak}}}$, and the size of the energy gap where non-adiabatic coupling is strongest $\hbar\omega(\boldsymbol{q}_{\boldsymbol{d}_{\mathrm{peak}}})$ for the simple avoided crossing system [1] for the values of the diabatic coupling constants $C = 0.0005, 0.001$ and 0.002.

C	$\boldsymbol{d}_{\mathrm{peak}}$(a.u.)	$w_{0.5}$(a.u.)	$\boldsymbol{q}_{\boldsymbol{d}_{\mathrm{peak}}}$(a.u.)	$\hbar\omega(\boldsymbol{q}_{\boldsymbol{d}_{\mathrm{peak}}})$(a.u.)
0.0005	-16	0.06	0.0	0.001
0.0010	-8	0.10	0.0	0.002
0.0020	-4	0.16	0.0	0.004

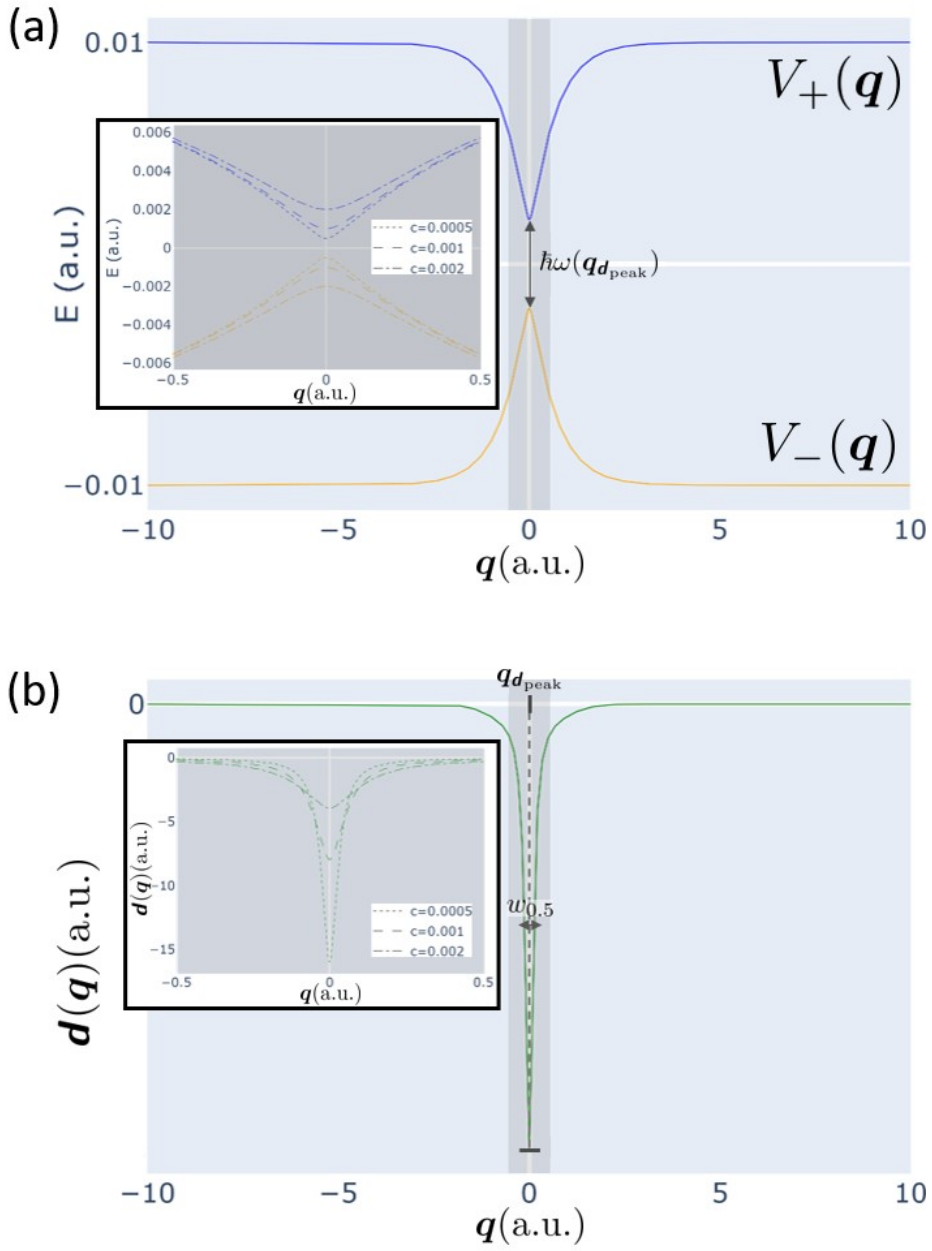

Figure 1.1: The grey shaded region spans the region of strong adiabatic coupling. The inset image shows an enlarged image of the grey shaded region. The dotted, dashed, and dashdotted lines in the inset images correspond to the diabatic coupling constants of $C = 0.0005$, $C = 0.001$, and $C = 0.002$, respectively. **(a)** Adiabatic potential energy surfaces (PESs) for the modified Tully's simple avoided crossing model. The upper surface is labeled $V_+(q)$ and the lower surface is labeled $V_-(\boldsymbol{q})$. The parameter $\hbar\omega(\boldsymbol{q}_{\boldsymbol{d}_{\text{peak}}})$ shows the size of the energy gap where the adiabatic coupling is strongest. The inset shows the the energy gap increases with the strength of the diabatic coupling. **(b)** Non-adiabatic coupling $\boldsymbol{d}(\boldsymbol{q})$ for the modified Tully's simple avoided crossing model. The parameter $\boldsymbol{d}_{\text{peak}}$ indicates the maximum strength of the adiabatic coupling, and $w_{0.5,\text{peak}}$ indicates the width of the adiabatic coupling at half maximum.

Table 1.2: Summary of the parameters maximum strength of the adiabatic coupling $\boldsymbol{d}_{\text{peak1}}$, the width of the non-adiabatic coupling at half maximum $w_{0.5,\text{peak1}}$, the position of strongest non-adiabatic coupling $\boldsymbol{q}_{\boldsymbol{d}_{\text{peak1}}}$, and the size of the energy gap where non-adiabatic coupling is strongest $\hbar\omega(\boldsymbol{q}_{\boldsymbol{d}_{\text{peak1}}})$ for the dual avoided crossing system [1] for the values of the diabatic coupling constants $C = 0.0015, 0.003$ and 0.006.

C	**Peak 1**			
	$\boldsymbol{d}_{\text{peak}}$(a.u.)	$w_{0.5,\text{peak}}$(a.u.)	$\boldsymbol{q}_{\boldsymbol{d}_{\text{peak}}}$(a.u.)	$\hbar\omega(\boldsymbol{q}_{\boldsymbol{d}_{\text{peak}}})$(a.u.)
0.0015	-8.50	0.12	-1.57	0.0026
0.0030	-4.25	0.22	-1.57	0.0052
0.0060	-2.13	0.47	-1.57	0.0104

Table 1.3: Summary of the parameters maximum strength of the adiabatic coupling $\boldsymbol{d}_{\text{peak2}}$, the width of the non-adiabatic coupling at half maximum $w_{0.5,\text{peak2}}$, the position of strongest non-adiabatic coupling $\boldsymbol{q}_{\boldsymbol{d}_{\text{peak2}}}$, and the size of the energy gap where non-adiabatic coupling is strongest $\hbar\omega(\boldsymbol{q}_{\boldsymbol{d}_{\text{peak2}}})$ for the dual avoided crossing system [1] for the values of the diabatic coupling constants $C = 0.0015, 0.003$ and 0.006.

C	**Peak 2**			
	$\boldsymbol{d}_{\text{peak}}$(a.u.)	$w_{0.5,\text{peak}}$(a.u.)	$\boldsymbol{q}_{\boldsymbol{d}_{\text{peak}}}$(a.u.)	$\hbar\omega(\boldsymbol{q}_{\boldsymbol{d}_{\text{peak}}})$(a.u.)
0.0015	8.50	0.12	1.57	0.0026
0.0030	4.25	0.22	1.57	0.0052
0.0060	2.13	0.47	1.57	0.0104

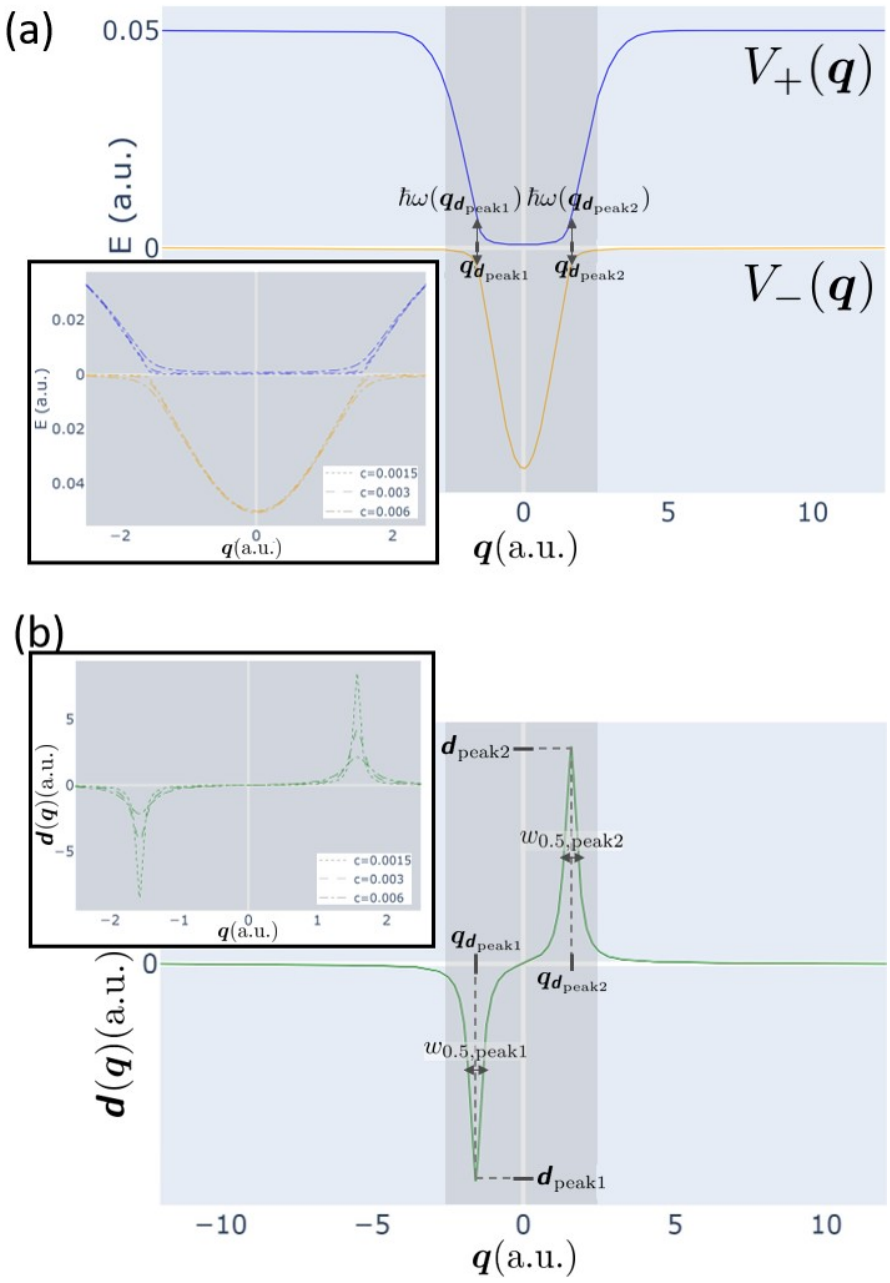

Figure 1.2: The grey shaded region spans the two regions of strong adiabatic coupling. The inset image shows an enlarged image of the grey shaded region. The dotted, dashed, and dashdotted lines in the inset images correspond to the diabatic coupling constants of $C = 0.0015$, $C = 0.003$, and $C = 0.006$, respectively. **(a)** Adiabatic potential energy surfaces (PESs) for the modified Tully's dual avoided crossing model. The upper surface is labeled $V_+(\boldsymbol{q})$ and the lower surface is labeled $V_-(\boldsymbol{q})$. The parameters $\hbar\omega(\boldsymbol{q}_{\boldsymbol{d}_{\text{peak1}}})$ and $\hbar\omega(\boldsymbol{q}_{\boldsymbol{d}_{\text{peak2}}})$ show the size of the energy gap where the adiabatic couplings are strongest. The inset shows that the energy gaps increase with increasing diabatic coupling strength. **(b)** Non-adiabatic coupling $\boldsymbol{d}(\boldsymbol{q})$ for the modified Tully's dual avoided crossing model. The parameters $\boldsymbol{d}_{\text{peak1}}$ and $\boldsymbol{d}_{\text{peak2}}$ indicate the maximum strengths of the non-adiabatic coupling, and $w_{0.5,\text{peak1}}$ and $w_{0.5,\text{peak2}}$ indicate the width of each region of strong adiabatic coupling at half maximum.

1.6.1 Chemical Relevance

The Tully 1D systems [1], while simple, are chemically relevant, and the performance of QTSH [62, 63] for these systems will inform us of whether QTSH would be a suitable predictive model to study the on-the-fly dynamics of various molecules with one or two avoided crossings.

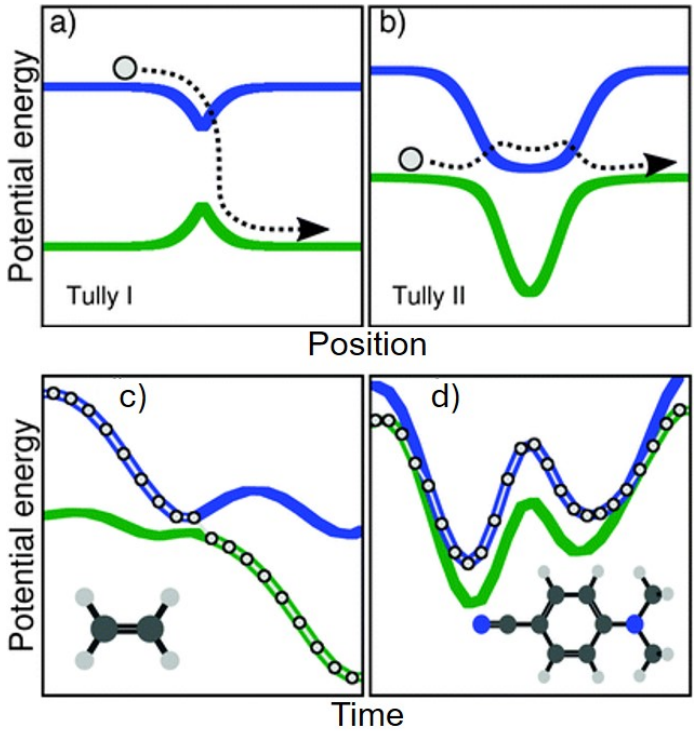

Figure 1.3: Schematic depiction of the potential energy curves as a function of a one-dimensional reactive coordinate for the (a) Tully simple avoided crossing model, and the (b) Tully dual avoided crossing model, and the time traces of the potential energies for trajectory surface hopping for Ibele-Curchod molecular models for (c) ethene that corresponds to the simple avoided crossing model, and (d) 4-N,N-Dimethylaminobenzonitrile (DMABN). The path described by the one-dimensional particle (circle and arrow) exemplifies a possible outcome of the dynamics probed by each model. Lower panel: Time traces of the potential energies along a trajectory surface hopping trajectory for ethylene (d), DMABN (e), and fulvene (f). The excited-state dynamics for each molecular Tully model mimics the particle dynamics of the corresponding one-dimensional Tully models depicted in the upper panel. Reproduced from L. M. Ibele and B. F. E. Curchod, *Phys. Chem. Chem. Phys.*, 2020, **22**, 15183 **DOI:** 10.1039/D0CP01353F (Ref [2]), with permission from the PCCP Owner Societies.

The molecular equivalent of Tully's simple one-dimensional systems, also known as the Ibele-Curchod (IC) systems have recently been proposed by Ibele et al. [2], and have been used as a benchmark to study on-the-fly direct dynamics variational multi-configuration Gaussian (DD-vMCG) method [84]. The potential energy time trace of ethene, the IC-1 system, illustrated by Fig 1.3(c) imitates Tully's simple avoided crossing system (Fig 1.3(a)), and that of 4-N,N-Dimethylaminobenzonitrile (DMABN), the IC-2 system, illustrated by Fig 1.3(d) imitates the potential energy surfaces for the dual avoided crossing system (Fig 1.3(b)).

We expect that if QTSH [62, 63] is accurate for Tully's simple avoided crossing and dual avoided crossing systems [1], that QTSH would also, by extension, produce accurate on-the-fly molecular dynamics results for molecules like ethene and DMABN.

1.7 Dissertation Outline

This dissertation explores the unique features of QTSH - energy conservation on the ensemble level without the imposition of *ad hoc* momentum rescaling and its independence of representation - that distinguishes it from the most popular [50] trajectory surface hopping method, FSSH [1]. We utilize the modified Tully 1D systems, as described in Section 1.6 to do so. This dissertation is organized as follows.

Chapter 2 explores the role of quantum forces - that arise naturally in QTSH from the inclusion of quantum effects in its derivation from the QCLE [38–40] - in energy conservation on the ensemble level. Here, we show the relation between the work done by the quantum force during electronic transitions that act to conserve energy at the *ensemble* level, and the *ad hoc* momentum 'jumps' to conserve classical energy on the *trajectory* level in FSSH. We also analyze the feedback between the classical nuclear degrees of freedom and quantum electronic degrees of freedom [3] that are mediated by quantum forces in QTSH.

Chapter 3 explores the representation invariance of QTSH. Here we perform the the diabatic-to-adiabatic (d2a) and adiabatic-to-diabatic (a2d) transformations of the Wigner distribution [74, 75] and the forces, both classical and quantum, in the quantum-classical limit, and within the *independent* trajectory framework. In doing so, we derive the expressions for transforming the system phase space averages of these quantities from one representation to another. We then test the representation invariance of QTSH by utilizing the derived equations to perform the d2a transformation of QTSH results in the diabatic representation, and the a2d transformation of QTSH results in the adiabatic representation, and comparing its results.

Chapter 4 shows how a highly non-classical system in the adiabatic representation can be highly classical in the diabatic representation. We show this by providing a simple derivation to show that the total force in the adiabatic representation in the limit of localized and complete population transfer is in fact equal to the classical force on a single diabatic PES. We then present QTSH results to demonstrate its validity. Finally, we show how the representation invariance of QTSH, as presented in Chapter 3 can be utilized to improve the accuracy of QTSH results in the adiabatic representation.

Chapter 5 is a standalone chapter that outlines how the relation between chemical work [85], Gibbs free energy changes, and spontaneity can be introduced in a chemically relevant yet accessible way to students in Introductory Chemistry classes.

Chapter 2

Role of Quantum Forces in QTSH

2.1 Introduction

The quantum forces in QTSH arise naturally from its derivation from the quantum-classical Liouville equation [38] using an *independent* trajectory ensemble ansatz [62, 63]. The quantum force couples the electronic transitions to the evolution of trajectories, making their evolution non-classical, and is responsible for the conservation of the quantum-classical energy on the ensemble level [62, 63].

In this chapter, we explore the role of quantum forces in energy conservation during electronic transitions in the limit of complete localized population transfer. By analyzing the quantum-classical energy budget of QTSH in this limit, we provide a simple but rigorous derivation

of the *ad hoc* FSSH momentum jumps. We also use QTSH in this limit to explain the frustrated hops in FSSH, and to illustrate the implied self-consistency between the classically treated nuclear degrees of freedom and the quantum mechanically treated electronic degrees of freedom, due to the inclusion of the quantum forces in QTSH (Fig 2.1).

We use a localized wavepacket/trajectory undergoing a non-adiabatic transition from the upper adiabatic state to the lower adiabatic state, and a localized wavepacket/trajectory undergoing a non-adiabatic transition from the lower to the upper adiabatic state at an avoided crossing in modified Tully's simple avoided crossing system [1] (As introduced in Section 1.6) to perform this analysis.

Finally, we test the aspect of energy conservation, and the feedback between nuclear and electronic degrees of freedom [3] (Fig 2.1) numerically with QTSH [62, 63] simulations in the adiabatic representation. Although conceptually derived from the modified simple avoided crossing systems [1], the derived results should also hold for other systems with avoided crossings. As such, we provide QTSH results for both the modified simple avoided crossing, and dual avoided crossing systems [1], as described in Section 1.6.

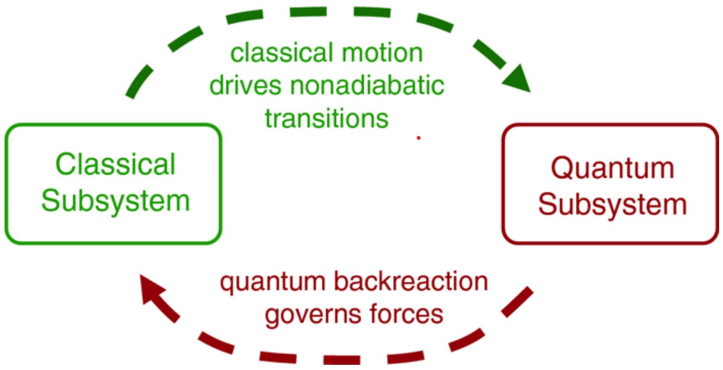

Figure 2.1: Self-consistency between the classical nuclear and quantum electronic subsystems as a result of the quantum backreaction that occurs following an electronic transition. Reprinted from John C. Tully; Perspective: non-adiabatic dynamics theory. *J. Chem. Phys.* 14 December 2012; 137 (22): 22A301. (Ref [3]), with the permission of AIP Publishing.

2.2 Derivation of FSSH Momentum Jumps

A simple two state model of a localized non-adiabatic transition is considered. We consider a system that is initially on the upper adiabatic surface and experiences an electronic transition that occurs in a localized region around it to the lower adiabatic state.

The initial adiabatic density matrix for this process is of the form

$$\rho^{\mathrm{A}}(t_0) = \begin{pmatrix} \rho(t_0) & 0 \\ 0 & 0 \end{pmatrix}, \tag{2.1}$$

with all probability on the upper state, while the final density matrix is

$$\rho^{\mathrm{A}}(t_{\mathrm{f}}) = \begin{pmatrix} 0 & 0 \\ 0 & \rho(t_{\mathrm{f}}) \end{pmatrix}, \tag{2.2}$$

with complete population transfer to the lower state. Here t_0 and t_{f} are the initial and final times, respectively. We take the quantity $\rho(\boldsymbol{q}, \boldsymbol{p}, t)$ to be a localized state in phase space evolving under coupled electron-nuclear dynamics. In the limit of complete localization, one can consider

$$\rho(\boldsymbol{q}, \boldsymbol{p}, t) = \delta\big(\boldsymbol{q} - \boldsymbol{q}(t)\big)\delta\big(\boldsymbol{p} - \boldsymbol{p}(t)\big), \tag{2.3}$$

in other words, a single trajectory.

In the diabatic representation, the initial and final density matrices correspond to the same diabatic state being populated, so $\rho^{\mathrm{D}}(t)$ can be written throughout the process as

$$\rho^{\mathrm{D}}(t) = \begin{pmatrix} \rho(t) & 0 \\ 0 & 0 \end{pmatrix}. \tag{2.4}$$

We assume this form holds approximately for all $t \in (t_0, t_\mathrm{f})$. In this limit, the adiabatic density matrix can, to a good approximation, be written as

$$\rho^{\mathrm{A}}(t_\mathrm{f}) = \begin{pmatrix} \frac{1}{2}\big(1+\cos\phi(t)\big) & -\frac{1}{2}\sin\phi(t) \\ -\frac{1}{2}\sin\phi(t) & \frac{1}{2}\big(1-\cos\phi(t)\big) \end{pmatrix} \rho(t), \tag{2.5}$$

where the angle $\phi(t)$ is evaluated at the center of the localized state $\rho(\boldsymbol{q}, \boldsymbol{p}, t)$. Here we have employed the transformation given in Eqns 1.22-1.24 and the diabatic state ansatz (Eqn 2.4).

Similarly, the initial adiabatic density matrix for the same two state model of a localized non-adiabatic transition where the system starts on the lower adiabatic surface and experiences an electronic transition that occurs in a localized region around it to the upper adiabatic state gives the initial adiabatic density matrix

$$\rho^{\mathrm{A}}(t_0) = \begin{pmatrix} 0 & 0 \\ 0 & \rho(t_0) \end{pmatrix}, \tag{2.6}$$

with all probability on the lower state, and the final density matrix

$$\rho^{\mathrm{A}}(t_\mathrm{f}) = \begin{pmatrix} \rho(t_\mathrm{f}) & 0 \\ 0 & 0 \end{pmatrix}, \tag{2.7}$$

with complete population transfer to the upper state.

In the diabatic representation, $\rho^{\mathrm{D}}(t)$ can be written throughout the process as

$$\rho^{\mathrm{D}}(t) = \begin{pmatrix} 0 & 0 \\ 0 & \rho(t) \end{pmatrix}, \tag{2.8}$$

allowing us to write the approximate adiabatic density matrix

$$\rho^{\mathrm{A}}(t_{\mathrm{f}}) = \begin{pmatrix} \frac{1}{2}\big(1-\cos\phi(t)\big) & \frac{1}{2}\sin\phi(t) \\ \frac{1}{2}\sin\phi(t) & \frac{1}{2}\big(1+\cos\phi(t)\big) \end{pmatrix} \rho(t). \tag{2.9}$$

Note that the real part of the off-diagonal coherence changes sign in comparison to Eqn 2.5.

In Fig 2.2, we depict schematically the non-adiabatic transition of a localized state in one dimension. The system begins on the upper adiabatic state potential $V_+(\boldsymbol{q})$ and evolves until it encounters an avoided crossing with the lower adiabatic state at $\boldsymbol{q}^* = 0$. At this point, the population transfers to the lower adiabatic potential $V_-(\boldsymbol{q})$, indicated by the grey arrow, where it resumes its evolution. The motion is in the positive $\boldsymbol{q}$ direction, indicating that the kinematic momentum $\boldsymbol{p}_{\mathrm{kin}}$ is positive. During the transition, we expect the value of $\boldsymbol{p}_{\mathrm{kin}}$ to become larger and the kinetic energy $\frac{p_{\mathrm{kin}}^2}{2m}$ to increase by a quantity equal to the energy gap $\hbar\omega(\boldsymbol{q}^*)$. The state is localized in coordinate space (and in momentum space) throughout the process. Fig 2.3 shows the corresponding process in the diabatic representation, where the system evolves along the same diabatic potential $V_1(\boldsymbol{q})$ throughout.

Depicted in Fig 2.4, the reverse process with the system starting on the lower adiabatic state potential $V_+(\boldsymbol{q})$ and evolving until it encounters the avoided crossing at $\boldsymbol{q}^* = 0$ where the population transfers to the upper adiabatic potential $V_+(\boldsymbol{q})$ where it continues its evolution. The change in $\boldsymbol{p}_{\mathrm{kin}}$ is expected to be negative, decreasing by a quantity equal to the energy gap $\hbar\omega(\boldsymbol{q}^*)$. We assume that the localized state has sufficient energy for the non-adiabatic transition to take place. The corresponding process in the diabatic representation is depicted in Fig 2.5, where the system evolves along the same diabatic potential $V_2(\boldsymbol{q})$ throughout.

The details of the systems depicted in Figures 2.2-2.5 will be described in Section 2.3.1.

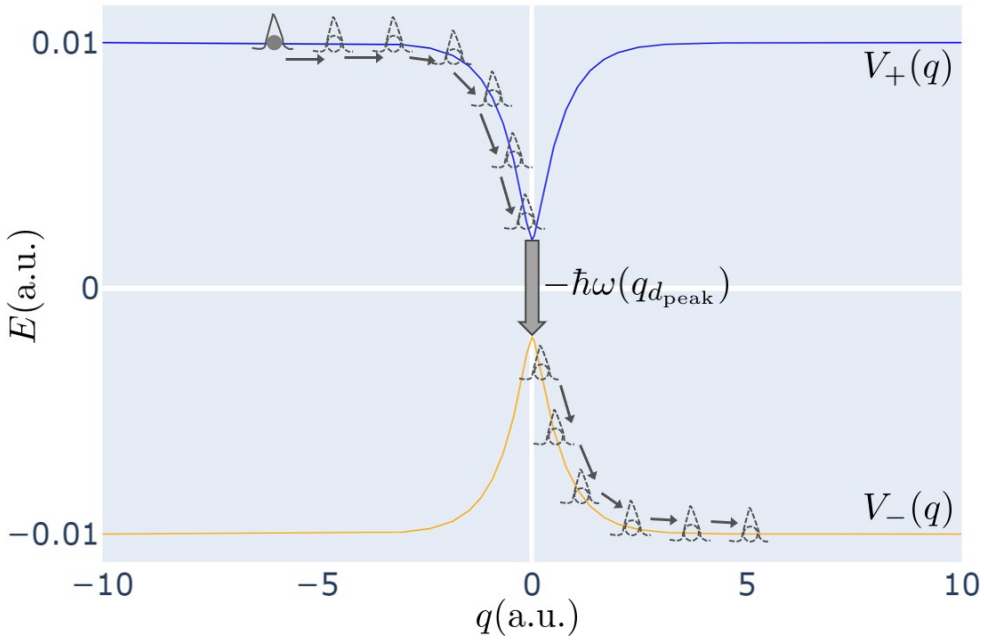

Figure 2.2: Schematic representation of a localized quantum state/trajectory undergoing a non-adiabatic transition from the upper to the lower adiabatic state at the avoided crossing. Diabatic potentials for the simple avoided crossing system are given in Eqns 1.83-1.84.

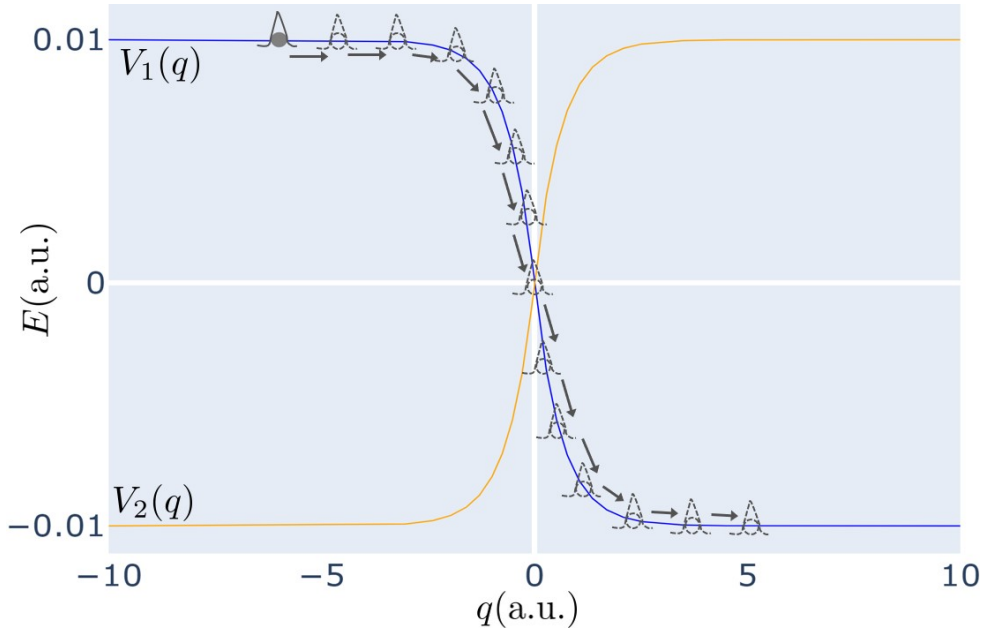

Figure 2.3: Schematic representation of a localized quantum state/trajectory traveling along the diabatic potential $V_1(q)$, corresponding to the process in Fig 2.2. Diabatic potentials for the simple avoided crossing system are given in Eqns 1.83-1.84.

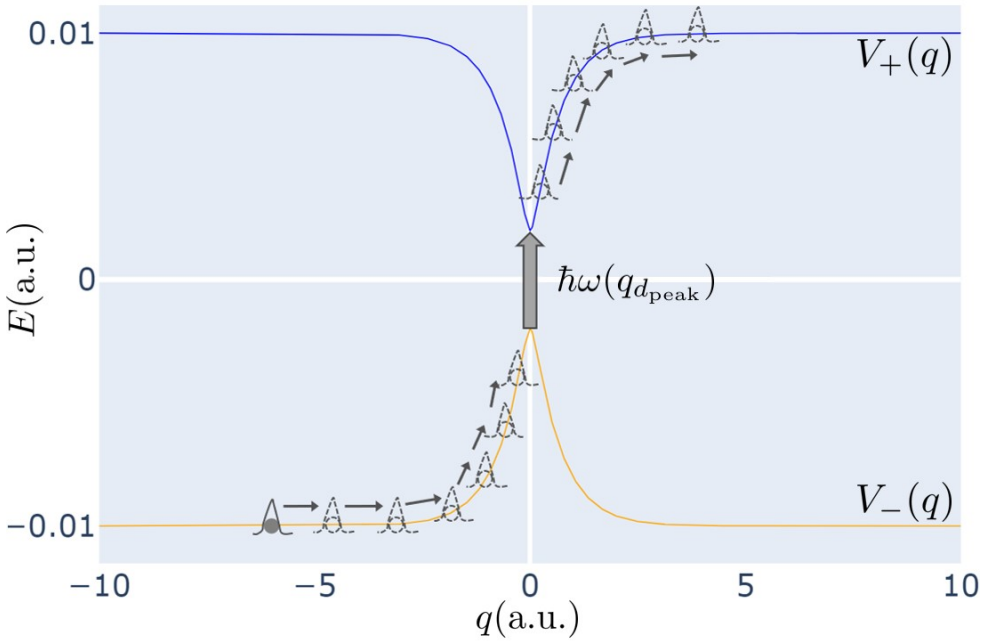

Figure 2.4: Schematic representation of a localized quantum state/trajectory undergoing a non-adiabatic transition from the lower to the upper adiabatic state at the avoided crossing. Diabatic potentials for the simple avoided crossing system are given in Eqns 1.83-1.84.

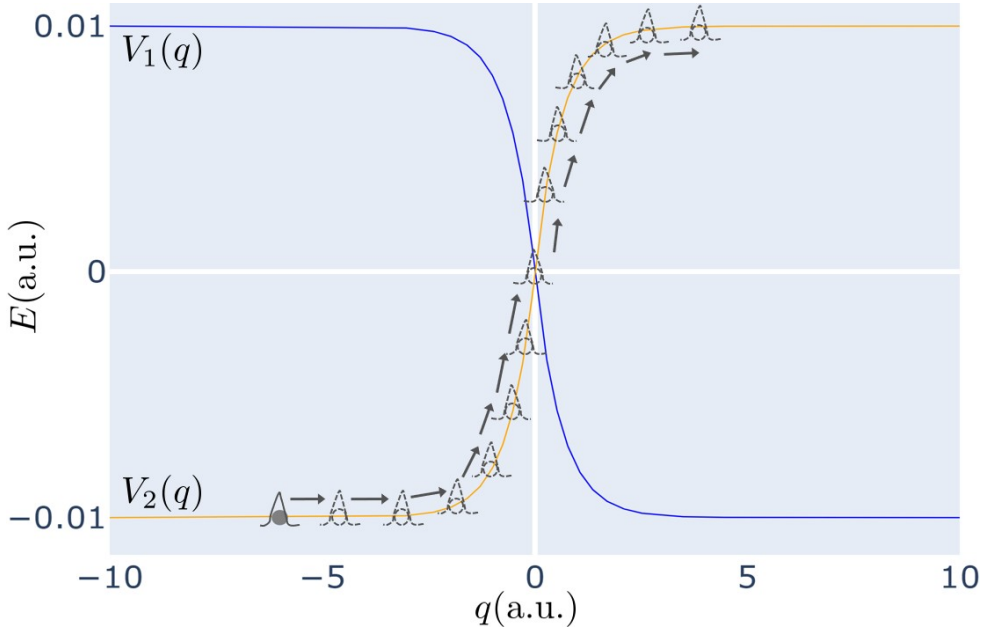

Figure 2.5: Schematic representation of a localized quantum state/trajectory traveling along the diabatic potential $V_2(\boldsymbol{q})$, corresponding to the process in Fig 2.4. Diabatic potentials for the simple avoided crossing system are given in Eqns 1.83-1.84.

In Fig 2.2, we show (a) the non-adiabatic mixing angle $\phi(\boldsymbol{q})$, (b) the non-adiabatic coupling vector $\boldsymbol{d}(\boldsymbol{q})$, (c) the real part of the coherence $\alpha(\boldsymbol{q})$, and (d) the quantum force $\boldsymbol{F}_{\text{quant}}(\boldsymbol{q}) = 2\hbar\omega(\boldsymbol{q})\boldsymbol{d}(\boldsymbol{q})\alpha(\boldsymbol{q})$ given by the modified potentials, with varying diabatic coupling constant parameters $C = 0.0005,\ 0.001$ and 0.002 for the process depicted in Fig 2.2. The coupling, coherence, and quantum force are non-zero in a relatively localized region around the avoided crossing, in qualitative agreement with the limit considered analytically here. The coupling $\boldsymbol{d}(\boldsymbol{q})$ and the coherence $\alpha(\boldsymbol{q})$ are both negative for this process. The localized quantum force, on the other hand, is a positive impulsive term, consistent with its role in increasing the momentum and kinetic energy of the nuclear motion.

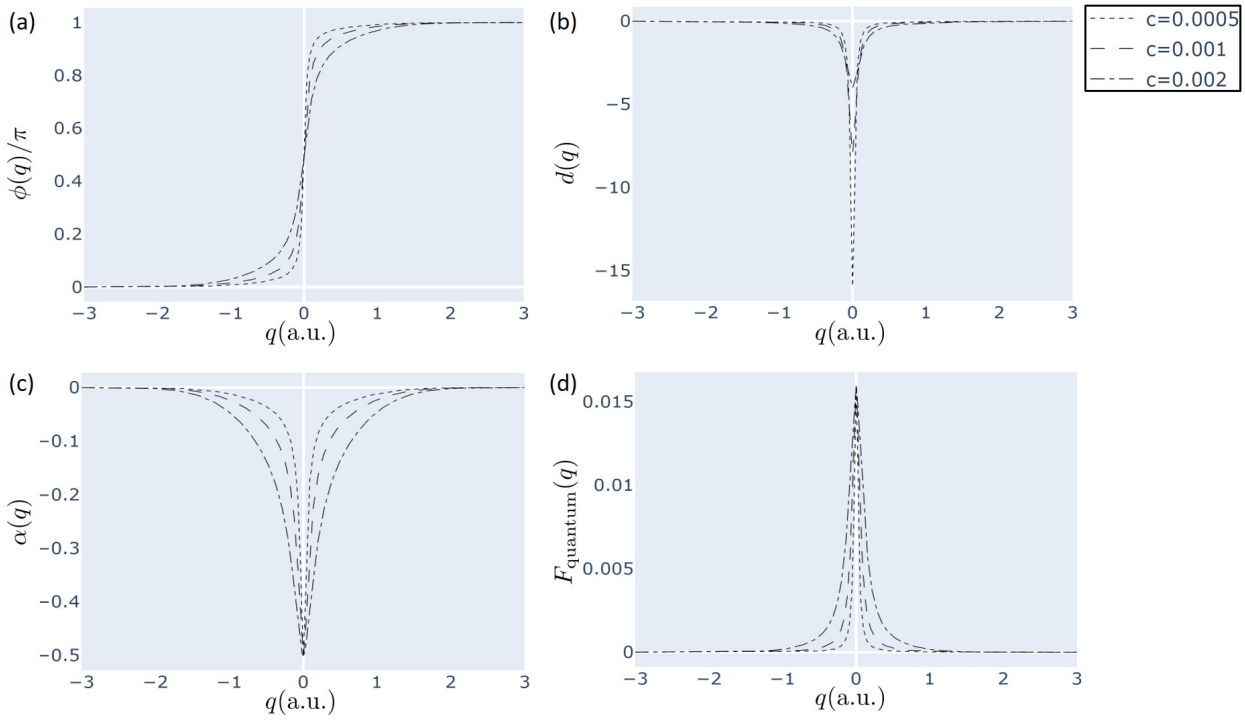

Figure 2.6: (a) The non-adiabatic mixing angle $\phi(\boldsymbol{q})$, (b) the non-adiabatic coupling vector $\boldsymbol{d}(\boldsymbol{q})$, (c) the real part of the coherence $\alpha(\boldsymbol{q})$, and (d) the quantum force $F_{\text{quant}}(\boldsymbol{q})$ for the process shown in Fig 2.2, as described in text. The dotted, dashed, and dashdotted lines represent the models where $C = 0.0005$, $C = 0.001$, and $C = 0.002$, respectively.

While $\phi(\boldsymbol{q})$ and $\boldsymbol{d}(\boldsymbol{q})$ as depicted in Figs 2.6(a) and (b) are specific to the modified simple avoided crossing as described by the diabatic potentials given by Eqns 1.83-1.84, and remain unchanged for the reverse process of a non-adiabatic transition from the lower to the upper

adiabatic state as depicted in Fig 2.4, $\alpha(\boldsymbol{q})$ (Fig 2.7(a)) and consequently, the quantum force $F_{\text{quant}}(\boldsymbol{q})$ (Fig 2.7(a)) changes sign. In this process, $\alpha(\boldsymbol{q})$ is positive, and the localized quantum force is a negative impulsive term, consistent with its role in decreasing the momentum and kinetic energy of the nuclear motion due to the upward electronic transition.

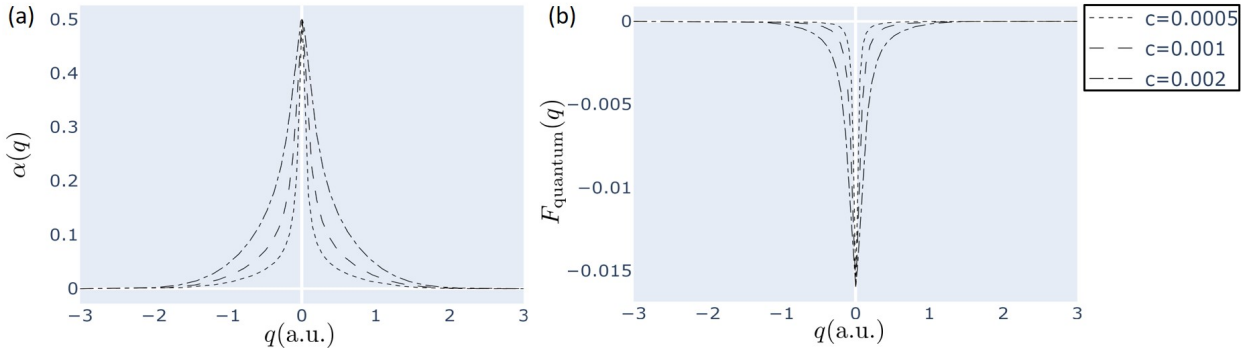

Figure 2.7: (a) The real part of the coherence $\alpha(q)$, and (b) the quantum force $F_{\text{quant}}(\boldsymbol{q})$ for the process shown in Fig 2.4, as described in text. The dotted, dashed, and dashdotted lines represent the models where $C = 0.0005$, $C = 0.001$, and $C = 0.002$, respectively.

The total energy of the state of the system is given by $E(t) = \text{Tr}\big(\mathbf{H}^{\text{A}}(\boldsymbol{q},\boldsymbol{p})\boldsymbol{\rho}^{\text{A}}(\boldsymbol{q},\boldsymbol{p},t)\big)$. Using the Hamiltonian and density matrix, this becomes

$$E(t) = \overbrace{\frac{\boldsymbol{p}^2}{2m} + V\left(\boldsymbol{q},\sigma(t)\right)}^{\text{canonical classical energy}} \underbrace{-2\hbar\beta(t)\boldsymbol{d}(\boldsymbol{q})\cdot\frac{\boldsymbol{p}_{\text{kin}}}{m}}_{\text{coherence/quantum energy}}, \tag{2.10}$$

where $\big(\boldsymbol{q}(t),\boldsymbol{p}(t)\big)$ is our trajectory and $V\left(\boldsymbol{q},\sigma(t)\right) = \sigma(t)V_+\big(\boldsymbol{q}\big) + \left(1-\sigma(t)\right)V_-\big(\boldsymbol{q}\big)$. (Our ensemble here has reduced to a single trajectory, and so we have dropped the subscript j.) The canonical classical energy in the first two terms is augmented by a *coherence* energy $E_{\text{coh}}(t) = -2\hbar\beta(t)\boldsymbol{d}(\boldsymbol{q})\cdot\frac{\boldsymbol{p}_{\text{kin}}}{m}$.

As noted above, the energy can be written more simply in terms of the kinematic momentum $\boldsymbol{p}_{\text{kin}} = \boldsymbol{p} - 2\hbar\beta(t)\boldsymbol{d}\big(\boldsymbol{q}\big)$. We find

$$E(t) = \frac{\boldsymbol{p}_{\text{kin}}^2}{2m} + V\left(\boldsymbol{q},\sigma(t)\right) = \frac{\boldsymbol{p}_{\text{kin}}^2}{2m} + \sigma(t)\hbar\omega\big(\boldsymbol{q}\big) + V_-\left(\boldsymbol{q}\right), \tag{2.11}$$

where $\hbar\omega(\boldsymbol{q}) = V_+(\boldsymbol{q}) - V_-(\boldsymbol{q})$.

Using the kinematic momentum, we can separate the energy into two terms: the electronic state-dependent potential energy

$$E_{\text{elec}}(t) = V(\boldsymbol{q}, \sigma(t)), \tag{2.12}$$

and the classical kinetic energy

$$E_{\text{kin}}(t) = \frac{\boldsymbol{p}_{\text{kin}}^2}{2m}, \tag{2.13}$$

that depends only on the nuclear motion. In this representation, the coherence energy does not appear in the energy budget. Quantum effects are nonetheless still present.

In the Born-Oppenheimer approximation, the electronic parameter $\sigma_j(t)$ is constant, assuming values of 0 or 1. In this limit, the nuclear dynamics of a single trajectory $\Delta\sigma_j(t) = 0$ are governed by purely *classical* motion on the appropriate adiabatic potential, $V_+(\boldsymbol{q}_j(t))$ or $V_-(\boldsymbol{q}_j(t))$, for $\sigma_j(t) = 1$ or $\sigma_j(t) = 0$, respectively. Note that we have included the subscript j to emphasize that these equations are applied for a single trajectory j. The equations of motion for the classical variables and electronic state parameters in the Born-Oppenheimer limit are

$$\begin{aligned}
\dot{\boldsymbol{q}}_j(t) &= \frac{\boldsymbol{p}_{\text{kin},j}(t)}{m}, && (2.14)\\
\dot{\boldsymbol{p}}_{\text{kin},j}(t) &= -\nabla_{\boldsymbol{q}_j} V\big(\boldsymbol{q}_j(t), \sigma_j(t)\big), && (2.15)\\
\dot{\sigma}_j(t) &= 0, && (2.16)\\
\dot{\alpha}_j(t) &= \omega\big(\boldsymbol{q}_j(t)\big)\beta_j(t), && (2.17)\\
\dot{\beta}_j(t) &= -\omega\big(\boldsymbol{q}_j(t)\big)\alpha_j(t). && (2.18)
\end{aligned}$$

When non-adiabatic transitions occur, however, *non-classical* forces appear, as described by the QTSH formalism. The equations of motion for a single trajectory, assuming complete and localized population transfer are generalized to

$$\begin{aligned}
\dot{\boldsymbol{q}}_j(t) &= \frac{\boldsymbol{p}_{\mathrm{kin},j}(t)}{m}, && (2.19)\\
\dot{\boldsymbol{p}}_{\mathrm{kin},j}(t) &= -\nabla_{\boldsymbol{q}_j} V\big(\boldsymbol{q}_j(t), \sigma_j(t)\big) + 2\hbar\omega\big(\boldsymbol{q}_j(t)\big)\boldsymbol{d}\big(\boldsymbol{q}_j(t)\big)\alpha_j(t), && (2.20)\\
\dot{\sigma}_j(t) &= -2\frac{\boldsymbol{d}\big(\boldsymbol{q}_j(t)\big)\cdot\boldsymbol{p}_{\mathrm{kin},j}(t)}{m}\alpha_j(t), && (2.21)\\
\dot{\alpha}_j(t) &= \omega\big(\boldsymbol{q}_j(t)\big)\beta_j(t) + \frac{\boldsymbol{d}\big(\boldsymbol{q}_j(t)\big)\cdot\boldsymbol{p}_{\mathrm{kin},j}(t)}{m}(2\sigma_j(t)-1), && (2.22)\\
\dot{\beta}_j(t) &= -\omega\big(\boldsymbol{q}(t)\big)\alpha_j(t). && (2.23)
\end{aligned}$$

As in presenting the equations of motion in the Born-Oppenheimer limit, we have included the subscript j to emphasize that these equations are applied for a single trajectory j.

Here, we have made the substitution of the stochastic integer parameter σ for the continuous electronic population a_{++}. In the limit of complete and localized population transfer, the electronic of a single trajectory j would result in $\Delta\sigma_j(t) = 1$ or $\Delta\sigma_j(t) = -1$, justifying the assumption that $\sigma_j(t) = a_{++,j}(t)$ that we have made here.

The consistency of surface hopping is equivalent to assuming that the average σ is equal to the continuous population parameter across a trajectory ensemble: $\langle\sigma(t)\rangle \approx \langle a_{++}(t)\rangle$. For localized transitions resulting in complete population transfer, both of these quantities are integers except during a brief excursion, where their values change by unity. We now drop the subscript j to make derived expressions more concise.

Such transitions occur at a localized crossing time $t = t^*$, or equivalently, around a localized configuration $\boldsymbol{q}(t^*) = \boldsymbol{q}^*$. We shall calculate the changes in the constituents of the total

energy as well as the work done by the quantum forces that the electronic and nuclear degrees of freedom exert on each other during that transition.

The electronic transition from the upper ($\sigma = 1$) state to the lower ($\sigma = 0$) state - as depicted in Fig 2.2 - is assumed to be localized within a short time interval of duration 2ϵ that is symmetric around $t = t^*$. During this interval, we assume that the classical forces and dynamics leave $\boldsymbol{q}$ and $\boldsymbol{p}_{\text{kin}}$ unchanged. The change in $\sigma(t)$ during this interval is given by

$$\Delta\sigma(t^*) = -1. \tag{2.24}$$

For a fixed nuclear coordinate $\boldsymbol{q}(t^*) = \boldsymbol{q}^*$, the change in electronic energy during the transition is

$$\Delta E_{\text{elec}}(t^*) = \hbar\omega(\boldsymbol{q}^*)\Delta\sigma(t^*) = -\hbar\omega(\boldsymbol{q}^*). \tag{2.25}$$

This change in electronic energy for the transition from the upper to lower state as shown in Eqn 2.25 is negative. To conserve energy, the classical kinetic energy must increase by the same amount,

$$\Delta E_{\text{kin}}(t^*) = -\Delta E_{\text{elec}}(t^*) = +\hbar\omega(\boldsymbol{q}^*). \tag{2.26}$$

The FSSH method imposes this conservation in an *ad hoc* manner by artificially rescaling the momentum by a "jump," chosen to satisfy

$$\frac{\left(\boldsymbol{p}_{\text{kin}}(t^*) + \Delta\boldsymbol{p}_{\text{kin}}(t^*)\right)^2}{2m} = \frac{\boldsymbol{p}_{\text{kin}}(t^*)^2}{2m} + \hbar\omega(\boldsymbol{q}^*). \tag{2.27}$$

Similarly, for the electronic transition from the lower ($\sigma = 0$) state to the upper ($\sigma = 1$) state - as depicted in Fig 2.4 - change in σ during the short time interval that is symmetric about $t = t^*$ is $\Delta\sigma = +1$, with the change in electronic energy for a fixed nuclear coordinate $\boldsymbol{q}(t^*) = \boldsymbol{q}^*$ during the transition is

$$\Delta E_{\text{elec}}(t^*) = \hbar\omega(\boldsymbol{q}^*), \tag{2.28}$$

the corresponding change in kinetic energy is

$$\Delta E_{\text{kin}}(t^*) = -\Delta E_{\text{elec}}(t^*) = -\hbar\omega(\boldsymbol{q}^*), \tag{2.29}$$

and the *ad hoc* momentum "jump" imposed by the FSSH method would be chosen satisfy

$$\frac{\big(\boldsymbol{p}_{\text{kin}}(t^*) + \Delta\boldsymbol{p}_{\text{kin}}(t^*)\big)^2}{2m} = \frac{\boldsymbol{p}_{\text{kin}}(t^*)^2}{2m} - \hbar\omega(\boldsymbol{q}^*). \tag{2.30}$$

The momentum jump $\Delta\boldsymbol{p}_{\text{kin}}(t^*)$ is chosen to solve the quadratic equations Eqns 2.27 for the transition corresponding to $\Delta\sigma(t^*) = -1$ and 2.30 for the transition corresponding to $\Delta\sigma(t^*) = +1$, in the direction parallel to the non-adiabatic coupling vector $\boldsymbol{d}(\boldsymbol{q}^*)$ [50].

Practical implementations have rules for selecting which root to choose, and what to do if no solution can be be found due to insufficient energy or directional constraints (a "frustrated" hop). [29, 86]

We now analyze the energy budget from the QTSH perspective. From the equations of motion, we have

$$\dot{\boldsymbol{p}}_{\text{kin}}(t) = -\nabla_{\boldsymbol{q}} V\big(\boldsymbol{q}(t), \sigma(t)\big) + 2\hbar\omega\big(\boldsymbol{q}(t)\big)\boldsymbol{d}\big(\boldsymbol{q}(t)\big)\alpha(t), \tag{2.31}$$

where the classical force is represented by

$$\boldsymbol{F}_{\text{class}}(t) = -\nabla_{\boldsymbol{q}} V\big(\boldsymbol{q}(t), \sigma(t)\big), \tag{2.32}$$

and the quantum force is represented by

$$\boldsymbol{F}_{\text{quant}}(t) = 2\hbar\omega\big(\boldsymbol{q}(t)\big)\boldsymbol{d}\big(\boldsymbol{q}(t)\big)\alpha(t). \tag{2.33}$$

The change in kinematic momentum results from two contributions: the classical force derived from the currently occupied adiabatic potential and a quantum force resulting from the electronic energy transition. This change of electronic states does work in what follows.

During the localized transition, the classical force does not have an appreciable effect on the nuclear dynamics. We consider only the impulsive quantum force during the transition. Here, we can take the coordinate $\boldsymbol{q} = \boldsymbol{q}^*$ to be constant. The integrated effect of this force on the momentum during this transition can be computed as

$$\Delta\boldsymbol{p}_{\text{kin}} = 2\hbar\omega(\boldsymbol{q}^*)\boldsymbol{d}(\boldsymbol{q}^*)\int_{t^*-\epsilon}^{t^*+\epsilon}\alpha(t)\mathrm{d}t. \tag{2.34}$$

The only time-dependent quantity during this transition is the electronic coherence, which is rapidly created and then dispersed by the flow of electronic population.

For the flow of electronic population from the upper to the lower state, we showed above that this coherence can be described simply in terms of the non-adiabatic mixing angle,

$$\alpha(t) = -\frac{1}{2}\sin\phi(t), \tag{2.35}$$

and for the flow of electronic population from the lower to the upper state, we showed above

that this coherence can be described simply in terms of the non-adiabatic mixing angle,

$$\alpha(t) = \frac{1}{2}\sin\phi(t). \tag{2.36}$$

The value of ϕ transitions rapidly from $\phi = 0$ for $t < t^*$ to $\phi = \pi$ for $t > t^*$. To simplify the integral, we change integration variables from t to ϕ. We note that

$$\mathrm{d}\phi = \dot{\phi}\mathrm{d}t. \tag{2.37}$$

We write $\dot{\phi}$ as

$$\dot{\phi} = \nabla_{\boldsymbol{q}}\phi \cdot \dot{\boldsymbol{q}} = \nabla_{\boldsymbol{q}}\phi \cdot \frac{\boldsymbol{p}_{\mathrm{kin}}}{m}. \tag{2.38}$$

Using the definition of the non-adiabatic coupling vector

$$\boldsymbol{d}(\boldsymbol{q}^*) = -\frac{1}{2}\nabla_{\boldsymbol{q}}\phi \tag{2.39}$$

then gives

$$\mathrm{d}t = -\left(\frac{m}{2\boldsymbol{d}(\boldsymbol{q}^*)\cdot\boldsymbol{p}_{\mathrm{kin}}}\right)\mathrm{d}\phi. \tag{2.40}$$

For the flow of electronic population from the upper to the lower state, the momentum jump can be expressed as

$$\Delta\boldsymbol{p}_{\mathrm{kin}} = \frac{1}{2}\hbar\omega(\boldsymbol{q}^*)\boldsymbol{d}(\boldsymbol{q}^*)\left(\frac{m}{2\boldsymbol{d}(\boldsymbol{q}^*)\cdot\boldsymbol{p}_{\mathrm{kin}}}\right)\int_0^\pi \sin\phi\ \mathrm{d}\phi, \tag{2.41}$$

and for the flow of electronic population from the lower to the upper state,

$$\Delta \boldsymbol{p}_{\text{kin}} = -\frac{1}{2}\hbar\omega(\boldsymbol{q}^*)\boldsymbol{d}(\boldsymbol{q}^*)\left(\frac{m}{2\boldsymbol{d}(\boldsymbol{q}^*)\cdot\boldsymbol{p}_{\text{kin}}}\right)\int_0^{\pi}\sin\phi\ \mathrm{d}\phi. \tag{2.42}$$

Noting that $\int_0^{\pi}\sin\phi\ \mathrm{d}\phi = 2$, we obtain the final result for the flow of electronic population from the upper to the lower state,

$$\Delta \boldsymbol{p}_{\text{kin}} = \hbar\omega(\boldsymbol{q}^*)\boldsymbol{d}(\boldsymbol{q}^*)\left(\frac{m}{2\boldsymbol{d}(\boldsymbol{q}^*)\cdot\boldsymbol{p}_{\text{kin}}}\right), \tag{2.43}$$

and for the flow of electronic population from the lower to the upper state,

$$\Delta \boldsymbol{p}_{\text{kin}} = -\hbar\omega(\boldsymbol{q}^*)\boldsymbol{d}(\boldsymbol{q}^*)\left(\frac{m}{2\boldsymbol{d}(\boldsymbol{q}^*)\cdot\boldsymbol{p}_{\text{kin}}}\right). \tag{2.44}$$

The explicit expressions for the momentum jumps for the downward electronic transition (Eqn 2.43) or the upward electronic transition (Eqn 2.44) resolves any ambiguity of the quadratic equation root choice inherent in the FSSH methodology [1, 29, 30].

From the perspective of the energy budget, the quantum force $\boldsymbol{F}_{\text{quant}}$ does work $W_{\text{e}\to\text{n}}$ [87] on the nuclear degrees of freedom, which changes the kinetic energy by an amount ΔE_{kin},

$$W_{\text{e}\to\text{n}} = \Delta E_{\text{kin}} = \int_{t^*-\epsilon}^{t^*+\epsilon} \boldsymbol{F}_{\text{quant}}(t)\cdot\dot{\boldsymbol{q}}\ \mathrm{d}t. \tag{2.45}$$

In our localized approximation, this becomes

$$W_{\text{e}\to\text{n}} = \Delta E_{\text{kin}} = \frac{\boldsymbol{p}_{\text{kin}}}{m}\cdot\Delta\boldsymbol{p}_{\text{kin}}. \tag{2.46}$$

For the flow of electronic population from the upper to the lower state, the change in the

kinetic energy in the localized approximation is

$$\Delta E_{\text{kin}} = \hbar\omega(\boldsymbol{q}^*), \tag{2.47}$$

and for the flow of electronic population from the lower to the upper state,

$$\Delta E_{\text{kin}} = -\hbar\omega(\boldsymbol{q}^*). \tag{2.48}$$

We have recovered the energy conservation expected on physical grounds: The electronic energy change $-\hbar\omega(\boldsymbol{q}^*)$ that accompanies the downward electronic transition, or the electronic energy change $\hbar\omega(\boldsymbol{q}^*)$ that accompanies the upward electronic transition, appears or disappears as kinetic energy of the classical nuclear motion, respectively. The quantum force $\boldsymbol{F}_{\text{quant}}$ that accompanies the loss or gain of electronic energy does work on the nuclear degrees of freedom and quantitatively transfers this energy into a gain or loss of nuclear kinetic energy, respectively.

2.2.1 Frustrated Hops

We now incorporate the consideration of available energy in examining upward electronic transitions.

As shown above, the momentum jump $\Delta\boldsymbol{p}_{\text{kin}}$ associated with the upward transition is given by Eqn 2.44, with the boundary conditions of $\phi = 0$ for $t < t^*$ and $\phi = \pi$ for $t > t^*$.

For upward transitions, an additional consideration of available energy enters the analysis. In particular, there has to be sufficient nuclear kinetic energy available to make the transition to the upper state. This corresponds to the positive kinetic energy before the transition $\frac{\boldsymbol{p}_{\text{kin}}^2}{2m}$ to be at least as large in magnitude as the negative ΔE_{kin} accompanying the electronic

excitation. Otherwise the hop is "frustrated," as previously discussed.

We can examine frustrated hops from the context of our analysis based on QTSH. In order for ϕ to fully transition from $\phi = 0$ to $\phi = \pi$, there must be enough kinetic energy to keep the nuclear motion proceeding in the initial positive direction. If this is not the case, the sign of $\boldsymbol{p}_{\text{kin}}$ will reverse before complete population transfer will be a change in the sign of $\dot{\phi}$, so that ϕ has the time history $0 \rightarrow \phi_{\text{max}} \rightarrow 0$ rather than $0 \rightarrow \pi$ for a successful upward transition, where ϕ_{max} is the value reached by the mixing angle when the momentum reversal occurs. The total work done by the quantum force in this case is $\Delta E_{\text{kin}} = 0$, the expected accompaniment for the $\Delta\sigma = 0$ failed transition. Correspondingly, the electronic degrees of freedom do zero net work on the nuclear motion for frustrated hops.

For the model of a localized and complete transition, employed here, one can show that the adiabatic plus quantum force, Eqn 2.31, is identical to the *diabatic* force $\boldsymbol{F}_1 = -\nabla_{\boldsymbol{q}} V_1(\boldsymbol{q})$ for the downward transition, and $\boldsymbol{F}_2 = -\nabla_{\boldsymbol{q}} V_2(\boldsymbol{q})$ for the upward transition. This will be discussed in Section 4.2.3 in Chapter 4.

From this perspective, the trajectory must have enough energy to reach the *crossing point* of the diabatic potentials and, further, to leave the region of transition, to avoid its motion being stopped and reversed.

We note that our analysis suggests that the correct way to treat frustrated hops in FSSH is to *reverse* the momentum when a frustrated hop is encountered (at least in one-dimensional systems).

In the general QTSH method, frustrated hops are not imposed externally. Electronic transitions occur solely based on the stochastic hopping algorithm with no attention paid to the energetics. The quantum forces of QTSH act in the manner described above to guide the trajectories and, if insufficient energy is available, will redirect the motion back through the interaction region. The reversal of momentum changes the sign of the hopping probability,

increasing the likelihood of a second downward transition. However, as we have emphasized, individual trajectories do not conserve energy, nor are the state residencies necessarily consistent with their classical motion. It is at the *ensemble* level that consistency of population energetics is achieved.

2.2.2 Energy Conservation & Quantum Backreaction

The change in electronic energy associated with the electronic transition is completely counterbalanced by the change in kinetic energy associated with the momentum jump of the nuclear degrees of freedom initiated by the quantum force. The quantum force can be said to work to conserve energy as a result of an electronic transition.

The quantum backreaction (Fig 2.1) describes the self-consistency between the classically treated nuclear degrees of freedom and the quantum mechanically treated electronic degrees of freedom. The nuclear dynamics that gives rise to changes in the electronic Hamiltonian induces electronic transitions that as a result produces a quantum force that alters the nuclear motion in the form of a momentum jump when transitions are localized.

The work done *on* the electronic degrees of freedom *by* the nuclear degrees of freedom $W_{\mathrm{n}\to\mathrm{e}}$ can be expressed as the change in the electronic energy ΔE_{elec}, represented by the expression

$$W_{\mathrm{n}\to\mathrm{e}}(t) = \Delta E_{\mathrm{elec}}(t). \tag{2.49}$$

Since the change in the electronic energy ΔE_{elec} occurs as a result of electronic transitions that results in $\Delta\sigma$, ΔE_{elec} can be expressed as

$$\Delta E_{\mathrm{elec}}(t) = \hbar\omega(\boldsymbol{q}(t))\Delta\sigma(t). \tag{2.50}$$

By using the equation of motion for $\sigma(t)$, Eqn 2.22, the change in σ during a transition that takes 2ϵ time can be found by solving the differential equation $\dot{\sigma}(t)$ with respect to time

$$\Delta\sigma(t) = \int_{t_\mathrm{i}}^{t_\mathrm{f}} \dot{\sigma}(t)\ \mathrm{d}t = -2\int_{t^*-\epsilon}^{t^*+\epsilon} \frac{\boldsymbol{d}(\boldsymbol{q})\cdot\boldsymbol{p}_\mathrm{kin}}{m}\alpha(t)\mathrm{d}t, \tag{2.51}$$

from the time before the transition $t_\mathrm{i} = t^* - \epsilon$ to the time after the transition $t_\mathrm{f} = t^* + \epsilon$.

We note here that we have omitted the subscript j that indicates that that the above calculations are for a single trajectory. Under the assumption of localized and complete population transfer, each trajectory has $\Delta a_{++,j}(t) = +1$ for a hop from $- \rightarrow +$, or $\Delta a_{++,j}(t) = +1$ for a hop from $+ \rightarrow -$, implying that $\Delta a_{++,j}(t) = \Delta\sigma_j(t)$, or $\dot{a}_{++,j}(t) = \dot{\sigma}_j(t)$.

We note that $\Delta\sigma(t)$ in Eqn 2.51 is more generally $\Delta a_{++}(t)$ when the assumption of complete and localized population transfer is not made.

By substituting Eqn 2.51 into Eqn 2.50, the change in the electronic energy ΔE^*_elec can be expressed as

$$\Delta E_\mathrm{elec} = -2\hbar\omega(\mathbf{q})\int_{t^*-\epsilon}^{t^*+\epsilon} \frac{\boldsymbol{d}(\boldsymbol{q})\cdot\boldsymbol{p}_\mathrm{kin}}{m}\alpha(t)\mathrm{d}t. \tag{2.52}$$

Given that $\dot{\boldsymbol{q}} = \frac{\boldsymbol{p}_\mathrm{kin}}{m}$ and the quantum force, Eqn 2.33, the change in the electronic energy is represented by

$$\Delta E_\mathrm{elec} = -\int_{t^*-\epsilon}^{t^*+\epsilon} \mathbf{F}_\mathrm{quant}(\boldsymbol{q})\cdot\dot{\boldsymbol{q}}\ \mathrm{d}t. \tag{2.53}$$

Since the work done *on* the electronic degrees of freedom *by* the nuclear degrees of freedom $W_{\mathrm{n}\rightarrow\mathrm{e}}$ is equal to the change in electronic energy during an electronic transition (Eqn 2.49),

$$W_{\mathrm{n}\rightarrow\mathrm{e}} = -\int_{t^*-\epsilon}^{t^*+\epsilon} \mathbf{F}_\mathrm{quant}(\boldsymbol{q})\cdot\dot{\boldsymbol{q}}\ \mathrm{d}t. \tag{2.54}$$

The above expression is the negative of the work done *on* the nuclear degrees of freedom *by* the electonic degrees of freedom $W_{\mathrm{e}\to\mathrm{n}}$ (Eqn 2.45), where

$$W_{\mathrm{n}\to\mathrm{e}} = -W_{\mathrm{e}\to\mathrm{n}}. \tag{2.55}$$

Rearranging the above gives

$$W_{\mathrm{n}\to\mathrm{e}} + W_{\mathrm{e}\to\mathrm{n}} = 0, \tag{2.56}$$

implying self-consistency between the classically treated nuclear degrees of freedom and the quantum mechanically treated electronic degrees of freedom. The nuclear dynamics that gives rise to changes in the electronic Hamiltonian induces electronic transitions that as a result produces a quantum force that alters the nuclear motion in the form of a momentum jump when transitions are localized. This is also known as the quantum backreaction (Fig 2.1).

2.3 Methods

2.3.1 Systems

Simple Avoided Crossing System

We consider a two-state system of a single localized adiabatic transitions. We will consider the process where the system starts on the upper adiabatic state and experiences an electronic transition to the lower adiabatic surface (Fig 2.2), and the process where the system starts on the lower adiabatic state and experiences an electronic transition to the upper adiabatic surface (Fig 2.4). In both of these processes, the electronic transition is accompanied by

nuclear dynamics. We made the assumption that the electronic transitions occurs in a localized region where the population transfer is complete, and that the population continues to evolve on the lower adiabatic or upper adiabatic state, respectively.

The potentials used to produce Figures 2.2-2.5 are the potentials for Tully's simple avoided crossing system given in Eqns 1.83-1.84.

These potentials are as given in Tully's original simple avoided crossing system [1], with modifications made to the off-diagonal diabatic coupling by reducing the size of the constant C. We vary the value of the potential parameter $C = 0.0005$, $C = 0.001$, and $C = 0.002$, which changes the strength of the diabatic coupling $V_{12}(\boldsymbol{q})$. These modifications give rise to a stronger and more localized non-adiabatic coupling in our systems, in comparison to the original system by Tully which has the value of $C = 0.005$. The effect of these modifications to the simple avoided crossing system [1] are illustrated in Fig 1.1.

Dual Avoided Crossing System

We also consider a more complex two state system of two localized adiabatic transitions where the system starts on the lower adiabatic state and experiences an electronic transition to the upper adiabatic surface that is accompanied by nuclear dynamics. We assume that the transition occurs in a localized region where the population transfer is complete. The system then continues on the upper adiabatic surface before experiencing a second electronic transition to the lower adiabatic surface (Fig 2.8).

The corresponding process in the diabatic representation is given by Fig 2.9, where the population remains on the horizontal diabatic surface 1 throughout the process.

The potentials used to produce Figures 2.8-2.9 are the potentials for Tully's dual avoided crossing system [1] given in Eqns 1.86-1.87.

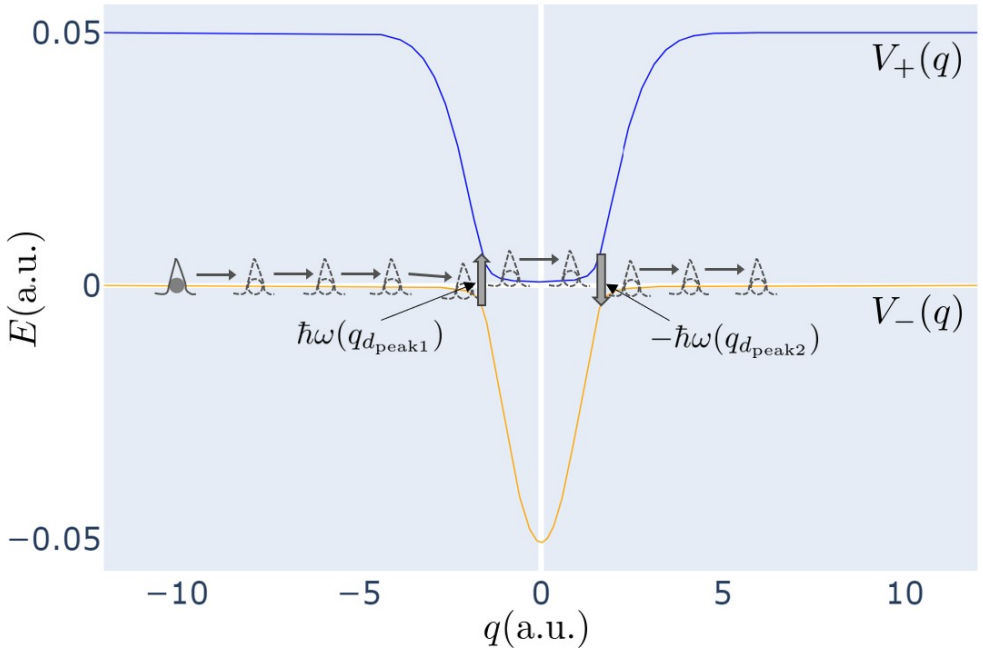

Figure 2.8: Schematic representation of a localized quantum state/trajectory undergoing a non-adiabatic transition from the lower to the upper adiabatic state at the avoided crossing, traveling on the upper adiabatic surface, and finally undergoing another non-adiabatic transition from the upper to the lower adiabatic state. Diabatic potentials for the dual avoided crossing system are given in Eqns 1.86-1.87.

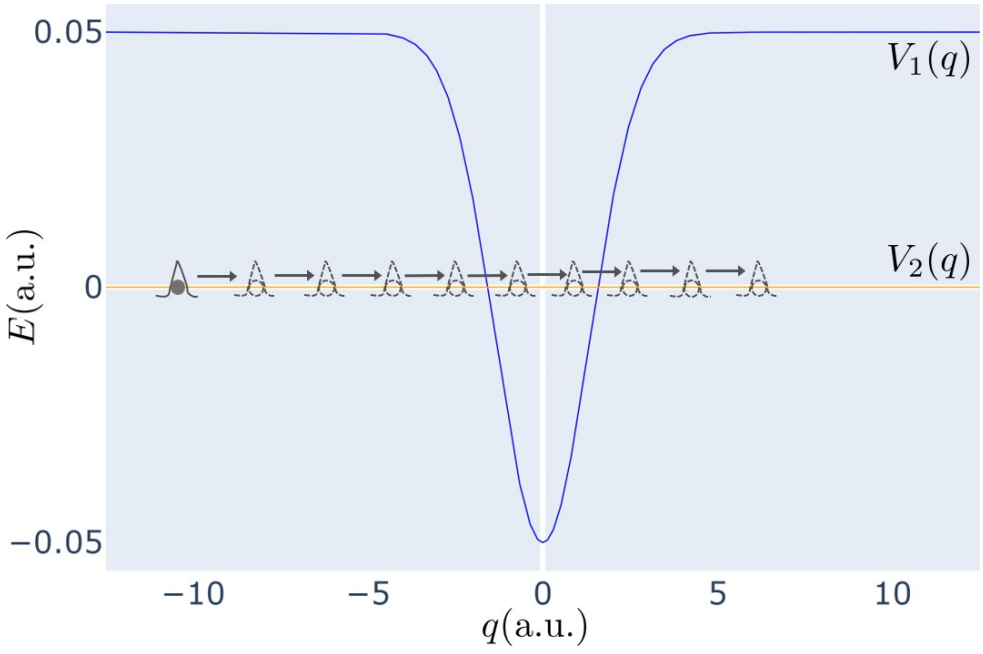

Figure 2.9: Schematic representation of a localized quantum state/trajectory traveling along the diabatic potential $V_2(\boldsymbol{q})$, corresponding to the process in Fig 2.8. Diabatic potentials for the dual avoided crossing system are given in Eqns 1.86-1.87.

These potentials are as given in Tully's original dual avoided crossing system [1], with modifications made to the off-diagonal diabatic coupling by reducing the size of the constant C. We vary the value of the potential parameter $C = 0.0015$, $C = 0.003$, and $C = 0.006$, which changes the strength of the diabatic coupling $V_{12}(\boldsymbol{q})$. These modifications give rise to a stronger and more localized non-adiabatic coupling in our systems, in comparison to the original system by Tully which has the value of $C = 0.015$. The effect of these modifications to the simple dual crossing system [1] are illustrated in Fig 1.2.

We note that the approximate adiabatic density matrix in terms of the non-adiabatic mixing angle $\phi(t)$, by virtue of the same diabatic state being populated throughout the process (Fig 2.9), is Eqn 2.9.

The definition of the adiabatic matrix at different times and the derivation of 2.9 can be found in the Appendix A.

2.3.2 Simulation Details

The numerical results for the QTSH simulations for each of the systems described above were obtained with 2000 trajectories ($N = 2000$) randomly sampled from a minimum uncertainty phase-space Gaussian distribution width $\sigma_{\boldsymbol{q}} = 1.0$. The mean initial positions were $\boldsymbol{q}_0 = -6.0$ for the simple avoided crossing systems, $\boldsymbol{q}_0 = -10.0$ for the dual crossing systems.

The results of the quantum wavepacket simulations that the QTSH results were compared against were performed using the split operator method by Kosloff [88, 89]. The initial wavepacket for the two-state system was a Gaussian wavepacket centered around $\boldsymbol{q}_0 = -6.0$ for the simple avoided crossing systems, and $\boldsymbol{q}_0 = -10.0$ and for the dual crossing systems.

The initial mean momenta $\boldsymbol{p}_0 = \hbar\boldsymbol{k}_0$ used for the simple avoided crossing system [1] was $\hbar\boldsymbol{k}_0 = 15$ a.u., and for the dual crossing system [1], $\hbar\boldsymbol{k}_0 = 40.3$ a.u.. The initial mean

momenta $\hbar\boldsymbol{k}_0 = 15$ for the simple avoided crossing system [1] was chosen to ensure that there would be sufficient kinetic energy for complete transition to take place between adiabatic states. The initial mean momenta $\hbar\boldsymbol{k}_0 = 40.3$ for the dual avoided crossing system [1] was chosen since almost complete population transfer from the lower to upper adiabatic state takes place, leaving a significantly small population on the lower adiabatic state to interfere with the population transferring from the upper to lower adiabatic state during the second transition.

The QTSH and quantum simulations were run with timesteps $\Delta t = 0.5$ a.u. long, and for a total length of 8533 a.u. and 1588 a.u. for the simple avoided crossing and dual avoided crossing systems, respectively.

The phase space averaged values of the elements of the Wigner distribution were computed at every timestep of the QTSH simulation were calculated with the following expressions

$$\langle \rho_{++}(t) \rangle = \frac{1}{N} \sum_{j}^{N} \sigma_j(t), \tag{2.57}$$

$$\langle \rho_{--}(t) \rangle = \frac{1}{N} \sum_{j}^{N} \left(1 - \sigma_j(t)\right), \tag{2.58}$$

$$\langle \alpha(t) \rangle = \frac{1}{N} \sum_{j}^{N} \alpha_j(t), \tag{2.59}$$

$$\langle \beta(t) \rangle = \frac{1}{N} \sum_{j}^{N} \beta_j(t). \tag{2.60}$$

The phase space averaged accumulated work done on the nuclear degrees of freedom by the electronic degrees of freedom $W_{\mathrm{e}\to\mathrm{n}}$ in QTSH was calculated with

$$\langle W_{\mathrm{e}\to\mathrm{n}}(t) \rangle = \frac{1}{N} \sum_{j}^{N} \int \boldsymbol{F}_{\mathrm{quant},j} \cdot \frac{\boldsymbol{p}_{\mathrm{kin},j}}{m} \, \mathrm{d}t. \tag{2.61}$$

The phase space averaged accumulated work done on the electronic degrees of freedom by the nuclear degrees of freedom were calculated in two ways

$$\langle W^{\sigma}_{\mathrm{n}\to\mathrm{e}}(t)\rangle = \frac{1}{N}\sum_{j}\hbar\omega(\boldsymbol{q}_j)\Delta\sigma_j(t)\ \mathrm{d}t, \tag{2.62}$$

where $\Delta\sigma_j(t) = \sigma_j(t) - \sigma_j(t-\Delta t)$, and

$$\langle W^{a}_{\mathrm{n}\to\mathrm{e}}(t)\rangle = \frac{1}{N}\sum_{j}\int\hbar\omega(\boldsymbol{q}_j)\dot{a}_{++,j}(t)\ \mathrm{d}t, \tag{2.63}$$

where $\dot{a}_{++,j}(t)$ is defined in Eqn 1.56. Note that we have not used $\dot{\sigma}_j(t)$ as in Eqn 2.22 since we have assumed that $\dot{a}_{++,j}(t) = \dot{\sigma}_j(t)$ in the limit of localized and complete population transfer/single trajectory in Eqn 2.22. As QTSH utilizes an ensemble of *independent* trajectories, the nuclear dynamics is non-local in electronic and phase space [1, 8], and we can no longer assume that $\dot{\sigma}_j(t) = \dot{a}_{++,j}(t)$.

2.4 Results & Discussion

We now present numerical QTSH results for the modified simple avoided crossing system [1] given in Figs 2.2 and 2.4, and the modified Tully dual avoided crossing system [1] given in Fig 2.8.

2.4.1 Wigner Distribution Dynamics

Here we present the QTSH results of the dynamics of the phase space averaged elements of Wigner distribution against the exact quantum results. The Eqns 2.58-2.60 were used to obtain the plots presented in this section.

In Figs 2.10 and 2.11, we present the comparison of QTSH results with exact quantum results for the simple avoided crossing system [1], with the process starting on the upper adiabatic surface with trajectories hopping to the lower adiabatic surface (Fig 2.2), and the process starting on the lower adiabatic surface with trajectories hopping to the upper adiabatic surface (Fig 2.4), respectively.

In Fig 2.12, we present the comparison of QTSH results with exact quantum results for the dual avoided crossing system [1], with the process starting on the lower adiabatic surface with trajectories hopping to the upper adiabatic surface (Fig 2.2), and then with trajectories hopping from the upper adiabatic surface to the lower adiabatic surface (Fig 2.8).

With reference to Figs 2.10 and 2.11, we observed that the transfer of population that occurs during the time interval between $t \approx 10$ fs and $t \approx 30$ fs, is almost complete. The size of the population transfer is largest when the non-adiabatic coupling $\boldsymbol{d}(\boldsymbol{q})$ is strongest and most localized (i.e. smallest C).

With reference to Figs 2.10 and 2.11, we observed that QTSH results for the real part of the coherence $\langle \alpha(t) \rangle$ and the the imaginary part of the coherence $\langle \beta(t) \rangle$ are in good agreement with the quantum result, with the best agreement when the non-adiabatic coupling $\boldsymbol{d}(\boldsymbol{q})$ is strongest and most localized (i.e. smallest C).

In Fig 2.10, we observe an increase in $\langle \rho_{--}(t) \rangle$ between $t \approx 10$ fs and $t \approx 30$ fs as a result of trajectory hops from $+ \rightarrow -$, before an asymptotic value is reached. The asymptotic value of the QTSH results for $\langle \rho_{--}(t) \rangle$ deviates from the exact quantum results the most when $C = 0.002$ and the least when $C = 0.0005$. We observe the same trend in Fig 2.11 for the $\langle \rho_{++}(t) \rangle$ results instead of $\langle \rho_{++}(t) \rangle$, since the trajectory hops occur from $+ \rightarrow -$ instead. The largest asymptotic value of the QTSH result for $\langle \rho_{--}(t) \rangle$ and $\langle \rho_{++}(t) \rangle$ were found in Figs 2.2 and 2.4, respectively, when $C = 0.0005$, and smallest when $C = 0.002$.

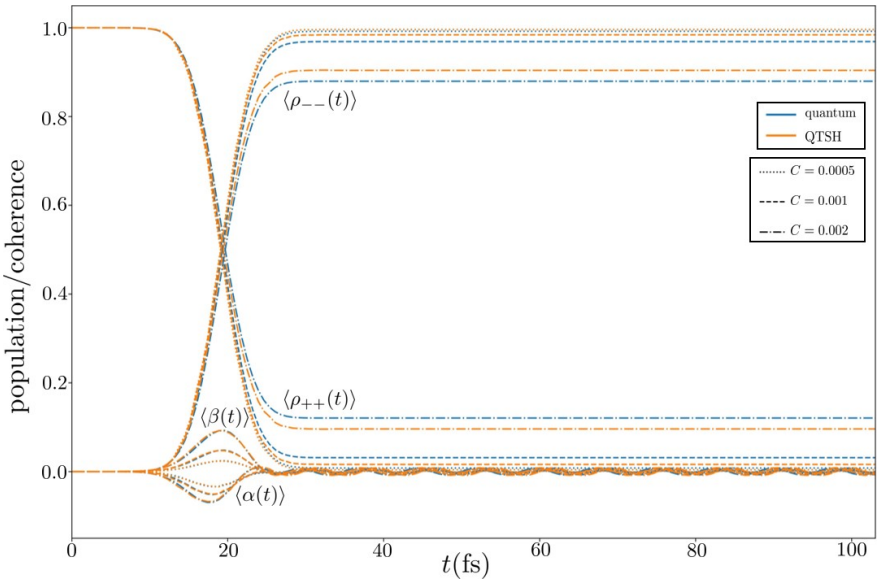

Figure 2.10: Comparison of the phase space averaged populations on the upper adiabatic PES $\langle \rho_{++}(t) \rangle$ and the lower adiabatic PES $\langle \rho_{--}(t) \rangle$, and the real and imaginary parts of the coherence, $\langle \alpha(t) \rangle$ and $\langle \beta(t) \rangle$, respectively, obtained from QTSH with exact quantum results for the modified Tully's simple avoided crossing system with a starting population on the upper adiabatic state at an initial average momentum $\hbar k_0 = 15$ a.u., and $C = 0.0005, 0.001$ and 0.002.

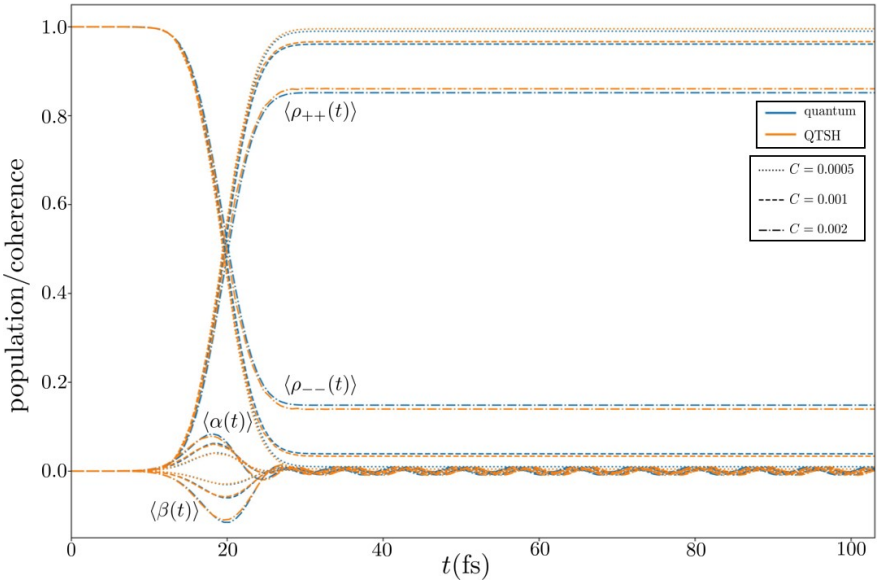

Figure 2.11: Comparison of the phase space averaged populations on the upper adiabatic PES $\langle \rho_{++}(t) \rangle$ and the lower adiabatic PES $\langle \rho_{--}(t) \rangle$, and the real and imaginary parts of the coherence, $\langle \alpha(t) \rangle$ and $\langle \beta(t) \rangle$, respectively, obtained from QTSH with exact quantum results for the modified Tully's simple avoided crossing system with a starting population on the lower adiabatic state at an initial average momentum $\hbar k_0 = 15$ a.u., and $C = 0.0005, 0.001$ and 0.002.

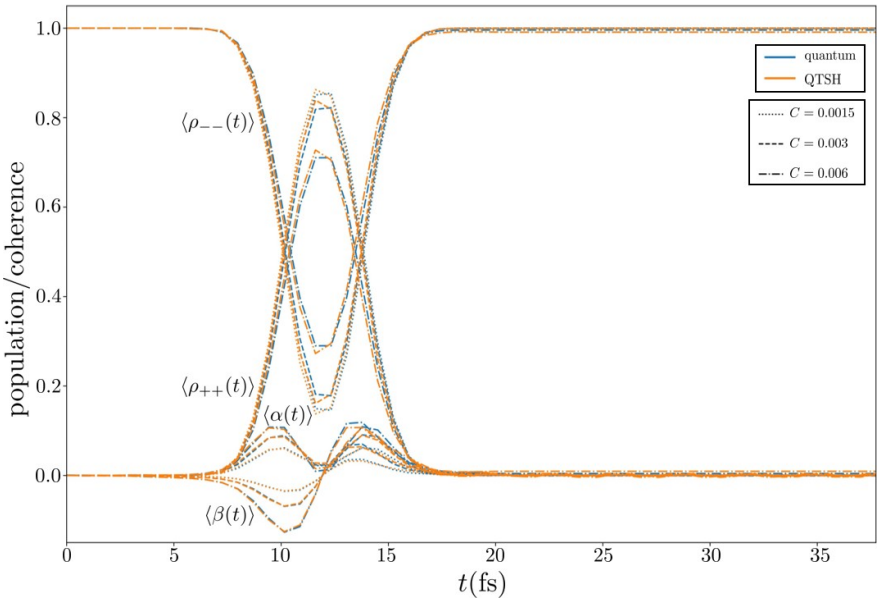

Figure 2.12: Comparison of the phase space averaged populations on the upper adiabatic PES $\langle\rho_{++}(t)\rangle$ and the lower adiabatic PES $\langle\rho_{--}(t)\rangle$, and the real and imaginary parts of the coherence, $\langle\alpha(t)\rangle$ and $\langle\beta(t)\rangle$, respectively, obtained from QTSH with exact quantum results for the modified Tully's dual avoided crossing system with a starting population on the lower adiabatic state at an initial average momentum $\hbar k_0 = 40.3$ a.u., and $C = 0.0015, 0.003$ and 0.006.

With reference to Figs 2.12, we observed that the transfer of population from the lower adiabatic surface to the upper adiabatic state that occurs during the time interval between $t \approx 7.5$ fs and $t \approx 11.4$ fs, is significantly large, followed by an almost complete transfer from the upper adiabatic surface to the lower adiabatic surface during the time interval between $t \approx 12$ fs and $t \approx 17.5$ fs. The size of the initial population transfer is largest when the non-adiabatic coupling $\boldsymbol{d}(\boldsymbol{q})$ is strongest and most localized (i.e. smallest C).

In Fig 2.12, we observe an increase in $\langle\rho_{++}(t)\rangle$ between $t \approx 7.5$ fs and $t \approx 11.4$ fs as a result of trajectory hops from $- \rightarrow +$. During the time interval between $t \approx 11.4$ fs and $t \approx 12$ fs where the quantum result for $\langle\rho_{++}(t)\rangle$ shows no change, the QTSH result exhibits as slight decrease, indicating that the second population transfer due to trajectory hops from $+ \rightarrow -$ occurs at a slow rate in this region. A decrease of the QTSH result for $\langle\rho_{++}(t)\rangle$ to close to zero, as in the case for the exact quantum result occurs during the time interval between

$t \approx 12$ fs and $t \approx 17.5$ fs The QTSH results for $\langle \rho_{++}(t) \rangle$ deviates from the exact quantum results the most when $C = 0.006$ and the least when $C = 0.0015$.

With reference to Figs 2.12, we observed that QTSH results for the real part of the coherence $\langle \alpha(t) \rangle$ and the the imaginary part of the coherence $\langle \beta(t) \rangle$ are in good agreement with the quantum result, with the best agreement when the non-adiabatic coupling $\boldsymbol{d}(\boldsymbol{q})$ is strongest and most localized (i.e. smallest C). The deviation of the QTSH results from the quantum results also increases after the first transition.

From the observations we have made in Figs 2.10-2.12, we conclude that the stronger and more localized $\boldsymbol{d}(\boldsymbol{q})$ is (i.e. the smaller the value of C), the more complete and localized the population transfer, and the smaller the discrepancy the QTSH results for the populations and coherence with the exact quantum result.

2.4.2 Feedback between Nuclear and Electronic Degrees of Freedom

We now examine the self-consistency between the classically treated nuclear degrees of freedom and the quantum mechanically treated electronic degrees of freedom using the analysis of the quantum-classical energy budget of QTSH.

The phase space averaged work done by the electronic degrees of freedom on the nuclear degrees of freedom $\langle W_{\mathrm{e}\to\mathrm{n}} \rangle$ (Eqn 2.61) - in the form of work done by the quantum force $\boldsymbol{F}_{\mathrm{quant}}$ in QTSH to instantaneously change the kinetic energy due to trajectories hopping $\langle \Delta E_{\mathrm{kin}}(t) \rangle$ - that are analogous to the *ad hoc* trajectory level momentum jump $\Delta \boldsymbol{p}_{\mathrm{kin},j}$ in the limit of localized and complete population transfer.

Since the quantum forces $\boldsymbol{F}_{\mathrm{quant}}$ in QTSH act to conserve energy when trajectories hop from one adiabatic surface to another, $\langle W_{\mathrm{e}\to\mathrm{n}} \rangle = \langle \Delta E_{\mathrm{kin}}(t) \rangle$.

Under the assumption of localized and complete population transfer, each trajectory has $\Delta a_{++,j}(t) = +1$ for a hop from $- \rightarrow +$, or $\Delta a_{++,j}(t) = +1$ for a hop from $+ \rightarrow -$, implying that $\Delta a_{++,j}(t) = \Delta\sigma_j(t)$, or $\dot{a}_{++,j}(t) = \dot{\sigma}_j(t)$.

As such, we have utilized both $\dot{a}_{++,j}(t)$ and $\Delta\sigma_j(t)$ to calculate the work done by the nuclear degrees of freedom on the electronic degrees of freedom $\langle W^a_{\mathrm{n}\rightarrow\mathrm{e}}(t)\rangle$ (Eqn 2.63) and $\langle W^\sigma_{\mathrm{n}\rightarrow\mathrm{e}}(t)\rangle$ (Eqn 2.62), respectively.

Since the actual change in electronic energy due to the hopping of trajectories in QTSH corresponds to $\Delta\sigma_j(t)$ rather than the change in the population of the proxy density matrix $\Delta a_{++,j}(t)$, $\langle \Delta E_{\mathrm{elec}}(t)\rangle = \langle W^\sigma_{\mathrm{n}\rightarrow\mathrm{e}}(t)\rangle$.

If there was self-consistency between the classically treated nuclear degrees of freedom and the quantum mechanically treated electronic degrees of freedom due to the effect of the quantum backreaction

$$\langle W_{\mathrm{e}\rightarrow\mathrm{n}}\rangle + \langle W^\sigma_{\mathrm{n}\rightarrow\mathrm{e}}(t)\rangle = 0, \tag{2.64}$$

conserving energy since

$$\langle \Delta E_{\mathrm{kin}}(t)\rangle + \langle \Delta E_{\mathrm{elec}}(t)\rangle = 0. \tag{2.65}$$

If the populations are perfectly localized and complete, we would expect that $\langle W^a_{\mathrm{n}\rightarrow\mathrm{e}}\rangle = \langle W^\sigma_{\mathrm{n}\rightarrow\mathrm{e}}\rangle = \langle \Delta E_{\mathrm{elec}}(t)\rangle$.

In Figs 2.13 and 2.14 we present the plots for $\langle W_{\mathrm{e}\rightarrow\mathrm{n}}\rangle$, $\langle W^a_{\mathrm{n}\rightarrow\mathrm{e}}\rangle$, and $\langle W_{\mathrm{e}\rightarrow\mathrm{n}}\rangle + \langle W^a_{\mathrm{n}\rightarrow\mathrm{e}}\rangle$ for the simple avoided crossing system [1] for the process involving electronic transitions from the upper to the lower adiabatic surface (Fig 2.2), and from the lower to the upper adiabatic surface (Fig 2.4), respectively.

In Fig 2.15 we present the plot for $\langle W_{\mathrm{e}\to\mathrm{n}}\rangle$, $\langle W^a_{\mathrm{n}\to\mathrm{e}}\rangle$, and $\langle W_{\mathrm{e}\to\mathrm{n}}\rangle + \langle W^a_{\mathrm{n}\to\mathrm{e}}\rangle$ for the dual avoided crossing system [1] with the trajectories initially populating the lower adiabatic surface, for the process depicted in Fig 2.8.

With reference to Fig 2.13 we observe that during the time interval $t \approx 10$ fs to $t \approx 30$ fs, when the trajectories hop from $+ \to -$, we find that $\langle W^a_{\mathrm{n}\to\mathrm{e}}\rangle \approx \langle \Delta E_{\mathrm{elec}}(t)\rangle$ drops before reaching an asymptotic value. This agrees with the decrease in electronic energy as a result of the $+ \to -$ electronic transition. While $\langle W^a_{\mathrm{n}\to\mathrm{e}}\rangle$ is not the exact $\langle \Delta E_{\mathrm{elec}}(t)\rangle$, we find that $\langle W_{\mathrm{e}\to\mathrm{n}}\rangle = \langle \Delta E_{\mathrm{kin}}(t)\rangle$, the work done by the quantum force to reduce the kinetic energy to conserve the quantum-classical energy, perfectly offsets $\langle W^a_{\mathrm{n}\to\mathrm{e}}\rangle$, where $\langle W_{\mathrm{e}\to\mathrm{n}}\rangle + \langle W^a_{\mathrm{n}\to\mathrm{e}}\rangle = 0$.

We make the same observation in Fig 2.14 with the change in $\langle W^a_{\mathrm{e}\to\mathrm{n}}\rangle$ and $\langle W^a_{\mathrm{n}\to\mathrm{e}}\rangle$ changing in opposite directions than in Fig 2.13 since the trajectories hop in the opposite direction $- \to +$.

With reference to Fig 2.15, we observe that $\langle W^a_{\mathrm{n}\to\mathrm{e}}\rangle \approx \langle \Delta E_{\mathrm{elec}}(t)\rangle$ increases during the time interval $t \approx 7.5$ fs and $t \approx 11.4$ fs as a result of an increase in electronic energy that occurs as trajectories hop from $- \to +$. As observed in Fig 2.12 where a very small number of trajectories hop from $+ \to -$ during the time interval between $t \approx 11.4$ fs and $t \approx 12$ fs, $\langle W^a_{\mathrm{n}\to\mathrm{e}}\rangle \approx \langle \Delta E_{\mathrm{elec}}(t)\rangle$ decreases slightly during that time interval. Following which, a large change in $\langle W^a_{\mathrm{n}\to\mathrm{e}}\rangle \approx \langle \Delta E_{\mathrm{elec}}(t)\rangle$ corresponding to the large number of trajectories hopping from $+ \to -$, was observed during the time interval between $t \approx 12$ fs and $t \approx 17.5$ fs. As in Figs 2.13 and 2.14, we also observe that $\langle W_{\mathrm{e}\to\mathrm{n}}\rangle = \langle \Delta E_{\mathrm{kin}}(t)\rangle$ perfectly offsets $\langle W^a_{\mathrm{n}\to\mathrm{e}}\rangle$, where $\langle W_{\mathrm{e}\to\mathrm{n}}\rangle + \langle W^a_{\mathrm{n}\to\mathrm{e}}\rangle = 0$.

The observation of $\langle W_{\mathrm{e}\to\mathrm{n}}\rangle + \langle W^a_{\mathrm{n}\to\mathrm{e}}\rangle = 0$ in Figs 2.13-2.15 implies that the feedback between the classical nuclear degrees of freedom and the quantum electronic degrees of freedom [3] would be properly incorporated in QTSH, ensuring that the quantum-classical energy is perfectly conserved on *average*, if surface hopping was consistent, where $\langle \rho_{++}(t)\rangle = \langle a_{++}(t)\rangle$.

As expected, we also observed that $|\langle W_{\mathrm{e}\to\mathrm{n}}(t_{\mathrm{final}})\rangle|$ in Figs 2.13 and 2.14 were approximately equal to the energy gap as summarized in Table 1.1, and the values of $\langle W_{\mathrm{e}\to\mathrm{n}}(t)\rangle$ at $t \approx 11.4$ fs in Fig 2.15 were approximately equal to the energy gap as summarized in Tables 1.2 and 1.3, for the various values of C. This agrees with our derivation of $W_{\mathrm{e}\to\mathrm{n}}$ in the limit of complete and localized population transfer (Eqn 2.46).

We now explore the surface hopping consistency and its effect on the feedback between the classical nuclear degrees of freedom and the quantum electronic degrees of freedom [3] that are responsible for properly capturing energy conservation in QTSH.

In Figs 2.16(a) and 2.17(a) we present the plots for $\langle W_{\mathrm{e}\to\mathrm{n}}(t)\rangle$, $\langle W^{\sigma}_{\mathrm{n}\to\mathrm{e}}(t)\rangle$, and $\langle W_{\mathrm{e}\to\mathrm{n}}(t)\rangle + \langle W^{a}_{\mathrm{n}\to\mathrm{e}}(t)\rangle$, and in Figs 2.16(b) and 2.17(b), we present the corresponding plots for $\langle \rho_{++}(t)\rangle$, $\langle a_{++}(t)\rangle$, and the surface hopping consistency $\langle \rho_{++}(t)\rangle - \langle a_{++}(t)\rangle$, for the simple avoided crossing system [1] for the process involving electronic transitions from the upper to the lower adiabatic surface (Fig 2.2), and from the lower to the upper adiabatic surface (Fig 2.4), respectively.

In Fig 2.18(a) we present the plot for $\langle W_{\mathrm{e}\to\mathrm{n}}(t)\rangle$, $\langle W^{\sigma}_{\mathrm{n}\to\mathrm{e}}(t)\rangle$, and $\langle W_{\mathrm{e}\to\mathrm{n}}(t)\rangle + \langle W^{a}_{\mathrm{n}\to\mathrm{e}}(t)\rangle$, and in Fig 2.18(b), we present the corresponding plots for $\langle \rho_{++}(t)\rangle$, $\langle a_{++}(t)\rangle$, and the surface hopping consistency $\langle \rho_{++}(t)\rangle - \langle a_{++}(t)\rangle$, for the dual avoided crossing system [1] with the trajectories initially populating the lower adiabatic surface, for the process depicted in Fig 2.8.

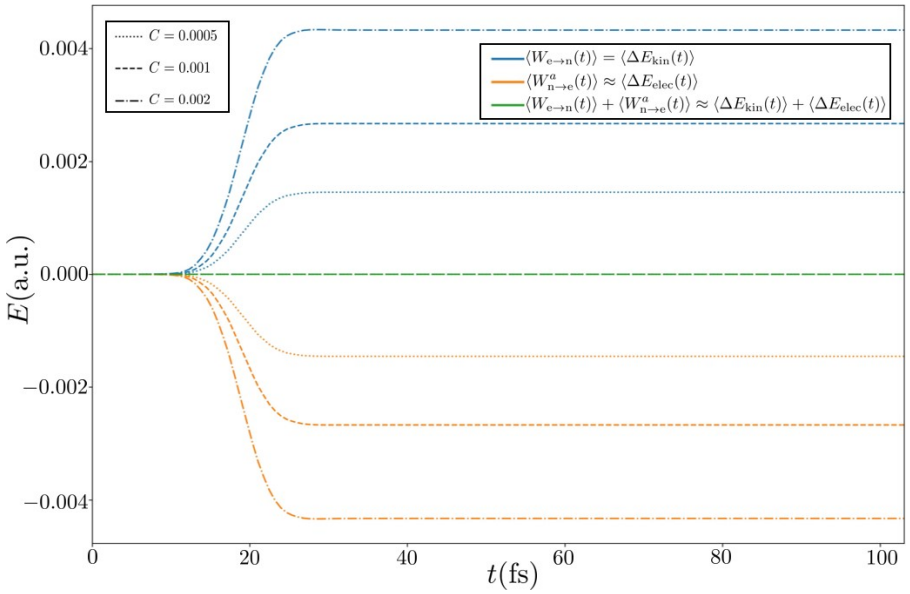

Figure 2.13: QTSH results for the phase space averaged work done by the electronic degrees of freedom on the nuclear degrees of freedom $\langle W_{e\to n}(t)\rangle$ and the work done by the nuclear degrees of freedom on the electronic degrees of freedom calculated with $\dot{a}_{++}(t)$, $\langle W^a_{n\to e}(t)\rangle$, and its sum $\langle W_{e\to n}(t)\rangle + \langle W^a_{n\to e}(t)\rangle$ for the modified Tully's simple avoided crossing system at an initial average momentum $\hbar k_0 = 15$, with the initial population on the upper surface.

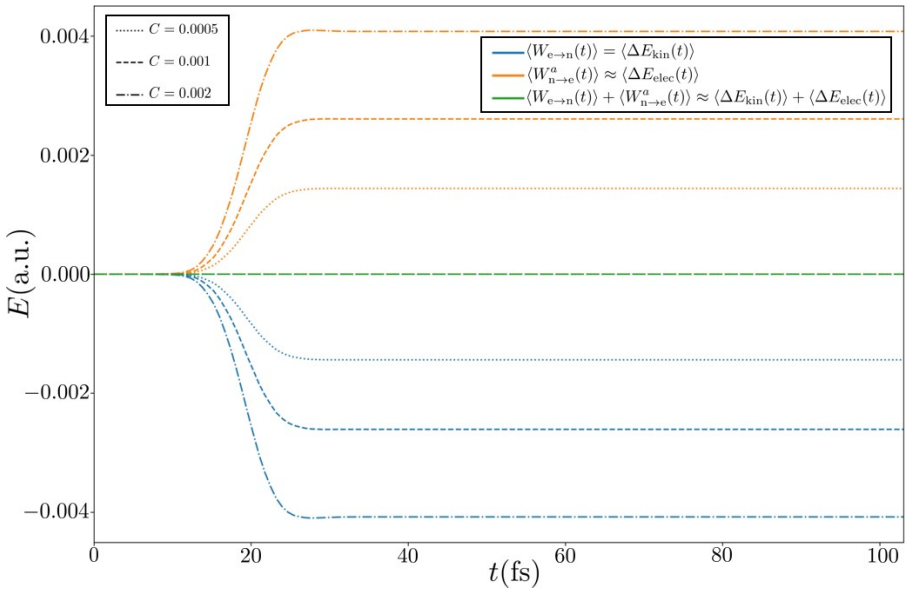

Figure 2.14: QTSH results for the phase space averaged work done by the electronic degrees of freedom on the nuclear degrees of freedom $\langle W_{e\to n}(t)\rangle$ and the work done by the nuclear degrees of freedom on the electronic degrees of freedom calculated with $\dot{a}_{++}(t)$, $\langle W^a_{n\to e}(t)\rangle$, and its sum $\langle W_{e\to n}(t)\rangle + \langle W^a_{n\to e}(t)\rangle$ for the modified Tully's simple avoided crossing system at an initial average momentum $\hbar k_0 = 15$, with the initial population on the lower surface.

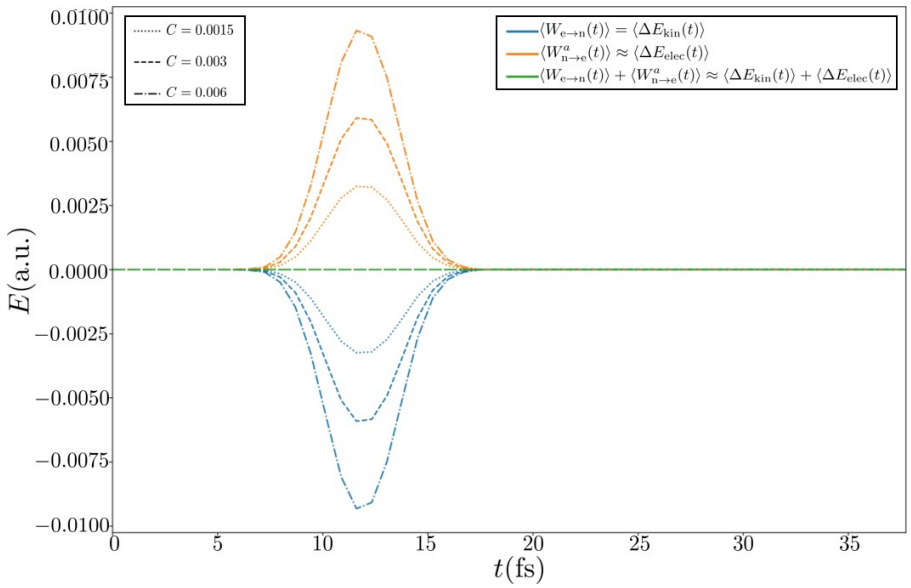

Figure 2.15: QTSH results for the phase space averaged work done by the electronic degrees of freedom on the nuclear degrees of freedom $\langle W_{e\to n}(t)\rangle$ and the work done by the nuclear degrees of freedom on the electronic degrees of freedom calculated with $\dot{a}_{++}(t)$, $\langle W^a_{n\to e}(t)\rangle$, and its sum $\langle W_{e\to n}(t)\rangle + \langle W^a_{n\to e}(t)\rangle$ for the modified Tully's dual avoided crossing system at an initial average momentum $\hbar k_0 = 40.3$, with the initial population on the lower surface.

With reference to Fig 2.16(a), and Fig 2.17(a) we observed that the sum $\langle W_{e\to n}(t)\rangle + \langle W^\sigma_{n\to e}(t)\rangle$ deviate positively from zero, and negatively from zero, respectively. We also observed that the deviation increases as C increases, with the smallest deviation when $C = 0.0005$, and the largest deviation when $C = 0.002$. This shows that the feedback between the classical nuclear degrees of freedom and the quantum electronic degrees of freedom [3] have not been properly incorporated, resulting in while good, less-than-perfect energy conservation. The deviation begins at $t \approx 10$ fs when the trajectories first start to hop, and increases in size until $t \approx 30$ fs, when the asymptotic value of $\langle \rho_{++}(t)\rangle\,(t)$ is reached in Figs 2.16(b) and 2.17(b).

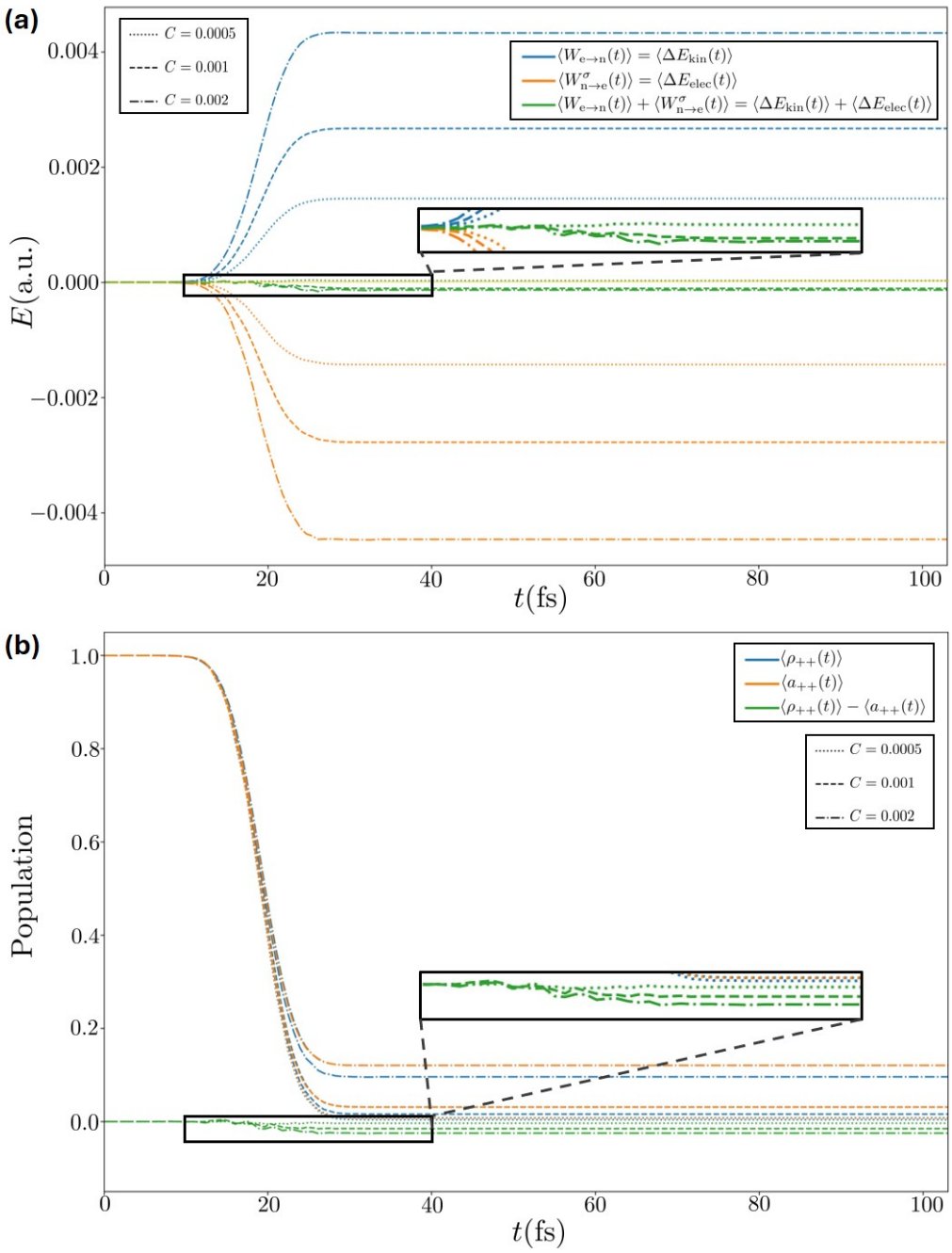

Figure 2.16: QTSH results for the phase space averaged (a) work done by the electronic degrees of freedom on the nuclear degrees of freedom $\langle W_{e\to n}(t)\rangle$ and the work done by the nuclear degrees of freedom on the electronic degrees of freedom calculated with $\Delta\sigma(t)$, $\langle W^{\sigma}_{n\to e}(t)\rangle$, its sum $\langle W_{e\to n}(t)\rangle + \langle W^{\sigma}_{n\to e}(t)\rangle$, and (b) population on the upper adiabatic PES $\langle \rho_{++}(t)\rangle$, proxy population on the upper adiabatic PES $\langle a_{++}(t)\rangle$, and the surface hopping consistency $\langle \rho_{++}(t)\rangle - \langle a_{++}(t)\rangle$ for the modified Tully's simple avoided crossing system at an initial average momentum $\hbar k_0 = 15$, with the initial population on the upper adiabatic surface. The inset shows a magnified portion of the plot for the time interval between $t = 10$ fs and $t = 40$ fs

.

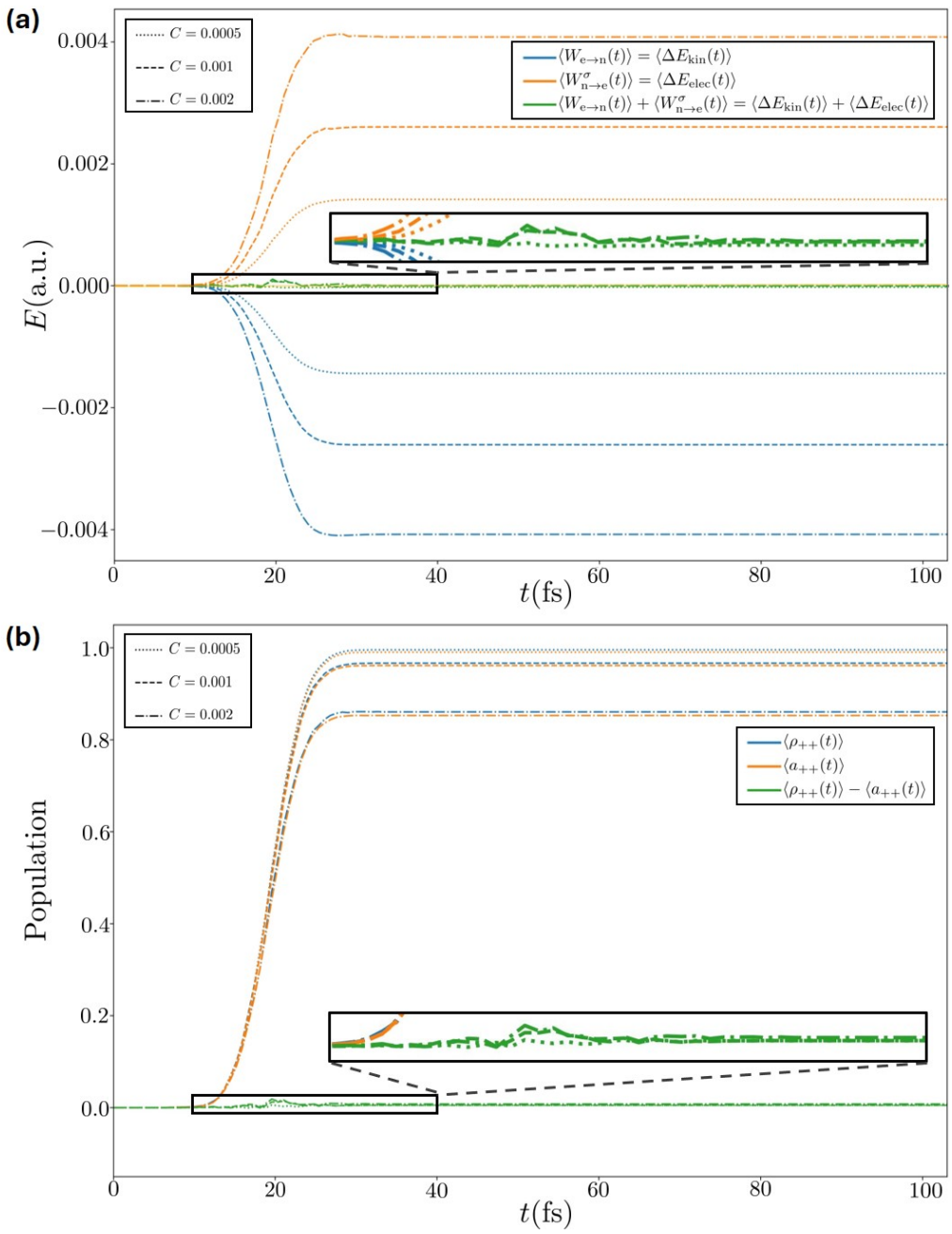

Figure 2.17: QTSH results for the phase space averaged (a) work done by the electronic degrees of freedom on the nuclear degrees of freedom $\langle W_{e\to n}(t)\rangle$ and the work done by the nuclear degrees of freedom on the electronic degrees of freedom calculated with $\Delta\sigma(t)$, $\langle W^{\sigma}_{n\to e}(t)\rangle$, its sum $\langle W_{e\to n}(t)\rangle + \langle W^{\sigma}_{n\to e}(t)\rangle$, and (b) population on the upper adiabatic PES $\langle \rho_{++}(t)\rangle$, proxy population on the upper adiabatic PES $\langle a_{++}(t)\rangle$, and the surface hopping consistency $\langle \rho_{++}(t)\rangle - \langle a_{++}(t)\rangle$ for the modified Tully's simple avoided crossing system at an initial average momentum $\hbar k_0 = 15$, with the initial population on the lower adiabatic surface. The inset shows a magnified portion of the plot for the time interval between $t = 10$ fs and $t = 40$ fs

.

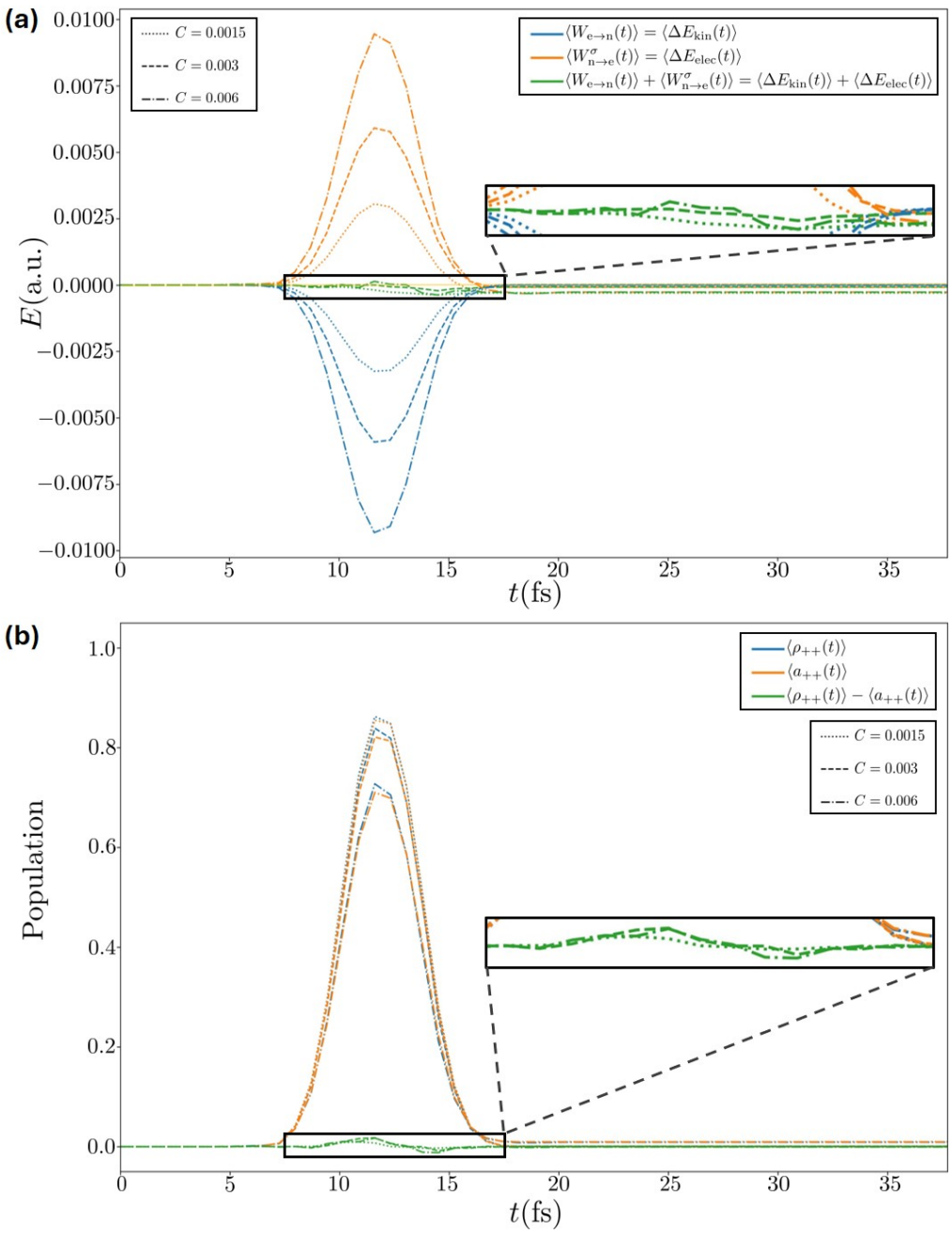

Figure 2.18: QTSH results for the phase space averaged (a) work done by the electronic degrees of freedom on the nuclear degrees of freedom $\langle W_{e\to n}(t)\rangle$ and the work done by the nuclear degrees of freedom on the electronic degrees of freedom calculated with $\Delta\sigma(t)$, $\langle W^{\sigma}_{n\to e}(t)\rangle$, its sum $\langle W_{e\to n}(t)\rangle + \langle W^{\sigma}_{n\to e}(t)\rangle$, and (b) population on the upper adiabatic PES $\langle \rho_{++}(t)\rangle$, proxy population on the upper adiabatic PES $\langle a_{++}(t)\rangle$, and the surface hopping consistency $\langle \rho_{++}(t)\rangle - \langle a_{++}(t)\rangle$ for the modified Tully's dual avoided crossing system at an initial average momentum $\hbar k_0 = 40.3$, with the initial population on the lower adiabatic surface. The inset shows a magnified portion of the plot for the time interval between $t = 7.5$ fs and $t = 17.5$ fs

.

Comparing Fig 2.16(a) with Fig 2.16(b), and Fig 2.17(a) with Fig 2.17(b), we observe that the deviation of the surface hopping consistency $\langle \rho_{++}(t) \rangle - \langle a_{++}(t) \rangle$ from zero in Figs 2.16(b) 2.17(b) match the deviation of $\langle W_{\mathrm{e}\to\mathrm{n}}(t) \rangle + \langle W^{\sigma}_{\mathrm{n}\to\mathrm{e}}(t) \rangle$ from zero. This shows that the surface hopping consistency of QTSH impacts the proper incorporation of the feedback between the classical and quantum subsystems [3] that determines the quality of energy conservation on *average*.

With reference to Fig 2.18(a) we observed that the sum $\langle W_{\mathrm{e}\to\mathrm{n}}(t) \rangle + \langle W^{\sigma}_{\mathrm{n}\to\mathrm{e}}(t) \rangle$ deviate positively from zero from $t = 10$ fs onwards. We also observed that the deviation increases as C increases, with the smallest deviation when $C = 0.0005$, and the largest deviation when $C = 0.002$. This shows that the feedback between the classical nuclear degrees of freedom and the quantum electronic degrees of freedom [3] have not been properly incorporated, resulting in while good, less-than-perfect energy conservation. The deviation begins at $t \approx 10$ fs when the trajectories first start to hop, with fluctuations until $t = 17.5$ fs, when the asymptotic value of $\langle \rho_{++}(t) \rangle \, (t)$ is reached in Fig 2.18(b).

Comparing Fig 2.18(a) with Fig 2.18(b), we observed that the deviation of the surface hopping consistency $\langle \rho_{++}(t) \rangle - \langle a_{++}(t) \rangle$ from zero in Fig 2.18(b) match the deviation of $\langle W_{\mathrm{e}\to\mathrm{n}}(t) \rangle + \langle W^{\sigma}_{\mathrm{n}\to\mathrm{e}}(t) \rangle$ from zero. This shows that the surface hopping consistency of QTSH impacts the proper incorporation of the feedback between the classical and quantum subsystems [3] that determines the quality of energy conservation on *average*.

While not perfect, there is sufficiently good feedback between the nuclear and electronic degrees of freedom in QTSH.

These results demonstrate the essentially quantitative accuracy of the QTSH method for these simple systems that involve one or two non-adiabatic transitions. We note that for these systems and initial conditions, FSSH give results that are essentially indistinguishable from the QTSH observables. Differences occur between the trajectory approaches when

processes are more non-classical, and the more "quantum" treatment of the energy budget allows QTSH to simulate such processes where the strict classical energy conservation of FSSH leads to significant errors [63].

2.5 Conclusions

In this chapter, we have investigated the energetics of mixed quantum-classical systems from the perspective provided by QTSH, where energy is conserved by the action of the quantum forces on an ensemble level. This is in contrast to FSSH where energy conservation is imposed on the trajectory level in the form of momentum jumps.

We have shown that QTSH, in the limit of complete and localized population transfer reproduce the momentum jumps of FSSH, further validating that the quantum forces in QTSH act to conserve energy on an *average* ensemble level. This more accurately reflects reality since quantum effects arise naturally as a result of the relaxation of strict classical constraints on individual trajectories [53, 54, 79]. From the perspective of the foundations of quantum mechanics, trajectories are *hidden variables*, and as Bell's theorem established [90], a faithful hidden variable theory must be *non-local*. The non-locality shows up in QTSH as the relaxation of individual trajectory energy conservation.

In the limit of localized non-adiabatic transitions, where the physical assumptions behind the FSSH algorithm becomes quantitatively valid, the momentum jumps should emerge from an exact theory. We established this connection by deriving the FSSH algorithm from the QTSH equations of motion.

For general non-adiabatic transitions that are not localized in time and space, the FSSH momentum jumps are no longer rigorously valid. Finally, we have found that the feedback between nuclear and electronic degrees of freedom, while not perfect, is well-incorporated in

QTSH, mediated by the quantum forces that work to conserve the quantum-classical energy on *average* without artificial external momentum rescaling. Improving the surface hopping consistency of QTSH would result in the improvement of the feedback between nuclear and electronic degrees of freedom, and as a result energy conservation.

Chapter 3

An Investigation of the Representation Invariance of QTSH

3.1 Introduction

In quantum trajectory surface hopping (QTSH) [62, 63], the quantum-classical description of multistate systems is derived rigorously from the quantum-classical limit of the multistate Liouville equation, the quantum-classical Liouville equation (QCLE) [38–40], within the framework of the independent trajectory approximation. QTSH in contrast to FSSH, is well-defined in both the diabatic and adiabatic representations [62, 63].

If implemented correctly, QTSH should, in principle, be representation invariant. We should be able to transform the results obtained from QTSH from one representation to another.

In this chapter, we derive the unitary transformation between the diabatic and the adiabatic representations, in terms of the populations, coherences, and forces (both classical and quantum) at the quantum-classical limit, within the framework of *independent* trajectories.

In doing so, we find the transformation between QTSH results for these quantities in the diabatic and adiabatic representations.

Finally, we perform QTSH simulations on the modified Tully's simple avoided crossing and dual avoided crossing systems [1] to test the representation invariance of QTSH [62, 63]. We will do so by running QTSH in both the diabatic and adiabatic representations, utilizing the derived equations for phase space averaged quantities to convert the QTSH results in one representation to the other representation at every timestep (Fig 3.1). We will then compare the transformed QTSH results with the results obatined directly in the representation of interest to test its invariance.

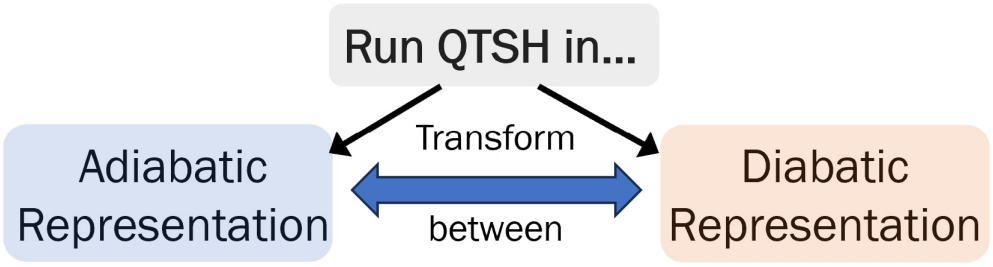

Figure 3.1: Two sets of data can be obtained to test the representation invariance of Quantum Trajectory Surface Hopping (QTSH). Running QTSH in the adiabatic representation and converting the results to the diabatic representation (a2d QTSH), and running QTSH in the diabatic representation and converting the results to the adiabatic representation (d2a QTSH).

3.2 Transformation Theory in the Quantum-Classical Limit

In this section, we derive the diabatic-to-adiabatic (d2a) unitary transformation, and the inverse adiabatic-to-diabatic (a2d) unitary transformation of the Wigner distribution [74, 75], and the Weyl functions [71] for forces - both classical and quantum.

We then incorporate the framework of independent trajectories to find the system phase space averages of the populations and coherences, and the forces - both classical and quantum, to obtain equations that can be used to transform QTSH results from one representation to another.

3.2.1 Wigner Distribution

The Wigner distribution [74, 75] in the adiabatic representation $\boldsymbol{\rho}^{\mathrm{A}}(\boldsymbol{q},\boldsymbol{p},t)$ and the diabatic representation $\boldsymbol{\rho}^{\mathrm{D}}(\boldsymbol{q},\boldsymbol{p},t)$ are related by the Weyl functions [71] of the transformation matrices $\boldsymbol{U}(\boldsymbol{q})$ and $\boldsymbol{U}^{\dagger}(\boldsymbol{q})$, similar to operators as given in Eqns 1.1-1.2, but taking the star product (Eqn 1.16) [91], in place of the matrix product, between the Weyl functions [71] and the Wigner distribution [74, 75].

This can be expressed as the diabatic-to-adiabatic (d2a) transformation,

$$\boldsymbol{\rho}^{\mathrm{A}}(\boldsymbol{q},\boldsymbol{p},t) = \boldsymbol{U}^{\dagger}(\boldsymbol{q}) \star \boldsymbol{\rho}^{\mathrm{D}}(\boldsymbol{q},\boldsymbol{p},t) \star \boldsymbol{U}(\boldsymbol{q}), \tag{3.1}$$

and the adiabatic-to-diabatic (a2d) transformation,

$$\boldsymbol{\rho}^{\mathrm{D}}(\boldsymbol{q},\boldsymbol{p},t) = \boldsymbol{U}(\boldsymbol{q}) \star \boldsymbol{\rho}^{\mathrm{A}}(\boldsymbol{q},\boldsymbol{p},t) \star \boldsymbol{U}^{\dagger}(\boldsymbol{q}). \tag{3.2}$$

For the two-state system as described in Eqn 1.20, the star product as given in Eqn 3.1 was computed to obtain the populations/diagonal elements of the d2a transformed Wigner distribution [74, 75] in the adiabatic representation $\boldsymbol{\rho}^{\mathrm{A}}(\boldsymbol{q},\boldsymbol{p},t)$, to $\mathcal{O}(\hbar^2)$, in terms of elements of $\boldsymbol{\rho}^{\mathrm{D}}(\boldsymbol{q},\boldsymbol{p},t)$.

The population/diagonal elements of the d2a transformed $\boldsymbol{\rho}^{\mathrm{A}}(\boldsymbol{q},\boldsymbol{p},t)$ were found to be

$$\begin{aligned}
\rho^{\mathrm{A}}_{++}(\boldsymbol{q},\boldsymbol{p},t) &= \frac{\rho^{\mathrm{D}}_{11}(\boldsymbol{q},\boldsymbol{p},t)+\rho^{\mathrm{D}}_{22}(\boldsymbol{q},\boldsymbol{p},t)}{2}+\frac{\rho^{\mathrm{D}}_{11}(\boldsymbol{q},\boldsymbol{p},t)-\rho^{\mathrm{D}}_{22}(\boldsymbol{q},\boldsymbol{p},t)}{2}\cos\phi(\boldsymbol{q})\\
&\quad+\alpha^{\mathrm{D}}(\boldsymbol{q},\boldsymbol{p},t)\sin\phi(\boldsymbol{q})-\hbar\boldsymbol{d}(\boldsymbol{q})\nabla_{\boldsymbol{p}}\beta^{\mathrm{D}}(\boldsymbol{q},\boldsymbol{p},t)\\
&\quad-\frac{\hbar^2}{4}\nabla_{\boldsymbol{q}}\boldsymbol{d}(\boldsymbol{q})\left(\frac{\nabla^2_{\boldsymbol{p}}\big(\rho^{\mathrm{D}}_{11}(\boldsymbol{q},\boldsymbol{p},t)-\rho^{\mathrm{D}}_{22}(\boldsymbol{q},\boldsymbol{p},t)\big)}{2}\sin\phi(\boldsymbol{q})-\nabla^2_{\boldsymbol{p}}\alpha^{\mathrm{D}}(\boldsymbol{q},\boldsymbol{p},t)\cos\phi(\boldsymbol{q})\right)\\
&\quad+\frac{\hbar^2}{2}\boldsymbol{d}^2(\boldsymbol{q})\frac{\nabla^2_{\boldsymbol{p}}\big(\rho^{\mathrm{D}}_{11}(\boldsymbol{q},\boldsymbol{p},t)+\rho^{\mathrm{D}}_{22}(\boldsymbol{q},\boldsymbol{p},t)\big)}{2}+\mathcal{O}(\hbar^3), \qquad (3.3)
\end{aligned}$$

$$\begin{aligned}
\rho^{\mathrm{A}}_{--}(\boldsymbol{q},\boldsymbol{p},t) &= \frac{\rho^{\mathrm{D}}_{11}(\boldsymbol{q},\boldsymbol{p},t)+\rho^{\mathrm{D}}_{22}(\boldsymbol{q},\boldsymbol{p},t)}{2}-\frac{\rho^{\mathrm{D}}_{11}(\boldsymbol{q},\boldsymbol{p},t)-\rho^{\mathrm{D}}_{22}(\boldsymbol{q},\boldsymbol{p},t)}{2}\cos\phi(\boldsymbol{q})\\
&\quad-\alpha^{\mathrm{D}}(\boldsymbol{q},\boldsymbol{p},t)\sin\phi(\boldsymbol{q})-\hbar\boldsymbol{d}(\boldsymbol{q})\nabla_{\boldsymbol{p}}\beta^{\mathrm{D}}(\boldsymbol{q},\boldsymbol{p},t)\\
&\quad+\frac{\hbar^2}{4}\nabla_{\boldsymbol{q}}\boldsymbol{d}(\boldsymbol{q})\left(\frac{\nabla^2_{\boldsymbol{p}}\big(\rho^{\mathrm{D}}_{11}(\boldsymbol{q},\boldsymbol{p},t)-\rho^{\mathrm{D}}_{22}(\boldsymbol{q},\boldsymbol{p},t)\big)}{2}\sin\phi(\boldsymbol{q})-\nabla^2_{\boldsymbol{p}}\alpha^{\mathrm{D}}(\boldsymbol{q},\boldsymbol{p},t)\cos\phi(\boldsymbol{q})\right)\\
&\quad+\frac{\hbar^2}{2}\boldsymbol{d}^2(\boldsymbol{q})\frac{\nabla^2_{\boldsymbol{p}}\big(\rho^{\mathrm{D}}_{11}(\boldsymbol{q},\boldsymbol{p},t)+\rho^{\mathrm{D}}_{22}(\boldsymbol{q},\boldsymbol{p},t)\big)}{2}+\mathcal{O}(\hbar^3). \qquad (3.4)
\end{aligned}$$

The coherence/off-diagonal elements of the d2a transformed $\boldsymbol{\rho}^{\mathrm{A}}(\boldsymbol{q},\boldsymbol{p},t)$ were found to be

$$\begin{aligned}
\rho^{\mathrm{A}}_{+-}(\boldsymbol{q},\boldsymbol{p},t) &= -\frac{\rho^{\mathrm{D}}_{11}(\boldsymbol{q},\boldsymbol{p},t)-\rho^{\mathrm{D}}_{22}(\boldsymbol{q},\boldsymbol{p},t)}{2}\sin\phi(\boldsymbol{q})+\alpha^{\mathrm{D}}(\boldsymbol{q},\boldsymbol{p},t)\cos\phi(\boldsymbol{q})\\
&\quad-\frac{\hbar^2}{4}\nabla_{\boldsymbol{q}}\boldsymbol{d}(\boldsymbol{q})\left(\frac{\nabla^2_{\boldsymbol{p}}\big(\rho^{\mathrm{D}}_{11}(\boldsymbol{q},\boldsymbol{p},t)-\rho^{\mathrm{D}}_{22}(\boldsymbol{q},\boldsymbol{p},t)\big)}{2}\cos\phi(\boldsymbol{q})+\nabla^2_{\boldsymbol{p}}\alpha^{\mathrm{D}}(\boldsymbol{q},\boldsymbol{p},t)\sin\phi(\boldsymbol{q})\right)\\
&\quad+i\beta^{\mathrm{D}}(\boldsymbol{q},\boldsymbol{p},t)-i\hbar\boldsymbol{d}(\boldsymbol{q})\frac{\nabla_{\boldsymbol{p}}\big(\rho^{\mathrm{D}}_{11}(\boldsymbol{q},\boldsymbol{p},t)+\rho^{\mathrm{D}}_{22}(\boldsymbol{q},\boldsymbol{p},t)\big)}{2}\\
&\quad+i\frac{\hbar^2}{2}\boldsymbol{d}^2(\boldsymbol{q})\nabla^2_{\boldsymbol{p}}\beta^{\mathrm{D}}(\boldsymbol{q},\boldsymbol{p},t)+\mathcal{O}(\hbar^3), \qquad (3.5)
\end{aligned}$$

$$
\begin{aligned}
\rho^{\mathrm{A}}_{-+}(\boldsymbol{q},\boldsymbol{p},t) &= -\frac{\rho^{\mathrm{D}}_{11}(\boldsymbol{q},\boldsymbol{p},t)-\rho^{\mathrm{D}}_{22}(\boldsymbol{q},\boldsymbol{p},t)}{2}\sin\phi(\boldsymbol{q})+\alpha^{\mathrm{D}}(\boldsymbol{q},\boldsymbol{p},t)\cos\phi(\boldsymbol{q}) \\
&\quad -\frac{\hbar^2}{4}\nabla_{\boldsymbol{q}}\boldsymbol{d}(\boldsymbol{q})\left(\frac{\nabla^2_{\boldsymbol{p}}\big(\rho^{\mathrm{D}}_{11}(\boldsymbol{q},\boldsymbol{p},t)-\rho^{\mathrm{D}}_{22}(\boldsymbol{q},\boldsymbol{p},t)\big)}{2}\cos\phi(\boldsymbol{q})+\nabla^2_{\boldsymbol{p}}\alpha^{\mathrm{D}}(\boldsymbol{q},\boldsymbol{p},t)\sin\phi(\boldsymbol{q})\right) \\
&\quad -i\beta^{\mathrm{D}}(\boldsymbol{q},\boldsymbol{p},t)+i\hbar\boldsymbol{d}(\boldsymbol{q})\frac{\nabla_{\boldsymbol{p}}\big(\rho^{\mathrm{D}}_{11}(\boldsymbol{q},\boldsymbol{p},t)+\rho^{\mathrm{D}}_{22}(\boldsymbol{q},\boldsymbol{p},t)\big)}{2} \\
&\quad -i\frac{\hbar^2}{2}\boldsymbol{d}^2(\boldsymbol{q})\nabla^2_{\boldsymbol{p}}\beta^{\mathrm{D}}(\boldsymbol{q},\boldsymbol{p},t)+\mathcal{O}(\hbar^3), \qquad (3.6)
\end{aligned}
$$

where $\mathrm{Re}\left(\rho^{\mathrm{A}}_{+-}(\boldsymbol{q},\boldsymbol{p},t)\right)=\mathrm{Re}\left(\rho^{\mathrm{A}}_{-+}(\boldsymbol{q},\boldsymbol{p},t)\right)=\alpha^{\mathrm{A}}(\boldsymbol{q},\boldsymbol{p},t)$, and
$\mathrm{Im}\left(\rho^{\mathrm{A}}_{+-}(\boldsymbol{q},\boldsymbol{p},t)\right)=-\mathrm{Im}\left(\rho^{\mathrm{A}}_{-+}(\boldsymbol{q},\boldsymbol{p},t)\right)=\beta^{\mathrm{A}}(\boldsymbol{q},\boldsymbol{p},t)$.

The details of this Wigner-Moyal [91] transformation are documented in Appendix B.1. To $\mathcal{O}(\hbar^0)$, the results agree with the findings in Ref [76].

With reference to Eqns 3.1 and 3.2, we observed that the unitary transformation for the adiabatic-to-diabatic (a2d) transformation was the inverse of the of diabatic-to-adiabatic (d2a) transformation.

Since the unitary matrix for the two-state system given by Eqn 1.6 consists of sines and cosines of half the transformation angle $\frac{\phi(\boldsymbol{q})}{2}$, the a2d transformation of the Wigner distribution [74, 75] was performed by replacing the transformation angle $\phi(\boldsymbol{q})$ in the d2a equations (Eqns 3.4-3.6) with the negative of the transformation angle $-\phi(\boldsymbol{q})$.

Since cosine is an even function, and sine is an odd function,

$$
\begin{aligned}
\cos\big(-\phi(\boldsymbol{q})\big) &= \cos\phi(\boldsymbol{q}), \qquad (3.7)\\
\sin\big(-\phi(\boldsymbol{q})\big) &= -\sin\phi(\boldsymbol{q}). \qquad (3.8)
\end{aligned}
$$

Utilizing the above, we found the population/diagonal elements of the a2d transformed Wigner distribution [74, 75] in the diabatic representation $\rho^{\mathrm{D}}(\boldsymbol{q},\boldsymbol{p},t)$ to $\mathcal{O}(\hbar^2)$, in terms of elements of $\rho^{\mathrm{A}}(\boldsymbol{q},\boldsymbol{p},t)$ to be

$$\begin{aligned}
\rho^{\mathrm{D}}_{11}(\boldsymbol{q},\boldsymbol{p},t) &= \frac{\rho^{\mathrm{A}}_{++}(\boldsymbol{q},\boldsymbol{p},t)+\rho^{\mathrm{A}}_{--}(\boldsymbol{q},\boldsymbol{p},t)}{2}+\frac{\rho^{\mathrm{A}}_{++}(\boldsymbol{q},\boldsymbol{p},t)-\rho^{\mathrm{A}}_{--}(\boldsymbol{q},\boldsymbol{p},t)}{2}\cos\phi(\boldsymbol{q})\\
&-\alpha^{\mathrm{A}}(\boldsymbol{q},\boldsymbol{p},t)\sin\phi(\boldsymbol{q})-\hbar\boldsymbol{d}(\boldsymbol{q})\nabla_{\boldsymbol{p}}\beta^{\mathrm{A}}(\boldsymbol{q},\boldsymbol{p},t)\\
&+\frac{\hbar^2}{4}\nabla_{\boldsymbol{q}}\boldsymbol{d}(\boldsymbol{q})\bigg(\frac{\nabla^2_{\boldsymbol{p}}\big(\rho^{\mathrm{A}}_{++}(\boldsymbol{q},\boldsymbol{p},t)-\rho^{\mathrm{A}}_{--}(\boldsymbol{q},\boldsymbol{p},t)\big)}{2}\sin\phi(\boldsymbol{q})+\nabla^2_{\boldsymbol{p}}\alpha^{\mathrm{A}}(\boldsymbol{q},\boldsymbol{p},t)\cos\phi(\boldsymbol{q})\bigg)\\
&+\frac{\hbar^2}{2}\boldsymbol{d}^2(\boldsymbol{q})\frac{\nabla^2_{\boldsymbol{p}}\big(\rho^{\mathrm{A}}_{++}(\boldsymbol{q},\boldsymbol{p},t)+\rho^{\mathrm{A}}_{--}(\boldsymbol{q},\boldsymbol{p},t)\big)}{2}+\mathcal{O}(\hbar^3), \qquad (3.9)
\end{aligned}$$

$$\begin{aligned}
\rho^{\mathrm{D}}_{22}(\boldsymbol{q},\boldsymbol{p},t) &= \frac{\rho^{\mathrm{A}}_{++}(\boldsymbol{q},\boldsymbol{p},t)+\rho^{\mathrm{A}}_{--}(\boldsymbol{q},\boldsymbol{p},t)}{2}-\frac{\rho^{\mathrm{A}}_{++}(\boldsymbol{q},\boldsymbol{p},t)-\rho^{\mathrm{A}}_{--}(\boldsymbol{q},\boldsymbol{p},t)}{2}\cos\phi(\boldsymbol{q})\\
&+\alpha^{\mathrm{A}}(\boldsymbol{q},\boldsymbol{p},t)\sin\phi(\boldsymbol{q})-\hbar\boldsymbol{d}(\boldsymbol{q})\nabla_{\boldsymbol{p}}\beta^{\mathrm{A}}(\boldsymbol{q},\boldsymbol{p},t)\\
&-\frac{\hbar^2}{4}\nabla_{\boldsymbol{q}}\boldsymbol{d}(\boldsymbol{q})\bigg(\frac{\nabla^2_{\boldsymbol{p}}\big(\rho^{\mathrm{A}}_{++}(\boldsymbol{q},\boldsymbol{p},t)-\rho^{\mathrm{A}}_{--}(\boldsymbol{q},\boldsymbol{p},t)\big)}{2}\sin\phi(\boldsymbol{q})+\nabla^2_{\boldsymbol{p}}\alpha^{\mathrm{A}}(\boldsymbol{q},\boldsymbol{p},t)\cos\phi(\boldsymbol{q})\bigg)\\
&+\frac{\hbar^2}{2}\boldsymbol{d}^2(\boldsymbol{q})\frac{\nabla^2_{\boldsymbol{p}}\big(\rho^{\mathrm{A}}_{++}(\boldsymbol{q},\boldsymbol{p},t)+\rho^{\mathrm{A}}_{--}(\boldsymbol{q},\boldsymbol{p},t)\big)}{2}+\mathcal{O}(\hbar^3). \qquad (3.10)
\end{aligned}$$

The coherence/off-diagonal elements of the a2d transformed Wigner distribution [74, 75] in the diabatic representation $\rho^{\mathrm{D}}(\boldsymbol{q},\boldsymbol{p},t)$, to $\mathcal{O}(\hbar^2)$, in terms of elements of $\rho^{\mathrm{A}}(\boldsymbol{q},\boldsymbol{p},t)$ were found to be

$$\begin{aligned}
\rho^{\mathrm{D}}_{12}(\boldsymbol{q},\boldsymbol{p},t) &= \frac{\rho^{\mathrm{A}}_{++}(\boldsymbol{q},\boldsymbol{p},t)-\rho^{\mathrm{A}}_{--}(\boldsymbol{q},\boldsymbol{p},t)}{2}\sin\phi(\boldsymbol{q})+\alpha^{\mathrm{A}}(\boldsymbol{q},\boldsymbol{p},t)\cos\phi(\boldsymbol{q})\\
&-\frac{\hbar^2}{4}\nabla_{\boldsymbol{q}}\boldsymbol{d}(\boldsymbol{q})\bigg(\frac{\nabla^2_{\boldsymbol{p}}\big(\rho^{\mathrm{A}}_{++}(\boldsymbol{q},\boldsymbol{p},t)-\rho^{\mathrm{A}}_{--}(\boldsymbol{q},\boldsymbol{p},t)\big)}{2}\cos\phi(\boldsymbol{q})-\nabla^2_{\boldsymbol{p}}\alpha^{\mathrm{A}}(\boldsymbol{q},\boldsymbol{p},t)\sin\phi(\boldsymbol{q})\bigg)\\
&+i\beta^{\mathrm{A}}(\boldsymbol{q},\boldsymbol{p},t)-i\hbar\boldsymbol{d}(\boldsymbol{q})\frac{\nabla_{\boldsymbol{p}}\big(\rho^{\mathrm{A}}_{++}(\boldsymbol{q},\boldsymbol{p},t)+\rho^{\mathrm{A}}_{--}(\boldsymbol{q},\boldsymbol{p},t)\big)}{2}\\
&+i\frac{\hbar^2}{2}\boldsymbol{d}^2(\boldsymbol{q})\nabla^2_{\boldsymbol{p}}\beta^{\mathrm{A}}(\boldsymbol{q},\boldsymbol{p},t)+\mathcal{O}(\hbar^3), \qquad (3.11)
\end{aligned}$$

$$\begin{aligned}\rho_{21}^{\mathrm{D}}(\boldsymbol{q},\boldsymbol{p},t) &= \frac{\rho_{++}^{\mathrm{A}}(\boldsymbol{q},\boldsymbol{p},t)-\rho_{--}^{\mathrm{A}}(\boldsymbol{q},\boldsymbol{p},t)}{2}\sin\phi(\boldsymbol{q})+\alpha^{\mathrm{A}}(\boldsymbol{q},\boldsymbol{p},t)\cos\phi(\boldsymbol{q})\\ &\quad -\frac{\hbar^2}{4}\nabla_{\boldsymbol{q}}\boldsymbol{d}(\boldsymbol{q})\Bigg(\frac{\nabla_{\boldsymbol{p}}^2\big(\rho_{++}^{\mathrm{A}}(\boldsymbol{q},\boldsymbol{p},t)-\rho_{--}^{\mathrm{A}}(\boldsymbol{q},\boldsymbol{p},t)\big)}{2}\cos\phi(\boldsymbol{q})-\nabla_{\boldsymbol{p}}^2\alpha^{\mathrm{A}}(\boldsymbol{q},\boldsymbol{p},t)\sin\phi(\boldsymbol{q})\Bigg)\\ &\quad -i\beta^{\mathrm{A}}(\boldsymbol{q},\boldsymbol{p},t)+i\hbar\boldsymbol{d}(\boldsymbol{q})\frac{\nabla_{\boldsymbol{p}}\big(\rho_{++}^{\mathrm{A}}(\boldsymbol{q},\boldsymbol{p},t)+\rho_{--}^{\mathrm{A}}(\boldsymbol{q},\boldsymbol{p},t)\big)}{2}\\ &\quad -i\frac{\hbar^2}{2}\boldsymbol{d}^2(\boldsymbol{q})\nabla_{\boldsymbol{p}}^2\beta^{\mathrm{A}}(\boldsymbol{q},\boldsymbol{p},t)+\mathcal{O}(\hbar^3),\end{aligned} \tag{3.12}$$

where $\mathrm{Re}\left(\rho_{12}^{\mathrm{D}}(\boldsymbol{q},\boldsymbol{p},t)\right)=\mathrm{Re}\left(\rho_{21}^{\mathrm{D}}(\boldsymbol{q},\boldsymbol{p},t)\right)=\alpha^{\mathrm{D}}(\boldsymbol{q},\boldsymbol{p},t)$, and
$\mathrm{Im}\left(\rho_{12}^{\mathrm{A}}(\boldsymbol{q},\boldsymbol{p},t)\right)=-\mathrm{Im}\left(\rho_{21}^{\mathrm{A}}(\boldsymbol{q},\boldsymbol{p},t)\right)=\beta^{\mathrm{D}}(\boldsymbol{q},\boldsymbol{p},t)$.

As QTSH is carried out within the framework of *independent* trajectories, the phase space averages of a quantity for each trajectory were found at every timestep, and the average of its sum was taken to be system phase space average of the quantity.

The phase space averaged elements of the Wigner distributions [74, 75] for each *independent* trajectory $\langle\rho_{ik,j}(t)\rangle$ were found by taking the integral over phase space given by

$$\begin{aligned}\langle\rho_{ik,j}(t)\rangle &= \int\int\rho_{ik}(\boldsymbol{q}_j,\boldsymbol{p}_j,t)\mathrm{d}\boldsymbol{q}\mathrm{d}\boldsymbol{p}\\ &= \int\int\rho_{ik,j}(t)\delta\big(\boldsymbol{q}-\boldsymbol{q}_j(t)\big)\delta\big(\boldsymbol{p}-\boldsymbol{p}_j(t)\big)\mathrm{d}\boldsymbol{q}\mathrm{d}\boldsymbol{p},\end{aligned} \tag{3.13}$$

and the phase space averaged elements of the Wigner distributions [74, 75] for the system $\langle\rho_{ik}(t)\rangle$ were found by taking the average of the trajectory averages,

$$\langle\rho_{ik}(t)\rangle=\frac{1}{N}\sum_{j}^{N}\langle\rho_{ik,j}(t)\rangle\,. \tag{3.14}$$

To $\mathcal{O}(\hbar^0)$, the trajectory phase space averaged element $\left\langle \rho^{\mathrm{A}}_{++,j}(\boldsymbol{q},\boldsymbol{p},t)\right\rangle$ for the element $\rho^{\mathrm{A}}_{++}(\boldsymbol{q},\boldsymbol{p},t)$ of the d2a transformed Wigner distribution given by Eqn 3.4, in terms of the elements of the Wigner distribution of the trajectories in the diabatic representation given by Eqns 1.36-1.38 was found to be

$$\begin{aligned}
\sigma^{\mathrm{A}}_j(t) &= \left\langle \rho^{\mathrm{A}}_{++,j}(t)\right\rangle \\
&= \int\int \left(\frac{1}{2} + \frac{2\sigma^{\mathrm{D}}_j(t)-1}{2}\cos\phi(\boldsymbol{q}) + \alpha^{\mathrm{D}}_j(t)\sin\phi(\boldsymbol{q})\right)\delta\big(\boldsymbol{q}-\boldsymbol{q}_j(t)\big)\delta\big(\boldsymbol{p}-\boldsymbol{p}_j(t)\big)\mathrm{d}\boldsymbol{q}\mathrm{d}\boldsymbol{p} + \mathcal{O}(\hbar) \\
&= \frac{1}{2} + \frac{2\sigma^{\mathrm{D}}_j(t)-1}{2}\cos\phi(\boldsymbol{q}_j) + \alpha^{\mathrm{D}}_j(t)\sin\phi(\boldsymbol{q}_j) + \mathcal{O}(\hbar). \qquad (3.15)
\end{aligned}$$

Similarly, to $\mathcal{O}(\hbar^0)$ the trajectory phase space averages of the other elements of the d2a transformed Wigner distribution in the adiabatic representation were found to be

$$\begin{aligned}
1-\sigma^{\mathrm{A}}_j(t) &= \left\langle \rho^{\mathrm{A}}_{--,j}(t)\right\rangle \\
&= \frac{1}{2} - \frac{2\sigma^{\mathrm{D}}_j(t)-1}{2}\cos\phi(\boldsymbol{q}_j) - \alpha^{\mathrm{D}}_j(t)\sin\phi(\boldsymbol{q}_j) + \mathcal{O}(\hbar), \qquad (3.16) \\
\alpha^{\mathrm{A}}_j(t) &= \left\langle \frac{\rho^{\mathrm{A}}_{+-,j}(t)+\rho^{\mathrm{A}}_{-+,j}(t)}{2}\right\rangle \\
&= \frac{2\sigma^{\mathrm{D}}_j(t)-1}{2}\sin\phi(\boldsymbol{q}_j) + \alpha^{\mathrm{D}}_j(t)\cos\phi(\boldsymbol{q}_j) + \mathcal{O}(\hbar), \qquad (3.17) \\
\beta^{\mathrm{A},j}(t) &= -i\left\langle \frac{\rho^{\mathrm{A}}_{+-,j}(t)-\rho^{\mathrm{A}}_{-+,j}(t)}{2}\right\rangle \\
&= \beta^{\mathrm{D}}_j(t) + \mathcal{O}(\hbar). \qquad (3.18)
\end{aligned}$$

The system phase space average of the d2a transformed Wigner distribution element $\rho^{\mathrm{A}}_{++}(\boldsymbol{q},\boldsymbol{p},t)$ in the framework of independent trajectories, $\left\langle \rho^{\mathrm{A}}_{++}(t)\right\rangle$ was the average over all trajectories,

$$\begin{aligned}\left\langle \rho^{\mathrm{A}}_{++}(t)\right\rangle &= \frac{1}{N}\sum_{j}^{N}\sigma^{\mathrm{A}}_{j}(t) \\ &= \frac{1}{N}\sum_{j}^{N}\left(\frac{1}{2}+\frac{2\sigma^{\mathrm{D}}_{j}(t)-1}{2}\cos\phi(\boldsymbol{q}_j)+\alpha^{\mathrm{D}}_{j}(t)\sin\phi(\boldsymbol{q}_j)\right)+\mathcal{O}(\hbar). \end{aligned} \tag{3.19}$$

The same procedure was performed on the other elements of the d2a transformed Wigner distribution in the adiabatic representation. The system phase space averages of the other elements of the d2a transformed Wigner distribution were found, to $\mathcal{O}(\hbar^0)$, to be

$$\left\langle \rho^{\mathrm{A}}_{--}(t)\right\rangle = \frac{1}{N}\sum_{j}\left(\frac{1}{2}-\frac{2\sigma^{\mathrm{D}}_{j}(t)-1}{2}\cos\phi(\boldsymbol{q}_j)-\alpha^{\mathrm{D}}_{j}(t)\sin\phi(\boldsymbol{q}_j)\right)+\mathcal{O}(\hbar), \tag{3.20}$$

$$\left\langle \alpha^{\mathrm{A}}(t)\right\rangle = \frac{1}{N}\sum_{j}\left(-\frac{2\sigma^{\mathrm{D}}_{j}(t)-1}{2}\sin\phi(\boldsymbol{q}_j)+\alpha^{\mathrm{D}}_{j}(t)\cos\phi(\boldsymbol{q}_j)\right)+\mathcal{O}(\hbar), \tag{3.21}$$

$$\left\langle \beta^{\mathrm{A}}(t)\right\rangle = \frac{1}{N}\sum_{j}\beta^{\mathrm{D}}_{j}(t)+\mathcal{O}(\hbar). \tag{3.22}$$

By substituting Eqns 3.7-3.8 into Eqns 3.19-3.22, we found the system phase space averages of the a2d transformed Wigner distribution [74, 75], to $\mathcal{O}(\hbar^0)$, to be

$$\left\langle \rho^{\mathrm{D}}_{11}(t)\right\rangle = \frac{1}{N}\sum_{j}^{N}\left(\frac{1}{2}+\frac{2\sigma^{\mathrm{A}}_{j}(t)-1}{2}\cos\phi(\boldsymbol{q}_j)-\alpha^{\mathrm{A}}_{j}(t)\sin\phi(\boldsymbol{q}_j)\right)+\mathcal{O}(\hbar), \tag{3.23}$$

$$\left\langle \rho^{\mathrm{D}}_{22}(t)\right\rangle = \frac{1}{N}\sum_{j}\left(\frac{1}{2}-\frac{2\sigma^{\mathrm{A}}_{j}(t)-1}{2}\cos\phi(\boldsymbol{q}_j)+\alpha^{\mathrm{A}}_{j}(t)\sin\phi(\boldsymbol{q}_j)\right)+\mathcal{O}(\hbar), \tag{3.24}$$

$$\left\langle \alpha^{\mathrm{D}}(t) \right\rangle = \frac{1}{N} \sum_{j} \left(\frac{2\sigma_j^{\mathrm{A}}(t) - 1}{2} \sin \phi(\boldsymbol{q}_j) + \alpha_j^{\mathrm{A}}(t) \cos \phi(\boldsymbol{q}_j) \right) + \mathcal{O}(\hbar), \tag{3.25}$$

$$\left\langle \beta^{\mathrm{D}}(t) \right\rangle = \frac{1}{N} \sum_{j} \beta_j^{\mathrm{A}}(t) + \mathcal{O}(\hbar). \tag{3.26}$$

In performing these derivations, we have assumed that the trajectories in both the diabatic and adiabatic representations are represented by the same delta functions $\delta\big(\boldsymbol{q} - \boldsymbol{q}_j(t)\big)\delta\big(\boldsymbol{p} - \boldsymbol{p}_j(t)\big)$. Making this assumption does not impact the transformed Wigner distribution [74, 75] to $\mathcal{O}(\hbar^0)$, but does not hold when higher order terms are included in the transformation.

Preliminary work done on the transformation theory of independent trajectories by Martens [92] will be briefly introduced in Section 3.6.

3.2.2 Forces

The classical forces in QTSH [62, 63] are related to the negative gradient of the diagonal elements of the Weyl functions [71] for potential energy, and the quantum forces in QTSH [62, 63] are related to the coupling of the nuclear and electronic degrees of freedom that are associated with the off-diagonal elements of the Hamiltonian and the off-diagonal elements/coherences of the Wigner distribution [74, 75].

We first perform the d2a unitary and the inverse a2d unitary transformation on the Weyl functions [71] for potential energy, before taking its negative gradient to obtain the Weyl functions [71] for is corresponding force.

The 2×2 Weyl function [71] for the potential energy of the two-state system in the diabatic representation $\boldsymbol{V}^{\mathrm{D}}(\boldsymbol{q})$, can be represented in terms of diabatic potentials as

$$\boldsymbol{V}^{\mathrm{D}}(\boldsymbol{q}) = \begin{pmatrix} V_1(\boldsymbol{q}) & V_{12}(\boldsymbol{q}) \\ V_{12}(\boldsymbol{q}) & V_2(\boldsymbol{q}) \end{pmatrix}. \tag{3.27}$$

Since $\boldsymbol{V}^{\mathrm{D}}(\boldsymbol{q})$ only depends on $\boldsymbol{q}$, the star product (Eqn 1.16) [91] of the d2a unitary transformation of the Weyl function [71] given by Eqn 3.1 was equivalent to the matrix product

$$\boldsymbol{V}^{\mathrm{A}}(\boldsymbol{q}) \;=\; \boldsymbol{U}^{\dagger}(\boldsymbol{q})\boldsymbol{V}^{\mathrm{D}}(\boldsymbol{q})\boldsymbol{U}(\boldsymbol{q}) = \begin{pmatrix} V_+(\boldsymbol{q}) & 0 \\ 0 & V_-(\boldsymbol{q}) \end{pmatrix}, \tag{3.28}$$

where

$$V_{\pm}(\boldsymbol{q}) = \frac{V_1(\boldsymbol{q}) + V_2(\boldsymbol{q})}{2} \pm \left(\frac{V_1(\boldsymbol{q}) - V_2(\boldsymbol{q})}{2} \cos\phi(\boldsymbol{q}) + V_{12} \sin\phi(\boldsymbol{q}) \right), \tag{3.29}$$

and

$$V_{+-}(\boldsymbol{q}) = V_{-+}(\boldsymbol{q}) = -\frac{V_1(\boldsymbol{q}) - V_2(\boldsymbol{q})}{2} \sin\phi(\boldsymbol{q}) + V_{12}(\boldsymbol{q}) \cos\phi(\boldsymbol{q}) = 0. \tag{3.30}$$

As in the case of $\boldsymbol{V}^{\mathrm{D}}(\boldsymbol{q})$, $\boldsymbol{V}^{\mathrm{A}}(\boldsymbol{q})$ only depends on $\boldsymbol{q}$. Consequently, the star product (Eqn 1.16) [91] of the inverse a2d unitary transformation of the Weyl function [71] given by Eqn 3.2 was the matrix product

$$\boldsymbol{V}^{\mathrm{D}}(\boldsymbol{q}) \;=\; \boldsymbol{U}^{\dagger}(\boldsymbol{q})\boldsymbol{V}^{\mathrm{A}}(\boldsymbol{q})\boldsymbol{U}(\boldsymbol{q}) = \begin{pmatrix} V_1(\boldsymbol{q}) & V_{12}(\boldsymbol{q}) \\ V_{12}(\boldsymbol{q}) & V_2(\boldsymbol{q}) \end{pmatrix}, \tag{3.31}$$

where

$$V_{1/2}(\boldsymbol{q}) = \frac{V_+(\boldsymbol{q}) + V_-(\boldsymbol{q})}{2} \pm \frac{V_+(\boldsymbol{q}) - V_-(\boldsymbol{q})}{2} \cos\phi(\boldsymbol{q}), \tag{3.32}$$

and

$$V_{12}(\boldsymbol{q}) = \frac{V_+(\boldsymbol{q}) - V_-(\boldsymbol{q})}{2} \sin\phi(\boldsymbol{q}). \tag{3.33}$$

Having found the d2a and a2d transformed Weyl functions [71] for the potential energy in the adiabatic and diabatic representations, $\boldsymbol{V}^{\mathrm{A}}(\boldsymbol{q})$ and $\boldsymbol{V}^{\mathrm{D}}(\boldsymbol{q})$, respectively, we now find the corresponding d2a and a2d transformed Weyl functions [71] for the classical, quantum and total forces in the adiabatic and diabatic representations.

The d2a transformed Weyl function [71] for the classical force $\boldsymbol{F}^{\mathrm{A}}_{\mathrm{class}}(\boldsymbol{q})$ for the two-state system in the adiabatic representation was obtained by taking the negative gradient of the d2a transformed Weyl function [71] of the diagonal adiabatic potential $\boldsymbol{V}^{\mathrm{A}}(\boldsymbol{q})$ as given in Eqn 3.28

$$\boldsymbol{F}^{\mathrm{A}}_{\mathrm{class}}(\boldsymbol{q}) = -\nabla_{\boldsymbol{q}} \boldsymbol{V}^{\mathrm{A}}(\boldsymbol{q}) = \begin{pmatrix} \boldsymbol{F}_+(\boldsymbol{q}) & 0 \\ 0 & \boldsymbol{F}_-(\boldsymbol{q}) \end{pmatrix}, \tag{3.34}$$

where $\boldsymbol{F}_\pm(\boldsymbol{q}) = -\nabla_{\boldsymbol{q}} V_\pm(\boldsymbol{q})$.

Since $\boldsymbol{V}^{\mathrm{A}}(\boldsymbol{q})$ for the two-state system is diagonal, only the classical force in the adiabatic representation $\boldsymbol{F}^{\mathrm{A}}_{\mathrm{class}}(\boldsymbol{q})$ is related to $\boldsymbol{V}^{\mathrm{A}}(\boldsymbol{q})$.

The d2a transformed elements of the Weyl function $\boldsymbol{F}^{\mathrm{A}}_{\mathrm{class}}(\boldsymbol{q})$ in terms of diabatic potentials was obtained by taking the negative gradient of the adiabatic potential given by Eqn 3.29, giving the expression

$$\begin{aligned}\boldsymbol{F}^{\mathrm{A}}_{\pm}(\boldsymbol{q}) &= -\frac{\nabla_{\boldsymbol{q}}V_1(\boldsymbol{q})+\nabla_{\boldsymbol{q}}V_2(\boldsymbol{q})}{2} \\ &\quad \mp\left(\frac{\nabla_{\boldsymbol{q}}V_1(\boldsymbol{q})-\nabla_{\boldsymbol{q}}V_2(\boldsymbol{q})}{2}\cos\phi(\boldsymbol{q})+\nabla_{\boldsymbol{q}}V_{12}(\boldsymbol{q})\sin\phi(\boldsymbol{q})\right). \end{aligned} \tag{3.35}$$

Since Weyl function of the adiabatic potential (Eqn 3.28) is diagonal, the adiabatic quantum force arises from the off-diagonal elements of the Weyl function [71] for kinetic energy in the adiabatic representation, which is closely related to the momentum in the adiabatic representation $\boldsymbol{p}^{\mathrm{A}}(\boldsymbol{q},\boldsymbol{p})$.

The Weyl function [71] for momentum in the adiabatic representation $\boldsymbol{p}^{\mathrm{A}}(\boldsymbol{q},\boldsymbol{p})$ can be split into its diagonal and off-diagonal components

$$\boldsymbol{p}^{\mathrm{A}}_{\mathrm{diag}}+\boldsymbol{p}^{\mathrm{A}}_{\text{off-diag}}, \tag{3.36}$$

where

$$\boldsymbol{p}^{\mathrm{A}}_{\mathrm{diag}}=\begin{pmatrix}\boldsymbol{p} & 0\\ 0 & \boldsymbol{p}\end{pmatrix}, \tag{3.37}$$

and

$$\boldsymbol{p}^{\mathrm{A}}_{\text{off-diag}}=\begin{pmatrix}0 & -i\hbar\boldsymbol{d}(\boldsymbol{q})\\ i\hbar\boldsymbol{d}(\boldsymbol{q}) & 0\end{pmatrix}. \tag{3.38}$$

We note that the off-diagonal elements of the Weyl function [71] for momentum in the adiabatic representation $\boldsymbol{p}^{\mathrm{A}}_{\text{off-diag}}$ contains the non-adiabatic coupling vector $\boldsymbol{d}(\boldsymbol{q})$ that couples the electronic and nuclear degrees of freedom.

The trajectory phase space averaged off-diagonal momentum within the independent trajectory framework was found to be

$$\begin{aligned} \boldsymbol{p}^{\mathrm{A}}_{\text{off-diag,j}}(t) &= \mathrm{Tr}\left(\boldsymbol{p}^{\mathrm{A}}_{\text{off-diag}}\boldsymbol{\rho}^{\mathrm{A}}(\boldsymbol{q}_j,\boldsymbol{p}_j,t)\right) \\ &= -2\hbar\boldsymbol{d}(\boldsymbol{q}_j)\beta^{\mathrm{A}}_j(t), \end{aligned} \tag{3.39}$$

where $\boldsymbol{\rho}^{\mathrm{A}}(\boldsymbol{q}_j,\boldsymbol{p}_j,t) = \boldsymbol{\rho}^{\mathrm{A}}_j(t)\delta\big(\boldsymbol{q}-\boldsymbol{q}_j(t)\big)\delta\big(\boldsymbol{p}-\boldsymbol{p}_j(t)\big)$, and $\boldsymbol{\rho}^{\mathrm{A}}_j(t) = \begin{pmatrix} \sigma^{\mathrm{A}}_j(t) & \alpha^{\mathrm{A}}_j(t)+i\beta^{\mathrm{A}}_j(t) \\ \alpha^{\mathrm{A}}_j(t)-i\beta^{\mathrm{A}}_j(t) & 1-\sigma^{\mathrm{A}}_j(t) \end{pmatrix}$.

Since force is the time-derivative of momentum, the time-derivative of the off-diagonal momentum associated with the coherence terms of the Wigner distribution $\rho^{\mathrm{A}}(\boldsymbol{q},\boldsymbol{p},t)$ [74, 75] gave the quantum force $\boldsymbol{F}^{\mathrm{A}}_{\text{quant}}$. The phase space averaged quantum force for the trajectory j, $\left\langle \boldsymbol{F}^{\mathrm{A}}_{\text{quant},j}(t)\right\rangle$ was obtained by taking the time derivative of $\left\langle p^{\mathrm{A}}_{\text{off-diag,j}}(t)\right\rangle$

$$\begin{aligned} \left\langle \boldsymbol{F}^{\mathrm{A}}_{\text{quant},j}(t)\right\rangle &= \left\langle \dot{\boldsymbol{p}}^{\mathrm{A}}_{\text{off-diag,j}}(t)\right\rangle \\ &= -2\hbar\boldsymbol{d}(\boldsymbol{q}_j)\dot{\beta}^{\mathrm{A}}_j(t), \end{aligned} \tag{3.40}$$

noting that the non-adiabatic coupling vector $\boldsymbol{d}(\boldsymbol{q})$ can be expressed in terms of the diabatic potentials and $\hbar\omega^{\mathrm{A}}(\boldsymbol{q}) = V_{++}(\boldsymbol{q}) - V_{--}(\boldsymbol{q})$ as

$$\boldsymbol{d}(\boldsymbol{q}) = \frac{-\nabla_{\boldsymbol{q}}V_{12}(\boldsymbol{q})}{\hbar\omega^{\mathrm{A}}(\boldsymbol{q})}\cos\phi(\boldsymbol{q}) + \frac{\nabla_{\boldsymbol{q}}V_1(\boldsymbol{q}) - \nabla_{\boldsymbol{q}}V_2(\boldsymbol{q})}{2\hbar\omega^{\mathrm{A}}(\boldsymbol{q})}\sin\phi(\boldsymbol{q}). \tag{3.41}$$

When $\dot{\beta}_j^{\mathrm{A}}(t)$ in Eqn 2.23 was substituted into the above Eqn 3.40, the trajectory phase space average quantum force for the system in the adiabatic representation

$$\left\langle \boldsymbol{F}^{\mathrm{A}}_{\mathrm{quant},j}(t) \right\rangle \;=\; 2\hbar \boldsymbol{d}(\boldsymbol{q}_j)\omega^{\mathrm{A}}(\boldsymbol{q}_j)\alpha_j^{\mathrm{A}}(t). \tag{3.42}$$

The derived expression is congruous with our previous result given in Eqn 2.33.

Substituting Eqns 3.18 and 3.41, into Eqn 3.42, the d2a transformed trajectory phase space average quantum force for the system was found to be

$$\begin{aligned}
\left\langle \boldsymbol{F}^{\mathrm{A}}_{\mathrm{quant},j}(t) \right\rangle \;&=\; -2\alpha_j^{\mathrm{A}}(t)\Big(\nabla_{\boldsymbol{q}_j} V_{12}(\boldsymbol{q}_j)\cos\phi(\boldsymbol{q}_j) - \big(\nabla_{\boldsymbol{q}_j} V_1(\boldsymbol{q}_j) - \nabla_{\boldsymbol{q}} V_2(\boldsymbol{q}_j)\big)\sin\phi(\boldsymbol{q}_j)\Big) \\
&=\; \nabla_{\boldsymbol{q}_j} V_{12}(\boldsymbol{q}_j)\Big(\big(2\sigma_j^{\mathrm{D}}(t)-1\big)\sin\phi(\boldsymbol{q}_j)\cos\phi(\boldsymbol{q}_j) - 2\alpha_j^{\mathrm{D}}(t)\cos^2\phi(\boldsymbol{q}_j)\Big) \\
&\quad -\frac{\nabla_{\boldsymbol{q}_j}\big(V_1(\boldsymbol{q}_j)-V_2(\boldsymbol{q}_j)\big)}{2}\Big(\big(2\sigma_j^{\mathrm{D}}(t)-1\big)\sin^2\phi(\boldsymbol{q}_j)\Big) \\
&\quad +\frac{\nabla_{\boldsymbol{q}_j}\big(V_1(\boldsymbol{q}_j)-V_2(\boldsymbol{q}_j)\big)}{2}\Big(2\alpha_j^{\mathrm{D}}(t)\sin\phi(\boldsymbol{q}_j)\cos\phi(\boldsymbol{q}_j)\Big).
\end{aligned} \tag{3.43}$$

The Weyl function [71] for force in the adiabatic representation has both a classical and quantum component. The classical component was derived from the negative gradient of the potential energy $\boldsymbol{V}^A(\boldsymbol{q})$, and the quantum component was derived from the time derivative of the off-diagonal terms of the kinetic energy $\boldsymbol{p}^{\mathrm{A}}_{\text{off-diag}}(\boldsymbol{q})$.

Similarly, the Weyl function [71] for force in the diabatic representation $\boldsymbol{F}^{\mathrm{D}}_{\mathrm{cons}}(\boldsymbol{q})$ for the two-state system was obtained by taking the negative gradient of the Weyl function [71] of the adiabatic potential $\boldsymbol{V}^{\mathrm{D}}(\boldsymbol{q})$ as given in Eqn 3.31, and found to be

$$\boldsymbol{F}^{\mathrm{D}}_{\mathrm{cons}}(\boldsymbol{q}) = -\nabla_{\boldsymbol{q}}\boldsymbol{V}^{\mathrm{D}}(\boldsymbol{q}) = \overbrace{\begin{pmatrix} \boldsymbol{F}_1(\boldsymbol{q}) & 0 \\ 0 & \boldsymbol{F}_2(\boldsymbol{q}) \end{pmatrix}}^{\boldsymbol{F}^{\mathrm{D}}_{\mathrm{class}}(\boldsymbol{q})} + \underbrace{\begin{pmatrix} 0 & \boldsymbol{F}_{12}(\boldsymbol{q}) \\ \boldsymbol{F}_{12}(\boldsymbol{q}) & 0 \end{pmatrix}}_{\boldsymbol{F}^{\mathrm{D}}_{\mathrm{quant}}(\boldsymbol{q})}, \tag{3.44}$$

where $\boldsymbol{F}_{1/2}(\boldsymbol{q}) = -\nabla_{\boldsymbol{q}}V_{1/2}(\boldsymbol{q})$ and $\boldsymbol{F}_{12}(\boldsymbol{q}) = -\nabla_{\boldsymbol{q}}V_{12}(\boldsymbol{q})$.

Since $\boldsymbol{V}^{\mathrm{D}}(\boldsymbol{q})$ for the two-state system has off-diagonal terms, $\boldsymbol{F}^{\mathrm{D}}(\boldsymbol{q})$ can be broken down into a classical component $\boldsymbol{F}^{\mathrm{D}}_{\mathrm{class}}(\boldsymbol{q})$ with only diagonal terms, and a quantum component $\boldsymbol{F}^{\mathrm{D}}_{\mathrm{quant}}(\boldsymbol{q})$ with only off-diagonal terms.

The elements of the a2d transformed Weyl function $\boldsymbol{F}^{\mathrm{D}}(\boldsymbol{q})$ in terms of adiabatic potentials were obtained by taking the negative gradient of the diabatic potentials in Eqns 3.32-3.33 giving the expressions

$$\begin{aligned} \boldsymbol{F}^{\mathrm{D}}_{1/2}(\boldsymbol{q}) &= -\frac{\nabla_{\boldsymbol{q}}V_+(\boldsymbol{q}) + \nabla_{\boldsymbol{q}}V_-(\boldsymbol{q})}{2} \\ &\quad \mp\Big(\frac{\nabla_{\boldsymbol{q}}V_+(\boldsymbol{q}) - \nabla_{\boldsymbol{q}}V_-(\boldsymbol{q})}{2}\cos\phi(\boldsymbol{q}) + \big(V_+(\boldsymbol{q}) - V_-(\boldsymbol{q})\big)\boldsymbol{d}(\boldsymbol{q})\sin\phi(\boldsymbol{q})\Big), \end{aligned} \tag{3.45}$$

and

$$\boldsymbol{F}^{\mathrm{D}}_{12}(\boldsymbol{q}) = \frac{\nabla_{\boldsymbol{q}}V_1(\boldsymbol{q}) - \nabla_{\boldsymbol{q}}V_2(\boldsymbol{q})}{2}\sin\phi(\boldsymbol{q}) + \big(V_+(\boldsymbol{q}) - V_-(\boldsymbol{q})\big)\boldsymbol{d}(\boldsymbol{q})\sin\phi(\boldsymbol{q}), \tag{3.46}$$

where

$$\boldsymbol{F}^{\mathrm{D}}_{\mathrm{class}} = \begin{pmatrix} \boldsymbol{F}_1(\boldsymbol{q}) & 0 \\ 0 & \boldsymbol{F}_2(\boldsymbol{q}) \end{pmatrix}, \tag{3.47}$$

and

$$\boldsymbol{F}^{\mathrm{D}}_{\mathrm{quant}} = \begin{pmatrix} 0 & \boldsymbol{F}_{12}(\boldsymbol{q}) \\ \boldsymbol{F}_{12}(\boldsymbol{q}) & 0 \end{pmatrix}. \tag{3.48}$$

We now compute the system phase space averaged classical and quantum force components for the adiabatic and diabatic representations, obtained by performing the d2a and a2d transformations, respectively. These equations were used to obtain the d2a and a2d QTSH numerical results in Section 3.4.2.

The classical component of the d2a transformed Weyl function for force $\boldsymbol{F}^{\mathrm{A}}_{\mathrm{class}}(\boldsymbol{q})$ associates with the population/diagonal terms of the d2a Wigner distribution [74, 75]. The d2a phase space averaged classical force was found to be represented by

$$\begin{aligned}
\left\langle \boldsymbol{F}^{\mathrm{A}}_{\mathrm{class}}(t) \right\rangle &= \mathrm{Tr}\left(\boldsymbol{F}^{\mathrm{A}}_{\mathrm{class}}(\boldsymbol{q}) \boldsymbol{\rho}^{\mathrm{A}}(\boldsymbol{q},\boldsymbol{p},t) \right) \\
&= \frac{1}{N} \sum_{j}^{N} \boldsymbol{F}_{+}(\boldsymbol{q}_j) \sigma^{\mathrm{A}}_j(t) + \boldsymbol{F}_{-}(\boldsymbol{q}_j)\big(1 - \sigma^{\mathrm{A}}_j(t)\big) \\
&= \frac{1}{N} \sum_{j}^{N} \Bigg(- \frac{\nabla_{\boldsymbol{q}_j}\big(V_1(\boldsymbol{q}_j) + V_2(\boldsymbol{q}_j)\big)}{2} \\
&\quad - \frac{\nabla_{\boldsymbol{q}_j}\big(V_1(\boldsymbol{q}_j) - V_2(\boldsymbol{q}_j)\big)}{2} \Big(\big(2\sigma^{\mathrm{D}}_j(t) - 1\big) \cos^2\phi(\boldsymbol{q}_j) + 2\alpha^{\mathrm{D}}_j(t) \sin\phi(\boldsymbol{q}_j) \cos\phi(\boldsymbol{q}_j) \Big) \\
&\quad - \nabla_{\boldsymbol{q}_j} V_{12}(\boldsymbol{q}_j) \Big(\big(2\sigma^{\mathrm{D}}_j(t) - 1\big) \sin\phi(\boldsymbol{q}_j) \cos\phi(\boldsymbol{q}_j) + 2\alpha^{\mathrm{D}}_j(t) \sin^2\phi(\boldsymbol{q}_j) \Big) \Bigg).
\end{aligned} \tag{3.49}$$

Taking the ensemble average of the d2a transformed trajectory phase space averaged quantum force $\left\langle \boldsymbol{F}^{\mathrm{A}}_{\mathrm{quant},j}(t)\right\rangle$ in terms of diabatic potentials given by Eqn 3.43, the expression for the d2a transformed system phase space averaged quantum force in the adiabatic representation, $\left\langle \boldsymbol{F}^{\mathrm{A}}_{\mathrm{quant}}(t)\right\rangle$ was found to be

$$\begin{aligned}
\left\langle \boldsymbol{F}^{\mathrm{A}}_{\mathrm{quant}}(t)\right\rangle &= \frac{1}{N}\sum_{j}^{N}\left\langle \boldsymbol{F}^{\mathrm{A}}_{\mathrm{quant},j}(t)\right\rangle \\
&= \frac{1}{N}\sum_{j}^{N}\Bigg(\nabla_{\boldsymbol{q}_j}V_{12}(\boldsymbol{q}_j)\Big(\big(2\sigma^{\mathrm{D}}_j(t)-1\big)\sin\phi(\boldsymbol{q}_j)\cos\phi(\boldsymbol{q}_j)-2\alpha^{\mathrm{D}}_j(t)\cos^2\phi(\boldsymbol{q}_j)\Big) \\
&\quad -\frac{\nabla_{\boldsymbol{q}_j}\big(V_1(\boldsymbol{q}_j)-V_2(\boldsymbol{q}_j)\big)}{2}\Big(\big(2\sigma^{\mathrm{D}}_j(t)-1\big)\sin^2\phi(\boldsymbol{q}_j)\Big) \\
&\quad +\frac{\nabla_{\boldsymbol{q}_j}\big(V_1(\boldsymbol{q}_j)-V_2(\boldsymbol{q}_j)\big)}{2}\Big(2\alpha^{\mathrm{D}}_j(t)\sin\phi(\boldsymbol{q}_j)\cos\phi(\boldsymbol{q}_j)\Big)\Bigg). \qquad (3.50)
\end{aligned}$$

The d2a transformed phase space averaged total force was found by taking the sum of the d2a transformed phase space averaged classical (Eqn 3.49) and quantum force (Eqn 3.50)

$$\begin{aligned}
\left\langle \boldsymbol{F}^{\mathrm{A}}_{\mathrm{tot}}(t)\right\rangle &= \left\langle \boldsymbol{F}^{\mathrm{A}}_{\mathrm{class}}(t)\right\rangle + \left\langle \boldsymbol{F}^{\mathrm{A}}_{\mathrm{quant}}(t)\right\rangle \\
&= \frac{1}{N}\sum_{j}^{N}\Bigg(-\frac{\nabla_{\boldsymbol{q}_j}\big(V_1(\boldsymbol{q}_j)+V_2(\boldsymbol{q}_j)\big)}{2}-\frac{\nabla_{\boldsymbol{q}_j}\big(V_1(\boldsymbol{q}_j)-V_2(\boldsymbol{q}_j)\big)}{2}\big(2\sigma^{\mathrm{D}}_j(t)-1\big) \\
&\quad -2\nabla_{\boldsymbol{q}_j}V_{12}(\boldsymbol{q}_j)\alpha^{\mathrm{D}}_j(t)\Bigg). \qquad (3.51)
\end{aligned}$$

With reference to Eqn 1.66, where the equation of motion for momentum is the force for a trajectory in the diabatic representation, we find that the expression for $\left\langle \boldsymbol{F}^{\mathrm{A}}_{\mathrm{tot}}(t)\right\rangle$ in Eqn 3.51 is in fact the phase space averaged total force in the diabatic representation $\left\langle \boldsymbol{F}^{\mathrm{D}}_{\mathrm{tot}}(t)\right\rangle$,

$$\left\langle \boldsymbol{F}^{\mathrm{A}}_{\mathrm{tot}}(t)\right\rangle = \left\langle \boldsymbol{F}^{\mathrm{D}}_{\mathrm{tot}}(t)\right\rangle. \qquad (3.52)$$

Since the classical component of the a2d transformed Weyl function for force $\boldsymbol{F}^{\mathrm{D}}_{\mathrm{class}}(\boldsymbol{q})$ associates with the population/diagonal terms of the a2d transformed Wigner distribution [74, 75], the a2d transformed phase space averaged classical force was represented by

$$\begin{aligned}
\left\langle \boldsymbol{F}^{\mathrm{D}}_{\mathrm{class}}(t) \right\rangle &= \mathrm{Tr}\left(\boldsymbol{F}^{\mathrm{D}}_{\mathrm{class}}(\boldsymbol{q}) \boldsymbol{\rho}^{\mathrm{D}}(\boldsymbol{q},\boldsymbol{p},t) \right) \\
&= \frac{1}{N} \sum_{j}^{N} \boldsymbol{F}_1(\boldsymbol{q}_j) \sigma^{\mathrm{D}}_j(t) + \boldsymbol{F}_2(\boldsymbol{q}_j)\big(1 - \sigma^{\mathrm{D}}_j(t)\big) \\
&= \frac{1}{N} \sum_{j}^{N} \Bigg(- \frac{\nabla_{\boldsymbol{q}_j}\big(V_+(\boldsymbol{q}_j) + V_-(\boldsymbol{q}_j)\big)}{2} \\
&\quad - \frac{\nabla_{\boldsymbol{q}_j}\big(V_+(\boldsymbol{q}_j) - V_-(\boldsymbol{q}_j)\big)}{2} \Big(\big(2\sigma^{\mathrm{A}}_j(t) - 1\big) \cos^2\phi(\boldsymbol{q}_j) - 2\alpha^{\mathrm{D}}_j(t) \sin\phi(\boldsymbol{q}_j) \cos\phi(\boldsymbol{q}_j) \Big) \\
&\quad - \hbar\omega^{\mathrm{A}}(\boldsymbol{q}_j) \boldsymbol{d}(\boldsymbol{q}) \Big(\big(2\sigma^{\mathrm{A}}_j(t) - 1\big) \sin\phi(\boldsymbol{q}_j) \cos\phi(\boldsymbol{q}_j) - 2\alpha^{\mathrm{A}}_j(t) \sin^2\phi(\boldsymbol{q}_j) \Big), \qquad (3.53)
\end{aligned}$$

where $\hbar\omega^{\mathrm{A}}(\boldsymbol{q}_j) = V_+(\boldsymbol{q}_j) + V_-(\boldsymbol{q}_j)$.

Since $\boldsymbol{F}^{\mathrm{D}}_{\mathrm{quant}}(\boldsymbol{q})$ only has off-diagonal elements that associates with the coherence/off-diagonal terms of the a2d transformed Wigner distribution [74, 75], the a2d transformed phase space averaged quantum force was represented by

$$\begin{aligned}
\left\langle \boldsymbol{F}^{\mathrm{D}}_{\mathrm{quant}}(t) \right\rangle &= \mathrm{Tr}\left(\boldsymbol{F}^{\mathrm{D}}_{\mathrm{quant}}(\boldsymbol{q}) \boldsymbol{\rho}^{\mathrm{D}}(\boldsymbol{q},\boldsymbol{p},t) \right) \\
&= \frac{1}{N} \sum_{j}^{N} 2\boldsymbol{F}_{12}(\boldsymbol{q}_j) \alpha^{\mathrm{D}}_j(t) \\
&= \frac{1}{N} \sum_{j}^{N} \Bigg(- \frac{\nabla_{\boldsymbol{q}_j}\big(V_+(\boldsymbol{q}_j) - V_-(\boldsymbol{q}_j)\big)}{2} \big(2\sigma^{\mathrm{A}}_j(t) - 1\big) \sin^2\phi(\boldsymbol{q}_j) \\
&\quad - \frac{\nabla_{\boldsymbol{q}_j}\big(V_+(\boldsymbol{q}_j) - V_-(\boldsymbol{q}_j)\big)}{2} 2\alpha^{\mathrm{A}}_j(t) \sin\phi(\boldsymbol{q}_j) \cos\phi(\boldsymbol{q}_j) \\
&\quad + \hbar\omega^{\mathrm{A}}(\boldsymbol{q}_j) \boldsymbol{d}(\boldsymbol{q}) \Big(\big(2\sigma^{\mathrm{A}}_j(t) - 1\big) \sin\phi(\boldsymbol{q}_j) \cos\phi(\boldsymbol{q}_j) + 2\alpha^{\mathrm{A}}_j(t) \cos^2\phi(\boldsymbol{q}_j) \Big). \qquad (3.54)
\end{aligned}$$

The a2d transformed phase space averaged total force in the diabatic representation in terms of the adiabatic potentials was found by taking the sum of the a2d transformed phase space averaged classical (Eqn 3.53) and quantum force (Eqn 3.54)

$$\begin{aligned}\left\langle \boldsymbol{F}^{\mathrm{D}}_{\mathrm{tot}}(t)\right\rangle &= \left\langle \boldsymbol{F}^{\mathrm{D}}_{\mathrm{class}}(t)\right\rangle + \left\langle \boldsymbol{F}^{\mathrm{D}}_{\mathrm{quant}}(t)\right\rangle \\ &= \frac{1}{N}\sum_{j}^{N}\Bigg(-\frac{\nabla_{\boldsymbol{q}_j}\big(V_{+}(\boldsymbol{q}_j)+V_{-}(\boldsymbol{q}_j)\big)}{2} - \frac{\nabla_{\boldsymbol{q}_j}\big(V_{+}(\boldsymbol{q}_j)-V_{-}(\boldsymbol{q}_j)\big)}{2}\big(2\sigma^{\mathrm{D}}_{j}(t)-1\big) \\ &\quad +2\hbar\omega^{\mathrm{A}}(\boldsymbol{q}_j)\alpha^{\mathrm{A}}_{j}(t)\boldsymbol{d}(\boldsymbol{q})\Bigg). \end{aligned} \tag{3.55}$$

With reference to Eqn 1.69, where the equation of motion for the kinematic momentum is the force for a trajectory in the adiabatic representation, we find that the expression for $\left\langle \boldsymbol{F}^{\mathrm{A}}_{\mathrm{tot}}(t)\right\rangle$ in Eqn 3.51 is equal to the phase space averaged total force in the adiabatic representation $\left\langle \boldsymbol{F}^{\mathrm{A}}_{\mathrm{tot}}(t)\right\rangle$, recovering the derived Eqn 3.52.

While the same system are apparently different in the adiabatic and the diabatic representation, the total forces acting on the trajectories in each representation are identical, although the classical force components and quantum force components, given by Eqns 3.49 and 3.50 in the adiabatic representation, and Eqns 3.53 and 3.54 in the diabatic representation, respectively, are vastly different.

While a non-adiabatic process in each representation can involve differing degrees of classical or non-classical effects of forces, the trajectories in either representation experience the same phase space averaged force at any given time.

We will explore the classical and non-classical effects of forces and representation in Chapter 4.

3.3 Computational Details

The description of the systems used and the simulation details are as given in Section 2.3 of Chapter 2, with the following additions.

In this chapter, we ran QTSH in both the adiabatic and diabatic representations.

We utilized the derived d2a and a2d equations for the phase space averaged Wigner distribution [74, 75], and forces in Section 3.2 to transform the QTSH results in the diabatic representation to the adiabatic representation (d2a QTSH), and to transform the QTSH results in the adiabatic representation to the diabatic representation (a2d QTSH).

3.4 Results & Discussion

In this section we compare the adiabatic QTSH and d2a QTSH results, and the diabatic QTSH and a2d QTSH results for the elements of the Wigner distribution [74, 75] and the forces. We also show that, as derived in Section 3.2.2, while the system is apparently different in the diabatic and adiabatic representations, the total forces acting on trajectories are the same in both representations (Eqn 3.52).

3.4.1 Wigner Distribution

We first examine the dynamics of the elements of the Wigner distribution [74, 75].

To obtain the d2a QTSH and a2d QTSH results for the elements of the Wigner distribution [74, 75] in the adiabatic and diabatic representations, respectively, we applied Eqns 3.19-3.22 to the diabatic QTSH results, and applied Eqns 3.23-3.26 to the adiabatic QTSH results, respectively.

We now present the d2a and a2d QTSH results for the populations and coherence for the processes in the simple avoided crossing and the dual avoided crossing systems [1].

We first consider the populations/diagonal elements of the Wigner distribution [74, 75].

In Figs 3.2-3.4, we present (a) the comparison of the adiabatic QTSH and d2a QTSH results for the phase space averaged adiabatic population $\langle \rho_{++}(t) \rangle$ against the exact quantum results, and (b) the comparison of the diabatic QTSH and a2d QTSH results for the phase space averaged diabatic population $\langle \rho_{11}(t) \rangle$ against the exact quantum results, for the non-adiabatic processes in the simple avoided crossing and dual avoided crossing systems [1].

Fig 3.2 shows the QTSH results for the non-adiabatic process in the simple avoided crossing system [1] that involves the $+ \rightarrow -$ electronic transition in the adiabatic representation (Fig 2.2), and its corresponding process in the diabatic representation depicted in Fig 2.3. Fig 3.3 shows the QTSH results for the non-adiabatic process in the simple avoided crossing system [1] that involves the $- \rightarrow +$ electronic transition in the adiabatic representation (Fig 2.4), and its corresponding process in the diabatic representation depicted in Fig 2.5.

Fig 3.4 shows the QTSH results for the non-adiabatic process in the dual avoided crossing system [1] that involves a non-adiabatic transition $- \rightarrow +$, followed by a second non-adiabatic transition $+ \rightarrow -$ in the adiabatic representation (Fig 2.8), and its corresponding process in the diabatic representation depicted in Fig. 2.9.

We first provide a cursory analysis of the representation invariance of the phase space average populations/diagonal terms of the Wigner distribution [74, 75] by comparing the adiabatic QTSH results and d2a QTSH results for $\langle \rho_{++}(t) \rangle$, and the diabatic QTSH results and a2d QTSH results for $\langle \rho_{11}(t) \rangle$.

With reference to Figs 3.2(a), 3.3(a) and 3.4(a), and Figs 3.2(b), 3.3(b) and 3.4(b), the agreement between the adiabatic QTSH results and d2a QTSH results for $\langle \rho_{++}(t) \rangle$, and the agreement between the diabatic QTSH results and a2d QTSH results for $\langle \rho_{11}(t) \rangle$ are essentially quantitative with slight deviations.

Since the d2a QTSH results and the adiabatic QTSH results in the adiabatic representation, and the a2d QTSH results and the diabatic QTSH results, are in good agreement, the system phase space averaged components of the diagonal/population elements of the Wigner distribution [74, 75] computed by the QTSH method can be considered to be representation invariant, with slight discrepancies.

We now provide a more in-depth analysis of the accuracy of the phase space average populations/diagonal terms of the Wigner distribution [74, 75] by comparing the adiabatic QTSH results and d2a QTSH results for $\langle \rho_{++}(t) \rangle$ with the exact quantum results, and the diabatic QTSH results and a2d QTSH results for $\langle \rho_{11}(t) \rangle$ with the exact quantum results.

We first examine the $\langle \rho_{++}(t) \rangle$ results in the adiabatic representation.

With reference to Figs 3.2(a) and 3.3(a), we found that the population transfer from $+ \rightarrow -$ and $- \rightarrow +$ occurs, observed in the plot as a change in $\langle \rho_{++}(t) \rangle$, during the transition time interval between $t \approx 10$ fs and $t \approx 30$ fs, before reaching an asymptotic value. The magnitude of the change in $\langle \rho_{++}(t) \rangle$ to the asymptotic value indicates the size/completeness of the population transfer. The completeness of the population transfer increased when the size of the diabatic coupling constant C was increased from $C = 0.0005$ to $C = 0.002$. The observation is consistent with the non-adiabatic coupling vector $\boldsymbol{d}(\boldsymbol{q}_j)$ being broadest with the smallest magnitude, for $C = 0.002$ (Fig 1.1(b)).

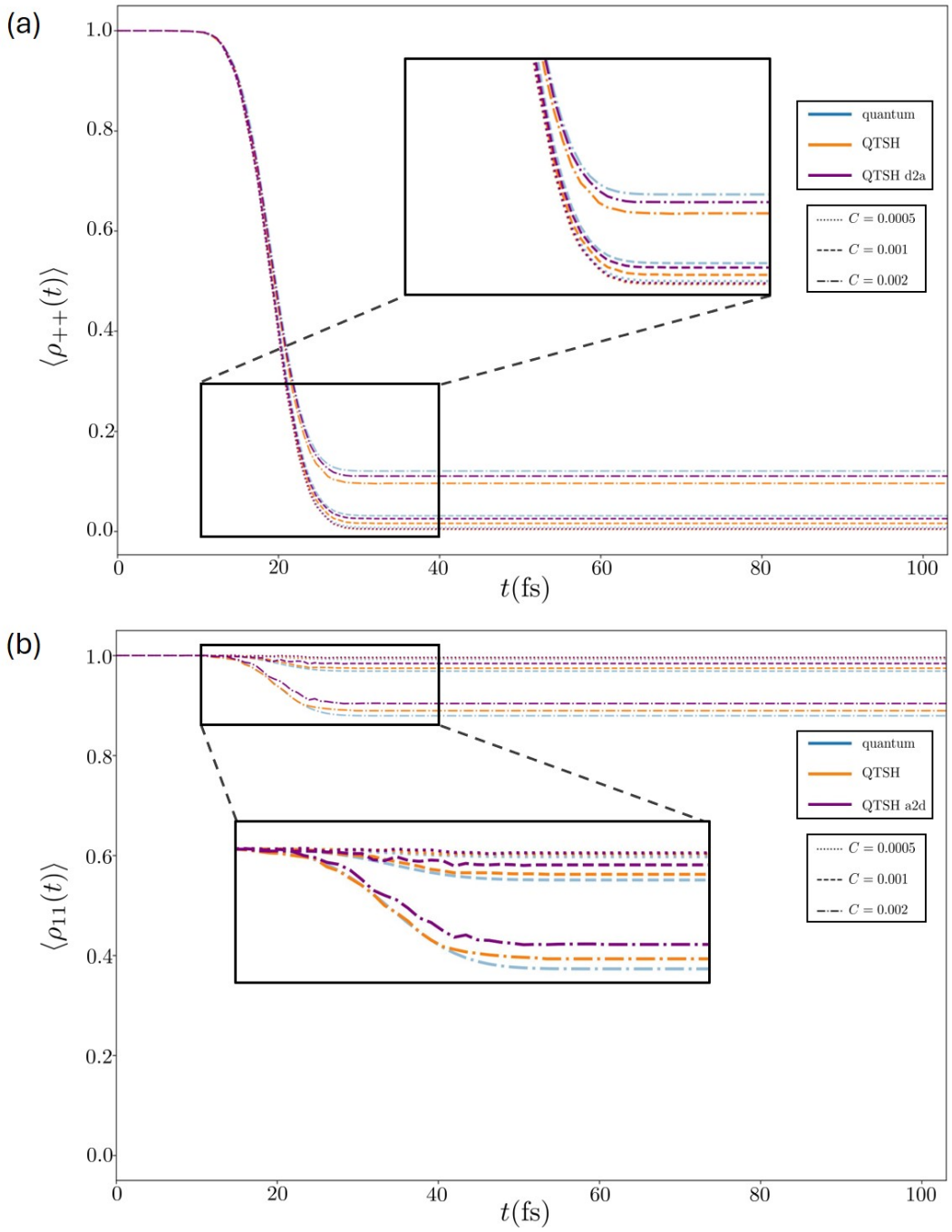

Figure 3.2: Comparison of exact quantum result for (a) the phase space average population $\langle \rho_{++}(t) \rangle$ with the adiabatic QTSH result and the transformed d2a QTSH result, and (b) the phase space average population $\langle \rho_{11}(t) \rangle$ with the diabatic QTSH result, and the transformed a2d QTSH result, for the for the processes described in Figs 2.2 and 2.3 for the simple avoided crossing system described by the diabatic potentials given by Eqns 1.83-1.84. The inset shows the magnified plot between $t = 10$ fs and $t = 40$ fs.

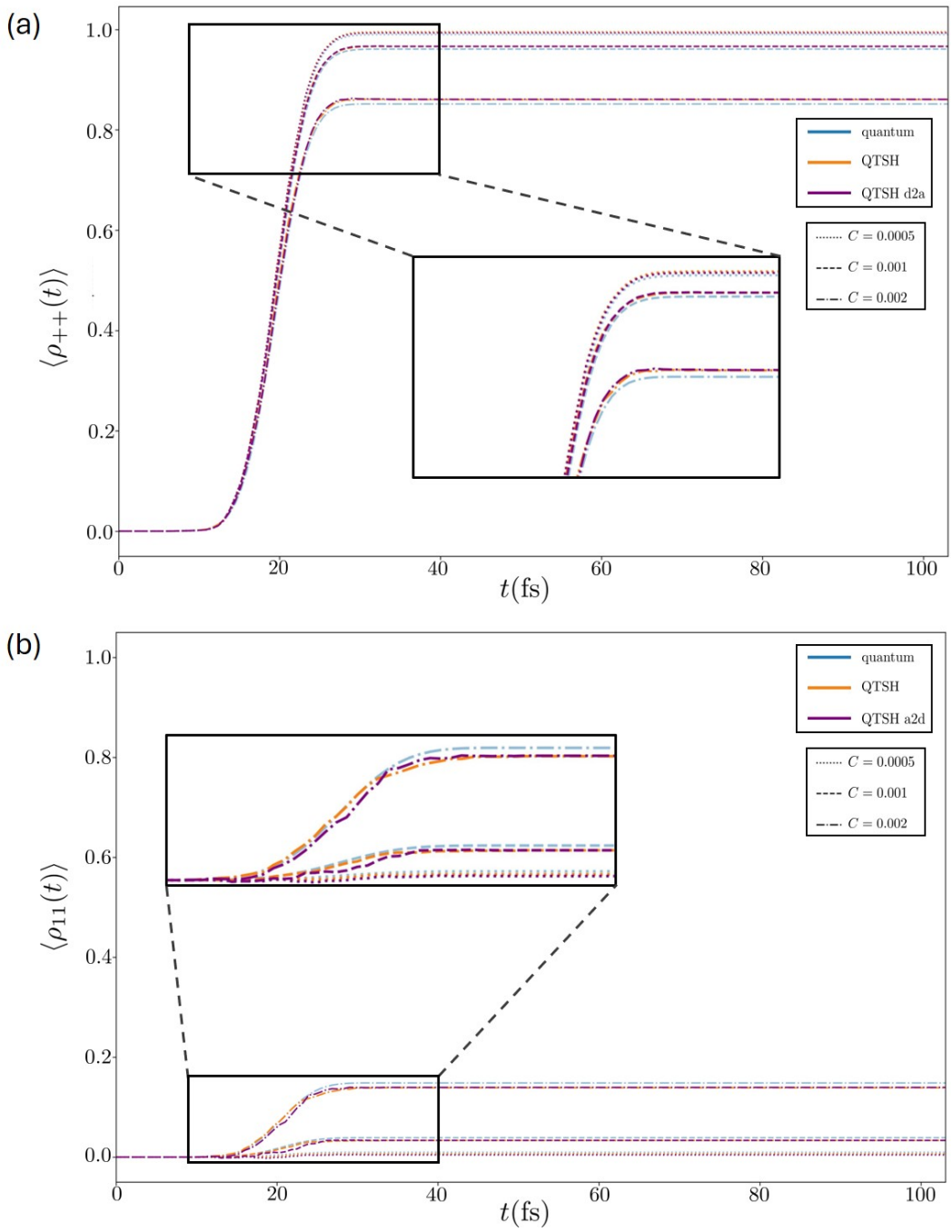

Figure 3.3: Comparison of exact quantum result for (a) the phase space average population $\langle \rho_{++}(t) \rangle$ with the adiabatic QTSH result and the transformed d2a QTSH result, and (b) the phase space average population $\langle \rho_{11}(t) \rangle$ with the diabatic QTSH result, and the transformed a2d QTSH result, for the for the processes described in Figs 2.4 and 2.5 for the simple avoided crossing system described by the diabatic potentials given by Eqns 1.83-1.84. The inset shows the magnified plot between $t = 10$ fs and $t = 40$ fs.

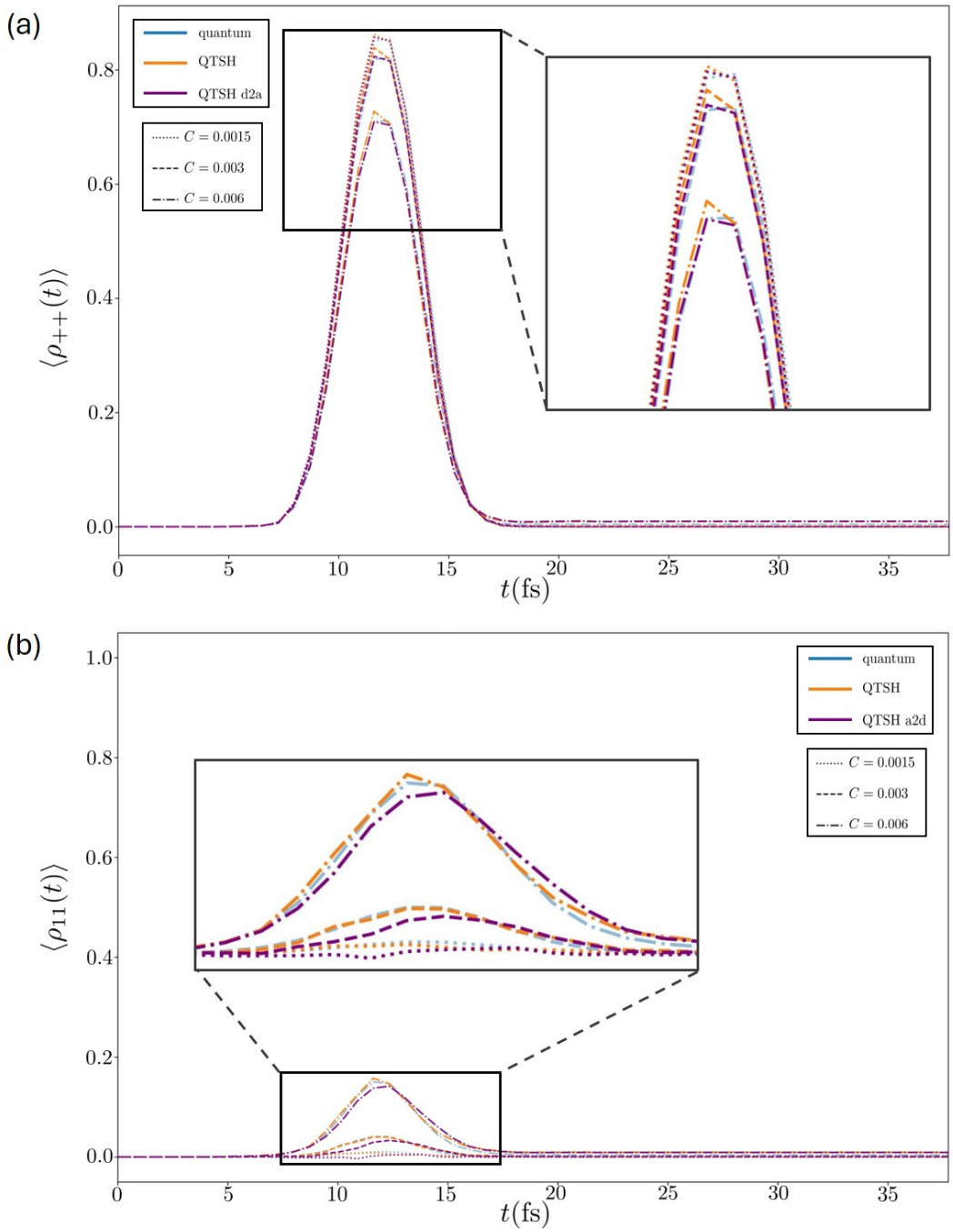

Figure 3.4: Comparison of exact quantum result for (a) the phase space average population $\langle \rho_{++}(t) \rangle$ with the adiabatic QTSH result and the transformed d2a QTSH result, and (b) the phase space average population $\langle \rho_{11}(t) \rangle$ with the diabatic QTSH result, and the transformed a2d QTSH result, for the for the processes described in Figs 2.8 and 2.9 for the dual avoided crossing system described by the diabatic potentials given by Eqns 1.86-1.87. The inset shows the magnified plot between $t = 7.5$ fs and $t = 17.5$ fs.

We also observed that the deviation of the adiabatic QTSH results and the d2a QTSH results from the exact quantum results decreased as C increased from $C = 0.0005$ to $C = 0.002$, in both Figs 3.2(a) and 3.3(a). This showed that the accuracy of QTSH in the adiabatic representation increased with the completeness and locality of the population transfer for both non-adiabatic processes occuring in the simple avoided crossing model [1].

With reference to Fig 3.2(a), we observed that the d2a QTSH result deviate from the exact quantum result to a smaller extent than the adiabatic QTSH result. The improved accuracy of the d2a QTSH result over the adiabatic QTSH result was most noticeable when C was largest. This suggests that the d2a QTSH result was slightly more accurate than the adiabatic QTSH result for the non-adiabatic process depicted by Fig 2.2 for the simple avoided crossing system [1], and that the most appreciable difference in accuracy was observed when population transfer was least complete and localized.

Since QTSH results in the adiabatic representation were less accurate than the d2a QTSH results, the non-adiabatic process involving the $+ \rightarrow -$ electronic transition, depicted by Fig 2.2 for the simple avoided crossing system [1] is likely to be captured more accurately in the diabatic representation.

With reference to Fig 3.3(a), the adiabatic QTSH result and d2a QTSH result were almost identical for all systems. This suggests that QTSH performed in either representation was likely to be similarly accurate for all values of C for the process depicted by Fig 2.4 for the simple avoided crossing model [1].

With reference to Fig 3.4(a), we found that the first population transfer from the lower adiabatic state $V_-(\boldsymbol{q})$ to the upper adiabatic state $V_+(\boldsymbol{q})$ occurs, observed in the plot as a decrease in $\langle \rho_{++}(t) \rangle$ over time, we find that the adiabatic QTSH and d2a QTSH results are in almost perfect agreement with the quantum results until $t \approx 10$ fs, with the highest accuracy for when C is smallest. From $t \approx 10$ fs to $t \approx 11.4$ fs we find that both the

adiabatic QTSH and d2a QTSH results are slightly higher than the quantum results. The first population transfer was most complete for the dual avoided crossing system [1] with the smallest $C = 0.0015$, and least complete for the dual avoided crossing system [1] with the largest $C = 0.006$.

From $t \approx 11.4$ fs to $t \approx 12$ fs, where the quantum results are constant indicating that no electronic transition occurred during that time period, the adiabatic QTSH and d2a QTSH results deviated slightly from the quantum result, with the size of the deviation being smaller for the d2a QTSH result than the adiabatic QTSH result. After $t \approx 12$ fs, the second population transfer from the upper adiabatic state $V_+(\boldsymbol{q})$ to the lower adiabatic state $V_-(\boldsymbol{q})$ occurs with a decrease in the adiabatic QTSH and d2a QTSH results, almost perfectly matching the quantum result to an asymptotic value close to zero, repopulating the initial lower adiabatic state $V_-(\boldsymbol{q})$.

Since the deviation from the quantum result that occurs mainly during the $t \approx 10$ fs to the $t \approx 12$ fs time period, with the d2a QTSH result being closer to the quantum result than the adiabatic result, it is plausible that QTSH in the diabatic representation is more accurate than in the adiabatic representation for the process depicted in Fig 2.8 for the dual avoided crossing system [1].

The inverse relation between the accuracy of the adiabatic QTSH and d2a QTSH results and the completeness of the population transfer, as observed in Figs 3.2(a) and 3.4(a) can be explained as follows. A larger population remains on the initial adiabatic state, when a smaller population transfer occurs. This makes the interference between the populations on the upper adiabatic state $V_+(\boldsymbol{q})$ and lower adiabatic state $V_-(\boldsymbol{q})$ more significant. As interference effects are poorly captured when *independent* trajectories are used [4], QTSH that utilizes independent trajectories [62, 63] gives less accurate results when interference effects are more significant.

We now examine the $\langle \rho_{11}(t) \rangle$ results in the diabatic representation.

With reference to Figs 3.2(b) and 3.3(b), a very small population transfer occurs from the diabatic state $V_1(\boldsymbol{q})$ to the diabatic state $V_2(\boldsymbol{q})$, indicated by the change in $\langle \rho_{11}(t) \rangle$ during the population transfer time interval between $t \approx 10$ fs and $t \approx 30$ fs, before reaching an asymptotic value. We found that converse to the corresponding process in the adiabatic representation, the largest magnitude of population transfer occurred when the size of the diabatic coupling constant was increased from $C = 0.0005$ to $C = 0.002$.

With reference to Fig 3.2(b), when $C = 0.0005$, the diabatic QTSH and a2d QTSH results almost perfectly match the quantum results with almost no population transfer. For the systems with $C = 0.001$ and $C = 0.002$, the diabatic QTSH and a2d QTSH results gave good agreement with the quantum results with the diabatic QTSH results being slightly more accurate than the a2d QTSH result in both systems.

This corroborates our earlier assertion that the process depicted by Fig 2.2 for the simple avoided crossing system [1] is likely to be captured more accurately in the diabatic representation.

We will explore how the representation invariance of QTSH can be exploited to obtain more accurate results in the representation of choice in Section 4.4.2 in Chapter 4.

With reference to Fig 3.3(b), the diabatic QTSH result and a2d QTSH result were almost identical for all systems. This suggests that QTSH performed in either representation was likely to be similarly accurate for all values of C for the process depicted by Fig 2.4 for the simple avoided crossing model [1].

This corroborates our earlier assertion that QTSH performed in either representation was likely to be similarly accurate for all values of C for the process depicted by Fig 2.4 for the simple avoided crossing model [1].

With reference to 3.4(b), we find that a small first population transfer from the diabatic state $V_2(\boldsymbol{q})$ to the diabatic state $V_1(\boldsymbol{q})$ occurs with $\langle\rho_{11}(t)\rangle$ increasing, with the largest population transfer occurring when C was largest, during the time period between $t = 0$ fs to $t \approx 12$ fs. For the system with $C = 0.0015$, the population transfer was very close to zero, with the diabatic QTSH result matching the exact quantum result almost exactly, while the a2d QTSH result deviated slightly from the quantum result, between $t \approx 10$ fs to $t \approx 11.4$ fs, reflecting inaccuracies in that time period found in the corresponding adiabatic QTSH result in Fig 3.4(a), as described above. For the time period between $t = 0$ fs to $t \approx 12$ fs, the diabatic QTSH result almost perfectly agrees with the quantum results, while the a2d QTSH results slightly deviates during this time period.

After $t \approx 12$ fs, the second population transfer from the diabatic state $V_1(\boldsymbol{q})$ to the diabatic state $V_2(\boldsymbol{q})$ occurs with a decrease in the diabatic QTSH and d2a QTSH results, almost perfectly matching the quantum result to an asymptotic value close to zero, repopulating the initial diabatic state $V_2(\boldsymbol{q})$.

Similar to the adiabatic representation, the deviation from the quantum result occurs mainly in the $t \approx 10$ fs to the $t \approx 12$ fs time period, with the diabatic QTSH result being closer to the quantum result than the a2d QTSH result.

This agrees with the earlier assertion that the QTSH in the diabatic representation being more accurate than QTSH in the adiabatic representation for this process. This will be further explored in Section 4.4.2 in Chapter 4.

Having examined the diagonal/population component of the Wigner distribution [74, 75], we now examine the real and imaginary parts of the off-diagonal/coherence components of the Wigner distribution [74, 75] for the same processes.

We will first examine the phase space averaged real part of the off-diagonal/coherence components of the Wigner distribution [74, 75] in the adiabatic and diabatic representations

$\left\langle \alpha^{\mathrm{A}}(t) \right\rangle$ and $\left\langle \alpha^{\mathrm{D}}(t) \right\rangle$.

In Figs 3.5 and 3.6, we present (a) the comparison of the adiabatic QTSH and d2a QTSH results for the phase space averaged adiabatic population $\left\langle \alpha^{\mathrm{A}}(t) \right\rangle$ against the exact quantum results, and (b) the comparison of the diabatic QTSH and a2d QTSH results for the phase space averaged diabatic population $\left\langle \alpha^{\mathrm{D}}(t) \right\rangle$ against the exact quantum results for the non-adiabatic processes occurring in the simple avoided crossing system [1] that involve the $+ \rightarrow -$ electronic transition (Fig 2.2), and the $- \rightarrow +$ electronic transition (Fig 2.4) in the adiabatic representation, respectively. The corresponding processes in the diabatic representation are depicted in Figs 2.3 and 2.5, respectively.

In Fig 3.7, we present (a) the comparison of the adiabatic QTSH and d2a QTSH results for the phase space averaged adiabatic population $\left\langle \alpha^{\mathrm{A}}(t) \right\rangle$ against the exact quantum results, and (b) the comparison of the diabatic QTSH and a2d QTSH results for the phase space averaged diabatic population $\left\langle \alpha^{\mathrm{D}}(t) \right\rangle$ against the exact quantum results, for the dual avoided crossing system [1] that involves the non-adiabatic transition from the lower adiabatic state to the upper adiabatic state $- \rightarrow +$, followed by a second non-adiabatic transition from the upper adiabatic state to the lower adiabatic state $+ \rightarrow -$ in the adiabatic representation (Fig 2.8). The corresponding process in the diabatic representation is depicted in Fig. 2.9.

We first provide a cursory analysis of the representation invariance of the phase space average of the real part of the coherences/off-diagonal terms of the Wigner distribution [74, 75] by comparing the adiabatic QTSH results and d2a QTSH results for $\left\langle \alpha^{\mathrm{A}}(t) \right\rangle$, and the diabatic QTSH results and a2d QTSH results for $\left\langle \alpha^{\mathrm{D}}(t) \right\rangle$.

With reference to Figs 3.5(a), 3.6(a) and 3.7(a), and Figs 3.5(b), 3.6(b) and 3.7(b), we found that the adiabatic QTSH results and d2a QTSH results for $\left\langle \alpha^{\mathrm{A}}(t) \right\rangle$, and the diabatic QTSH results and a2d QTSH results for $\left\langle \alpha^{\mathrm{D}}(t) \right\rangle$, are in good agreement with slight deviations.

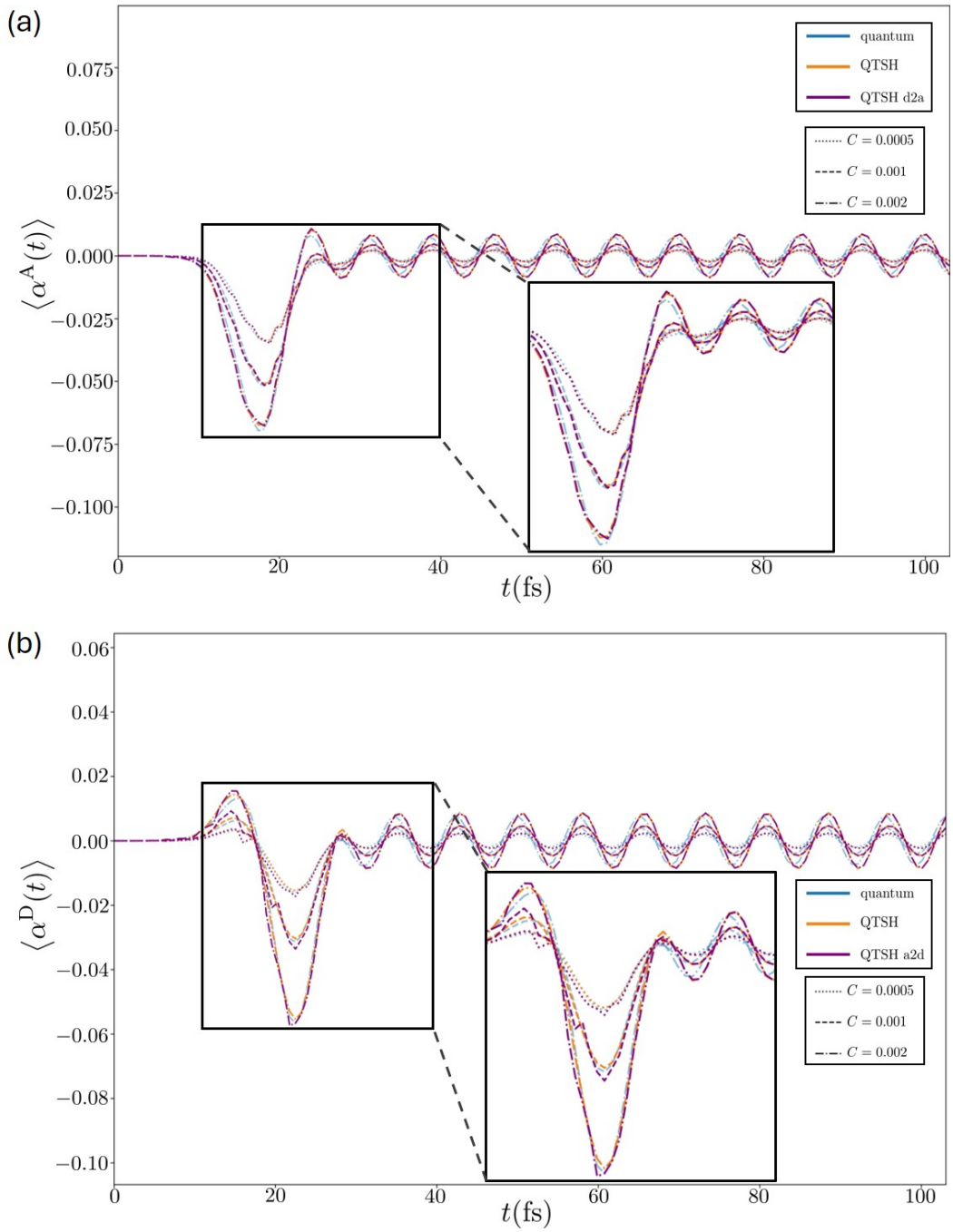

Figure 3.5: Comparison of exact quantum result for (a) the phase space averaged real part of the coherence $\langle \alpha^{\mathrm{A}}(t) \rangle$ with the adiabatic QTSH result and the transformed d2a QTSH result, and (b) the phase space averaged real part of the coherence $\langle \alpha^{\mathrm{D}}(t) \rangle$ with the diabatic QTSH result, and the transformed a2d QTSH result, for the for the processes described in Figs 2.2 and 2.3 for the simple avoided crossing system described by the diabatic potentials given by Eqns 1.83-1.84. The inset shows the magnified plot between $t = 10$ fs and $t = 40$ fs.

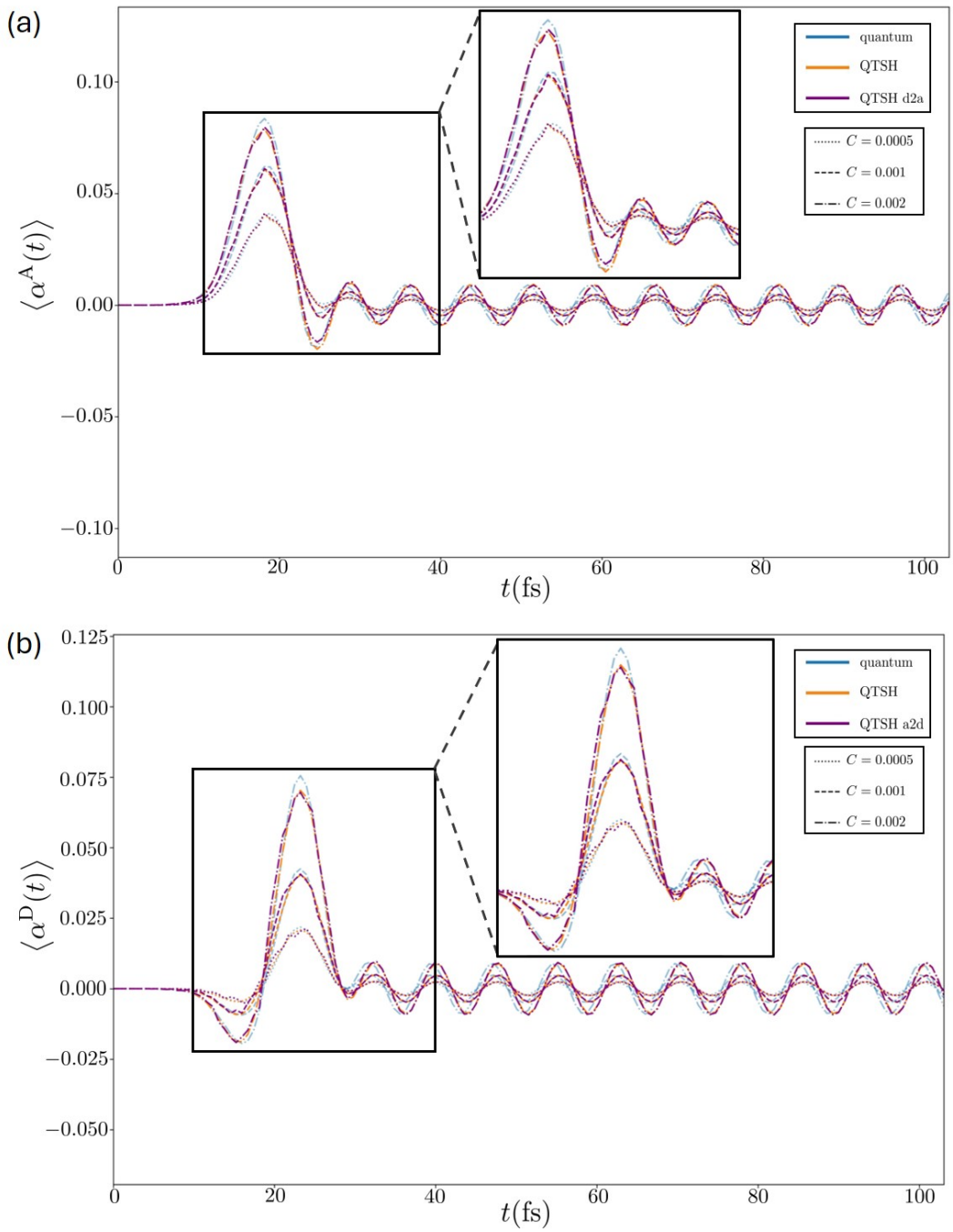

Figure 3.6: Comparison of exact quantum result for (a) the phase space averaged real part of the coherence $\langle \alpha^{\mathrm{A}}(t) \rangle$ with the adiabatic QTSH result and the transformed d2a QTSH result, and (b) the phase space averaged real part of the coherence $\langle \alpha^{\mathrm{D}}(t) \rangle$ with the diabatic QTSH result, and the transformed a2d QTSH result, for the for the processes described in Figs 2.4 and 2.5 for the simple avoided crossing system described by the diabatic potentials given by Eqns 1.83-1.84. The inset shows the magnified plot between $t = 10$ fs and $t = 40$ fs.

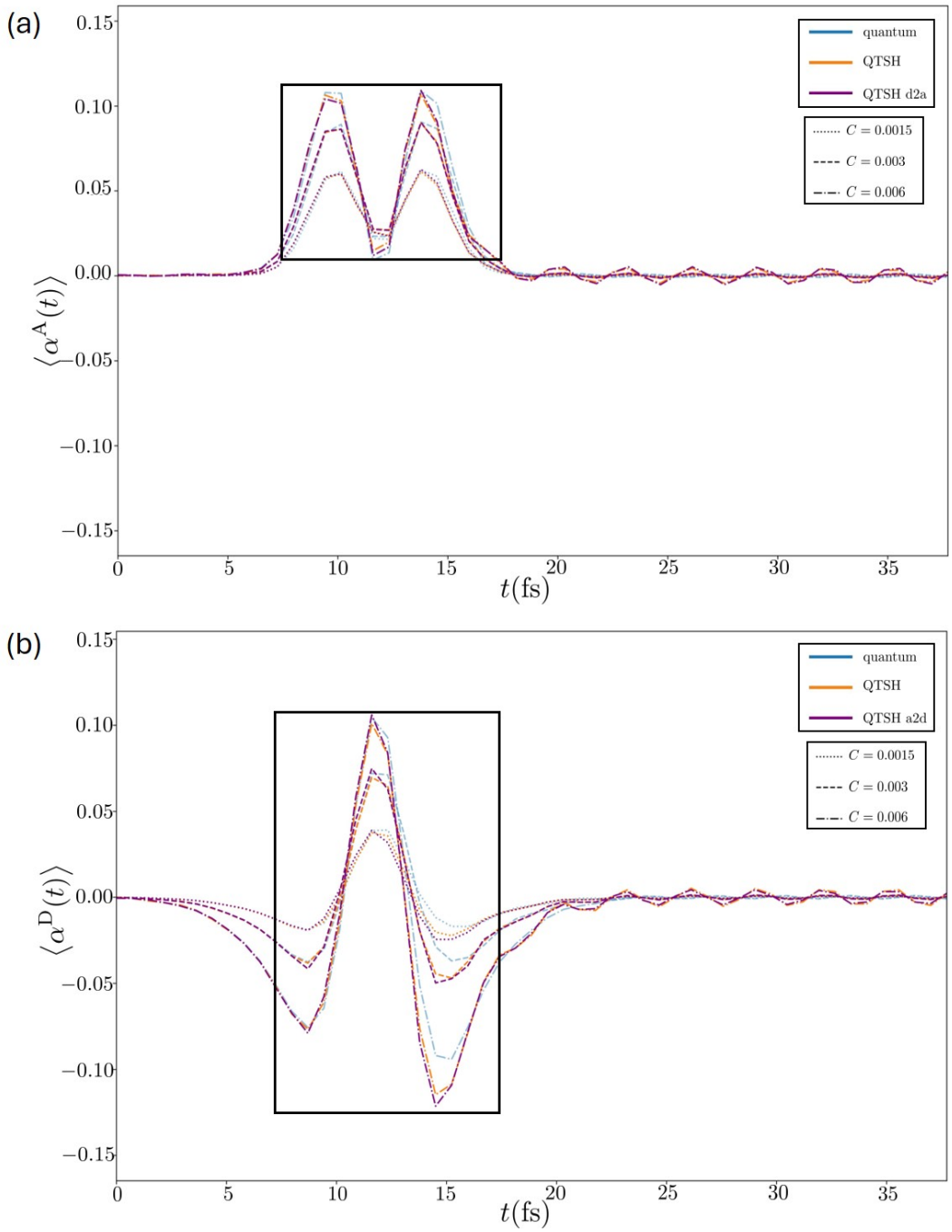

Figure 3.7: Comparison of exact quantum result for (a) the phase space averaged real part of the coherence $\langle \alpha^{\mathrm{A}}(t) \rangle$ with the adiabatic QTSH result and the transformed d2a QTSH result, and (b) the phase space averaged real part of the coherence $\langle \alpha^{\mathrm{D}}(t) \rangle$ with the diabatic QTSH result, and the transformed a2d QTSH result, for the for the processes described in Figs 2.8 and 2.9 for the dual avoided crossing system described by the diabatic potentials given by Eqns 1.86-1.87. The black box highlights the plot between $t = 7.5$ fs and $t = 17.5$ fs.

Since the d2a QTSH results and the QTSH results in the adiabatic representation, and the a2d QTSH results and the QTSH results in the diabatic representation are in good agreement, the system phase space averaged components of the real part of the off-diagonal/coherence elements of the Wigner distribution [74, 75] computed by QTSH is representation invariant, with the slight discrepancies.

We now provide a more in-depth analysis of the accuracy of the phase space average real part of the coherences/off-diagonal terms of the Wigner distribution [74, 75] by comparing the adiabatic QTSH results and d2a QTSH results for $\left\langle \alpha^{\mathrm{A}}(t) \right\rangle$ with the exact quantum results, and the diabatic QTSH results and a2d QTSH results for $\left\langle \alpha^{\mathrm{D}}(t) \right\rangle$ with the exact quantum results.

With reference to Figs 3.5(a) and 3.6(a), and Figs 3.5(b) and 3.6(b), we also found that the adiabtic QTSH and d2a QTSH results for $\left\langle \alpha^{\mathrm{A}}(t) \right\rangle$, and the diabatic QTSH and a2d QTSH results for $\left\langle \alpha^{\mathrm{D}}(t) \right\rangle$, in comparison to the exact quantum results, were slightly displaced in the positive direction and of larger magnitude after $t \approx 30$ fs. This effect was most pronounced for the systems with the largest diabatic coupling constant C. This overcoherence [1, 3] observed is a consequence of utilizing *independent* trajectories. In order to correctly capture the quantum coherence, trajectories have to be *interdependent* [39–41, 52–58].

With reference to Fig 3.7(a) and (b), we found that the adiabatic QTSH and d2a QTSH $\left\langle \alpha^{\mathrm{A}} \right\rangle$ results and the we found that the diabatic QTSH and a2d QTSH $\left\langle \alpha^{\mathrm{D}} \right\rangle$ results deviated more significantly the exact quantum result, after $t \approx 12$ fs, when the second transition from the upper adiabatic state $V_{+}(\boldsymbol{q})$ to the lower adiabatic state $V_{-}(\boldsymbol{q})$ takes place. The results were also slightly displaced in the positive direction and the oscillations are of larger amplitude than the exact quantum results after 12 fs. This effect was most pronounced for the systems with the largest diabatic coupling constant C.

The observation of the increase in the amplitude of oscillations after the first transition agrees with our understanding of the overcoherence of the QTSH method as a result of the *independent* trajectory approximation made [1, 3].

We now examine the phase space averaged imaginary part of the off-diagonal/coherence components of the Wigner distribution [74, 75] in the adiabatic and diabatic representations $\left\langle \beta^{\mathrm{A}}(t) \right\rangle$ and $\left\langle \beta^{\mathrm{D}}(t) \right\rangle$.

In Figs 3.8 and 3.9, we present (a) the comparison of the adiabatic QTSH and d2a QTSH results for the phase space averaged adiabatic population $\left\langle \beta^{\mathrm{A}}(t) \right\rangle$ against the exact quantum results, and (b) the comparison of the diabatic QTSH and a2d QTSH results for the phase space averaged diabatic population $\left\langle \beta^{\mathrm{D}}(t) \right\rangle$ against the exact quantum results, for the simple avoided crossing system [1] involving the non-adiabatic processes that include the $+ \rightarrow -$ electronic transition (Fig 2.2) and the $- \rightarrow +$ electronic transition (Fig 2.4) in the adiabatic representation, respectively. The corresponding processes in the diabatic representation are depicted in Figs 2.3 and 2.5, respectively.

In Fig 3.10, we present (a) the comparison of the adiabatic QTSH and d2a QTSH results for the phase space averaged adiabatic population $\left\langle \beta^{\mathrm{A}}(t) \right\rangle$ against the exact quantum results, and (b) the comparison of the diabatic QTSH and a2d QTSH results for the phase space averaged diabatic population $\left\langle \beta^{\mathrm{D}}(t) \right\rangle$ against the exact quantum results, for the non-adiabatic process in the dual avoided crossing system [1] that involves the non-adiabatic transition from the lower adiabatic state to the upper adiabatic state $- \rightarrow +$, followed by a second non-adiabatic transition from the upper adiabatic state to the lower adiabatic state $+ \rightarrow -$ in the adiabatic representation (Fig 2.8). The corresponding process in the diabatic representation is depicted in Fig. 2.9.

We provide a cursory analysis of the representation invariance of the phase space average of the imaginary part of the coherences/off-diagonal terms of the Wigner distribution [74, 75] by

comparing the adiabatic QTSH results and d2a QTSH results for $\langle \beta^{\mathrm{A}}(t) \rangle$, and the diabatic QTSH results and a2d QTSH results for $\langle \beta^{\mathrm{D}}(t) \rangle$.

With reference to Figs 3.8(a), 3.9(a) and 3.10(a), and Figs 3.8(b), 3.9(b) and 3.10(b), the adiabatic QTSH results and d2a QTSH results for $\langle \beta^{\mathrm{A}}(t) \rangle$, and the diabatic QTSH results and a2d QTSH results for $\langle \beta^{\mathrm{D}}(t) \rangle$ are in perfect agreement.

This proves the validity of the derived Eqns 3.22 and 3.26.

Since the d2a QTSH results and the adiabatic QTSH results for $\langle \beta^{\mathrm{A}}(t) \rangle$, and the a2d QTSH results and the diabatic QTSH results for $\langle \beta^{\mathrm{D}}(t) \rangle$ are in perfect agreement, the system phase space averaged components of the imaginary part of the off-diagonal/coherence elements of the Wigner distribution [74, 75] computed by the QTSH method is representation invariant.

We now provide a more in-depth analysis of the accuracy of the phase space average imaginary part of the coherences/off-diagonal terms of the Wigner distribution [74, 75] by comparing the adiabatic QTSH results and d2a QTSH results for $\langle \beta^{\mathrm{A}}(t) \rangle$ with the exact quantum results, and the diabatic QTSH results and a2d QTSH results for $\langle \beta^{\mathrm{D}}(t) \rangle$ with the exact quantum results.

With reference to Figs 3.8(a) and (b) we found that the adiabatic QTSH and d2a QTSH results for $\langle \beta^{\mathrm{A}}(t) \rangle$, and the diabatic QTSH and a2d QTSH results for $\langle \beta^{\mathrm{D}}(t) \rangle$ deviate from the quantum results after 25 fs. The results exhibit oscillations that are slightly out-of-phase with the quantum results.

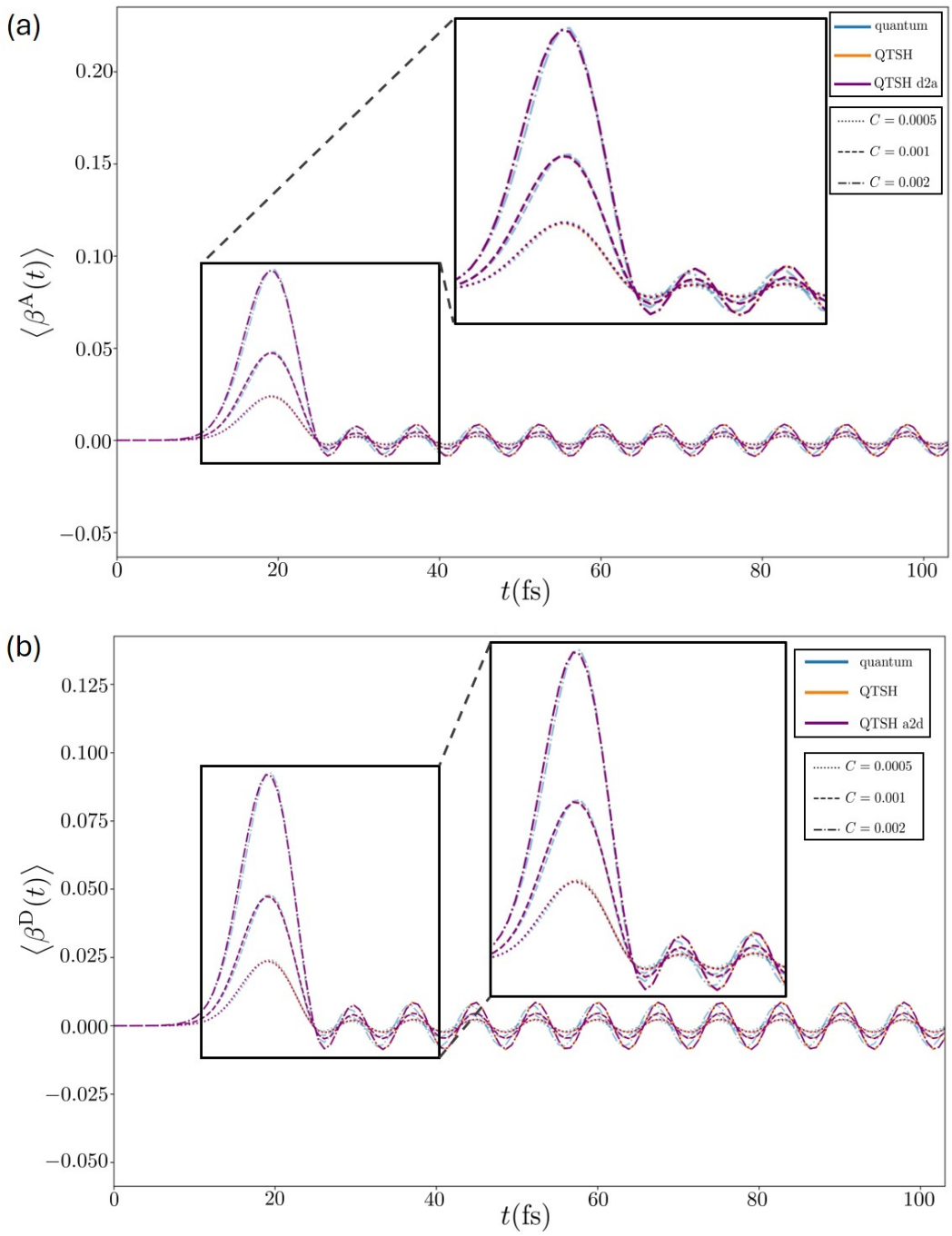

Figure 3.8: Comparison of exact quantum result for (a) the phase space averaged imaginary part of the coherence $\langle \beta^{A}(t) \rangle$ with the adiabatic QTSH result and the transformed d2a QTSH result, and (b) the phase space averaged imaginary part of the coherence $\langle \beta^{D}(t) \rangle$ with the diabatic QTSH result, and the transformed a2d QTSH result, for the for the processes described in Figs 2.2 and 2.3 for the simple avoided crossing system described by the diabatic potentials given by Eqns 1.83-1.84. The inset shows the magnified plot between $t = 10$ fs and $t = 40$ fs.

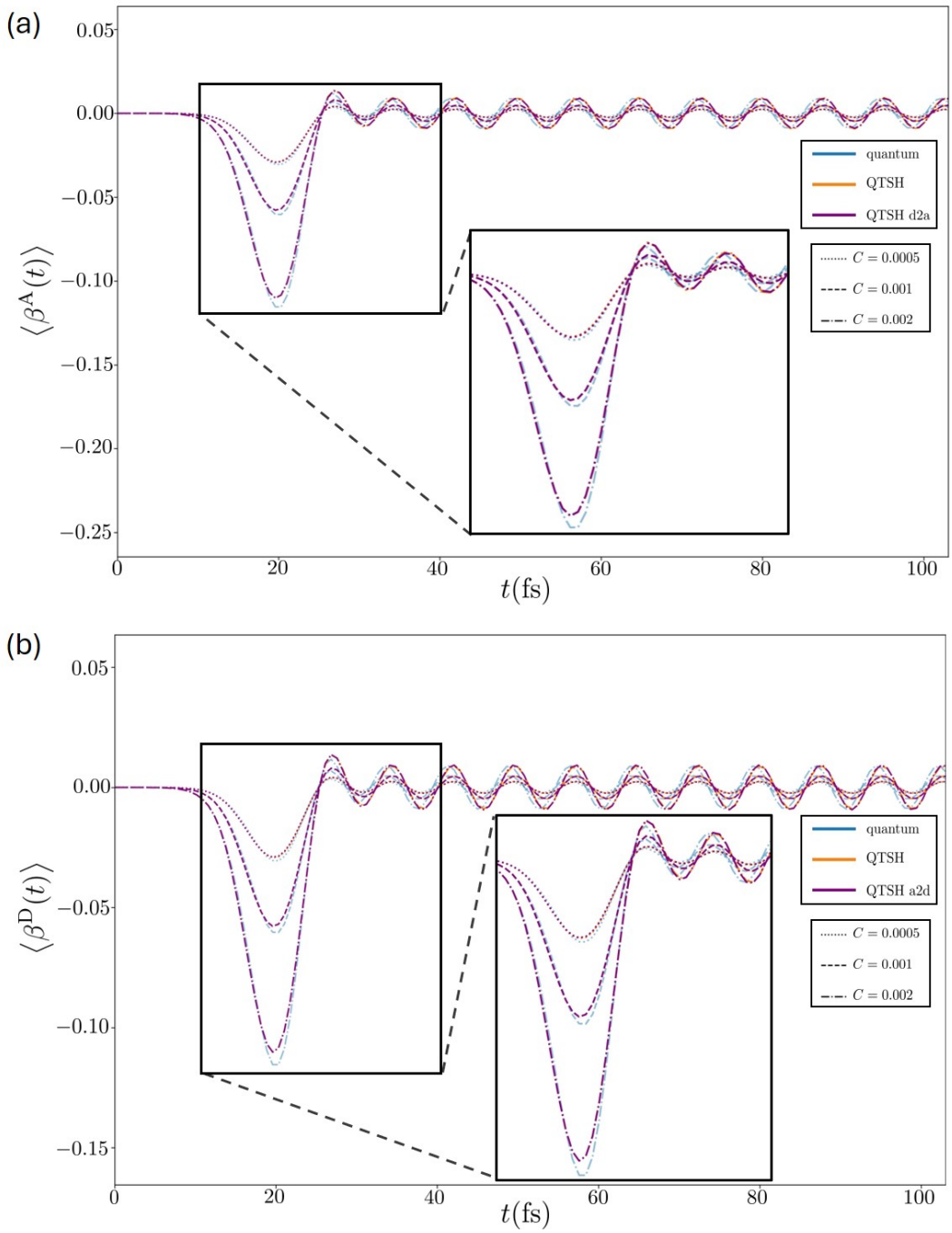

Figure 3.9: Comparison of exact quantum result for (a) the phase space averaged imaginary part of the coherence $\langle \beta^{A}(t) \rangle$ with the adiabatic QTSH result and the transformed d2a QTSH result, and (b) the phase space averaged imaginary part of the coherence $\langle \beta^{D}(t) \rangle$ with the diabatic QTSH result, and the transformed a2d QTSH result, for the for the processes described in Figs 2.4 and 2.5 for the simple avoided crossing system described by the diabatic potentials given by Eqns 1.83-1.84. The inset shows the magnified plot between $t = 10$ fs and $t = 40$ fs.

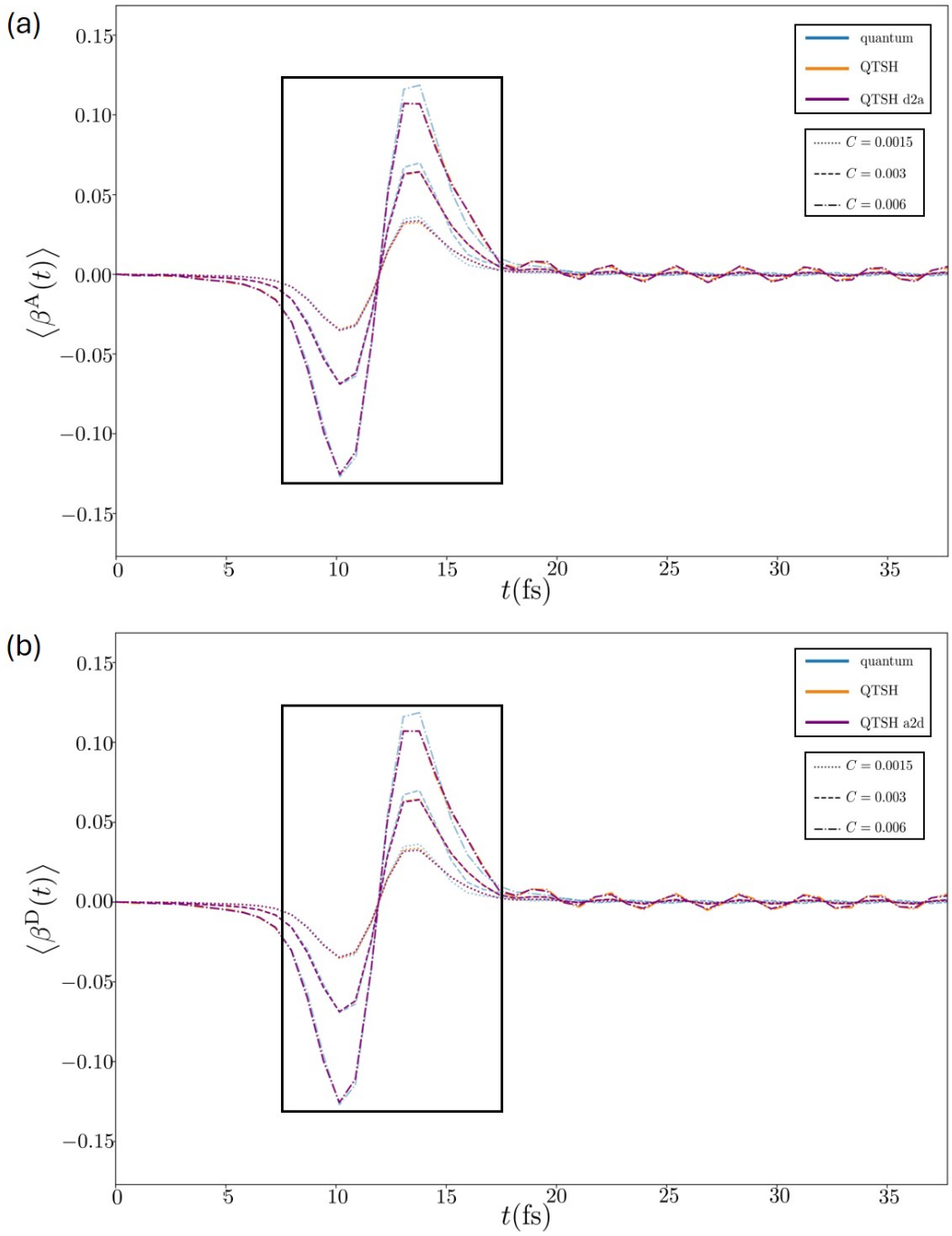

Figure 3.10: Comparison of exact quantum result for (a) the phase space averaged imaginary part of the coherence $\langle \beta^{\mathrm{A}}(t) \rangle$ with the adiabatic QTSH result and the transformed d2a QTSH result, and (b) the phase space averaged imaginary part of the coherence $\langle \beta^{\mathrm{D}}(t) \rangle$ with the diabatic QTSH result, and the transformed a2d QTSH result, for the for the processes described in Figs 2.8 and 2.9 for the dual avoided crossing system described by the diabatic potentials given by Eqns 1.86-1.87. The black box highlights the plot between $t = 7.5$ fs and $t = 17.5$ fs.

With reference to Figs 3.9(a) and (b), we found that the adiabatic QTSH and d2a QTSH results for $\left\langle \beta^{\mathrm{A}}(t) \right\rangle$, and the diabatic QTSH and a2d QTSH results for $\left\langle \beta^{\mathrm{D}}(t) \right\rangle$ deviate from the quantum results between $t \approx 18$ fs and $t \approx 22$ fs. After $t \approx 27$ fs, we find that the d2a QTSH and the adiabatic QTSH results for $\left\langle \beta^{\mathrm{A}}(t) \right\rangle$, and the a2d QTSH and the diabatic QTSH results for $\left\langle \beta^{\mathrm{D}}(t) \right\rangle$ have oscillations that are slightly out-of-phase in comparison to the quantum results.

This overcoherence [1, 3] observed is a consequence of utilizing *independent* trajectories. In order to correctly capture the quantum coherence, trajectories have to be *interdependent* [39–41, 52–58].

With reference to Figs 3.10(a) and (b) we found that the adiabatic QTSH and d2a QTSH results for $\left\langle \beta^{\mathrm{A}}(t) \right\rangle$, and the diabatic QTSH and a2d QTSH results for $\left\langle \beta^{\mathrm{D}}(t) \right\rangle$ deviate significantly from the quantum results after the first transition has taken place, after $t \approx 12$ fs. We also found that the adiabatic QTSH and d2a QTSH results for $\left\langle \beta^{\mathrm{A}}(t) \right\rangle$, and the diabatic QTSH and a2d QTSH results for $\left\langle \beta^{\mathrm{D}}(t) \right\rangle$ are slightly out-of-phase when compared with the quantum results after $t \approx 17.5$ fs.

The quantum interference effect in the dual avoided crossing system [1] that is not well-captured in QTSH as a result of the *independent* trajectories used [4, 8] in QTSH [62, 63] becomes significant after the first electronic transition, resulting in a decrease in the accuracy after the first electronic transition.

3.4.2 Forces

We now examine the dynamics of the forces in QTSH. To obtain the d2a QTSH and a2d QTSH results for the elements of the forces in the adiabatic and diabatic representations, we applied Eqns 3.49-3.51 to the diabatic QTSH results, and applied Eqns 3.53-3.55 to the adiabatic QTSH results, respectively.

We start by comparing the system phase space total force in the adiabatic representation $\left\langle \boldsymbol{F}_{\text{tot}}^{\text{A}}(t) \right\rangle$ and in the diabatic representation $\left\langle \boldsymbol{F}_{\text{tot}}^{\text{D}}(t) \right\rangle$ to verify its equivalence as described by Eqn 3.52.

Even though the simple avoided crossing and dual avoided crossing systems are apparently different in the adiabatic and the diabatic representation, the total forces governing the coupled electronic-nuclear dynamics in each representation should be identical.

In Figs 3.11 and 3.12, we compare $\left\langle \boldsymbol{F}_{\text{tot}}^{\text{D}}(t) \right\rangle$ and $\left\langle \boldsymbol{F}_{\text{tot}}^{\text{A}}(t) \right\rangle$ for the QTSH simulations of the simple avoided crossing system [1] for the processes involving the $+ \rightarrow -$ transition in the adiabatic representation (Fig 2.2), and involving the $- \rightarrow +$ transition in the adiabatic representation (Fig 2.4), respectively. The corresponding processes in the diabatic representation are described by Figs 2.3 and 2.5, respectively.

In Fig 3.13, we compare $\left\langle \boldsymbol{F}_{\text{tot}}^{\text{D}}(t) \right\rangle$ and $\left\langle \boldsymbol{F}_{\text{tot}}^{\text{A}}(t) \right\rangle$ for the QTSH simulations of the dual avoided crossing system [1] for the process that involves the non-adiabatic transition from $- \rightarrow +$, followed by a second non-adiabatic transition from $+ \rightarrow -$ in the adiabatic representation (Fig 2.8). The corresponding process in the diabatic representation is depicted in Fig. 2.9.

With reference to Figs 3.11 and Fig 3.12, we observed that $\left\langle \boldsymbol{F}_{\text{tot}}^{\text{A}}(t) \right\rangle \approx \left\langle \boldsymbol{F}_{\text{tot}}^{\text{D}}(t) \right\rangle$ for each diabatic coupling constant C used, for the processes described by Figs 2.2 and 2.4 in the adiabatic representation, and Figs 2.3 and 2.5 in the diabatic representation.

With reference to Figs 3.13, we observed that $\left\langle \boldsymbol{F}^{\mathrm{A}}_{\mathrm{tot}}(t) \right\rangle$ and $\left\langle \boldsymbol{F}^{\mathrm{D}}_{\mathrm{tot}}(t) \right\rangle$ agreed in terms of its overall shape - two peaks - a maximum during the time interval for the first $- \rightarrow +$ electronic transition, and a minimum for the second $+ \rightarrow -$ electronic transition in the adiabatic representation (Fig 2.8).

The above observations verifies Eqn 3.52 for the simple avoided crossing and dual avoided systems [1]. While imperfect, there is loose agreement between $\left\langle \boldsymbol{F}^{\mathrm{A}}_{\mathrm{total}}(t) \right\rangle$ and $\left\langle \boldsymbol{F}^{\mathrm{D}}_{\mathrm{total}}(t) \right\rangle$ for the dual avoided crossing system [1].

From a practical standpoint, the accuracy of QTSH might not be the same in both representations, resulting in the discrepancy in the phase space averaged total force in the diabatic and adiabatic representations. We will explore this further in Chapter 4.

With reference to Figs 3.11 and 3.12, we found that largest deviation occurred for $\left\langle \boldsymbol{F}^{\mathrm{A}}_{\mathrm{tot}}(t) \right\rangle$ and $\left\langle \boldsymbol{F}^{\mathrm{D}}_{\mathrm{tot}}(t) \right\rangle$ at $t \approx 20$ fs, where the fastest rate of $+ \rightarrow -$ and $- \rightarrow +$ electronic transitions occurred in the adiabatic representation, respectively. The best agreement was obtained for $C = 0.0005$, and the worst for $C = 0.002$. The agreement was best when the non-adiabatic coupling $\boldsymbol{d}(\boldsymbol{q})$, and consequently the population transfer was most localized and highest in the adiabatic representation.

With reference to Fig 3.13, we found that deviation between $\left\langle \boldsymbol{F}^{\mathrm{A}}_{\mathrm{tot}}(t) \right\rangle$ and $\left\langle \boldsymbol{F}^{\mathrm{D}}_{\mathrm{tot}}(t) \right\rangle$ shows up as a positive time shift of $\left\langle \boldsymbol{F}^{\mathrm{A}}_{\mathrm{tot}}(t) \right\rangle$ with respect to $\left\langle \boldsymbol{F}^{\mathrm{D}}_{\mathrm{tot}}(t) \right\rangle$. This implies that the electronic transitions in the adiabatic representation that occurs at a later time than in the diabatic representation for $C = 0.001$ and $C = 0.002$. The positive time shift was smaller for the dual avoided crossing system [1] with $C = 0.001$ than with $C = 0.002$. For the system $C = 0.0005$, no distinct peaks were present for both $\left\langle \boldsymbol{F}^{\mathrm{A}}_{\mathrm{tot}}(t) \right\rangle$ and $\left\langle \boldsymbol{F}^{\mathrm{D}}_{\mathrm{tot}}(t) \right\rangle$, appearing to exhibit fluctuations in the time interval $t = 7.5$ fs to $t = 17.5$ fs.

We will explore this in Section 4.4.2 of Chapter 4.

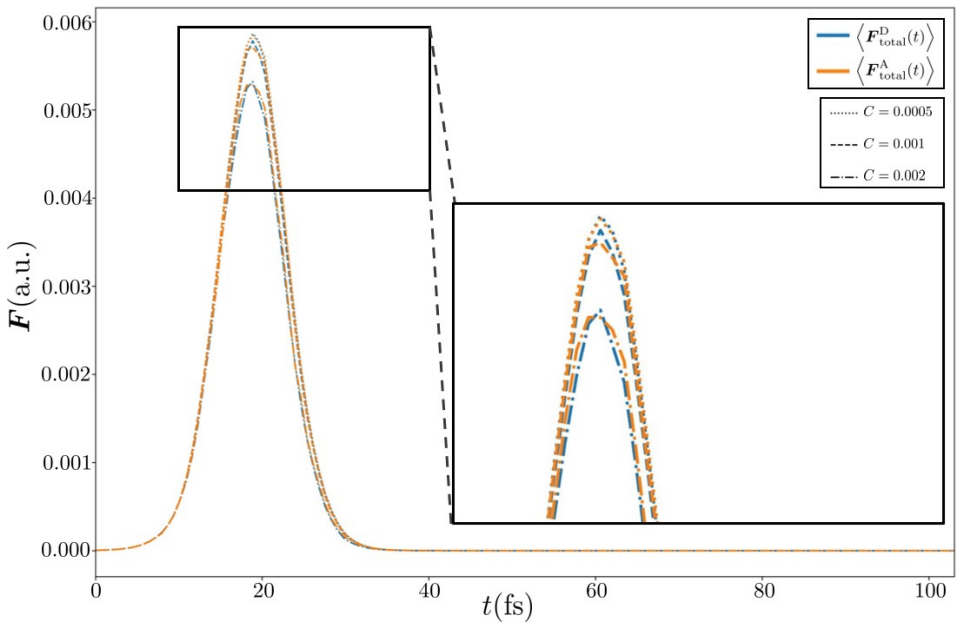

Figure 3.11: QTSH results for the phase space averaged total force in the diabatic and adiabatic representation, $\langle \boldsymbol{F}^{\mathrm{D}}_{\mathrm{total}} \rangle$ and $\langle \boldsymbol{F}^{\mathrm{A}}_{\mathrm{total}} \rangle$ for the processes described in Figs 2.2 and 2.3 for the simple avoided crossing system described by the diabatic potentials given by Eqns 1.83-1.84.

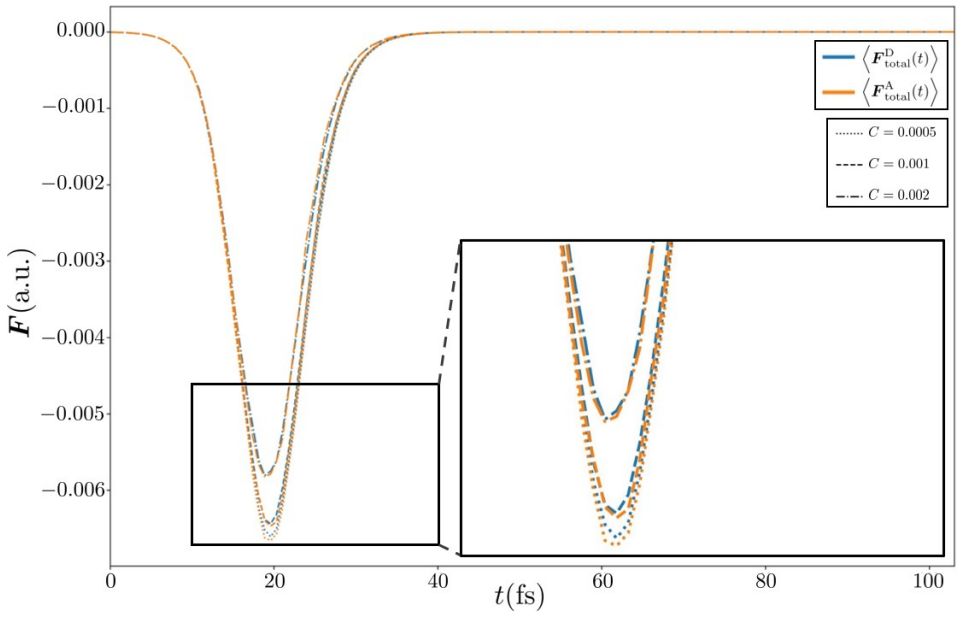

Figure 3.12: QTSH results for the phase space averaged total force in the diabatic and adiabatic representation, $\langle \boldsymbol{F}^{\mathrm{D}}_{\mathrm{total}} \rangle$ and $\langle \boldsymbol{F}^{\mathrm{A}}_{\mathrm{total}} \rangle$ for the processes described in Figs 2.4 and 2.5 for the simple avoided crossing system described by the diabatic potentials given by Eqns 1.83-1.84.

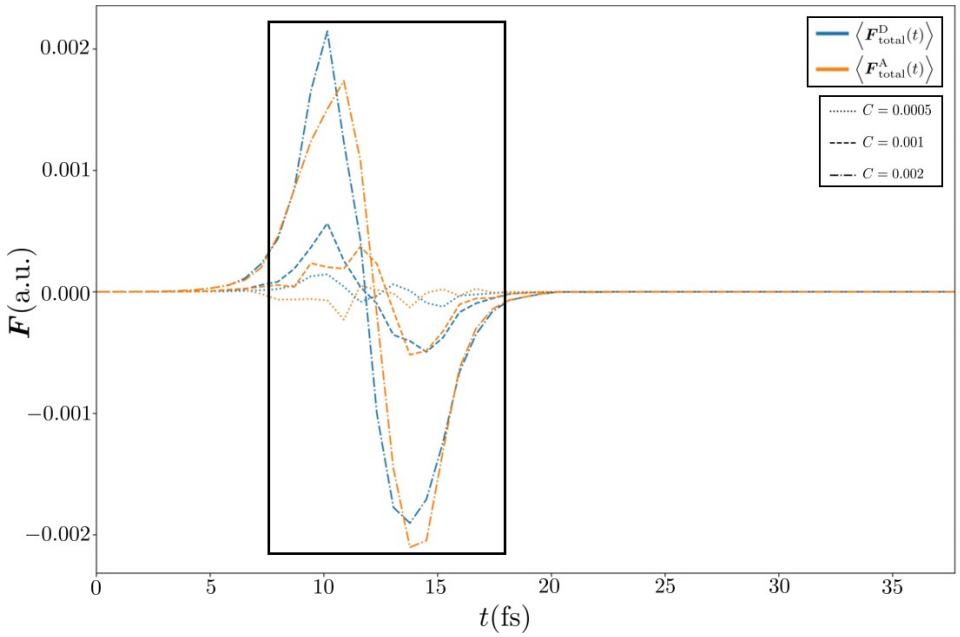

Figure 3.13: QTSH results for the phase space averaged total force in the diabatic and adiabatic representation, $\langle \boldsymbol{F}^{\mathrm{D}}_{\mathrm{total}} \rangle$ and $\langle \boldsymbol{F}^{\mathrm{A}}_{\mathrm{total}} \rangle$ for the processes described in Figs 2.8 and 2.9 for the dual avoided crossing system described by the diabatic potentials given by Eqns 1.86-1.87. The black box highlights the plot in the time interval $t = 7.5$ fs and $t = 17.5$ fs.

We now present the d2a and a2d QTSH for the classical, quantum and total forces for non-adiabatic processes occurring in the simple avoided crossing system, and dual avoided crossing system [1].

We first examine the adiabatic QTSH and d2a QTSH results for the system phase space averaged classical force $\langle \boldsymbol{F}^{\mathrm{A}}_{\mathrm{class}}(t) \rangle$, quantum force $\langle \boldsymbol{F}^{\mathrm{A}}_{\mathrm{quant}}(t) \rangle$, and total force $\langle \boldsymbol{F}^{\mathrm{A}}_{\mathrm{tot}}(t) \rangle$ in the adiabatic representation.

In Figs 3.14 and 3.15, we present the adiabatic QTSH and d2a QTSH results for $\langle \boldsymbol{F}^{\mathrm{A}}_{\mathrm{class}}(t) \rangle$, $\langle \boldsymbol{F}^{\mathrm{A}}_{\mathrm{quant}}(t) \rangle$, and $\langle \boldsymbol{F}^{\mathrm{A}}_{\mathrm{tot}}(t) \rangle$ when (a) the most local and complete population transfer ($C = 0.0005$) and (b) the least local and complete population transfer ($C = 0.002$) occurs in the simple avoided crossing system [1] for the process that involves the $+ \rightarrow -$ electronic transition (Fig 2.2), and the $- \rightarrow +$ electronic transition (Fig 2.4), respectively.

In Fig 3.16, we present the adiabatic QTSH and d2a QTSH results for $\left\langle \boldsymbol{F}^{\mathrm{A}}_{\mathrm{class}}(t) \right\rangle$, $\left\langle \boldsymbol{F}^{\mathrm{A}}_{\mathrm{quant}}(t) \right\rangle$, and $\left\langle \boldsymbol{F}^{\mathrm{A}}_{\mathrm{tot}}(t) \right\rangle$ when (a) the most local and complete population transfer ($C = 0.0015$) and (b) the least local and complete population transfer ($C = 0.006$) occurs in the dual avoided crossing system [1] for the process that involves an $-\ \rightarrow\ +$ electronic transition, and a subsequent $-\ \rightarrow\ +$ electronic transition (Fig 2.8).

With reference to Figs 3.14(a) and (b), and 3.15(a) and (b), we observed that each force component $\left\langle \boldsymbol{F}^{\mathrm{A}}_{\mathrm{class}}(t) \right\rangle$, $\left\langle \boldsymbol{F}^{\mathrm{A}}_{\mathrm{quant}}(t) \right\rangle$, and the total $\left\langle \boldsymbol{F}^{\mathrm{A}}_{\mathrm{tot}}(t) \right\rangle$, was in almost perfect agreement for the processes that occur in the simple avoided crossing system [1], for both the highly local and complete, and the less local and complete population transfer.

With reference to Fig 3.16(a) and (b), we observed that the quantum force component $\left\langle \boldsymbol{F}^{\mathrm{A}}_{\mathrm{quant}}(t) \right\rangle$ was in almost perfect agreement for the processes that occur in the dual avoided crossing system [1], for both the highly local and complete ($C = 0.0015$), and the less local and complete ($C = 0.006$) population transfer. On the other hand, the adiabatic QTSH and d2a QTSH results for the classical force component $\left\langle \boldsymbol{F}^{\mathrm{A}}_{\mathrm{class}}(t) \right\rangle$ that depends on the population on each surface deviated from each other, most noticeably in the time intervals of electronic transition $t \approx 7.5$ fs to $t \approx 11.4$ fs, and $t \approx 12$ fs to $t \approx 17.5$ fs. Since the resulting d2a QTSH result for the total force component $\left\langle \boldsymbol{F}^{\mathrm{A}}_{\mathrm{tot}}(t) \right\rangle$ shows a maximum and a minimum where the extrema for $\left\langle \boldsymbol{F}^{\mathrm{A}}_{\mathrm{class}}(t) \right\rangle$ and $\left\langle \boldsymbol{F}^{\mathrm{A}}_{\mathrm{quant}}(t) \right\rangle$ are, while the adiabatic QTSH results for $\left\langle \boldsymbol{F}^{\mathrm{A}}_{\mathrm{tot}}(t) \right\rangle$ results in a maximum and a minimum shifted in positive time from where the extrema for $\left\langle \boldsymbol{F}^{\mathrm{A}}_{\mathrm{class}}(t) \right\rangle$, QTSH in the diabatic representation is likely to produce a better estimate of the forces involved in QTSH. This effect is more noticeable for the system with less local and complete population transfer ($C = 0.006$). As discussed in Section 2.4.2 of Chapter 2, the reduced consistency of surface hopping is likely to explain the shift in the adiabatic QTSH results for $\left\langle \boldsymbol{F}^{\mathrm{A}}_{\mathrm{tot}}(t) \right\rangle$.

Along with the differing degrees of classical or non-classical effects, from a practical standpoint, the accuracy of QTSH might not be the same in both representations, resulting in the discrepancy in the phase space averaged total force in the diabatic and adiabatic representations. The interference effect that is significant in the adiabatic representation for the process occurring in the dual avoided crossing system [4, 8], exacerbates the impact of overcoherence [1, 3] due to the lack of *interdependence* of trajectories [39–41, 52–58] in the ensemble in QTSH. This overcoherence also presents itself in the breakdown of the consistency of surface hopping [50].

With the assertion of QTSH being more accurate in the diabatic representation for the dual avoided crossing model [1], we will explore this in Section 4.4.2 of Chapter 4.

We now consider the diabatic QTSH and a2d QTSH results for the system phase space averaged classical force $\left\langle \boldsymbol{F}^{\mathrm{D}}_{\mathrm{class}}(t)\right\rangle$, quantum force $\left\langle \boldsymbol{F}^{\mathrm{D}}_{\mathrm{quant}}(t)\right\rangle$, and total force $\left\langle \boldsymbol{F}^{\mathrm{D}}_{\mathrm{tot}}(t)\right\rangle$ in the diabatic represenation.

In Figs 3.17 and 3.18, we present the diabatic QTSH and a2d QTSH results for $\left\langle \boldsymbol{F}^{\mathrm{D}}_{\mathrm{class}}(t)\right\rangle$, $\left\langle \boldsymbol{F}^{\mathrm{D}}_{\mathrm{quant}}(t)\right\rangle$, and $\left\langle \boldsymbol{F}^{\mathrm{D}}_{\mathrm{tot}}(t)\right\rangle$ when (a) the least population transfer in the diabatic representation ($C = 0.0005$) and (b) the most population transfer in the diabatic representation ($C = 0.002$) occurs in the simple avoided crossing system [1] for the process that involves the evolution of the trajectories on diabatic surface 1 with little to no hopping (Fig 2.3), and the evolution of the trajectories on diabatic surface 2 with little to no hopping (Fig 2.5), respectively.

In Fig 3.16, we present the diabatic QTSH and a2d QTSH results for $\left\langle \boldsymbol{F}^{\mathrm{A}}_{\mathrm{class}}(t)\right\rangle$, $\left\langle \boldsymbol{F}^{\mathrm{D}}_{\mathrm{quant}}(t)\right\rangle$, and $\left\langle \boldsymbol{F}^{\mathrm{D}}_{\mathrm{tot}}(t)\right\rangle$ when (a) the least population transfer in the diabatic representation ($C = 0.0005$) and (b) the most population transfer in the diabatic representation ($C = 0.002$) occurs in the dual avoided crossing system [1] for the process that involves the evolution of the trajectories on diabatic surface 2 with little to no hopping (Fig 2.9).

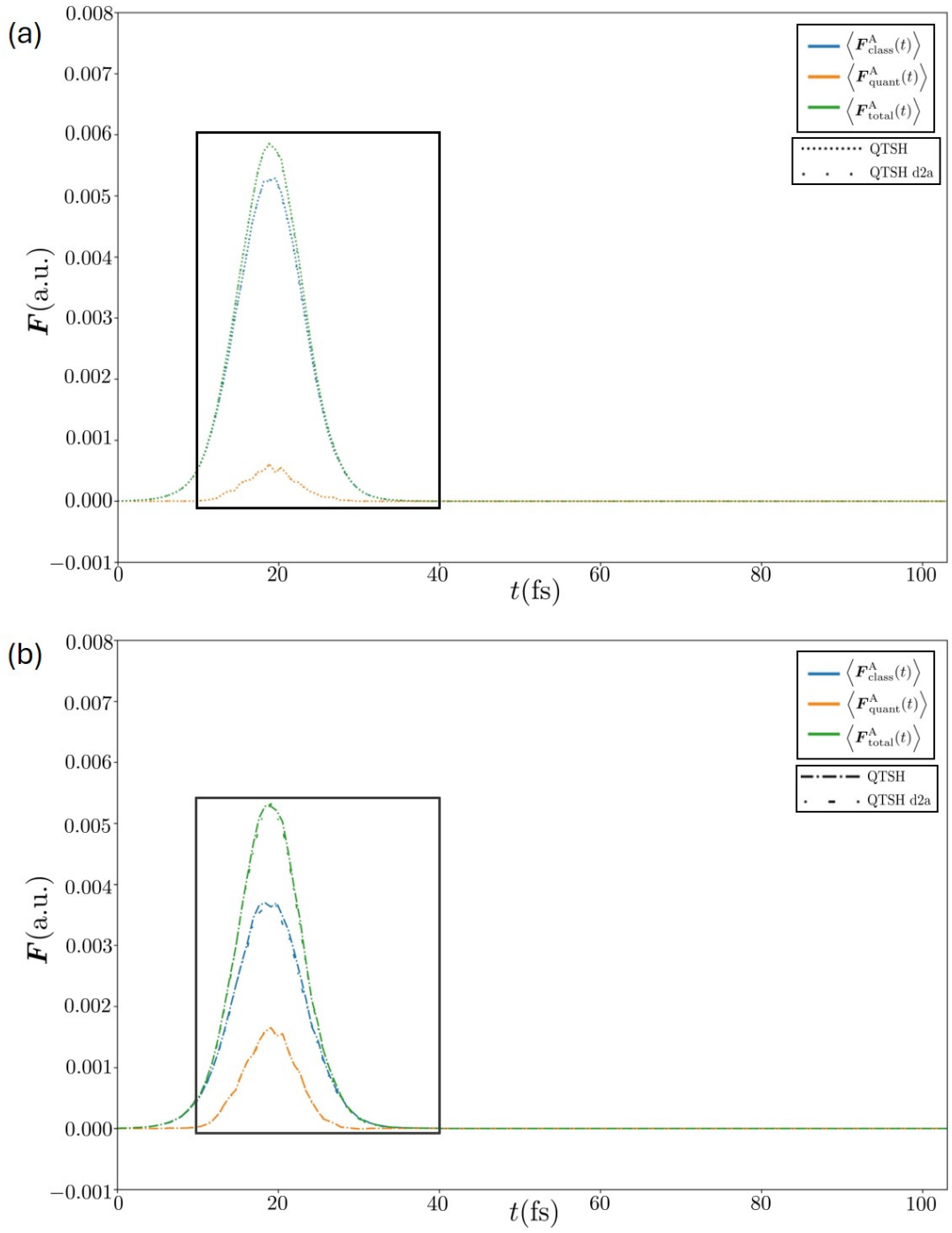

Figure 3.14: Comparison of the adiabatic QTSH and d2a QTSH results for the system phase space averaged classical force $\left\langle \boldsymbol{F}^{\mathrm{A}}_{\mathrm{class}}(t)\right\rangle$, quantum force $\left\langle \boldsymbol{F}^{\mathrm{A}}_{\mathrm{quant}}(t)\right\rangle$, and total force $\left\langle \boldsymbol{F}^{\mathrm{A}}_{\mathrm{total}}(t)\right\rangle$ in the adiabatic representation for the non-adiabatic process in the simple avoided crossing system depicted by Fig 2.2, with the diabatic coupling constants (a) $C = 0.0005$, and (b) $C = 0.002$. The inset shows a magnified view of the plot in the time interval $t = 10$ fs and $t = 40$ fs.

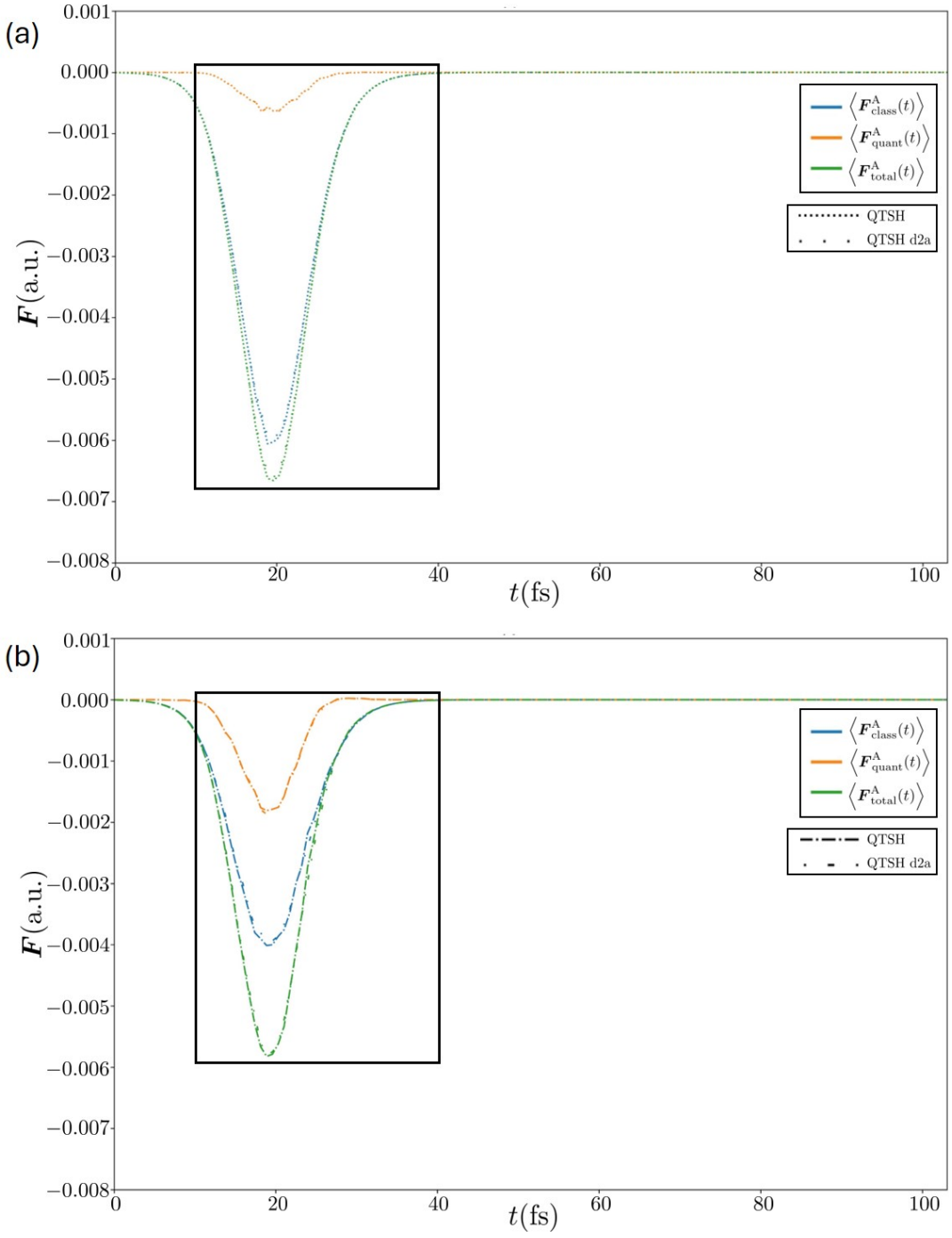

Figure 3.15: Comparison of the adiabatic QTSH and d2a QTSH results for the system phase space averaged classical force $\left\langle \boldsymbol{F}^{\mathrm{A}}_{\mathrm{class}}(t) \right\rangle$, quantum force $\left\langle \boldsymbol{F}^{\mathrm{A}}_{\mathrm{quant}}(t) \right\rangle$, and total force $\left\langle \boldsymbol{F}^{\mathrm{A}}_{\mathrm{total}}(t) \right\rangle$ in the adiabatic representation for the non-adiabatic process in the simple avoided crossing system depicted by Fig 2.4, with the diabatic coupling constants (a) $C = 0.0005$, and (b) $C = 0.002$. The inset shows a magnified view of the plot in the time interval $t = 10$ fs and $t = 40$ fs.

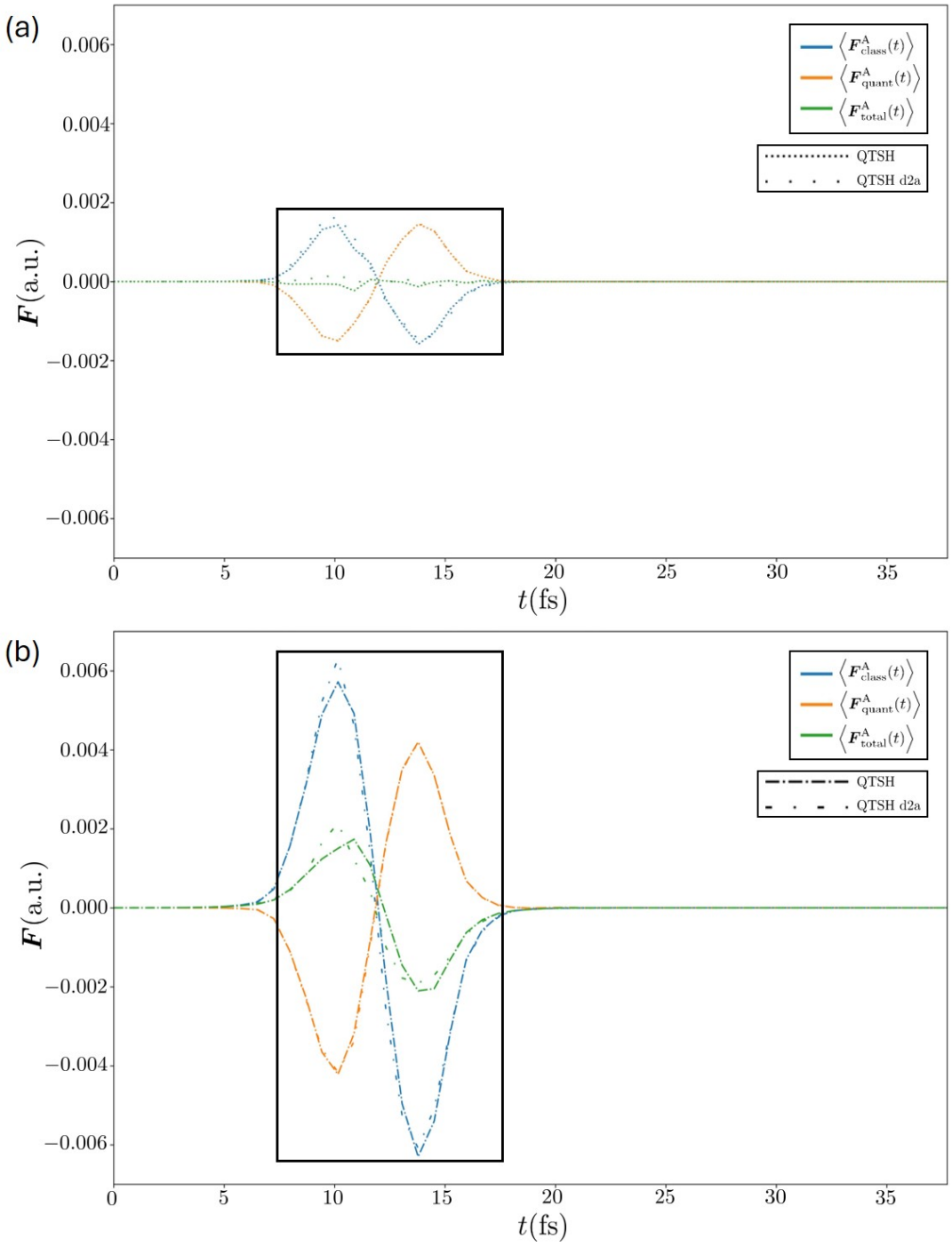

Figure 3.16: Comparison of the adiabatic QTSH and d2a QTSH results for the system phase space averaged classical force $\left\langle \boldsymbol{F}^{\mathrm{A}}_{\mathrm{class}}(t)\right\rangle$, quantum force $\left\langle \boldsymbol{F}^{\mathrm{A}}_{\mathrm{quant}}(t)\right\rangle$, and total force $\left\langle \boldsymbol{F}^{\mathrm{A}}_{\mathrm{total}}(t)\right\rangle$ in the diabatic representation for the non-adiabatic process in the dual avoided crossing system depicted by Fig 2.8, with the diabatic coupling constants (a) $C = 0.0015$, and (b) $C = 0.006$. The inset shows a magnified view of the plot in the time interval $t = 7.5$ fs and $t = 17.5$ fs.

With reference to Figs 3.17(a) and (b), and 3.18(a) and (b), we observed that each force component $\left\langle \boldsymbol{F}^{\mathrm{D}}_{\mathrm{class}}(t)\right\rangle$, $\left\langle \boldsymbol{F}^{\mathrm{D}}_{\mathrm{quant}}(t)\right\rangle$, and the total $\left\langle \boldsymbol{F}^{\mathrm{D}}_{\mathrm{tot}}(t)\right\rangle$, was in almost perfect agreement for the processes that occur in the simple avoided crossing system [1], for both the least ($C = 0.0005$), and the most population transfer ($C = 0.002$), in the diabatic representation.

With reference to Fig 3.19(a) and (b), we observed that the quantum force component $\left\langle \boldsymbol{F}^{\mathrm{D}}_{\mathrm{quant}}(t)\right\rangle$ was in almost perfect agreement for the processes that occur in the dual avoided crossing system [1], for both the least ($C = 0.0015$), and the most ($C = 0.006$) population transfer. We find that $\left\langle \boldsymbol{F}^{\mathrm{D}}_{\mathrm{quant}}(t)\right\rangle$ is very close to zero for $C = 0.0015$ since very little population transfer occurs for this system. The diabatic QTSH and a2d QTSH results for the classical force component $\left\langle \boldsymbol{F}^{\mathrm{D}}_{\mathrm{class}}(t)\right\rangle$ that depends on the population on each surface deviated from each other.

With reference to Fig 3.19(a) observed that the diabatic QTSH and a2d QTSH results for the classical force component $\left\langle \boldsymbol{F}^{\mathrm{D}}_{\mathrm{class}}(t)\right\rangle$ and the total force component $\left\langle \boldsymbol{F}^{\mathrm{D}}_{\mathrm{tot}}(t)\right\rangle$ differ from each other, and exhibits small fluctuations from zero. For the dual avoided crossing [1] with $C = 0.0015$, the lack of distinct extrema in the diabatic QTSH and a2d QTSH results for $\left\langle \boldsymbol{F}^{\mathrm{D}}_{\mathrm{class}}(t)\right\rangle$ and $\left\langle \boldsymbol{F}^{\mathrm{D}}_{\mathrm{tot}}(t)\right\rangle$ loosely agrees with the process depicted in Fig 2.9 where the trajectories evolving only on $V_2(\boldsymbol{q}) = 0$ would give $\left\langle \boldsymbol{F}^{\mathrm{D}}_{\mathrm{class}}(t)\right\rangle = \left\langle \boldsymbol{F}^{\mathrm{D}}_{\mathrm{tot}}(t)\right\rangle = 0$.

With reference to Fig 3.19(b) observed that the diabatic QTSH result for the classical force component $\left\langle \boldsymbol{F}^{\mathrm{D}}_{\mathrm{class}}(t)\right\rangle$ and the total force component $\left\langle \boldsymbol{F}^{\mathrm{D}}_{\mathrm{tot}}(t)\right\rangle$ has a maximum and minimum during the transition during the time intervals of electronic transition $t \approx 7.5$ fs to $t \approx 11.4$ fs, and $t \approx 12$ fs to $t \approx 17.5$ fs, while the maximum in the a2d QTSH results for $\left\langle \boldsymbol{F}^{\mathrm{D}}_{\mathrm{class}}(t)\right\rangle$ and $\left\langle \boldsymbol{F}^{\mathrm{D}}_{\mathrm{tot}}(t)\right\rangle$ falls outside of the $t \approx 7.5$ fs to $t \approx 11.4$ fs time interval. QTSH in the diabatic representation is likely to produce a better estimate of the forces involved in QTSH than in the adiabatic representation for $C = 0.006$.

With the assertion of QTSH being more accurate in the diabatic representation for the dual avoided crossing model [1], we will explore this in Section 4.4.2 of Chapter 4.

Since the adiabatic QTSH and d2a QTSH results, and the diabatic QTSH and a2d QTSH results for all force components almost perfectly agree for the simple avoided crossing system [1], making them representation invariant in QTSH for the processes depicted by Figs 2.2 and 2.4 in the adiabatic representation, and by Figs 2.3 and 2.5 in the diabatic representation, for the simple avoided crossing system [1].

The adiabatic QTSH and d2a QTSH results, and the diabatic QTSH and a2d QTSH results for the quantum force components almost perfectly agree with each other for the dual avoided crossing system [1], making the quantum force component representation invariant in QTSH for the process depicted by Fig 2.8 in the adiabatic representation, and by Fig 2.9 in the diabatic representation, for the dual avoided crossing system [1].

The adiabatic QTSH and d2a QTSH results, and the diabatic QTSH and a2d QTSH results for the classical force and total force components loosely agree with each other for the dual avoided crossing system [1], making these force components representation invariant in QTSH for the process depicted by Fig 2.8 in the adiabatic representation, and by Fig 2.9 in the diabatic representation, for the dual avoided crossing system [1]. Since the classical force component is highly dependent on the populations, the discrepancies are likely to be due to inconsistencies in surface hopping that arises as a result of overcoherence [50, 59].

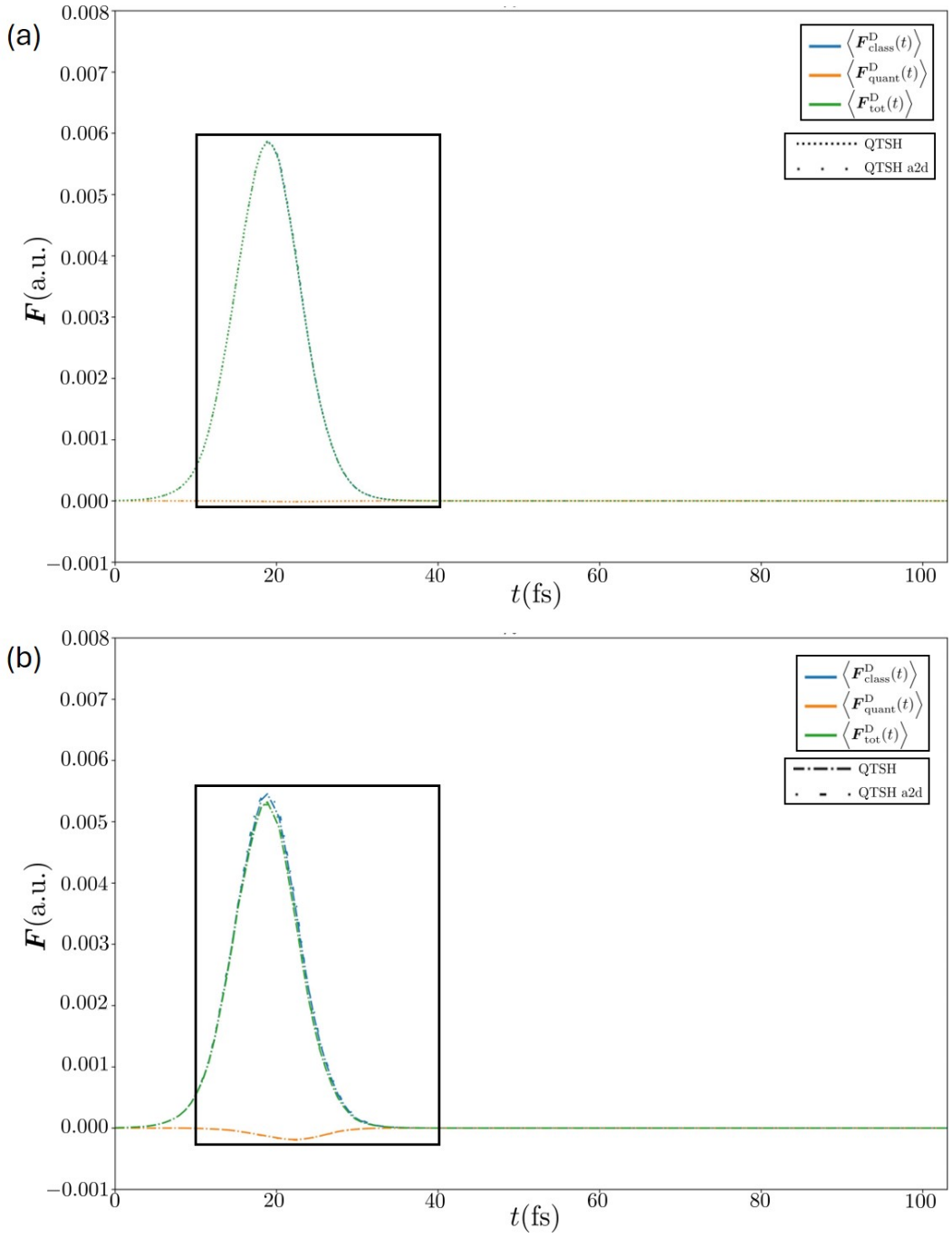

Figure 3.17: Comparison of the diabatic QTSH and a2d QTSH results for the system phase space averaged classical force $\left\langle \boldsymbol{F}^{\mathrm{D}}_{\mathrm{class}}(t) \right\rangle$, quantum force $\left\langle \boldsymbol{F}^{\mathrm{D}}_{\mathrm{quant}}(t) \right\rangle$, and total force $\left\langle \boldsymbol{F}^{\mathrm{D}}_{\mathrm{total}}(t) \right\rangle$ in the diabatic representation for the non-adiabatic process in the simple avoided crossing system depicted by Fig 2.3, with the diabatic coupling constants (a) $C = 0.0005$, and (b) $C = 0.002$. The inset shows a magnified view of the plot in the time interval $t = 10$ fs and $t = 40$ fs.

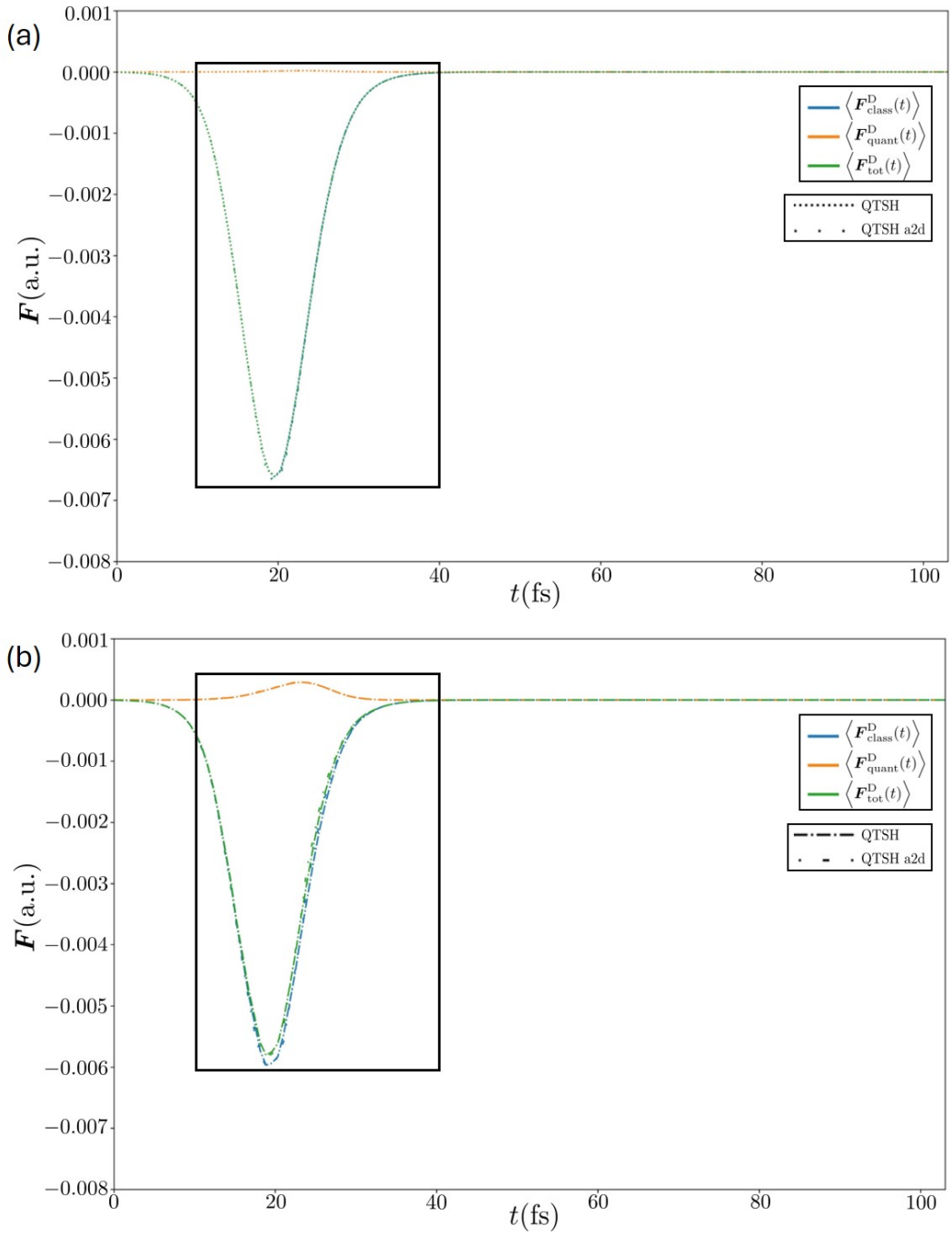

Figure 3.18: Comparison of the diabatic QTSH and a2d QTSH results for the system phase space averaged classical force $\left\langle \boldsymbol{F}^{\mathrm{D}}_{\mathrm{class}}(t)\right\rangle$, quantum force $\left\langle \boldsymbol{F}^{\mathrm{D}}_{\mathrm{quant}}(t)\right\rangle$, and total force $\left\langle \boldsymbol{F}^{\mathrm{D}}_{\mathrm{total}}(t)\right\rangle$ in the diabatic representation for the non-adiabatic process in the simple avoided crossing system depicted by Fig 2.5, with the diabatic coupling constants (a) $C = 0.0005$, and (b) $C = 0.002$. The inset shows a magnified view of the plot in the time interval $t = 10$ fs and $t = 40$ fs.

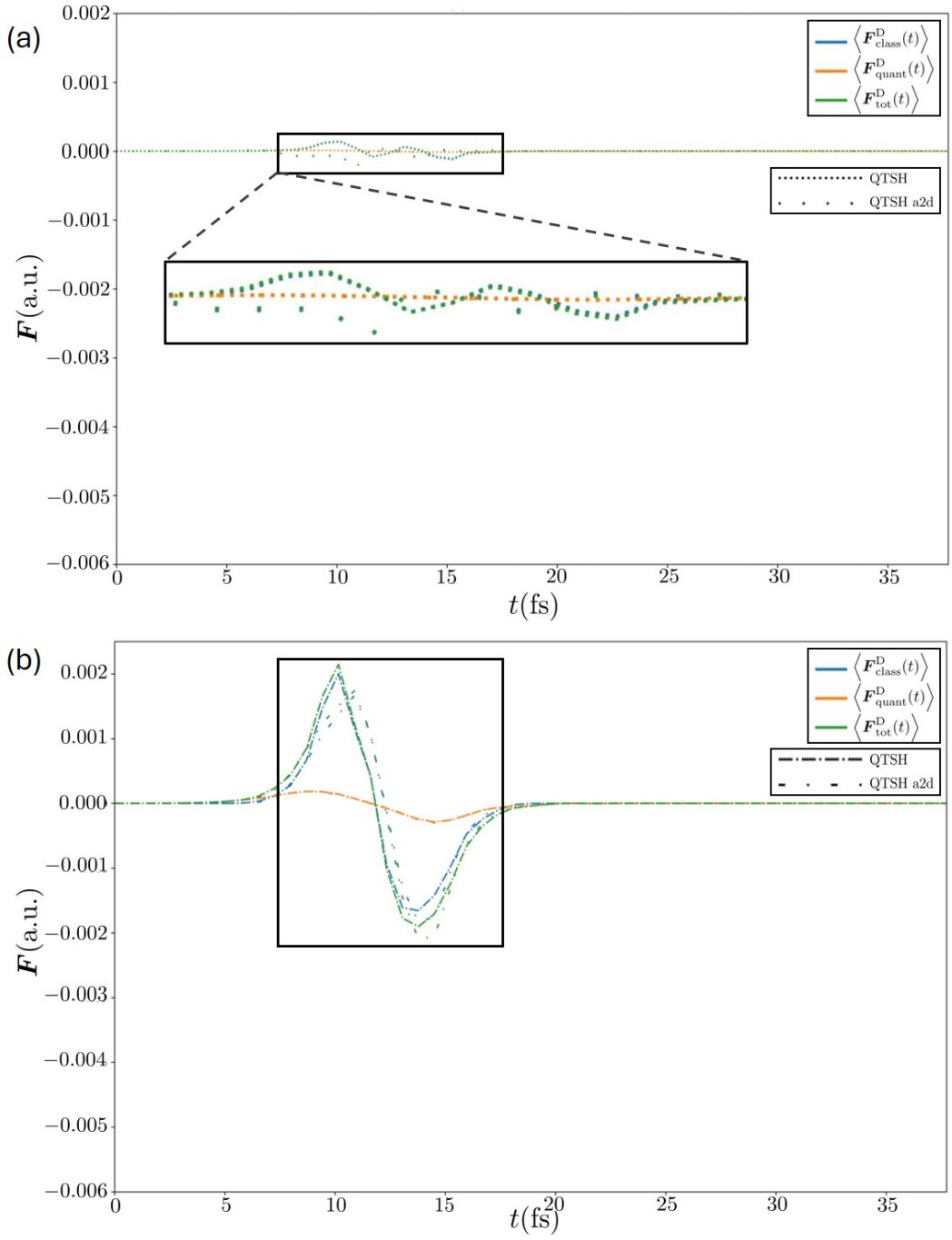

Figure 3.19: Comparison of the diabatic QTSH and a2d QTSH results for the system phase space averaged classical force $\langle \boldsymbol{F}^{\mathrm{D}}_{\mathrm{class}}(t)\rangle$, quantum force $\langle \boldsymbol{F}^{\mathrm{D}}_{\mathrm{quant}}(t)\rangle$, and total force $\langle \boldsymbol{F}^{\mathrm{D}}_{\mathrm{total}}(t)\rangle$ in the diabatic representation for the non-adiabatic process in the dual avoided crossing system depicted by Fig 2.9, with the diabatic coupling constants (a) $C = 0.0015$, and (b) $C = 0.006$. The inset shows a magnified view of the plot in the time interval $t = 7.5$ fs and $t = 17.5$ fs.

3.5 Conclusions

Since the d2a QTSH and adiabatic QTSH results, and the a2d QTSH and diabatic QTSH results, for the system phase space averaged components of the diagonal/population elements and off-diagonal/coherence elements of the Wigner distribution [74, 75], and the forces, are in good agreement - with the slight discrepancies - we conclude that the computation of the system phase space averages of these quantities by the QTSH method is representation invariant.

While the same system appears to be different in the adiabatic and the diabatic representation, the coupled electronic-nuclear dynamics governed by total forces acting on the trajectories in both representations are, as we would expect, to good approximation, the same. We found this to be true even though the classical force components and quantum force components, given by Eqns 3.49 and 3.50 in the adiabatic representation, and Eqns 3.53 and 3.54 in the diabatic representation, are vastly different. We will explore the interplay between the classical and non-classical effects of these forces and representation in Chapter 4.

We note that the results for the quantum force component obtained from the d2a QTSH and adiabatic QTSH simulations, and from the a2d QTSH and diabatic QTSH simulations, are in perfect agreement. Any deviations in the total force were due to deviations in the classical force components that are highly dependent on the potential energy surface that the trajectories are on. As such, the discrepencies can be explained by inconsistencies in surface hopping with QTSH in either representation. The breakdown of the consistency of surface hopping in QTSH is due to overcoherence [1, 3, 59] that results from the use of *independent* trajectories [62, 63].

An improvement of the transformation between representations is likely to be observed if the proper Wigner-Moyal [91] transformation of trajectories between representation was carried out and utilized (See Section 3.6), instead of assuming that the trajectories in the diabatic and adiabatic representations are equivalent.

3.6 Future Work

In ongoing work by Martens [92], it has been found that the trajectories in the diabatic and adiabatic representation are different.

Performing the Wigner-Moyal transformation [73, 91] to the trajectories in the diabatic representation results in the derivation of a different set of equations of motion, population dynamics equations, and equations for energy, force, and populations.

This extends beyond the $\mathcal{O}(\hbar^0)$ simplifications that we have made in the earlier part of this chapter. Here we present the result of performing the Wigner-Moyal [91] transformation [73, 91] on the diabatic trajectories to obtain the adiabatic trajectories.

In the semiclassical limit, the matrix representing the trajectory j, a localized state in phase space for the two-state system in the diabatic representation can be expressed as

$$\Delta_j^{\mathrm{D}}(\boldsymbol{q},\boldsymbol{p},t) = \begin{pmatrix} \delta(\boldsymbol{q}-\boldsymbol{q}_j)\delta(\boldsymbol{p}-\boldsymbol{p}_j) & 0 \\ 0 & \delta(\boldsymbol{q}-\boldsymbol{q}_j)\delta(\boldsymbol{p}-\boldsymbol{p}_j) \end{pmatrix}, \tag{3.56}$$

a diagonal matrix of delta functions in phase space.

The matrix representing the trajectory j in the adiabatic representation $\Delta_j^{\mathrm{A}}(\boldsymbol{q},\boldsymbol{p},t)$ derived by performing the Wigner-Moyal [91] transformation given by Eqn 1.15 on $\Delta_j^{\mathrm{D}}(\boldsymbol{q},\boldsymbol{p},t)$ was

found to be

$$\Delta_j^{\mathrm{A}}(\boldsymbol{q},\boldsymbol{p},t) = \begin{pmatrix} \delta_{\boldsymbol{q}_j}\frac{\delta_{\boldsymbol{p}_j-\hbar\boldsymbol{d}(\boldsymbol{q}_j)}+\delta_{\boldsymbol{p}_j+\hbar\boldsymbol{d}(\boldsymbol{q}_j)}}{2} & -i\ \delta_{\boldsymbol{q}_j}\frac{\delta_{\boldsymbol{p}_j-\hbar\boldsymbol{d}(\boldsymbol{q}_j)}-\delta_{\boldsymbol{p}_j+\hbar\boldsymbol{d}(\boldsymbol{q}_j)}}{2} \\ i\ \delta_{\boldsymbol{q}_j}\frac{\delta_{\boldsymbol{p}_j-\hbar\boldsymbol{d}(\boldsymbol{q}_j)}-\delta_{\boldsymbol{p}_j+\hbar\boldsymbol{d}(\boldsymbol{q}_j)}}{2} & \delta_{\boldsymbol{q}_j}\frac{\delta_{\boldsymbol{p}_j-\hbar\boldsymbol{d}(\boldsymbol{q}_j)}+\delta_{\boldsymbol{p}_j+\hbar\boldsymbol{d}(\boldsymbol{q}_j)}}{2} \end{pmatrix}, \tag{3.57}$$

where $\delta_{\boldsymbol{q}_j}$, $\delta_{\boldsymbol{p}_j-\hbar\boldsymbol{d}(\boldsymbol{q}_j)}$, and $\delta_{\boldsymbol{p}_j+\hbar\boldsymbol{d}(\boldsymbol{q}_j)}$ are shorthand for $\delta(\boldsymbol{q}-\boldsymbol{q}_j)$, $\delta\big(\boldsymbol{p}-(\boldsymbol{p}_j-\hbar\boldsymbol{d}(\boldsymbol{q}_j))\big)$, and $\delta\big(\boldsymbol{p}-(\boldsymbol{p}_j+\hbar\boldsymbol{d}(\boldsymbol{q}_j))\big)$, respectively.

Utilizing the adiabatic trajectories $\Delta_j^{\mathrm{A}}(\boldsymbol{q},\boldsymbol{p},t)$, we go beyond the $\mathcal{O}(\hbar^0)$ approximation we have m a more accurate QTSH method for future use.

Chapter 4

Classical and Non-classical Effects of Forces and Representation

This chapter contains verbatim excerpts from Dorothy Miaoyu Huang, Craig C. Martens; Nonclassical effects in molecular dynamics with electronic transitions (*Unpublished*).

4.1 Introduction

As introduced in Section 1.5.2 of Chapter 1, the QTSH forces in both the diabatic and adiabatic representations have a classical and a quantum force component [62, 63].

The QTSH classical force, like the FSSH force drives the motion of the trajectories along a single electronic potential surface in nuclear phase space [1, 50]. The quantum force component that is absent from the FSSH method [1], as shown in Chapter 2, mediates the feedback between the nuclear and electronic degrees of freedom, acting to conserve the quantum-classical energy on the *ensemble* level, even as non-adiabatic transitions occur [62, 63, 81] in QTSH. In the limit of complete and localized population transfer, we showed

that the work done by the QTSH quantum force is akin to the *ad hoc* momentum 'jumps' imposed to conserve the classical energy on the trajectory level in FSSH [81]. In systems where non-adiabatic transitions do not occur, the quantum force component should vanish, with the classical force being the only driver of the coupled electronic-nuclear dynamics in QTSH.

In this chapter, we will analyze the forces calculated by the QTSH method [62, 63], that act on a localized wavepacket/trajectory in the limit of complete and localized population transfer from one electronic state to another in the adiabatic representation. We also present a simple derivation of its equivalent force in the above mentioned limit in the diabatic representation. In doing so, we will demonstrate that non-adiabatic processes driven only by the classical force on a single electronic state in the diabatic representation are highly non-classical in the adiabatic representation, where both the classical and quantum force components play a significant role in the dynamics of the system, as a result of electronic transition(s) that take place.

We will then present numerical QTSH results in the diabatic and adiabatic representations to demonstrate the validity of the assertions made for the modified Tully's simple avoided crossing, and dual avoided crossing systems [1].

Finally, we utilize the representation invariance of the QTSH phase space averaged populations, as found in Chapter 3, to obtain more accurate phase space averaged population dynamics results for a highly non-classical process in the adiabatic representation. We do so by performing the QTSH method in the diabatic representation, for which the corresponding process is highly classical, before transforming the QTSH population dynamics results to the adiabatic representation (i.e. QTSH d2a).

4.2 Simple Derivation of Adiabatic Forces

In Chapter 3, we have shown that the phase space averaged total force in the adiabatic and diabatic representations, $\left\langle \boldsymbol{F}^{\mathrm{A}}_{\mathrm{total}}(t) \right\rangle$ and $\left\langle \boldsymbol{F}^{\mathrm{D}}_{\mathrm{total}}(t) \right\rangle$ are equivalent (Eqn 3.52) and verified this with QTSH results in both representations.

While we have shown the transformation theory of the forces in the diabatic and adiabatic representations in greater detail in the Chapter 3, we made simplifications by taking the limit of complete and localized population transfer - as we have done in the derivation of the FSSH momentum jumps in Chapter 2 - in this chapter. Note that the subscript j that indicates that the quantities derived in this section, are in fact trajectory phase space averaged quantities for the phase space coordinates associated with trajectory j, $\big(\boldsymbol{q}_j(t), \boldsymbol{p}_j(t)\big)$, are dropped since we are performing the analysis by utilizing a localized wavepacket/single trajectory.

In this limit, Eqn 3.52 can be rewritten as

$$\boldsymbol{F}^{\mathrm{A}}_{\mathrm{total}}(t) = \boldsymbol{F}^{\mathrm{D}}_{\mathrm{total}}(t). \tag{4.1}$$

For the rest of this section, we make the assumption of complete and localized population transfer in the adiabatic representation, unless otherwise stated.

4.2.1 Classical Force in the Adiabatic Representation

The adiabatic potentials for a two-state system $V_{\pm}(\boldsymbol{q})$ can be expressed in terms of the diabatic diagonal potentials $V_{1/2}(\boldsymbol{q})$, and the diabatic off-diagonal potential $V_{12}(\boldsymbol{q})$ as in Eqn 3.29.

Taking the negative gradient of $V_{\pm}(\boldsymbol{q})$ on both sides of Eqn 3.29, we obtain the adiabatic classical force $\boldsymbol{F}^{\mathrm{A}}_{\mathrm{class}}(t)$, where

$$\boldsymbol{F}^{\mathrm{A}}_{\pm}(t) = -\frac{\nabla_{\boldsymbol{q}} V_1(\boldsymbol{q}) + \nabla_{\boldsymbol{q}} V_2(\boldsymbol{q})}{2} \mp \left(\frac{\nabla_{\boldsymbol{q}} V_1(\boldsymbol{q}) - \nabla_{\boldsymbol{q}} V_2(\boldsymbol{q})}{2} \cos\phi(\boldsymbol{q}) + \nabla_{\boldsymbol{q}} V_{12}(\boldsymbol{q}) \sin\phi(\boldsymbol{q}) \right). \quad (4.2)$$

4.2.2 Quantum Force in the Adiabatic Representation

Taking the gradient of both sides of Equation 1.7, and utilizing Equation 1.9, the non-adiabatic coupling vector $\boldsymbol{d}(\boldsymbol{q})$ can be expressed in terms of the diabatic potentials as

$$\boldsymbol{d}(\boldsymbol{q}) = \frac{-\nabla_{\boldsymbol{q}} V_{12}(\boldsymbol{q}) \big(V_1(\boldsymbol{q}) - V_2(\boldsymbol{q})\big) + V_{12}(\boldsymbol{q}) \big(\nabla_{\boldsymbol{q}} V_1(\boldsymbol{q}) - \nabla_{\boldsymbol{q}} V_2(\boldsymbol{q})\big)}{\big(V_1(\boldsymbol{q}) - V_2(\boldsymbol{q})\big)^2 + 4V_{12}(\boldsymbol{q})^2}. \quad (4.3)$$

Noting that the difference in the adiabatic potentials $\hbar\omega^{\mathrm{A}}(\boldsymbol{q}) = V_+(\boldsymbol{q}) - V_-(\boldsymbol{q})$ is

$$\hbar\omega^{\mathrm{A}}(\boldsymbol{q}) = \sqrt{\big(V_1(\boldsymbol{q}) - V_2(\boldsymbol{q})\big)^2 + 4V_{12}(\boldsymbol{q})^2}, \quad (4.4)$$

the non-adiabatic coupling vector $\boldsymbol{d}(\boldsymbol{q})$ can be rewritten as

$$\boldsymbol{d}(\boldsymbol{q}) = \frac{-\nabla_{\boldsymbol{q}} V_{12}(\boldsymbol{q})}{\hbar\omega^{\mathrm{A}}(\boldsymbol{q})} \cos\phi(\boldsymbol{q}) + \frac{\nabla_{\boldsymbol{q}} V_1(\boldsymbol{q}) - \nabla_{\boldsymbol{q}} V_2(\boldsymbol{q})}{2\hbar\omega^{\mathrm{A}}(\boldsymbol{q})} \sin\phi(\boldsymbol{q}). \quad (4.5)$$

Substituting the above into the expression for the quantum force in the adiabatic representation given by Eqn 2.33, we found that the quantum force

$$\boldsymbol{F}^{\mathrm{A}}_{\mathrm{quant}}(t) = \Big(-2\nabla_{\boldsymbol{q}} V_{12}(\boldsymbol{q}) \cos\phi(\boldsymbol{q}) + \big(\nabla_{\boldsymbol{q}} V_1(\boldsymbol{q}) - \nabla_{\boldsymbol{q}} V_2(\boldsymbol{q})\big) \sin\phi(\boldsymbol{q}) \Big) \alpha^{\mathrm{A}}(t), \quad (4.6)$$

depends on the real part of the coherence in the adiabatic represenation $\alpha^{\mathrm{A}}(t)$.

4.2.3 Application to Tully's 1D Systems [1]

In this section we will analyze the QTSH forces for the modified simple avoided crossing and dual avoided crossing systems [1] in the adiabatic representation, where non-adiabatic transitions are involved, and derive the equivalent forces in the diabatic representation.

We begin with a brief description of the processes studied in the adiabatic representation.

The processes involving the simple avoided crossing system [1] involve an electronic transition, either from the upper adiabatic state $V_+(\boldsymbol{q})$ to the lower adiabatic state $V_-(\boldsymbol{q})$ (Fig 2.2), or from the lower adiabatic state $V_-(\boldsymbol{q})$ to the upper adiabatic state $V_+(\boldsymbol{q})$ (Fig 2.4). We will refer to these transitions in shorthand as $+ \rightarrow -$ and $- \rightarrow +$, respectively.

The process involving the dual avoided crossing system depicted in Fig 2.8 involves a $- \rightarrow +$ electronic transition, a short evolution on the upper adiabatic state $V_+(\boldsymbol{q})$ electronic state, and a subsequent $+ \rightarrow -$ electronic transition (Fig 2.8).

For the simple avoided crossing system [1] in the diabatic representation, the processes depicted in Fig 2.3, and Fig 2.5, involve no electronic transitions, with the trajectory evolving along the single diabatic state $V_1(\boldsymbol{q})$, and along the single diabatic state $V_2(\boldsymbol{q})$, respectively. This is equivalently expressed as the diabatic localized density matrix only having one term throughout the processes, the diagonal population term $\rho^{\mathrm{D}}_{11}(t)$ (Eqn 2.4) or $\rho^{\mathrm{D}}_{22}(t)$ (Eqn 2.8).

For the dual avoided crossing system [1], the process in the diabatic representation depicted in Fig 2.9 involves the trajectory evolving along the diabatic state $V_2(\boldsymbol{q}) = 0$. This is equivalently expressed as the diabatic localized density matrix only having one term, the diagonal population term $\rho^{\mathrm{D}}_{22}(t)$ (Eqn A.6), and no coherence terms throughout the process.

This suggests that the total force in the diabatic representation $\boldsymbol{F}^{\mathrm{D}}_{\mathrm{total}}(t)$ for the non-adiabatic processes occurring in the simple avoided crossing and dual avoided crossing systems [1]

described above has to be equal to the classical force associated with the diabatic surface ($V_1(\boldsymbol{q})$ or $V_2(\boldsymbol{q})$) that the trajectory is evolving on, $\boldsymbol{F}^{\mathrm{D}}_{\mathrm{class},1}(t)$ or $\boldsymbol{F}^{\mathrm{D}}_{\mathrm{class},2}(t)$.

The total diabatic force for the simple avoided crossing system [1] is

$$\boldsymbol{F}^{\mathrm{D}}_{\mathrm{total}}(t) = \boldsymbol{F}^{\mathrm{D}}_{\mathrm{class},1}(t), \tag{4.7}$$

for the non-adiabatic process depicted in Fig 2.3, and

$$\boldsymbol{F}^{\mathrm{D}}_{\mathrm{total}}(t) = \boldsymbol{F}^{\mathrm{D}}_{\mathrm{class},2}(t), \tag{4.8}$$

for the non-adiabatic process depicted in Fig 2.5.

Similarly, the total diabatic force for the non-adiabatic process in the dual avoided crossing system [1] depicted by Fig 2.9 is

$$\boldsymbol{F}^{\mathrm{D}}_{\mathrm{total}}(t) = \boldsymbol{F}^{\mathrm{D}}_{\mathrm{class},2}(t). \tag{4.9}$$

We now find the total adiabatic force $\boldsymbol{F}^{\mathrm{A}}_{\mathrm{total}}(t)$ for the corresponding non-adiabatic processes in the adiabatic representations by evaluating the classical and quantum force components of the adiabatic force $\boldsymbol{F}^{\mathrm{A}}_{\mathrm{class}}(t)$ and $\boldsymbol{F}^{\mathrm{A}}_{\mathrm{quant}}(t)$ *before*, *during*, and *after* the electronic transition(s), and show that the total force is the same in both the adiabatic and diabatic representations as given in Eqn 4.1.

We first perform the analysis of QTSH forces for the processes in the simple avoided crossing system with only one non-adiabatic transition, before performing a similar analysis for the process in the dual avoided crossing system that involves two non-adiabatic transitions.

Simple Avoided Crossing System

We now use the generalized expressions for the quantities $\alpha^{\mathrm{A}}(t)$ and $\boldsymbol{F}^{\mathrm{A}}_{\mathrm{quant}}(t)$ for the processes in the simple avoided crossing system system [1] (Figs 2.2 and 2.4).

For $+ \rightarrow -$ in the adiabatic representation, the generalized expressions for the quantities $\alpha^{\mathrm{A}}(t)$ and $\boldsymbol{F}^{\mathrm{A}}_{\mathrm{quant}}(t)$ were

$$\alpha^{\mathrm{A}}(t) = -\frac{1}{2}\sin\phi(\boldsymbol{q}), \tag{4.10}$$

and

$$\boldsymbol{F}^{\mathrm{A}}_{\mathrm{quant}}(t) = \nabla_{\boldsymbol{q}} V_{12}(\boldsymbol{q}) \sin\phi(\boldsymbol{q})\cos\phi(\boldsymbol{q}) - \frac{\big(\nabla_{\boldsymbol{q}} V_1(\boldsymbol{q}) - \nabla_{\boldsymbol{q}} V_2(\boldsymbol{q})\big)}{2}\sin^2\phi(\boldsymbol{q}). \tag{4.11}$$

For $- \rightarrow +$ in the adiabatic representation, the generalized expressions for the quantities $\alpha^{\mathrm{A}}(t)$ and $\boldsymbol{F}^{\mathrm{A}}_{\mathrm{quant}}(t)$ were

$$\alpha^{\mathrm{A}}(t) = \frac{1}{2}\sin\phi(\boldsymbol{q}), \tag{4.12}$$

and

$$\boldsymbol{F}^{\mathrm{A}}_{\mathrm{quant}}(t) = -\nabla_{\boldsymbol{q}} V_{12}(\boldsymbol{q}) \sin\phi(\boldsymbol{q})\cos\phi(\boldsymbol{q}) + \frac{\big(\nabla_{\boldsymbol{q}} V_1(\boldsymbol{q}) - \nabla_{\boldsymbol{q}} V_2(\boldsymbol{q})\big)}{2}\sin^2\phi(\boldsymbol{q}). \tag{4.13}$$

Since the real part of the coherence $\alpha^{\mathrm{A}}(t)$ and the quantum force $\boldsymbol{F}^{\mathrm{A}}_{\mathrm{quant}}(t)$ (Eqn 2.33) in the adiabatic representation depends on the diabatic populations, $\alpha^{\mathrm{A}}(t)$ and $\boldsymbol{F}^{\mathrm{A}}_{\mathrm{quant}}(t)$ were found to have opposite signs for the electronic transitions $+ \rightarrow -$ and $- \rightarrow +$. This agrees with the Figs 2.6(d) and 2.7(b).

As observed in Fig 2.6(b), in general, the strength of the adiabatic coupling $\boldsymbol{d}(\boldsymbol{q})$ for the one-

dimensional system becomes stronger and more localized as diabatic coupling constant C is decreased. In the limit $C \to 0$, the plot for the nonadiabatic mixing angle in one-dimension $\phi(\boldsymbol{q})$ in Fig 2.6(a) becomes a step function as depicted in Fig 4.1.

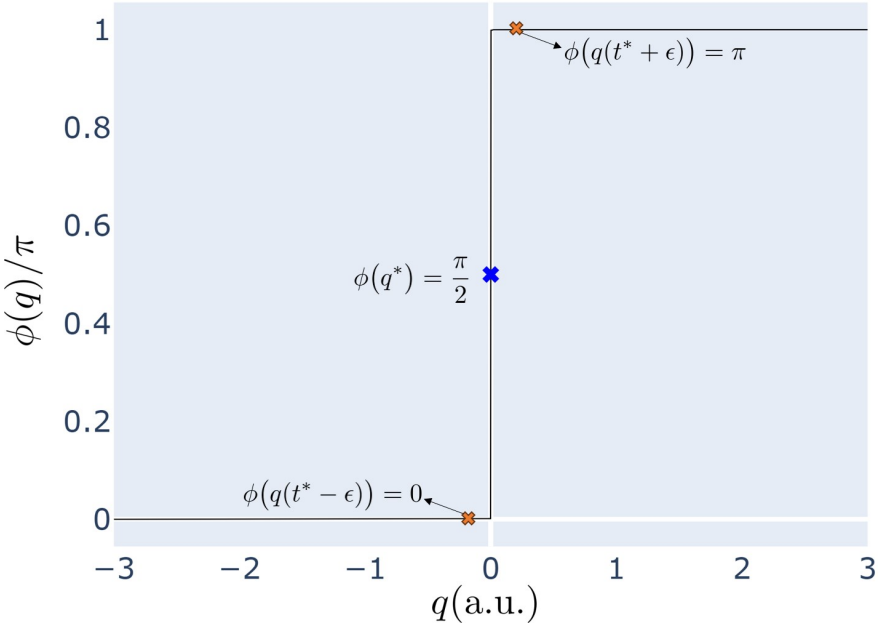

Figure 4.1: Nonadiabatic mixing angle for the simple avoided crossing system given by the diabatic potentials in Eqns 1.83-1.84, where the diabatic coupling constant $C \to 0$. The blue marker marks $\phi(0) = \frac{\pi}{2}$, $\phi(q)$ at the nuclear coordinate where the transition takes place at $q^* = 0$. The orange markers mark $\phi(q(t^* - \epsilon)) = 0$ and $\phi(q(t^* - \epsilon)) = \pi$, the nuclear coordinates the instant ϵ right before and right after the transition, $q(t^* - \epsilon)$ and $q(t^* + \epsilon)$, respectively.

We now find the adiabatic forces - both the quantum and classical - in terms of the diabatic potentials at three time points, the time of the instantaneous electronic transition $t = t^*$, the instant ϵ *before* the electronic transition $t = t^* - \epsilon$, and the instant ϵ *after* the electronic transition $t = t^* + \epsilon$.

For the processes depicted in Figs 2.2 and 2.4, in generalized coordinates $\boldsymbol{q}(t)$, the electronic transition taking place is completely localized and complete at the nuclear coordinate $\boldsymbol{q}(t^*) = 0$, where $\boldsymbol{q}^* \equiv \boldsymbol{q}(t^*)$. This corresponds to the vertical step in Fig 4.1. We took $\phi(\boldsymbol{q}^*) = \frac{\pi}{2}$ to be the midpoint of the step at $\boldsymbol{q}^*$.

At the instant ϵ *before* and *after* the transition, where the generalized coordinates were $\boldsymbol{q}(t^* - \epsilon)$ and $\boldsymbol{q}(t^* + \epsilon)$, respectively. The corresponding non-adiabatic mixing angles were $\phi\big(\boldsymbol{q}(t^* - \epsilon)\big) = 0$ and $\phi\big(\boldsymbol{q}(t^* + \epsilon)\big) = \pi$.

The total force $\boldsymbol{F}^{\mathrm{A}}_{\mathrm{total}}(t)$ in the adiabatic representation consists of a classical component $\boldsymbol{F}^{\mathrm{A}}_{\mathrm{class}}(t)$ and a quantum component $\boldsymbol{F}^{\mathrm{A}}_{\mathrm{quant}}(t)$ that can be expressed as the sum

$$\boldsymbol{F}^{\mathrm{A}}_{\mathrm{total}}(t) = \boldsymbol{F}^{\mathrm{A}}_{\mathrm{class}}(t) + \boldsymbol{F}^{\mathrm{A}}_{\mathrm{quant}}(t). \tag{4.14}$$

We proceed to compute classical forces $\boldsymbol{F}^{\mathrm{A}}_{\mathrm{class}}(t)$ and quantum forces $\boldsymbol{F}^{\mathrm{A}}_{\mathrm{quant}}(t)$, in the limit $C \to 0$.

At the instant before the electronic transition where $t = t^* - \epsilon$, the classical force involves only one adiabatic state, the upper adiabatic state $V_+(\boldsymbol{q})$ or the lower adiabatic state $V_-(\boldsymbol{q})$, for the non-adiabatic process that involved the $+ \to -$ (Fig 2.2) or $- \to +$ (Fig 2.4) electronic transitions, respectively.

Given that $\phi\left(\boldsymbol{q}(t^* - \epsilon)\right) = 0$,

$$\cos\phi\left(\boldsymbol{q}(t^* - \epsilon)\right) = 1, \tag{4.15}$$

and

$$\sin\phi\left(\boldsymbol{q}(t^* - \epsilon)\right) = 0. \tag{4.16}$$

Substituting Eqns 4.15-4.16 into the expression for the classical force in the adiabatic representation (Eqn 4.2), for the process involving the $+ \to -$ electronic transition (Fig 2.2), the

classical force was found to be

$$\boldsymbol{F}^{\mathrm{A}}_{\mathrm{class}}(t^* - \epsilon) = \boldsymbol{F}^{\mathrm{A}}_{+}(t^* - \epsilon) = -\nabla_{\boldsymbol{q}} V_1\big(\boldsymbol{q}(t^* - \epsilon)\big), \tag{4.17}$$

and for the process involving the $- \rightarrow +$ electronic transition (Fig 2.4), the classical force was found to be

$$\boldsymbol{F}^{\mathrm{A}}_{\mathrm{class}}(t^* - \epsilon) = \boldsymbol{F}^{\mathrm{A}}_{-}(t^* - \epsilon) = -\nabla_{\boldsymbol{q}} V_2\big(\boldsymbol{q}(t^* - \epsilon)\big). \tag{4.18}$$

Performing the same procedure for the quantum force, Eqn 4.6 for the process involving the $+ \rightarrow -$ electronic transition (Fig 2.2), and Eqn 4.13 for the process involving the $- \rightarrow +$ electronic transition (Fig 2.4), the quantum force at the instant before the electronic transition in the adiabatic representation $\boldsymbol{F}^{\mathrm{A}}_{\mathrm{quant}}(t^* - \epsilon)$ was found to be

$$\boldsymbol{F}^{\mathrm{A}}_{\mathrm{quant}}(t^* - \epsilon) = 0 \tag{4.19}$$

for both processes. This is consistent with our picture of complete and localized population transfer, where the quantum force is *instantaneous* and impulsive, vanishing when no electronic transition takes place.

The classical force for each process at $t = t^* - \epsilon$, Eqn 4.17 for the process with the $+ \rightarrow -$ transition, and Eqn 4.18 for the process with the $- \rightarrow +$ transition, combines with the corresponding quantum force (Eqn 4.19) to give the total force for each process in the adiabatic representation.

The total force in the adiabatic representation was found to be

$$\boldsymbol{F}^{\mathrm{A}}_{\mathrm{total}}(t^* - \epsilon) = -\nabla_{\boldsymbol{q}} V_1\big(\boldsymbol{q}(t^* - \epsilon)\big) = \boldsymbol{F}^{\mathrm{D}}_{\mathrm{class},1}(t^* - \epsilon), \tag{4.20}$$

the classical force associated with the evolution of a localized wavepacket/trajectory along the diabatic surface $V_1(\boldsymbol{q})$, for the process involving the $+ \rightarrow -$ electronic transition in the adiabatic representation (Fig 2.2), and

$$\boldsymbol{F}^{\mathrm{A}}_{\mathrm{total}}(t^* - \epsilon) = -\nabla_{\boldsymbol{q}} V_2\big(\boldsymbol{q}(t^* - \epsilon)\big) = \boldsymbol{F}^{\mathrm{D}}_{\mathrm{class},2}(t^* - \epsilon), \tag{4.21}$$

the classical force associated with the evolution of a localized wavepacket/trajectory along the diabatic surface $V_2(\boldsymbol{q})$, for the process involving the $- \rightarrow +$ electronic transition in the adiabatic representation (Fig 2.4).

We now derive the forces during the *instantaneous* transition at $t = t^*$, where the nuclear coordinate is $q^* = 0$.

Given that $\phi(\boldsymbol{q}^*) = \frac{\pi}{2}$,

$$\cos\phi(\boldsymbol{q}^*) = 0, \tag{4.22}$$

and

$$\sin\phi(\boldsymbol{q}^*) = 1. \tag{4.23}$$

Regardless of whether the electronic transition was from $+ \rightarrow -$ (Fig 2.2) or from $- \rightarrow +$ (Fig 2.4) in the adiabatic representation, the localized wavepacket/trajectory experiences both the upper and lower adiabatic potentials $V_+(\boldsymbol{q}^*)$ and $V_-(\boldsymbol{q}^*)$ equally at the instant of the transition t^*.

The classical adiabatic force for both systems were found to be given by the same expression

$$\begin{aligned} \boldsymbol{F}^{\mathrm{A}}_{\mathrm{class}}(t^*) &= -\frac{\nabla_{\boldsymbol{q}} V_+(\boldsymbol{q}^*) + \nabla_{\boldsymbol{q}} V_-(\boldsymbol{q}^*)}{2} \\ &= -\frac{\nabla_{\boldsymbol{q}} V_1(\boldsymbol{q}^*) + \nabla_{\boldsymbol{q}} V_2(\boldsymbol{q}^*)}{2}. \end{aligned} \tag{4.24}$$

Substituting Eqns 4.22-4.23 into the expression of the quantum force, Eqn 4.6 for the process involving the $+ \rightarrow -$ electronic transition (Fig 2.2), and Eqn 4.13 for the process involving the $- \rightarrow +$ electronic transition (Fig 2.4), the quantum force at the instant of transition t^* in the adiabatic representation $\boldsymbol{F}^{\mathrm{A}}_{\mathrm{quant}}(t^*)$ were found to be

$$\boldsymbol{F}^{\mathrm{A}}_{\mathrm{quant}}(t^*) = -\frac{\nabla_{\boldsymbol{q}} V_1(\boldsymbol{q}^*) - \nabla_{\boldsymbol{q}} V_2(\boldsymbol{q}^*)}{2}, \tag{4.25}$$

for the process involving the $+ \rightarrow -$ electronic transition (Fig 2.2), and

$$\boldsymbol{F}^{\mathrm{A}}_{\mathrm{quant}}(t^*) = \frac{\nabla_{\boldsymbol{q}} V_1(\boldsymbol{q}^*) - \nabla_{\boldsymbol{q}} V_2(\boldsymbol{q}^*)}{2}, \tag{4.26}$$

for the process involving the $- \rightarrow +$ electronic transition (Fig 2.4). Note the opposite sign of the quantum force for both processes. This is congruous with the acceleration of the localized wavepacket/trajectory for the $+ \rightarrow -$ electronic transition, and the deceleration of the localized wavepacket/trajectory for the $- \rightarrow +$ electronic transition.

Combining $\boldsymbol{F}^{\mathrm{A}}_{\mathrm{quant}}(t^*)$, Eqn 4.25 for the $+ \rightarrow -$ transition, and Eqn 4.26 for the $- \rightarrow +$ transition with $\boldsymbol{F}^{\mathrm{A}}_{\mathrm{class}}(t^*)$ (Eqn 4.24), the total force in the adiabatic representation at the instant of transition t^* was found to be

$$\boldsymbol{F}^{\mathrm{A}}_{\mathrm{total}}(t^*) = -\nabla_{\boldsymbol{q}} V_1(\boldsymbol{q}^*) = \boldsymbol{F}^{\mathrm{D}}_{\mathrm{class},1}(t^*), \tag{4.27}$$

the classical force acting on the localized wavepacket/trajectory along the single diabatic potential energy surface $V_1(\boldsymbol{q}^*)$, as depicted in Fig 2.3 for the $+ \rightarrow -$ transition, and

$$\boldsymbol{F}^{\mathrm{A}}_{\mathrm{total}}(t^*) = -\nabla_{\boldsymbol{q}} V_2(\boldsymbol{q}^*) = \boldsymbol{F}^{\mathrm{D}}_{\mathrm{class},2}(t^*), \tag{4.28}$$

the classical force acting on the localized wavepacket/trajectory along the single diabatic potential energy surface $V_2(\boldsymbol{q}^*)$, as depicted in Fig 2.5 for the $- \rightarrow +$ transition.

Finally, we derive the forces at the instant after the transition $t = t^* + \epsilon$.

Given that $\phi\left(\boldsymbol{q}(t^* + \epsilon)\right) = \pi$,

$$\cos\phi\left(\boldsymbol{q}(t^* + \epsilon)\right) = -1, \tag{4.29}$$

and

$$\sin\phi\left(\boldsymbol{q}(t^* + \epsilon)\right) = 0. \tag{4.30}$$

Substituting Eqns 4.29-4.30 into Eqn 4.2, the expression for the classical force (Eqn 4.2) was found to be

$$\boldsymbol{F}^{\mathrm{A}}_{\mathrm{class}}(t^* + \epsilon) = \boldsymbol{F}^{\mathrm{A}}_{-}(t^* + \epsilon) = -\nabla_{\boldsymbol{q}} V_1\big(\boldsymbol{q}(t^* + \epsilon)\big), \tag{4.31}$$

for the process involving the $+ \rightarrow -$ electronic transition, and

$$\boldsymbol{F}^{\mathrm{A}}_{\mathrm{class}}(t^* + \epsilon) = \boldsymbol{F}^{\mathrm{A}}_{+}(t^* + \epsilon) = -\nabla_{\boldsymbol{q}} V_2\big(\boldsymbol{q}(t^* + \epsilon)\big), \tag{4.32}$$

for the process involving the $- \rightarrow +$ electronic transition.

Substituting Eqns 4.29-4.30 into the expression of the quantum force, Eqn 4.11 for the system involving the $+ \rightarrow -$ electronic transition (Fig 2.2), and Eqn 4.13 for the system involving the $- \rightarrow +$ electronic transition (Fig 2.4), the quantum force at the instant after the electronic transition in the adiabatic representation $\boldsymbol{F}^{\mathrm{A}}_{\mathrm{quant}}(t^* + \epsilon)$ was found to be

$$\boldsymbol{F}^{\mathrm{A}}_{\mathrm{quant}}(t^* + \epsilon) = 0, \tag{4.33}$$

for both processes. As previously observed at the instant before the transition $t = t^* - \epsilon$, the adiabatic quantum force is *instantaneous* and impulsive, vanishing when no electronic transition takes place at $t = t^* + \epsilon$.

The classical force for each process at $t = t^* + \epsilon$, Eqn 4.31 for the process with the $+ \rightarrow -$ transition, and Eqn 4.32 for the process with the $- \rightarrow +$ transition, combines with the corresponding quantum force (Eqn 4.33) to give the total force for each process in the adiabatic representation.

The total force in the adiabatic representation at $t = t^* + \epsilon$ is

$$\boldsymbol{F}^{\mathrm{A}}_{\mathrm{total}}(t^* + \epsilon) = -\nabla_{\boldsymbol{q}} V_1\big(\boldsymbol{q}(t^* + \epsilon)\big) = \boldsymbol{F}^{\mathrm{D}}_{\mathrm{class},1}(t^* + \epsilon), \tag{4.34}$$

the classical force acting on the localized wavepacket/trajectory evolving along the diabatic potential energy surface $V_1(\boldsymbol{q}^* + \epsilon)$ for the process that involves the $+ \rightarrow -$ transition in the adiabatic representation, and

$$\boldsymbol{F}^{\mathrm{A}}_{\mathrm{total}}(t^* + \epsilon) = -\nabla_{\boldsymbol{q}} V_2\big(\boldsymbol{q}(t^* + \epsilon)\big) = \boldsymbol{F}^{\mathrm{D}}_{\mathrm{class},2}(t^* + \epsilon), \tag{4.35}$$

the classical force acting on the localized wavepacket/trajectory evolving along the diabatic potential energy surface $V_2(\boldsymbol{q}^* + \epsilon)$ for the process that involves the $- \rightarrow +$ transition in the adiabatic representation.

We have now shown that *before*, *during*, and *after* the complete and localized population transfer, the total adiabatic force $\boldsymbol{F}^{\mathrm{A}}_{\mathrm{tot}}(t)$ is equivalent the classical diabatic force experienced on a single electronic potential energy surface, reflecting the process occurring on a single electronic potential energy surface in the diabatic representation.

For the process involving the $+ \rightarrow -$ electronic transition in the adiabatic representation (Fig 2.2). Throughout the process, the total adiabatic force

$$\boldsymbol{F}^{\mathrm{A}}_{\mathrm{tot}}(t) = \boldsymbol{F}^{\mathrm{D}}_{\mathrm{class},1}(t), \tag{4.36}$$

the classical force acting to evolve the localized wavepacket/trajectory along a single diabatic surface $V_1(\boldsymbol{q})$, making the process in the diabatic representation (Fig 2.3) highly classical since the quantum force vanishes when no electronic transitions take place.

A similar conclusion can be drawn for the process involving the $- \rightarrow +$ electronic transition in the adiabatic representation (Fig 2.4). Throughout the process, the total adiabatic force

$$\boldsymbol{F}^{\mathrm{A}}_{\mathrm{tot}}(t) = \boldsymbol{F}^{\mathrm{D}}_{\mathrm{class},2}(t), \tag{4.37}$$

the classical force acting to evolve the localized wavepacket/trajectory along a single diabatic surface $V_2(\boldsymbol{q})$, making the process in the diabatic representation (Fig 2.5) highly classical since the quantum force vanishes when no electronic transitions take place.

Due to the non-adiabatic transition from one adiabatic state to another that occurs as a result of complete and localized electronic population transfer in the adiabatic representation, the processes depicted by Figs 2.2 and 2.4 that occur in the simple avoided system [1] are highly non-classical in the adiabatic representation, involving the quantum force that acts to conserve the quantum-classical energy on the ensemble level [62, 63, 81].

Substituting Eqn 4.7 into Eqn 4.36, and Eqn 4.8 into Eqn 4.37, we find that $\boldsymbol{F}^{\mathrm{A}}_{\mathrm{tot}}(t) = \boldsymbol{F}^{\mathrm{D}}_{\mathrm{tot}}(t)$.

While the non-adiabatic processes in the simple avoided crossing system [1] are apparently different in the adiabatic and the diabatic representations, the nuclear motion driven by the total forces in both representations was the same. While highly non-classical in the adiabatic representation, the non-adiabatic process is highly classical in the diabatic representation.

We will demonstrate the validity of these conclusions for the simple avoided crossing system [1] with QTSH results in Section 4.4.

Dual Avoided Crossing System

A similar procedure used to analyze the forces in non-adiabatic processes occuring in the simple avoided crossing system [1] in Section 4.2.3 was used to analyze the non-adiabatic process occurring in the dual avoided crossing system [1] (Fig 2.8).

Similar to the process depicted in Fig 2.4, the process outlined above for the dual avoided crossing system [1] in the diabatic representation only involves dynamics only on the diabatic state $V_2(\boldsymbol{q})$.

This resulted in the same generalized expression for quantities $\alpha^{\mathrm{A}}(t)$ and $\boldsymbol{F}^{\mathrm{A}}_{\mathrm{quant}}(t)$ given by Eqn 4.12 and Eqn 4.13, respectively.

The adiabatic forces - both the quantum and classical - in terms of the diabatic potentials were found at five timepoints, the time of the first instantaneous electronic transition $t = t_1^*$, the instant ϵ *before* the first electronic transition $t = t_1^* - \epsilon$, and the instant ϵ *after* the first electronic transition $t = t_1^* + \epsilon$, the time of the second instantaneous electronic transition $t = t_2^*$, the time interval between the instant *after* the first electronic transition and *before* the second electronic transition $t = \tau$, and the instant *after* the second electronic transition $t = t_2^* + \epsilon$. We note that the nuclear coordinate during electronic transitions are denoted by $\boldsymbol{q}(t_1^*) \equiv \boldsymbol{q}_1^*$ and $\boldsymbol{q}(t_2^*) \equiv \boldsymbol{q}_2^*$.

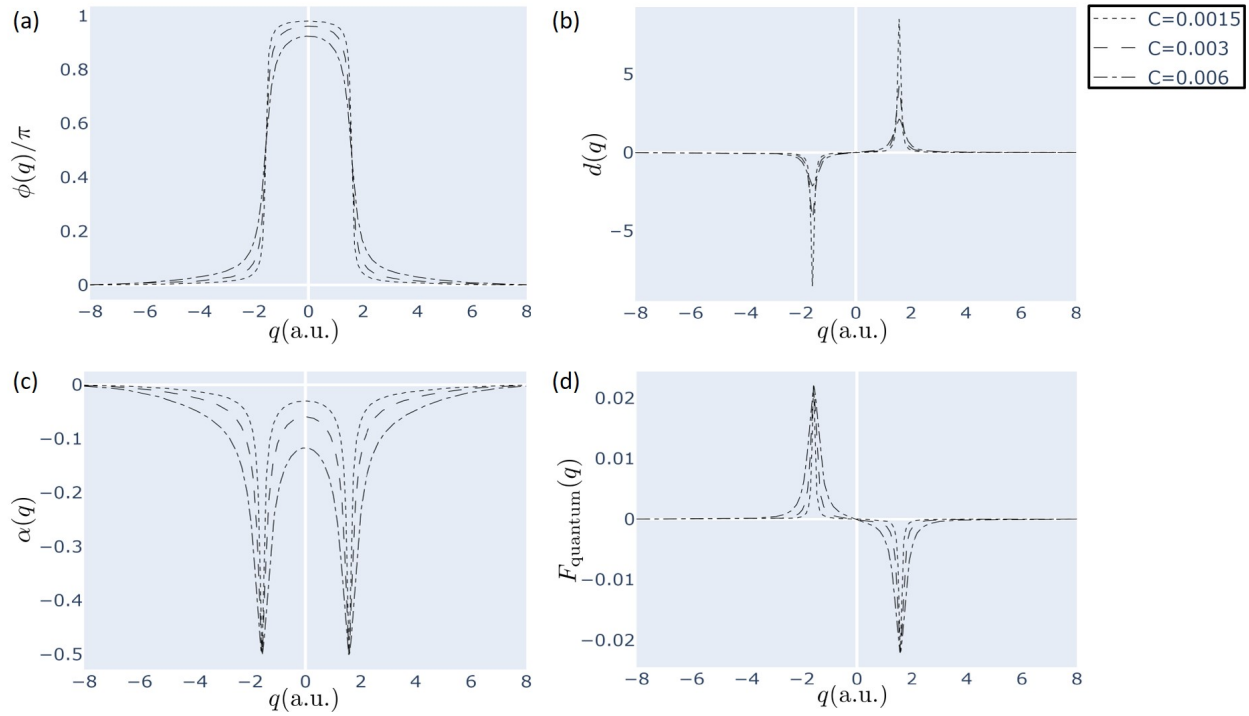

Figure 4.2: (a) The non-adiabatic mixing angle $\phi(q)$, (b) the non-adiabatic coupling vector $\boldsymbol{d}(\boldsymbol{q})$, (c) the real part of the coherence $\alpha(q)$, and (d) the quantum force $F_{\mathrm{quant}}(q)$ for the process shown in Fig 2.8, as described in text. The dotted, dashed, and dashdotted lines represent the models where $C = 0.0015, 0.003$, and 0.006, respectively.

As observed in Fig 4.2(b), in general, the strength of the adiabatic coupling $\boldsymbol{d}(\boldsymbol{q})$ for the one-dimensional system becomes stronger and more localized as diabatic coupling constant C is

decreased. In the limit $C \to 0$, the plot for the nonadiabatic mixing angle in one-dimension $\phi(\boldsymbol{q})$ in Fig 2.6(a) becomes a dual step function as depicted in Fig 4.3, with a step from $\phi(\boldsymbol{q}_1^*) = 0$ to $\phi(\boldsymbol{q}_1^*) = \pi$ at $q_1^* = -1.57$, and a step from $\phi(\boldsymbol{q}_2^*) = \pi$ to $\phi(\boldsymbol{q}_2^*) = 0$ at $q_2^* = 1.57$.

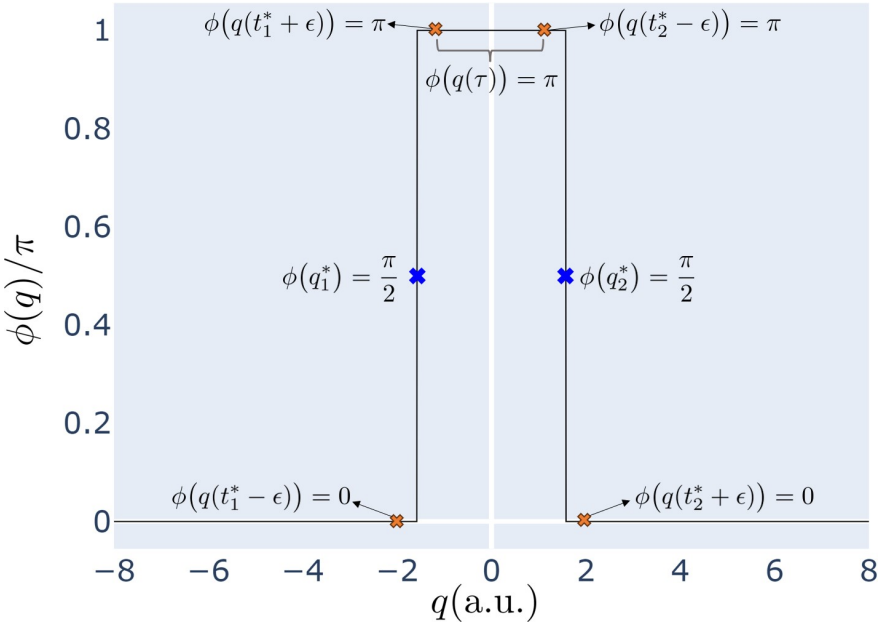

Figure 4.3: Nonadiabatic mixing angle for the simple avoided crossing system given by the diabatic potentials in Eqns 1.86-1.87, where the diabatic coupling constant $C \to 0$. The blue marker marks $\phi(-1.57) = \frac{\pi}{2}$ and $\phi(1.57) = \frac{\pi}{2}$, where a complete and localized transition from the lower to the upper adiabatic state takes place at $\boldsymbol{q}_1^* = -1.57$, and from the upper to the lower adiabatic state at $\boldsymbol{q}_2^* = 1.57$ in the adiabatic representation given by Fig 2.8.

The details of this analysis can be found in Appendix C.

Having performed the analysis, we found that the adiabatic quantum force $\boldsymbol{F}^{\mathrm{A}}_{\mathrm{quant}}(t)$ is only non-zero at the two instants of electronic transitions $t = t_1^*$ and $t = t_2^*$, consistent with our analysis of $\boldsymbol{F}^{\mathrm{A}}_{\mathrm{quant}}(t)$ acting to create FSSH-like momentum 'jumps' in the limit of complete and localized population transfer [81].

We also found that *before*, *during*, *between*, and *after* the **two** complete and localized population transfers, the total adiabatic force $\boldsymbol{F}^{\mathrm{A}}_{\mathrm{tot}}(t)$ is equivalent the classical diabatic force associated with the electronic diabatic potential energy surface $V_2(\boldsymbol{q})$.

In the adiabatic representation (Fig 2.8), throughout the process, the total adiabatic force

$$\boldsymbol{F}^{\mathrm{A}}_{\mathrm{tot}}(t) = \boldsymbol{F}^{\mathrm{D}}_{\mathrm{class},2}(t), \tag{4.38}$$

the classical force acting to evolve the localized wavepacket/trajectory along diabatic surface $V_2(\boldsymbol{q})$, making the process in the diabatic representation (Fig 2.9) highly classical since the quantum force vanishes when no electronic transitions take place.

Due to the two complete and localized electronic population transfers, the non-adiabatic process in the dual avoided crossing system [1] depicted by Fig 2.8 was highly non-classical in the adiabatic representation, involving the quantum force that acts to conserve the quantum-classical energy on the ensemble level when electronic transitions take place [62, 63, 81].

Substituting Eqn 4.9 into Eqn 4.38, we find that $\boldsymbol{F}^{\mathrm{A}}_{\mathrm{tot}}(t) = \boldsymbol{F}^{\mathrm{D}}_{\mathrm{tot}}(t)$.

While the non-adiabatic processes in the dual avoided crossing system [1] are apparently different in the adiabatic and the diabatic representations, the nuclear motion driven by the total forces in both representations was the same. While highly non-classical in the adiabatic representation, the non-adiabatic process is highly classical in the diabatic representation.

We will demonstrate the validity of these conclusions for the dual avoided crossing system [1] with QTSH results in Section 4.4.

4.3 Computational Details

The description of the systems used and the simulation details are as in Section 2.3 of Chapter 2, with the following changes.

In this chapter, QTSH was run in both the diabatic and adiabatic representations [62, 63]. We also ran QTSH [62, 63] in the adiabatic representation, and QTSH d2a (as outlined in Section 3.3 of Chapter 3) for the initial momenta condition $\boldsymbol{p}_0 = \hbar\boldsymbol{k}_0 = 8$ a.u. for the process starting on the lower adiabatic surface for the simple avoided crossing system [1] with $C = 0.001$, and the initial momenta condition $\boldsymbol{p}_0 = \hbar\boldsymbol{k}_0 = 77.2$ a.u. for the process starting on the lower adiabatic surface for the dual avoided crossing system [1] with $C = 0.0015$.

4.4 Results & Discussion

4.4.1 Classical and Non-classical Forces

In this section, we show that while the processes in the simple avoided crossing system [1] described by Figs 2.2 and 2.4, and the process in the dual avoided crossing system [1] described by Fig 2.8 in the adiabatic representation are non-classical due to non-adiabatic transitions that take place during the process, the corresponding processes for the simple avoided crossing system [1] described by Figs 2.3 and 2.5, and the process in the dual avoided crossing system [1] described in Fig 2.9 in the diabatic representation are highly classical.

We demonstrate that the quantum force component in the adiabatic representation $\boldsymbol{F}^{\mathrm{A}}_{\mathrm{quant}}$ becomes significant in the region where electronic transitions are taking place, and that the quantum force component in the diabatic representation $\boldsymbol{F}^{\mathrm{D}}_{\mathrm{quant}}$ makes minimal to no contributions to the total force in the diabatic representation $\boldsymbol{F}^{\mathrm{D}}_{\mathrm{total}}$ for the processes in the modified simple avoided crossing and dual avoided crossing systems [1].

We then applied the derived equations, Eqns 4.36-4.37 to the processes occuring in the modified Tully simple avoided crossing system [1], and Eqn 4.38 to the process occuring in the modified dual avoided crossing system [1], and test its validity with QTSH [62, 63] results

in the adiabatic and diabatic representations.

Finally, we show how we can utilize the representation invariance of QTSH [62, 63] as shown in Chapter 3 to obtain more accurate QTSH population results in the adiabatic representation by running d2a QTSH as described in Section 3.3 of Chapter 3.

The results of the QTSH simulations in the adiabatic representation were used to obtain the phase space averaged total adiabatic force that was computed as

$$\left\langle \boldsymbol{F}^{\mathrm{A}}_{\mathrm{total}}(t)\right\rangle = \left\langle \boldsymbol{F}^{\mathrm{A}}_{\mathrm{class}}(t)\right\rangle + \left\langle \boldsymbol{F}^{\mathrm{A}}_{\mathrm{quant}}(t)\right\rangle, \tag{4.39}$$

where the phase space averaged classical adiabatic force was computed as

$$\left\langle \boldsymbol{F}^{\mathrm{A}}_{\mathrm{class}}(t)\right\rangle = \frac{1}{N}\sum_{j}^{N} -\sigma^{\mathrm{A}}_{j}(t)\nabla_{\boldsymbol{q}_j} V_{+}(\boldsymbol{q}_j) - \left(1-\sigma^{\mathrm{A}}_{j}(t)\nabla_{\boldsymbol{q}_j}\right)V_{-}(\boldsymbol{q}_j), \tag{4.40}$$

and the phase space averaged quantum adiabatic force was computed as

$$\left\langle \boldsymbol{F}^{\mathrm{A}}_{\mathrm{quant}}(t)\right\rangle = \frac{1}{N}\sum_{j}^{N} 2\hbar\omega^{\mathrm{A}}_{j}\boldsymbol{d}(\boldsymbol{q}_j)\alpha^{\mathrm{A}}_{j}(t). \tag{4.41}$$

The results of the QTSH simulations in the diabatic representation were also used to obtain the phase space averaged total diabatic force that was computed as

$$\left\langle \boldsymbol{F}^{\mathrm{A}}_{\mathrm{total}}(t)\right\rangle = \left\langle \boldsymbol{F}^{\mathrm{D}}_{\mathrm{class}}(t)\right\rangle + \left\langle \boldsymbol{F}^{\mathrm{D}}_{\mathrm{quant}}(t)\right\rangle, \tag{4.42}$$

where the phase space averaged classical adiabatic force was computed as

$$\left\langle \boldsymbol{F}^{\mathrm{D}}_{\mathrm{class}}(t)\right\rangle = \frac{1}{N}\sum_{j}^{N} -\sigma^{\mathrm{D}}_{j}(t)\nabla_{\boldsymbol{q}_j} V_{1}(\boldsymbol{q}_j) - \left(1-\sigma^{\mathrm{D}}_{j}(t)\nabla_{\boldsymbol{q}_j}\right)V_{2}(\boldsymbol{q}_j), \tag{4.43}$$

and the phase space averaged quantum diabatic force was computed as

$$\left\langle \boldsymbol{F}^{\mathrm{A}}_{\mathrm{quant}}(t) \right\rangle = \frac{1}{N} \sum_{j}^{N} -2\alpha_j^{\mathrm{A}} \nabla_{\boldsymbol{q}_j} V_1(\boldsymbol{q}_j). \tag{4.44}$$

The results of the QTSH simulations in the diabatic representation were also used to obtain the phase space averaged classical diabatic force on separate single potential energy surfaces $V_1(\boldsymbol{q})$ and $V_2(\boldsymbol{q})$ that were computed as

$$\left\langle \boldsymbol{F}^{\mathrm{D}}_{\mathrm{class},1}(t) \right\rangle = \frac{1}{N} \sum_{j}^{N} -\sigma_j^{\mathrm{D}}(t) \nabla_{\boldsymbol{q}_j} V_1(\boldsymbol{q}_j), \tag{4.45}$$

and

$$\left\langle \boldsymbol{F}^{\mathrm{D}}_{\mathrm{class},2}(t) \right\rangle = \frac{1}{N} \sum_{j}^{N} -\big(1 - \sigma_j^{\mathrm{D}}(t)\big) \nabla_{\boldsymbol{q}_j} V_2(\boldsymbol{q}_j), \tag{4.46}$$

respectively.

From Fig 2.6(b), we observed that the non-adiabatic coupling vector $\boldsymbol{d}(\boldsymbol{q})$ was strongest and most localized when the diabatic coupling constant C in the expression for the diabatic coupling potential $V_{12}(\boldsymbol{q})$ given by Eqn 1.84, was $C = 0.0005$ for the simple avoided crossing system [1]. We make a similar observation for the dual avoided crossing system [1], where the value of the parameter $C = 0.0015$, associated with the diabatic coupling potential given in Eqn 1.87, gives rise to a strong and localized adiabatic coupling at $\boldsymbol{q} = -1.57$ and $\boldsymbol{q} = 1.57$ as shown in Fig 4.2(b).

Since we have made the assumption of complete and localized population transfer in the adiabatic representation, we only considered processes involving the simple avoided crossing system [1] where $C = 0.0005$, and the process involving the dual avoided crossing system [1] where $C = 0.0015$.

For the simple avoided crossing system [1] in the adiabatic representation that involves the processes with the $+ \rightarrow -$ transition (Fig 2.2) and the $- \rightarrow +$ transition (Fig 2.4), Figs 4.4(a) and 4.5(a) show that the dynamics of the trajectories in each process are driven by a phase space average classical force component $\left\langle \boldsymbol{F}^{\mathrm{A}}_{\mathrm{class}}(t) \right\rangle$ that act to accelerate or decelerate the trajectories along the electronic potential surfaces $V_{+}(\boldsymbol{q})$ or $V_{-}(\boldsymbol{q})$, respectively. Upon entering into the region of strong non-adiabatic coupling where trajectories begin to hop from $+ \rightarrow -$ or from $- \rightarrow +$ during the transition time interval between $t = 10$ fs and $t = 30$ fs, the trajectories experience a positive or negative system phase space averaged quantum force $\left\langle \boldsymbol{F}^{\mathrm{A}}_{\mathrm{quant}}(t) \right\rangle$, respectively. The $\left\langle \boldsymbol{F}^{\mathrm{A}}_{\mathrm{quant}}(t) \right\rangle$ acts to conserve the average quantum-classical energy due to the non-adiabatic transitions [62, 63, 81].

For the dual avoided crossing system [1] in the adiabatic representation that involves an initial $- \rightarrow +$ transition at $\boldsymbol{q}^{*}_{1}$ and a subsequent $+ \rightarrow -$ transition at $\boldsymbol{q}^{*}_{2}$ (Fig 2.8), Fig 4.14(a) shows that the dynamics of the trajectories are driven by a phase space average classical force component $\left\langle \boldsymbol{F}^{\mathrm{A}}_{\mathrm{class}}(t) \right\rangle$ as they move along $V_{-}(\boldsymbol{q})$ at constant velocity until they enter the region of strong coupling when the hopping of trajectories from $- \rightarrow +$ begins to take place at $t^{*} \approx 10.5$ fs. During the transition, the localized trajectories experience a simultaneous acceleration and deceleration by the phase space averaged classical force component $\left\langle \boldsymbol{F}^{\mathrm{A}}_{\mathrm{class}}(t) \right\rangle$ and the negative phase space averaged quantum force $\left\langle \boldsymbol{F}^{\mathrm{A}}_{\mathrm{quant}}(t) \right\rangle$, respectively. Shortly after, when the second non-adiabatic transition $+ \rightarrow -$ takes place at $t^{*} \approx 13$ fs, the trajectories experience a simultaneous deceleration and acceleration by $\left\langle \boldsymbol{F}^{\mathrm{A}}_{\mathrm{class}}(t) \right\rangle$ and $\left\langle \boldsymbol{F}^{\mathrm{A}}_{\mathrm{quant}}(t) \right\rangle$, respectively. The net effect of the oppositely acting $\left\langle \boldsymbol{F}^{\mathrm{A}}_{\mathrm{class}}(t) \right\rangle$ and $\left\langle \boldsymbol{F}^{\mathrm{A}}_{\mathrm{quant}}(t) \right\rangle$ gave rise to an approximately zero phase space averaged total force in the adiabatic representation $\left\langle \boldsymbol{F}^{\mathrm{A}}_{\mathrm{total}}(t) \right\rangle$, resulting in an approximately constant velocity of the trajectories throughout the process.

The significant contribution of $\left\langle \boldsymbol{F}^{\mathrm{A}}_{\mathrm{quant}}(t) \right\rangle$ to the system phase space averaged total force $\left\langle \boldsymbol{F}^{\mathrm{A}}_{\mathrm{total}}(t) \right\rangle$ as observed in Figs 4.4(a), 4.5(a) and 4.14(a), indicated that these processes

in the adiabatic representation for the simple avoided crossing and dual avoided crossing systems [1] are highly non-classical, with significant work being done by the quantum forces to conserve the system average quantum-classical energy [62, 63, 81].

As the corresponding processes in the simple avoided crossing system [1] depicted in Figs 2.3 and 2.5, and the corresponding process in the dual avoided crossing system [1] in the diabatic representation do not involve any electronic transitions, the trajectories evolve along a single diabatic state.

With reference to Figs 4.4(b), 4.5(b) and 4.14(b), the dynamics of trajectories in the diabatic representation is driven only by a phase space averaged classical force component $\left\langle \boldsymbol{F}^{\mathrm{D}}_{\mathrm{class}} \right\rangle$ with the quantum force $\left\langle \boldsymbol{F}^{\mathrm{D}}_{\mathrm{quant}} \right\rangle = 0$ throughout the process.

While the processes occurring in the simple avoided crossing and dual avoided crossing systems [1] in the adiabatic representation are highly non-classical due to the non-adiabatic transitions that take place, the corresponding processes are highly classical in the diabatic representation.

We have shown that the dynamics of trajectories of the non-adiabatic processes in the adiabatic representation are highly non-classical, with both the classical motion of trajectories along the adiabatic electronic potentials and the average quantum-classical energy conservation during electronic transitions [62, 63, 81] that are driven by $\left\langle \boldsymbol{F}^{\mathrm{A}}_{\mathrm{class}}(t) \right\rangle$ and $\left\langle \boldsymbol{F}^{\mathrm{A}}_{\mathrm{quant}}(t) \right\rangle$, respectively.

We have also shown that the dynamics of trajectories of the corresponding non-adiabatic processes in the diabatic representation are conversely highly classical, with only classical motion of trajectories along the diabatic electronic potentials, driven by $\left\langle \boldsymbol{F}^{\mathrm{D}}_{\mathrm{class}}(t) \right\rangle$.

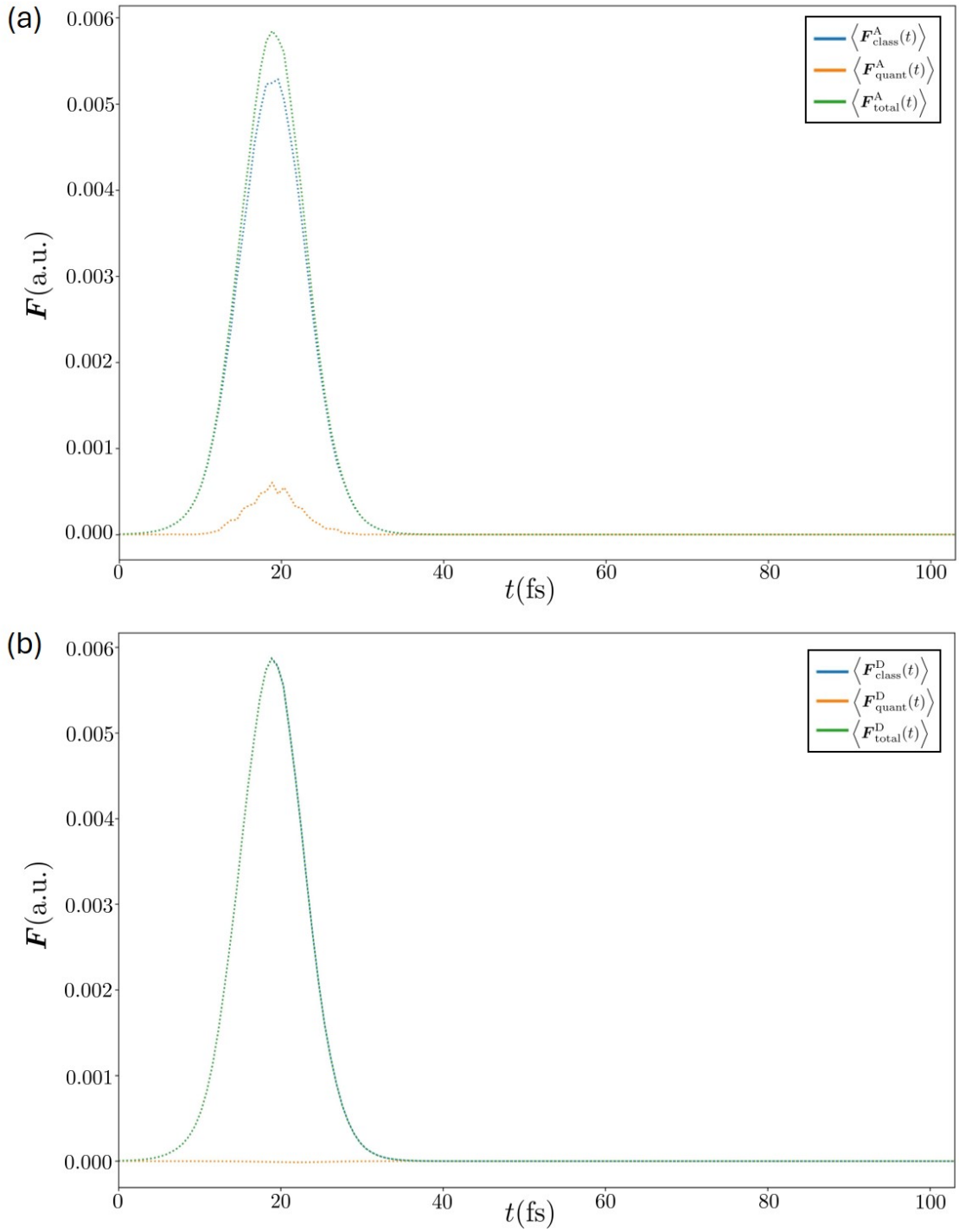

Figure 4.4: (a) Classical and quantum force components that make up the total force in the adiabatic representation for the process in Fig 2.2. (b) Classical and quantum force components that make up the total force in the diabatic representation for the process in Fig 2.3. Diabatic potentials for the simple avoided crossing system [1] are given in Eqns 1.83-1.84, with the diabatic potential coupling constant $C = 0.0005$.

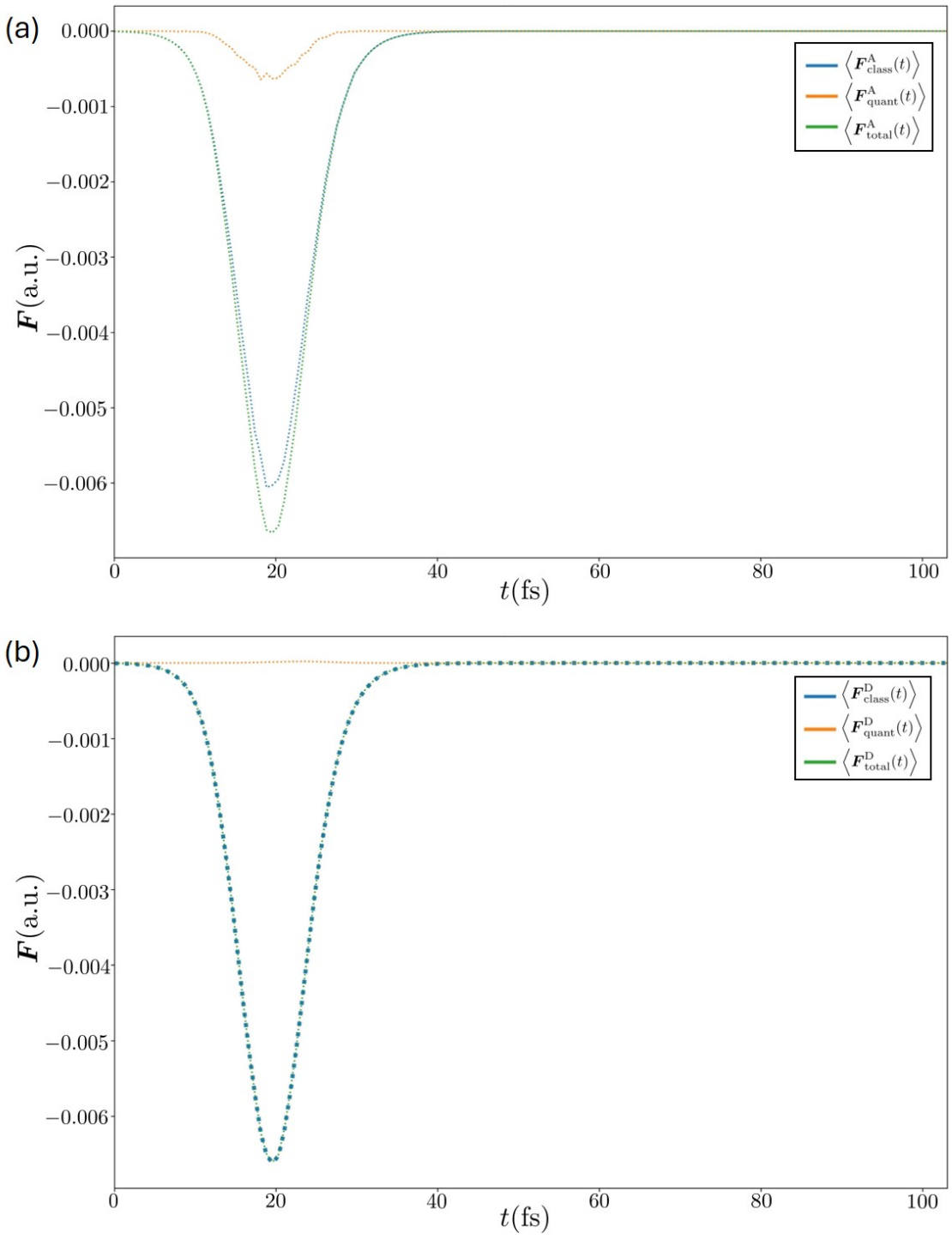

Figure 4.5: (a) Classical and quantum force components that make up the total force in the adiabatic representation for the process in Fig 2.4. (b) Classical and quantum force components that make up the total force in the diabatic representation for the process in Fig 2.5. Diabatic potentials for the simple avoided crossing system [1] are given in Eqns 1.83-1.84, with the diabatic potential coupling constant $C = 0.0005$.

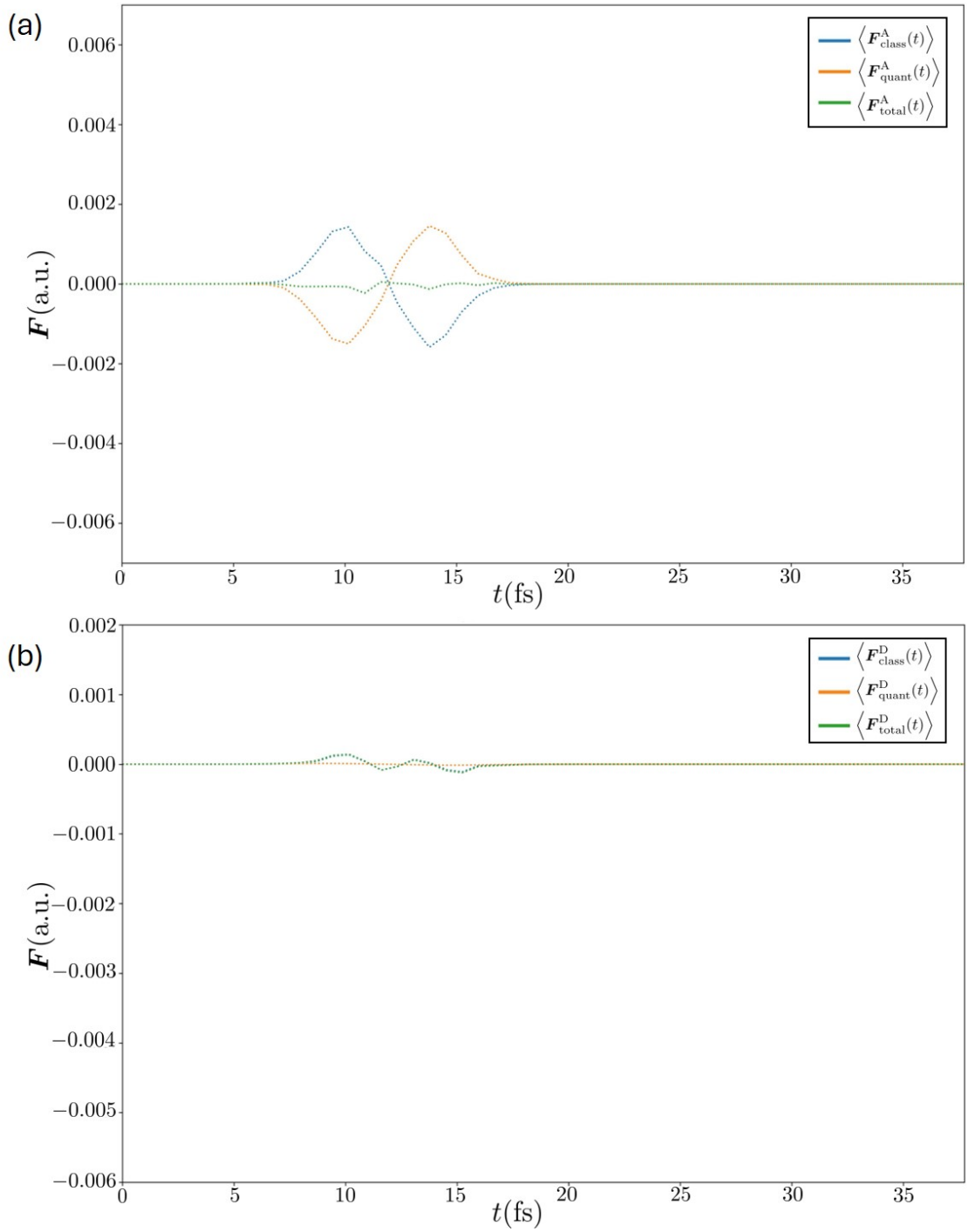

Figure 4.6: (a) Classical and quantum force components that make up the total force in the adiabatic representation for the process in Fig 2.8. (b) Classical and quantum force components that make up the total force in the diabatic representation for the process in Fig 2.9. Diabatic potentials for the simple avoided crossing system are given in Eqns 1.86-1.87, with the diabatic potential coupling constant $C = 0.0015$.

We now show that as derived in Section 4.2.3, that the system phase space averaged total force in the adiabatic representation $\left\langle \boldsymbol{F}^{\mathrm{A}}_{\mathrm{total}}(t) \right\rangle$ is in fact equivalent to the system phase space averaged classical force on a single diabatic surface, $\left\langle \boldsymbol{F}^{\mathrm{D}}_{\mathrm{class},1}(t) \right\rangle$ for the surface $V_1(\boldsymbol{q})$, or $\left\langle \boldsymbol{F}^{\mathrm{D}}_{\mathrm{class},2}(t) \right\rangle$ for surface $V_2(\boldsymbol{q})$ in the diabatic representation.

With reference to Fig 4.7, we found that for the non-adiabatic process in simple avoided crossing system [1] that involves the $+ \rightarrow -$ electronic transition (Fig 2.2) that is driven by $\left\langle \boldsymbol{F}^{\mathrm{A}}_{\mathrm{total}}(t) \right\rangle$ in the adiabatic representation, is equivalent to $\left\langle \boldsymbol{F}^{\mathrm{D}}_{\mathrm{class},1}(t) \right\rangle$, the classical force that acts to evolve trajectories along the single diabatic surface $V_1(\boldsymbol{q})$ in the diabatic represention (Fig 2.3). This agrees with Eqn 4.36 that we derived in Section 4.2.3.

With reference to Figs 4.8 and 4.9, we found that for the non-adiabatic process in simple avoided crossing system [1] that involves the $- \rightarrow +$ electronic transition (Fig 2.4) and the non-adiabatic process in dual avoided crossing system [1] (Fig 2.8) that is driven by $\left\langle \boldsymbol{F}^{\mathrm{A}}_{\mathrm{total}}(t) \right\rangle$ in the adiabatic representation, is equivalent to $\left\langle \boldsymbol{F}^{\mathrm{D}}_{\mathrm{class},2}(t) \right\rangle$, the classical force that acts to evolve trajectories along the single diabatic surface $V_2(\boldsymbol{q})$ in the diabatic represention (Figs 2.5 and 2.9). This agrees with Eqns 4.37 and 4.38 that we derived in Section 4.2.3.

While the agreement between $\left\langle \boldsymbol{F}^{\mathrm{A}}_{\mathrm{total}}(t) \right\rangle$ and $\left\langle \boldsymbol{F}^{\mathrm{D}}_{\mathrm{class},2}(t) \right\rangle$ in Fig 4.9 is not perfect, the deviation is sufficiently small.

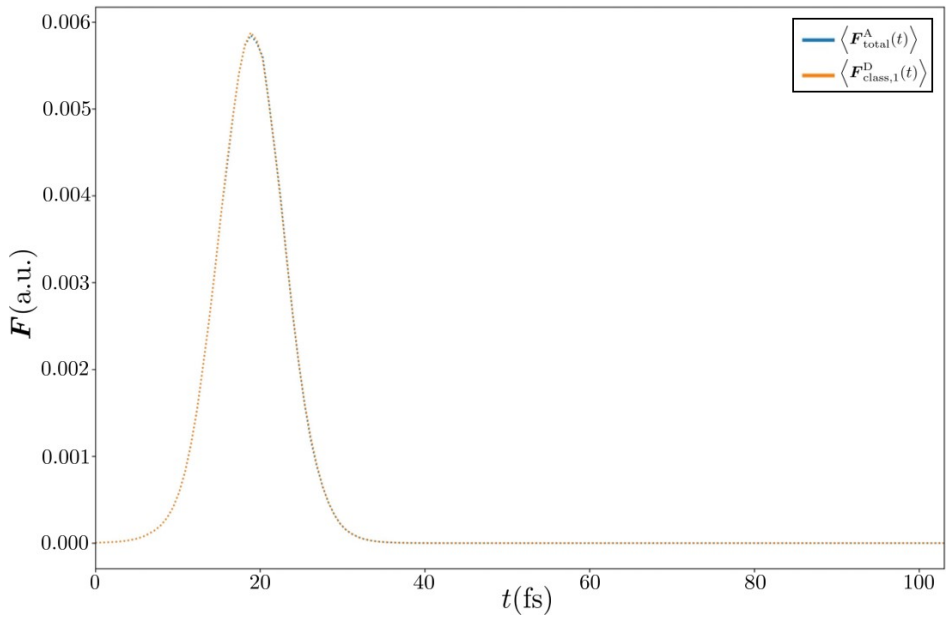

Figure 4.7: Phase space averaged classical diabatic force associated with the localized quantum states/trajectories traveling along the single diabatic potential energy surface $V_1(\boldsymbol{q})$, and the phase space averaged total adiabatic force corresponding to the process in Fig 2.2. Diabatic potentials for the simple avoided crossing system are given in Eqns 1.83-1.84, with the diabatic coupling constant $C = 0.0005$.

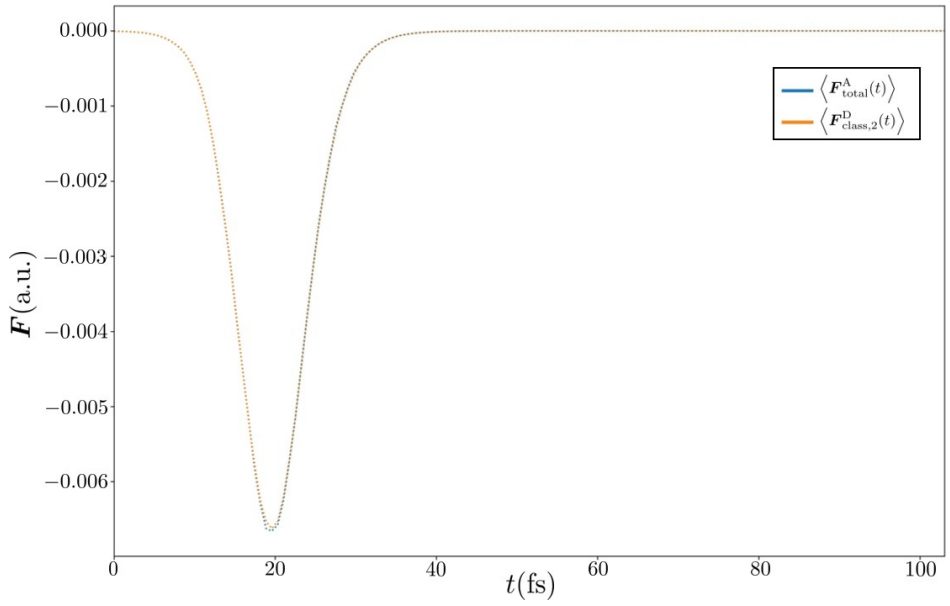

Figure 4.8: Phase space averaged classical diabatic force associated with the localized quantum states/trajectories traveling along the single diabatic potential energy surface $V_2(\boldsymbol{q})$, and the phase space averaged total adiabatic force corresponding to the process in Fig 2.4. Diabatic potentials for the simple avoided crossing system [1] are given in Eqns 1.83-1.84, with the diabatic coupling constant $C = 0.0005$.

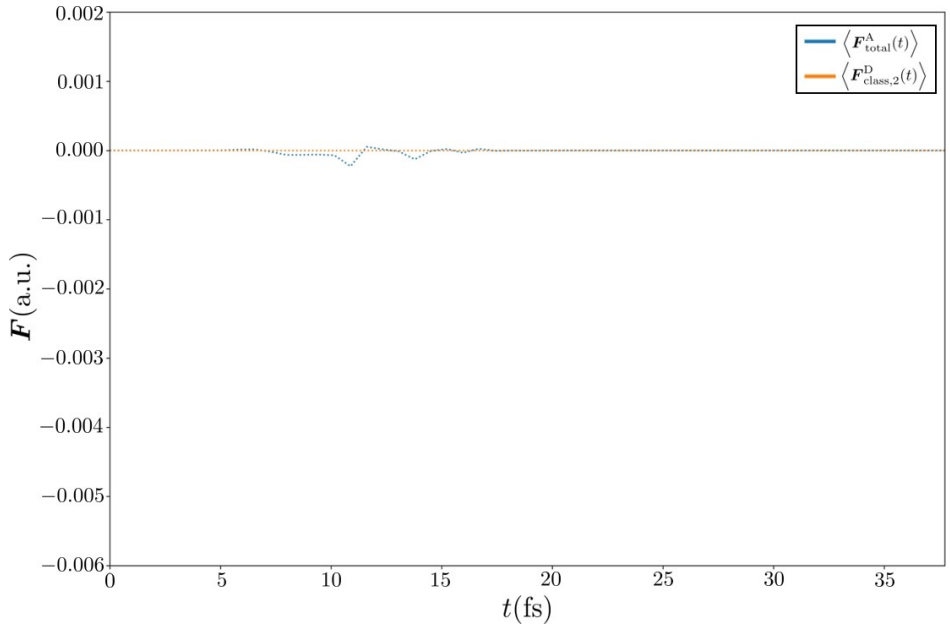

Figure 4.9: Phase space averaged classical diabatic force associated with the localized quantum states/trajectories traveling along the single diabatic potential energy surface $V_2(\boldsymbol{q})$, and the phase space averaged total adiabatic force corresponding to the process in Fig 2.8. Diabatic potentials for the dual avoided crossing system are given in Eqns 1.86-1.87, with the diabatic coupling constant $C = 0.0015$.

Being highly classical in the diabatic representation, the non-adiabatic processes in the simple and dual avoided crossing systems [1] are much simpler, evolving only along one diabatic electronic potential. This in contrast to the adiabatic representation where numerous trajectories hop from one surface to another. The imperfect feedback between the nuclear and electronic degrees of freedom as a result slight inconsistencies in surface hopping as found in Section 2.4.2 of Chapter 2 manifests in QTSH [62, 63] due to the *independence* of trajectories in QTSH [62, 63]. The quantum force as given in Eqn 2.33 is dependent on the real part of the coherence that can only be captured accurately if the trajectories are *interdependent* [39–41, 52–58].

QTSH [62, 63] results in the diabatic representation are likely to be more accurate for non-adiabatic processes that are highly non-classical in the adiabatic representation, but highly classical in the diabatic representation since any surface hopping inconsistencies that arise

will be minimized when few to no hops occur in QTSH.

Since QTSH [62, 63] provides a quantum-classical description of systems that is derived rigorously from QCLE [38–40], QTSH can be derived rigorously, and performed in both the diabatic and adiabatic representations, we can exploit its representation invariance, as discussed in Chapter 3 to perform QTSH d2a (as described in Section 3.3) for non-adiabatic processes that are highly classical in the diabatic representation, thereby improve the accuracy of the results obtained in the adiabatic representation.

4.4.2 Exploiting Representation Invariance

In Section 4.4, we found that for the simple avoided crossing system and dual avoided crossing systems [1], the dynamics in the diabatic representation was much more classical than that in the adiabatic representation, as a result of little to no population transfer in the diabatic representation.

Since QTSH [62, 63] is representation invariant, as shown in Chapter 3, we exploit this property of representation invariance to obtain more accurate QTSH results in the adiabatic representation by employing QTSH d2a.

We will demonstrate this with a process in the simple avoided crossing system [1] and a process in the dual avoided crossing system [1].

Simple Avoided Crossing System

From Sec 4.4, we found that for the simple avoided crossing system [1], involving the $- \rightarrow +$ transition in the adiabatic representation, both the classical and quantum forces were significant with the classical force acting to propagate trajectories along a single potential

energy surface, and the quantum force acting to create momentum jumps when a non-adiabatic transition takes place.

In reducing the initial momentum to $\boldsymbol{p_0} = \hbar \boldsymbol{k}_0 = 8$ a.u. for the simple avoided crossing system [1], and starting on the lower adiabatic surface $V_-(\boldsymbol{q})$, we found that because not trajectories that hop to the upper adiabatic surface $V_+(\boldsymbol{q})$ have sufficient energy to remain there, and undergo a subsequent hop to the lower adiabatic state $V_-(\boldsymbol{q})$. In systems where the same trajectory hops multiple times, the problem of overcoherence is more pronounced [3] in the adiabatic representation.

In Fig 4.10, the adiabatic QTSH results are compared with the exact quantum result for (a) the system phase space averaged population on adiabatic surface -, $\langle \rho_{--}(t) \rangle$ and (b) the system phase space averaged population on diabatic surface $V_2(\boldsymbol{q})$, $\langle \rho_{22}(t) \rangle$ for the simple avoided crossing system [1].

In Fig 4.11, we present the various system phase space averaged classical force, quantum force and total force (a) in the adiabatic representation, and (b) in the diabatic representation for the simple avoided crossing system [1].

With reference to Fig 4.10(a), the phase space averaged population for the lower adiabatic state, $\langle \rho_{--}(t) \rangle$ for QTSH was found to be in good agreement with the exact quantum results for the non-adiabatic transition $- \rightarrow +$ from $t = 0$ fs to $t \approx 45$ fs. A larger than expected population transfer of to the upper adiabatic state $V_+(\boldsymbol{q})$ then occurs with QTSH result between $t \approx 45$ fs and $t \approx 50$ fs. The population transfer due to the first non-adiabatic transition was ~ 0.9. A second non-adiabatic transition $+ \rightarrow -$ then occurs at a rate in agreement to the quantum results between $t \approx 50$ to $t \approx 70$ fs. Finally the rate of $+ \rightarrow -$ becomes increasingly slower that of the quantum results, giving rise to the asymptotic value of $\langle \rho_{--}(t) \rangle \approx 0.85$ that is ~ 0.1 lower than the asymptotic value for the exact quantum results.

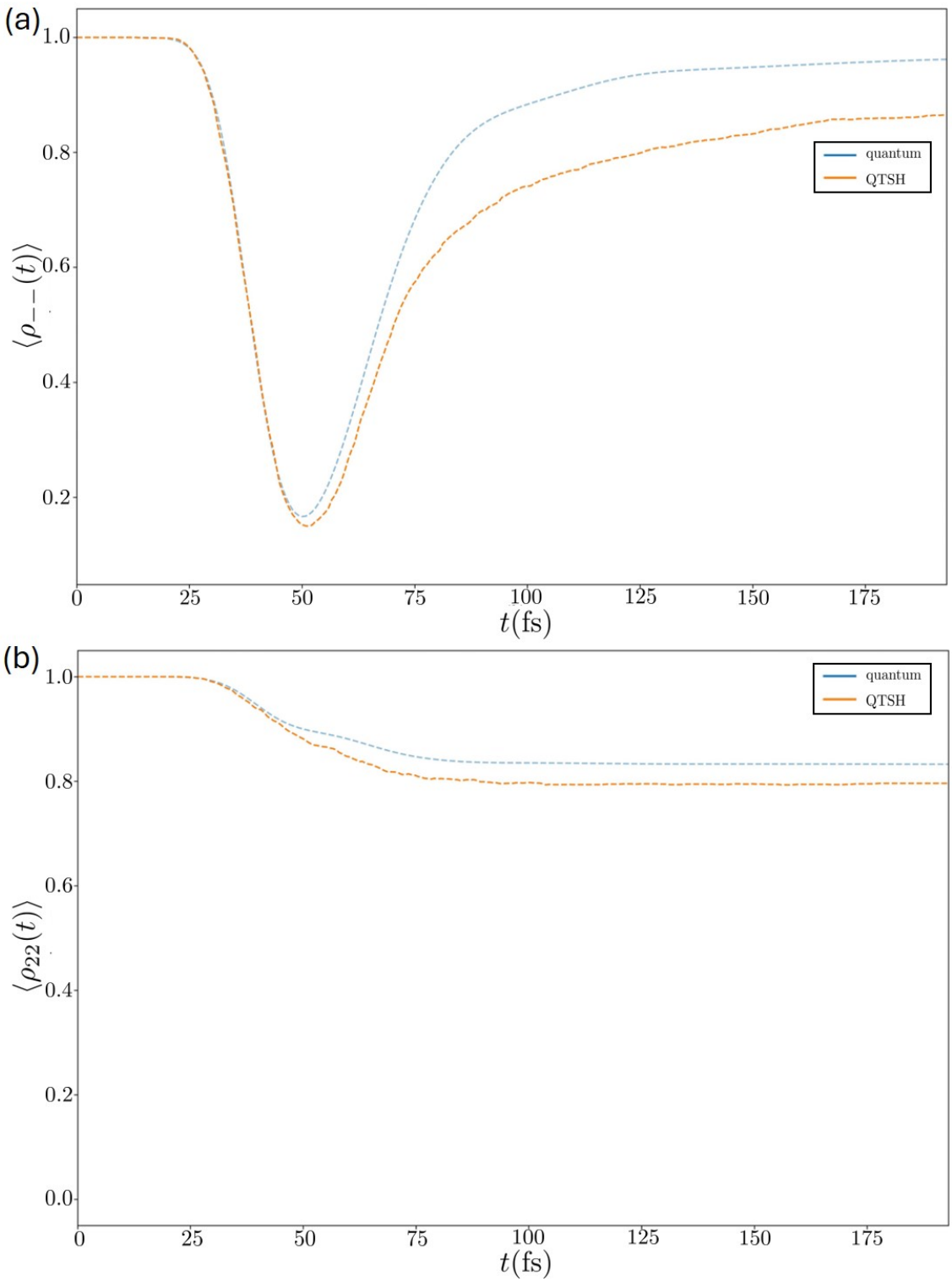

Figure 4.10: Comparison of QTSH against quantum wavepacket results (a) for $\langle \rho_{--}(t) \rangle$ in the adiabatic representation, for the process in the simple avoided crossing system with the initial population on the lower adiabatic surface, (b) and for $\langle \rho_{22}(t) \rangle$ in the diabatic representation, for the corresponding process in the diabatic representation. The trajectories had an average starting momentum of $\hbar k_0 = 8.0$, with the diabatic potential coupling constant $C = 0.001$.

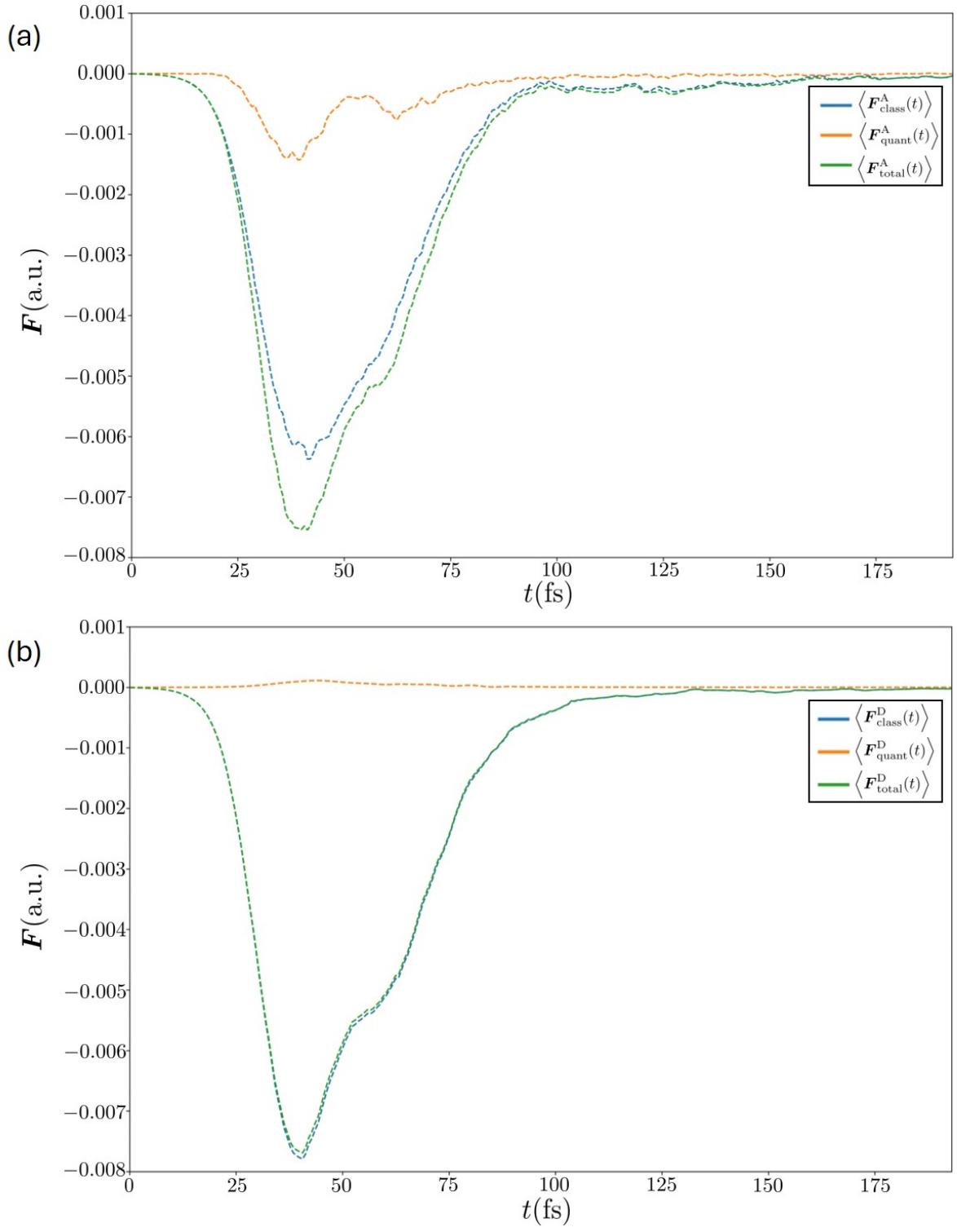

Figure 4.11: (a) Classical and quantum force components that make up the total force in the adiabatic representation for the process in the simple avoided crossing system with the initial population on the lower adiabatic surface. (b) Classical and quantum force components that make up the total force in the corresponding process in the diabatic representation. The trajectories had an average starting momentum of $\hbar k_0 = 8.0$, with the diabatic potential coupling constant $C = 0.001$.

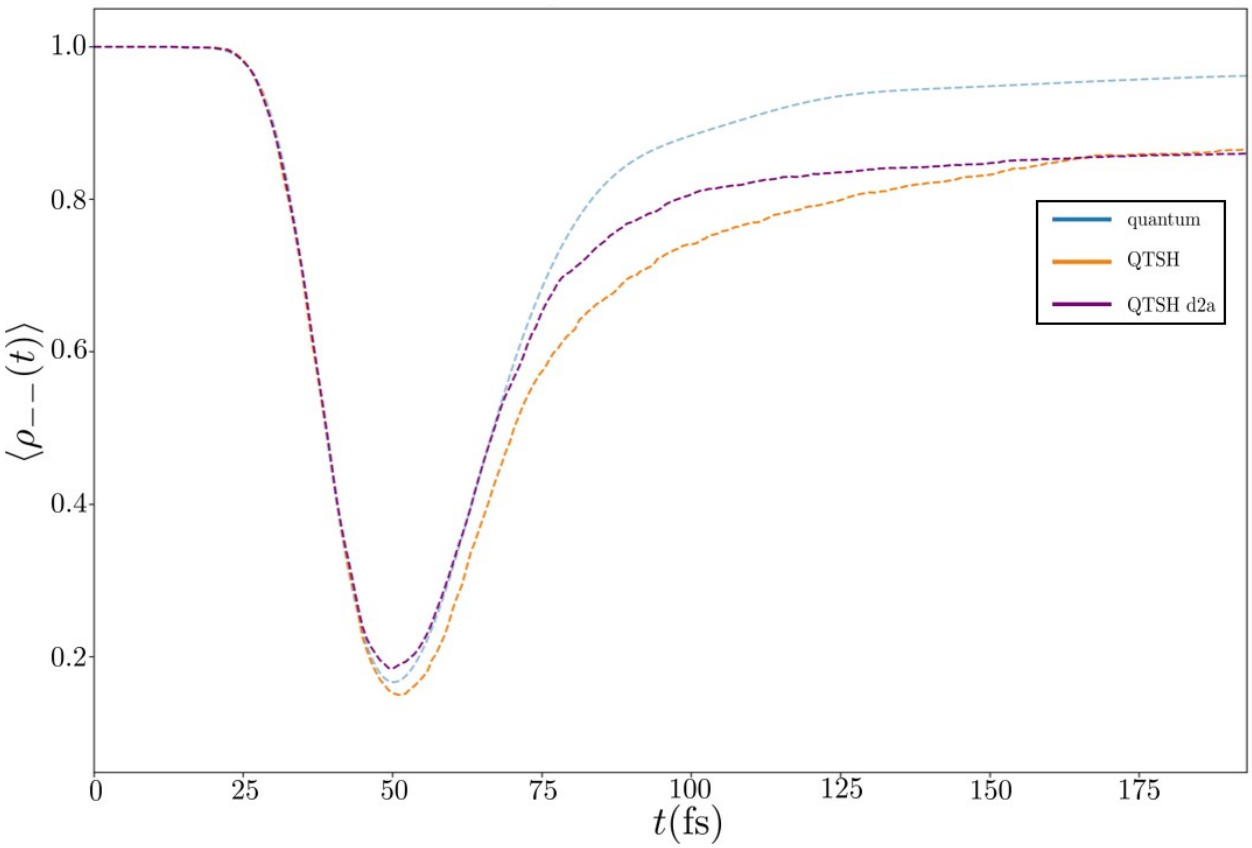

Figure 4.12: Comparison of QTSH, and the QTSH diabatic to adiabatic transformed (QTSH d2a) results against exact quantum results for $\langle \rho_{--}(t) \rangle$, for the simple avoided crossing system with the initial population on the lower adiabatic surface. The trajectories had an average starting momentum of $\hbar k_0 = 8.0$, with the diabatic potential coupling constant $C = 0.001$.

With reference to Fig 4.10(b), the phase space averaged population for the diabatic state $V_2(\boldsymbol{q})$, $\langle \rho_{22}(t) \rangle$ for QTSH [62, 63] was found to be in good agreement with the exact quantum results with non-adiabatic transitions $2 \rightarrow 1$ from $t = 0$ fs to $t \approx 45$ fs. A larger than expected population transfer to the diabatic state $V_1(\boldsymbol{q})$ then occurs with QTSH result between $t \approx 45$ fs and $t \approx 80$ fs. After $t \approx 80$ fs, the asymptotic value of $\langle \rho_{22}(t) \rangle \approx 0.8$ is reached, that is ~ 0.025 lower than the asymptotic value of the exact quantum results.

Given that a large population transfer of ~ 0.9 for the non-adiabatic transition $- \rightarrow +$, followed by a large population transfer of ~ 0.75 for the subsequent $+ \rightarrow -$ took place in the adiabatic representation, we find that the phase space averaged quantum force $\left\langle \boldsymbol{F}^{\mathrm{A}}_{\mathrm{quant}} \right\rangle$

- the force responsible for momentum jumps due to the non-adiabatic transitions - observed in Fig 4.10(a) has two distinct peaks corresponding to the two population transfers. The contribution of $\left\langle \boldsymbol{F}^{\mathrm{A}}_{\mathrm{quant}} \right\rangle$ to the total phase space averaged total force $\left\langle \boldsymbol{F}^{\mathrm{A}}_{\mathrm{total}} \right\rangle$ was significant. This shows that the process in the adiabatic representation is significantly non-classical.

In contrast, in the diabatic representation, only one transition with a small population transfer of ~ 0.2 occurs from diabatic state $2 \rightarrow 1$ in the diabatic representation, we find that the phase space averaged quantum force $\left\langle \boldsymbol{F}^{\mathrm{D}}_{\mathrm{quant}} \right\rangle$ observed in Fig 4.10(b) has a very weak single peak. The contribution of $\left\langle \boldsymbol{F}^{\mathrm{D}}_{\mathrm{quant}} \right\rangle$ to the total phase space averaged total force $\left\langle \boldsymbol{F}^{\mathrm{D}}_{\mathrm{total}} \right\rangle$ was negligible. The same process in the diabatic representation was largely classical with $\left\langle \boldsymbol{F}^{\mathrm{D}}_{\mathrm{total}} \right\rangle$ acting mainly to evolve the trajectories along the potential energy surfaces.

Since the more classical process in the diabatic representation is much simpler with fewer trajectory hops, the errors due to surface hopping inconsistencies [50] accumulated as a result are much smaller in the diabatic representation, giving more accurate QTSH results in the diabatic representation (Fig 4.11(b)) than in the adiabatic representation (Fig 4.11(a)).

With this reasoning, we used Eqn 3.4 to convert the results of the QTSH simulation in the diabatic representation, to obtain $\langle \rho_{--}(t) \rangle$. With reference to Fig 4.12, we observed that $\langle \rho_{--}(t) \rangle$ for the transformed QTSH (QTSH d2a) results of the second non-adiabatic transition $+ \rightarrow -$ between $t \approx 55$ fs and $t \approx 70$ fs exactly matches the quantum result. While the QTSH results at the same time interval has the same rate as the quantum result, $\langle \rho_{--}(t) \rangle$ is lower than the quantum result.

Obtaining QTSH [62, 63] in the diabatic representation, where the process is highly classical, and subsequently converting the QTSH result to the adiabatic representation (QTSH d2a) improves the accuracy of the QTSH [62, 63] results in the adiabatic representation by reducing the errors that accumulate with the imperfect surface hopping inconsistencies associated large population transfers in the adiabatic representation.

Dual Avoided Crossing System

From Sec 4.4, we found that for the dual avoided crossing system [1], involving the $- \rightarrow +$ transition followed by a subsequent $+ \rightarrow -$ transition in the adiabatic representation, both the classical and quantum forces were significant with the classical force acting to propagate trajectories along a single potential energy surface, and the quantum force acting to create momentum jumps when non-adiabatic transitions takes place.

The initial momentum used was $\boldsymbol{p_0} = \hbar \boldsymbol{k}_0 = 77.2$ a.u. for the dual avoided crossing system [1], starting on the lower adiabatic surface $V_-(\boldsymbol{q})$.

In Fig 4.13, the adiabatic QTSH results is compared with the exact quantum result for (a) the system phase space averaged population on adiabatic surface -, $\langle \rho_{--}(t) \rangle$ and (b) the system phase space averaged population on diabatic surface $V_2(\boldsymbol{q})$, $\langle \rho_{22}(t) \rangle$ for the dual avoided crossing system [1].

In Fig 4.14, we present the various system phase space averaged classical force, quantum force and total force (a) in the adiabatic representation, and (b) in the diabatic representation for the dual avoided crossing system [1].

With reference to Fig 4.13(a), the phase space averaged population for the lower adiabatic state, $\langle \rho_{--}(t) \rangle$ for QTSH was found to be in good agreement with the exact quantum results for the non-adiabatic transition $- \rightarrow +$ from $t = 0$ fs to $t \approx 6.5$ fs, and the second non-adiabatic transition $+ \rightarrow -$ from $t \approx 6.5$ fs to $t \approx 8$ fs. After $t \approx 8$, the rate of the second non-adiabatic transition $+ \rightarrow -$ becomes faster that of the quantum results, giving rise to the asymptotic value of $\langle \rho_{--}(t) \rangle \approx 1.0$ that is ~ 0.025 higher than the asymptotic value for the exact quantum results.

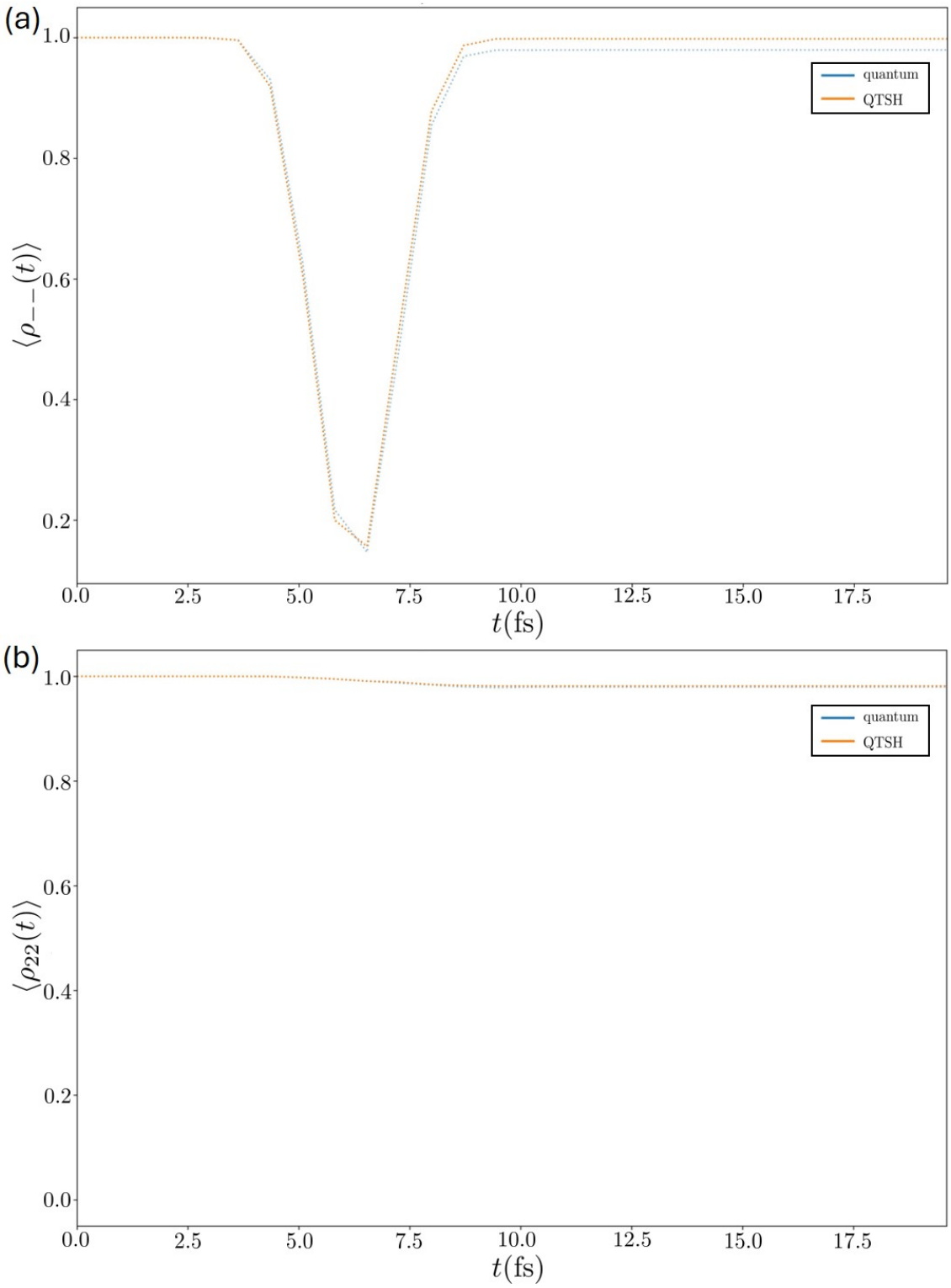

Figure 4.13: Comparison of QTSH against quantum wavepacket results (a) for $\langle \rho_{--}(t) \rangle$ in the adiabatic representation, for the process in the dual avoided crossing system with the initial population on the lower adiabatic surface, (b) and for $\langle \rho_{22}(t) \rangle$ in the diabatic representation, for the corresponding process in the diabatic representation. The trajectories had an average starting momentum of $\hbar k_0 = 77.2$ a.u., with the diabatic potential coupling constant $C = 0.0015$.

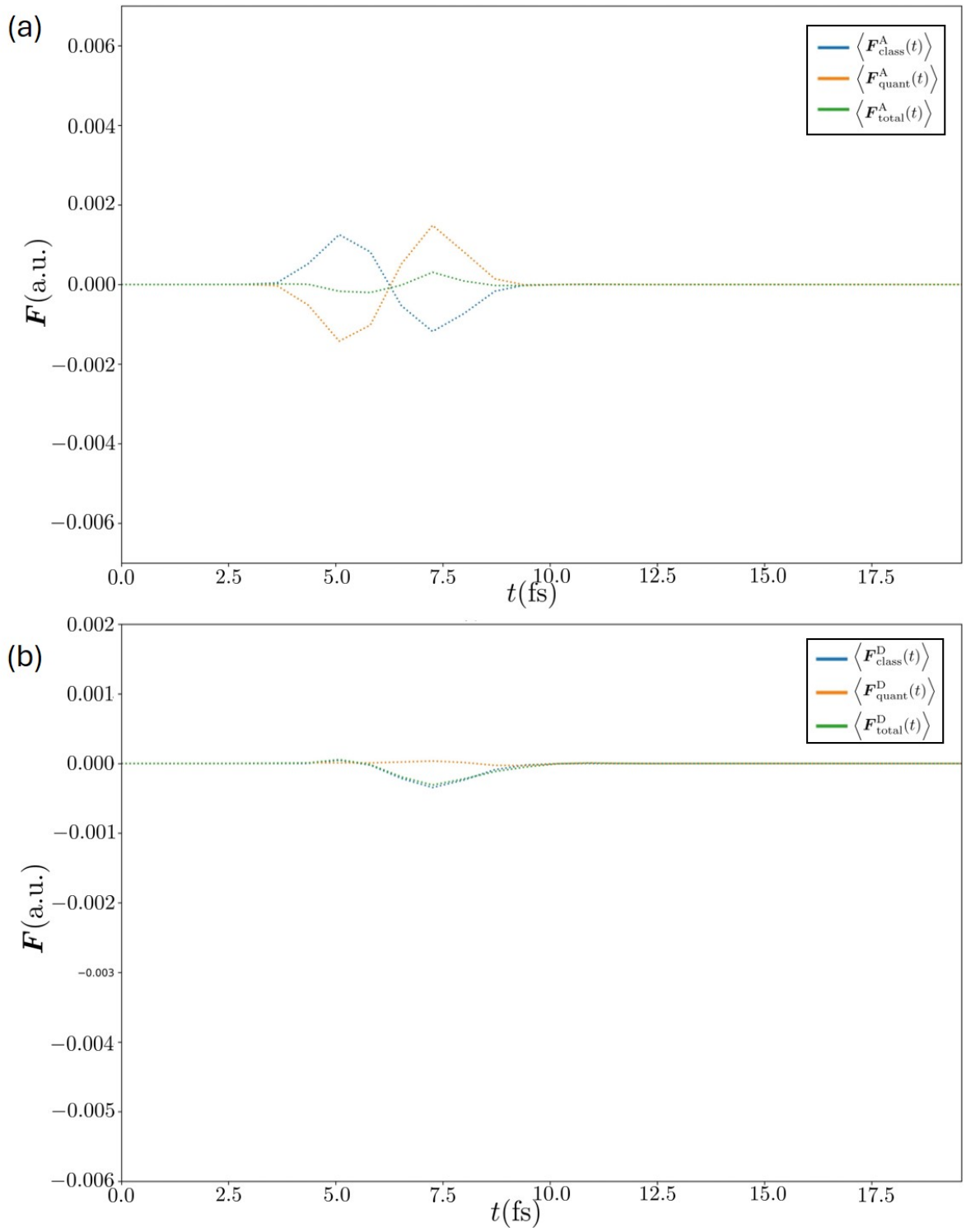

Figure 4.14: (a) Classical and quantum force components that make up the total force in the adiabatic representation for the process in the dual avoided crossing system with the initial population on the lower adiabatic surface. (b) Classical and quantum force components that make up the total force in the corresponding process in the diabatic representation. Diabatic potentials for the dual avoided crossing system are given in Eqns 1.86-1.87, with the diabatic potential coupling constant $C = 0.0015$.

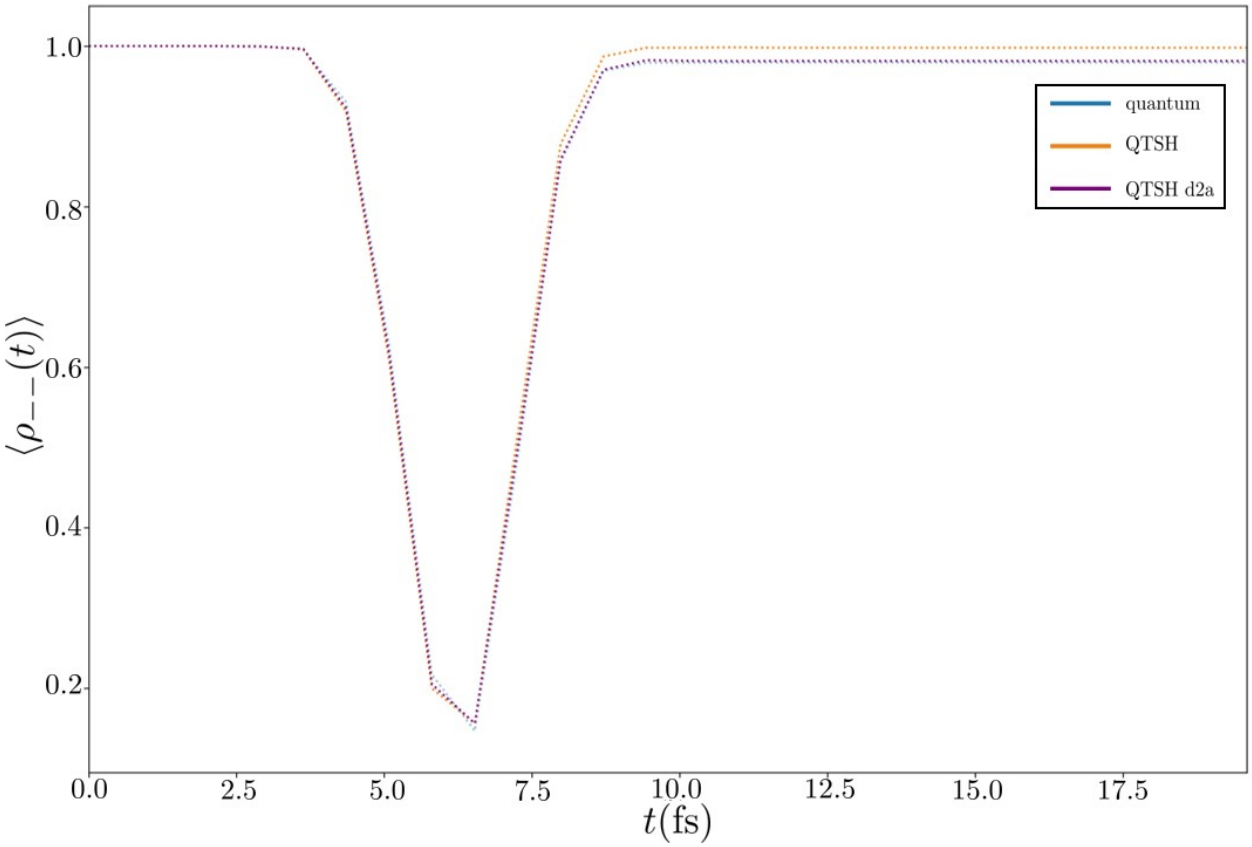

Figure 4.15: Comparison of QTSH, and the QTSH diabatic to adiabatic transformed (QTSH d2a) results against exact quantum results for $\langle \rho_{--}(t) \rangle$, for the dual avoided crossing system with the initial population on the lower adiabatic surface. The trajectories had an average starting momentum of $\hbar k_0 = 77.2$ a.u., with the diabatic potential coupling constant $C = 0.0015$.

With reference to Fig 4.13(b), the phase space averaged population for the diabatic state $V_2(\boldsymbol{q})$, $\langle \rho_{22}(t) \rangle$ for QTSH [62, 63] was found to be in good agreement with the exact quantum results throughout, with non-adiabatic transitions $2 \to 1$ from $t = 5$ fs to $t \approx 10$ fs, finally giving the asymptotic value of $\langle \rho_{22}(t) \rangle \approx 0.975$.

Given that a large population transfer of ~ 0.9 for the non-adiabatic transition $- \to +$, followed by a large population transfer of ~ 0.9 for the subsequent $+ \to -$ took place in the adiabatic representation, we find that the phase space averaged quantum force $\left\langle \boldsymbol{F}^{\mathrm{A}}_{\mathrm{quant}} \right\rangle$ - the force responsible for momentum jumps due to the non-adiabatic transitions - observed in Fig 4.13(a) has two distinct peaks corresponding to the two population transfers. The

contribution of $\left\langle \boldsymbol{F}^{\mathrm{A}}_{\mathrm{quant}} \right\rangle$ to the total phase space averaged total force $\left\langle \boldsymbol{F}^{\mathrm{A}}_{\mathrm{total}} \right\rangle$ was significant. This shows that the process in the adiabatic representation is significantly non-classical.

In contrast, in the diabatic representation, only one transition with a small population transfer of ~ 0.025 occurs from diabatic state $2 \rightarrow 1$ in the diabatic representation, we find that the phase space averaged quantum force $\left\langle \boldsymbol{F}^{\mathrm{D}}_{\mathrm{quant}} \right\rangle$ observed in Fig 4.13(b) has a very weak single peak. The contribution of $\left\langle \boldsymbol{F}^{\mathrm{D}}_{\mathrm{quant}} \right\rangle$ to the total phase space averaged total force $\left\langle \boldsymbol{F}^{\mathrm{D}}_{\mathrm{total}} \right\rangle$ was negligible. The same process in the diabatic representation was largely classical with $\left\langle \boldsymbol{F}^{\mathrm{D}}_{\mathrm{total}} \right\rangle$ acting mainly to evolve the trajectories along the potential energy surfaces.

As in the case of the simple avoided crossing system [1], since the more classical process in the diabatic representation is much simpler with a very small number of trajectory hops, the errors accumulated as a result of surface hopping inconsistencies [50] are much smaller in the diabatic representation, giving more accurate QTSH results in the diabatic representation (Fig 4.14(b)) than in the adiabatic representation (Fig 4.14(a)).

With reference to Fig 4.15, we observed that $\langle \rho_{--}(t) \rangle$ for the transformed QTSH (QTSH d2a) results of the rate of the second non-adiabatic transition $+ \rightarrow -$ after $t \approx 8$ fs exactly matches the quantum result. While the QTSH results at the same time interval had the same rate as the quantum result, but a $\langle \rho_{--}(t) \rangle$ that is higher than the quantum result.

Similar to the case in Sec 4.4.2, obtaining QTSH results in the diabatic representation, where the process is highly classical, and subsequently converting the QTSH [62, 63] result to the adiabatic representation (QTSH d2a) improves the accuracy of the QTSH [62, 63] results in the adiabatic representation by reducing the errors that accumulate with the imperfect surface hopping inconsistencies associated with large population transfers in the adiabatic representation.

4.5 Conclusions

In the limit of complete and localized population transfer, non-adiabatic processes in the adiabatic representation are highly non-classical, with quantum forces that act to create 'momentum' jumps associated with non-adiabatic transitions [81]. The corresponding non-adiabatic processes in the diabatic representation are highly classical with classical forces that act to evolve the trajectories along a *single* diabatic electronic surface. In the highly classical corresponding process in the diabatic representation, the quantum force vanishes since no adiabatic transitions take place.

When many trajectory hops occur and population transfer is incomplete, errors due to QTSH surface hopping inconsistencies [62, 63] accumulate as the problem of overcoherence [3, 50] becomes significant in QTSH. This makes QTSH [62, 63] results for highly classical non-adiabatic processes in the diabatic representation, where few to no trajectory hops occur, more accurate than the corresponding highly non-classical non-adiabatic processes in the adiabatic representation, where numerous trajectory hops take place.

We conclude that applying the d2a transformation to QTSH results in the diabatic representation (i.e. d2a QTSH), where the process is highly classical, minimized the errors associated with QTSH surface hopping inconsistencies, and improved the accuracy of the population dynamics results for the corresponding highly non-classical process in the adiabatic representation.

Chapter 5

Chemical Work, Gibbs Free Energy Change, and Spontaneity in Introductory Chemistry - Chemical Education

This chapter contains verbatim excerpts from Dorothy Miaoyu Huang, Ramesh D. Arasasingham; A Case for Introducing Chemical Work in Introductory Chemistry Courses: A Molecular Mechanics Point of View (*Unpublished*).

5.1 Motivation

In this chapter, we present a case for introducing chemical work [85] in an introductory Chemistry course. In this chapter, we define chemical work [85] as the maximum 'useful' work [93] that can be extracted from a change in the chemical composition as a result of

chemical reactions or phase changes, in the absence of external fields.

In traditional Introductory Chemistry courses that introduce thermodynamics, the form of work that is explained in detail is pressure-volume (P-V) expansion work. This fails to help students appreciate how non-expansion work can be extracted from chemical reactions or phase changes that are central to Chemistry.

In order to do so, the understanding of chemical potentials becomes important. As Introductory Chemistry courses do not necessarily have multivariable calculus as a prerequisite, the definition of chemical potential of a chemical species i, μ_i in terms of the partial derivative of the Gibbs free energy G with respect to the number of moles of the chemical species i, n_i, at constant pressure P and temperature T,

$$\mu_i = \left(\frac{\partial G}{\partial n_i}\right)_{P,T}, \tag{5.1}$$

would not be instructive to Introductory Chemistry students.

Giving Introductory Chemistry students a molecular perspective of what the standard chemical potential of a chemical species is would aid them in understanding how changes in chemical compositions - that occur due to a chemical reaction or phase change - can lead to a change in the total chemical potential energy of the system, that can be converted to 'useful' work [93] at standard state.

In current Physical Chemistry textbooks, [94, 95] a statistical thermodynamics approach is taken to the bridge properties on the molecular level to the macroscopic level. In statistical thermodynamics, the macroscopic property, chemical potential of a species i in a chemical system, accounting for both the chemical identity and phase, μ_i is associated with the thermally accessible states, given by the molar canonical partition function. The complexity of explaining statistical thermodynamics in Introductory Chemistry courses prohibits the

explanation of chemical work [85] to students in such courses.

Introducing students to chemical potential from a molecular mechanics point of view would help give students a diagrammatic and qualitative understanding of how chemical potential arises from molecular motion and intermolecular interactions, allowing them to connect the changes in these interactions to the change in the total chemical potential energy of the system that can extracted as chemical work [85].

Introducing chemical work [85] to students in Introductory Chemistry courses also has the added advantage of helping students to understand why the criteria for spontaneity and equilibrium in terms of the Gibbs free energy change ΔG is

$$\Delta G = 0 \tag{5.2}$$

for chemical equilibrium, and

$$\Delta G < 0 \tag{5.3}$$

for spontaneous chemical reactions.

5.2 Theoretical Background

5.2.1 Pressure-Volume Expansion and 'Useful' Non-expansion Work

Most generally, work w is described as the action of a force $\vec{F}$ in a specified direction $\vec{r}$, given by the general equation,

$$w = \vec{F} \cdot \vec{r}. \tag{5.4}$$

Perhaps since the effect of a force is most easily visualized in $P-V$ expansion work, the starting point for the discussion in General Chemistry and Physical Chemistry textbooks is often pressure-volume (P-V) expansion work [95–101].

We often express work as the sum of a pressure-volume expansion component w_{exp} and non-expansion component $w_{\text{non-exp}}$

$$w = w_{\text{exp}} + \overbrace{w_{\text{non-exp}}}^{w_{\text{useful}}}. \tag{5.5}$$

In Chemistry, the non-expansion component of work (Equation 5.5) is what we consider 'useful' work [93], since this is the work that can be extracted from the chemical system as a result of a chemical reaction or phase change. One form of useful work often studied in Chemistry is electrical work in a galvanic cell.

In this paper, we assume the absence of external fields. This limits our discussion of w_{exp} to P-V expansion work w_{PV}, and $w_{\text{non-exp}}$ to w_{useful}

$$w = w_{PV} + w_{\text{useful}}. \tag{5.6}$$

When work is maximized $w^{\max}$, the maximum 'useful' work $w_{\text{useful}}^{\max}$ equates to chemical work w_{chem}, the maximum non-expansion work that can be extracted from a change in the chemical composition as a result of chemical reactions or phase changes. This reduces work to the sum of P-V expansion work $w_{PV}^{\max}$, and chemical work w_{chem}

$$w^{\max} = w_{PV}^{\max} + w_{\text{chem}}. \tag{5.7}$$

Chemical Work

When the chemical composition of a chemical system changes as a result of a chemical reaction or phase change, the total potential energy of the chemical system E_{pot} is being converted to kinetic energy with 'useful' non-expansion work as the form of energy transfer.

Defined as the maximum 'useful' work that can be extracted from a chemical reaction or phase change in the absence of external fields, chemical work w_{chem} can be defined in terms of the change in the total potential energy of the chemical system ΔE_{pot} as

$$\Delta E_{\text{pot}} = w_{\text{chem}}. \tag{5.8}$$

Since heat can be dissipated due to the chemical reaction or phase change, the 'useful' work extracted obeys the inequality

$$|w_{\text{useful}}| \leq |w_{\text{chem}}|.$$

The chemical potential of a chemical species i, μ_i in a chemical system can be defined as the chemical potential energy that one mole of the chemical species i contributes to the *mixture* in a chemical system.

It then follows that the infinitesimal change in the total chemical potential energy $\mathrm{d}E_{\text{pot}}$, can be expressed as the sum of the product of the chemical potential of each chemical species i by the infinitesimal change in the number of moles of each chemical species i, $\mathrm{d}n_i$ given by the expression

$$\mathrm{d}E_{\text{pot}} = \sum_i \mu_i \mathrm{d}n_i. \tag{5.9}$$

Since the number of moles of each chemical species i changes in proportion the extent of the reaction ξ, with its stoichiometric coefficient in the chemical equation ν_i as the proportionality constant,

$$\mathrm{d}n_i = \nu_i \mathrm{d}\xi. \tag{5.10}$$

This reduces equation 5.9 to

$$\mathrm{d}E_{\mathrm{pot}} = \sum_i \nu_i \mu_i(\xi) \mathrm{d}\xi. \tag{5.11}$$

When the chemical system changes from the initial state ξ_{initial} to the final state ξ_{final}, the change in the chemical potential energy of the system and using its relation to w_{chem} (equation 5.8) gives,

$$w_{\mathrm{chem}} = \Delta E_{\mathrm{pot}} = \int_{\xi_{\mathrm{initial}}}^{\xi_{\mathrm{final}}} \left(\sum_i \nu_i \mu_i(\xi) \right) \mathrm{d}\xi. \tag{5.12}$$

5.2.2 Chemical Work, Spontaneity and the Sign Convention for Work

In much of Chemistry, the thermodynamic quantity, Gibbs free energy G is often used since many chemical reactions take place under constant temperature T and pressure P conditions. As such, the criterion for spontaneity at constant T and P conditions uses the Gibbs free energy change ΔG as a reference.

The criterion for spontaneity and equilibrium at constant T and P conditions is often refer-

enced in General Chemistry [98, 100, 101] as

$$\Delta G \leq 0, \tag{5.13}$$

and more precisely as $\mathrm{d}G_{\mathrm{rxn}} \leq 0$ in Physical Chemistry textbooks [96].

While Gibbs free energy change ΔG is often introduced as the maximum energy available to do work in some General Chemistry textbooks [98, 100]. The Gibbs free energy change is more specifically the maximum 'useful' work $w_{\mathrm{useful}}^{\mathrm{max}}$,[93] that can be done as a result of a chemical reaction or phase change in the absence of external field, which we have defined as chemical work w_{chem} [85] in this chapter.

This is given by

$$\Delta G = w_{\mathrm{useful}}^{\mathrm{max}} = w_{\mathrm{chem}}, \tag{5.14}$$

excluding pressure-volume expansion work w_{PV}, the form of work that is introduced in detail in Introductory Chemistry.

Fundamental Equation of Chemical Thermodynamics

In the absence of external fields, a thermodynamic function of T, P, and $\{n_i\}$, that is related to the internal energy $U\big(S, V, \{n_i\}\big)$ by a Legendre transform is the Gibbs' free energy $G\big(T, P, \{n_i\}\big)$.

The resulting equation in its differential form is the fundamental equation of chemical ther-

modynamics (Equation 5.15) [85, 96],

$$\mathrm{d}G\big(T,P,\{n_i\}\big) = V\mathrm{d}P - S\mathrm{d}T + \sum_i^N \mu_i \mathrm{d}n_i = V\mathrm{d}P - S\mathrm{d}T + \overbrace{\sum_i^N \nu_i \mu_i(\xi)\mathrm{d}\xi}^{\mathrm{d}E_{\mathrm{pot}} = đw_{\mathrm{chem}}}. \tag{5.15}$$

At constant T and constant P, where $\mathrm{d}T = 0$ and $\mathrm{d}P = 0$, the fundamental equation of chemical thermodynamics reduces to

$$\mathrm{d}G\big(T,P,\{n_i\}\big) = \sum_i^N \mu_i \mathrm{d}n_i = \overbrace{\sum_i^N \nu_i \mu_i(\xi)\mathrm{d}\xi}^{\mathrm{d}E_{\mathrm{pot}} = đw_{\mathrm{chem}}}, \tag{5.16}$$

As the Gibbs free energy change of reaction ΔG_{rxn} is the partial derivative,

$$\Delta G_{\mathrm{rxn}} = \left(\frac{\partial G}{\partial \xi}\right)_{T,P}, \tag{5.17}$$

at constant T and P, ΔG_{rxn} can be written in terms of chemical potentials μ_i as

$$\Delta G_{\mathrm{rxn}} = \sum_i^N \nu_i \mu_i(\xi). \tag{5.18}$$

Combining equations 5.16 and 5.11, in the absence of any external fields, the Gibbs free energy change ΔG at constant T and P when a chemical reaction or phase change occurs, taking the chemical system from state ξ_{initial} to ξ_{final} is,

$$\Delta G = \Delta E_{\mathrm{pot}} = w_{\mathrm{chem}} = \int_{\xi_{\mathrm{initial}}}^{\xi_{\mathrm{final}}} \Delta G_{\mathrm{rxn}} \mathrm{d}\xi. \tag{5.19}$$

5.2.3 Molecular View of Chemical Potential: Current Approach

In Physical Chemistry textbooks [94–96], the idea of chemical work [85] is often not mentioned, and the molecular interpretation of chemical potential is made from a statistical thermodynamics point of view.

While this approach addresses the molecular picture that Chemistry is concerned with, it requires multivariate calculus that is often not a requisite for Introductory Chemistry courses.

In statistical mechanics the chemical potential of a species i in a chemical system, accounting for both the chemical identity and phase, μ_i is associated with the thermally accessible translational, rotational, vibrational, and electronic states, given by the molar canonical partition functions $Q_{m,i}^{\text{trans}}$, $Q_{m,i}^{\text{rot}}$, $Q_{m,i}^{\text{vib}}$, and $Q_{m,i}^{\text{elec}}$, respectively.

The chemical potential μ_i at constant temperature T and pressure P is equivalent to the molar Gibbs free energy[85, 96][1],

$$\mu_i = -RT\ln(Q_{m,i}^{\text{trans}}Q_{m,i}^{\text{rot}}Q_{m,i}^{\text{vib}}Q_{m,i}^{\text{elec}}) + RTV\left(\frac{\partial \ln(Q_{m,i}^{\text{trans}}Q_{m,i}^{\text{rot}}Q_{m,i}^{\text{vib}}Q_{m,i}^{\text{elec}})}{\partial V}\right)_T, \tag{5.20}$$

where the potential energy due to intermolecular interactions E_{imf} are accounted for in the translational molar canonical partition function for species i, $Q_{m,i}^{\text{trans}}$ [94].

This can be expressed as

$$Q_{m,i}^{\text{trans}} = \frac{\int \mathrm{e}^{-\frac{E_{\text{imf}}}{k_{\text{B}}T}}\mathrm{d}\tau_1\mathrm{d}\tau_2\cdots\mathrm{d}\tau_{N_{\text{A}}}}{N_{\text{A}}!\Lambda^{3N_{\text{A}}}}, \tag{5.21}$$

where N_{A} and Λ represent Avogadro's number and the thermal de Broglie wavelength, respectively.

[1] This equation has been rewritten in a generalized form to allow for use with non-ideal fluids.

5.3 Chemical Work: A Molecular Mechanics Perspective

We suggest an approach that make reduces the complexity of chemical work and chemical potential using a molecular mechanics approach to make the concept of chemical work and chemical potential possible at an introductory Chemistry level.

Chemical systems at a given extent of a chemical reaction or phase change ξ have chemical potential energy in the form of bonds, and intermolecular interactions that occur between reactant molecules, between product molecules, and between reactant and product molecules.

From a molecular mechanics point of view, the change in the total potential energy of the system ΔE_{pot} due to changes in chemical composition when the chemical system progresses from its initial to final state $\Delta\xi$, involves the change in the total chemical potential energy associated with the molecular modes of motion are associated with bond stretching, angle bending, bond twisting, intermolecular rearrangement (Fig 5.1), and the bond breakage and formation that occurs between the reactant and product states.

It can then be said that the chemical potential of the chemical species i, μ_i is the average potential energy that one mole of the species i contributes to the state of the chemical system that exists as a mixture, due to the molecular modes of motions, and intermolecular interactions, as seen in Fig 5.1.

These changes result in a change in the total potential energy ΔE_{pot} that can be extracted to perform work. The maximum amount of work that can be extracted from this change is the chemical work w_{chem} [85].

Presenting this picture to students gives them a more diagrammatic view of what happens in chemical systems, helping them to better appreciate chemical thermodynamics.

5.3.1 Suggestions for the Classroom

For introductory chemistry, adapting from equation 5.19, w_{chem} can be presented as the difference between the sum of the product of the chemical potential and the stoichiometric coefficient of each product species, and sum of the product of the chemical potential and the stoichiometric coefficient of each reactant species, taking the change in the extent of reaction $\Delta\xi$ into account,

$$w_{\text{chem}} = \Bigg(\overbrace{\sum_{\text{products}} \nu_{\text{products}}\mu_{\text{products}}}^{\text{total potential energy of products}} - \underbrace{\sum_{\text{reactants}} \nu_{\text{reactants}}\mu_{\text{reactants}}}_{\text{total potential energy of reactants}} \Bigg) \Delta\xi. \tag{5.22}$$

Presenting the equation in this manner provides a familiar form to the calculation of the standard Gibbs free energy change of reaction $\Delta G^{\circ}_{\text{rxn}}$ from the standard molar Gibbs free energy G°_{m} of products and reactants that students are introduced to in introductory textbooks.[95–101]

This provides an opportunity to connect the standard molar Gibbs free energy of the chemical species i, $G^{\circ}_{\text{m},i}$ to the standard chemical potential μ°_i where the connection between the standard Gibbs free energy change of reaction $\Delta G^{\circ}_{\text{rxn}}$ is equal to the chemical work w_{chem} at constant T and P, since the reaction is assumed to go to completion, where $\Delta\xi = 1$. (Section 5.5)

Chemical Reaction Example

A diagrammatic example illustrating how these principles are applied can be illustrated with the following reaction

$$\text{H}_2(g) + \frac{1}{2}\text{O}_2(g) \longrightarrow \text{H}_2\text{O}(g). \tag{5.23}$$

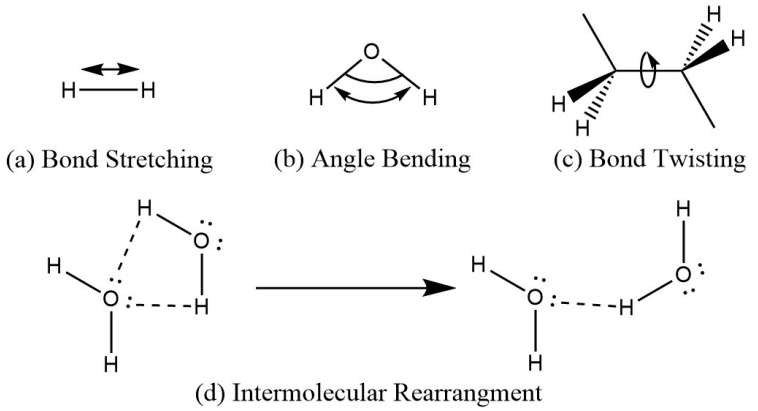

Figure 5.1: Potential energy associated with intramolecular interactions associated with (a) bond stretching, (b) angle bending, and (c) bond twisting. (d) Changes in potential energy associated with changes in intermolecular interactions such as hydrogen bonding, as a result of the rearrangement of molecules.

For this specific example, w_{chem} can be written in the form of equation 5.22 as

$$w_{\text{chem}} = \Bigg(\overbrace{\mu_{\text{H}_2\text{O}}}^{\text{total potential energy of product}} - \underbrace{\left(\mu_{\text{H}_2} + \frac{1}{2}\mu_{\text{O}_2}\right)}_{\text{total potential energy of reactants}} \Bigg) \Delta\xi. \tag{5.24}$$

With reference to Fig 5.2, the difference in the molecular modes of motion and intermolecular interaction for the reactants and products contribute to differences in the chemical potentials for each chemical species and demonstrates how a change in the composition from the initial to final state $\Delta\xi$, results in a change in the molecular modes of motion and intermolecular interactions.

Phase Change Example

A diagrammatic example illustrating how these principles are applied can be illustrated with the vaporization of water given by

$$\text{H}_2\text{O}(l) \longrightarrow \text{H}_2\text{O}(g), \tag{5.25}$$

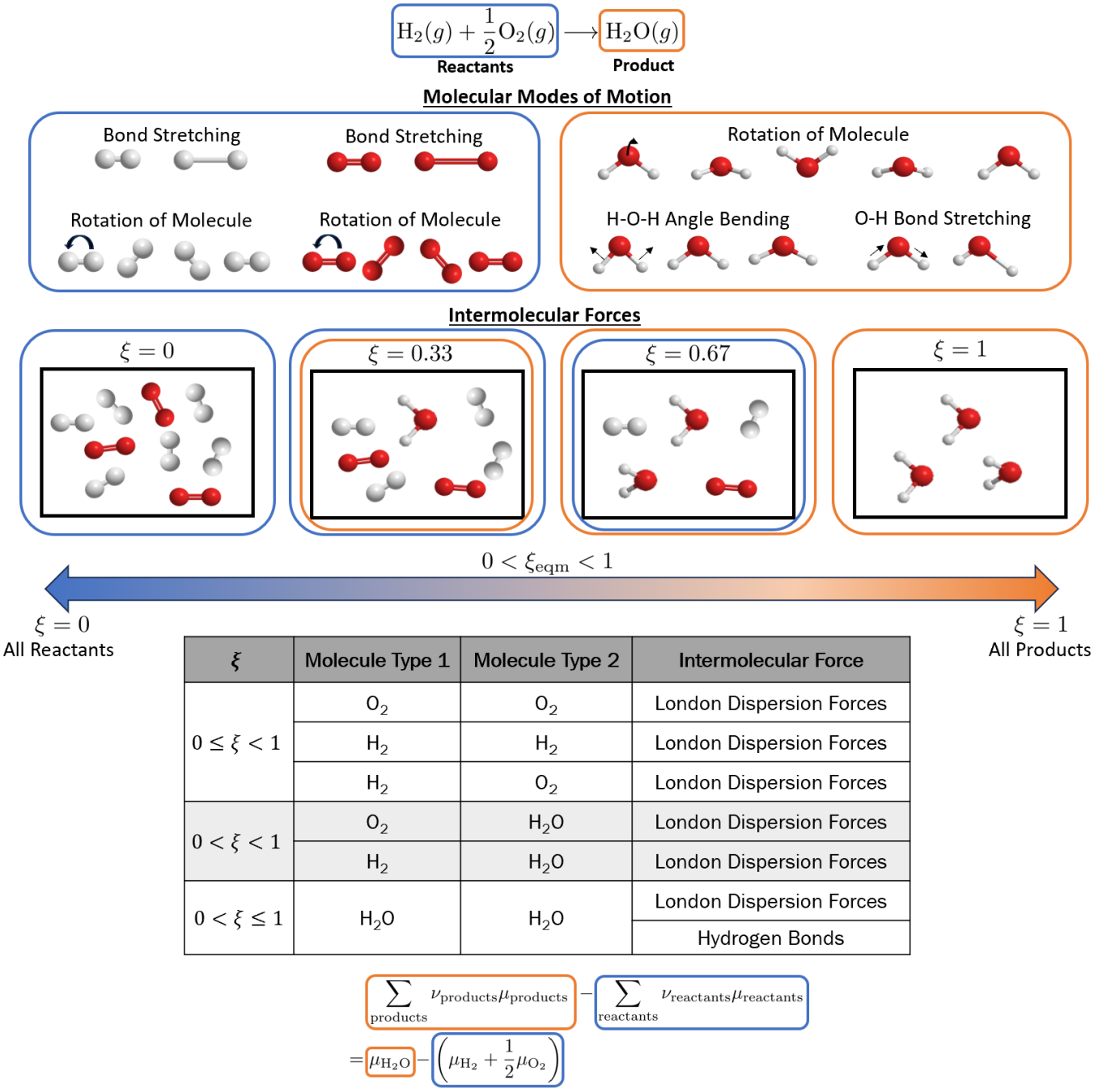

ξ	Molecule Type 1	Molecule Type 2	Intermolecular Force
$0 \leq \xi < 1$	O_2	O_2	London Dispersion Forces
	H_2	H_2	London Dispersion Forces
	H_2	O_2	London Dispersion Forces
$0 < \xi < 1$	O_2	H_2O	London Dispersion Forces
	H_2	H_2O	London Dispersion Forces
$0 < \xi \leq 1$	H_2O	H_2O	London Dispersion Forces
			Hydrogen Bonds

$$\sum_{\text{products}} \nu_{\text{products}} \mu_{\text{products}} - \sum_{\text{reactants}} \nu_{\text{reactants}} \mu_{\text{reactants}}$$
$$= \mu_{H_2O} - \left(\mu_{H_2} + \frac{1}{2} \mu_{O_2} \right)$$

Figure 5.2: Molecular modes of motion that contribute the the chemical potentials of the reactants, H_2 and O_2 include the bond stretching modes and rotational modes of H_2 molecules and O_2 molecules. Molecular modes of motion that contribute the the chemical potential of the product, H_2O include the bond stretching modes, rotational modes, and angle bending modes of H_2O molecules (not all bond stretching modes are displayed.). Depending on the extent of the reaction ξ, different intermolecular forces of attraction contribute the the chemical potentials, as summarized in the table.

when the phase change is irreversible at the given temperature and pressure conditions, and

$$\mathrm{H_2O}(l) \rightleftharpoons \mathrm{H_2O}(g), \tag{5.26}$$

when the phase change is reversible at the given temperature and pressure.

For this vaporization of water, w_{chem} can be written in the form of equation 5.22 as

$$w_{\text{chem}} = \big(\overbrace{\mu_{\mathrm{H_2O(g)}}}^{\text{product component}} - \underbrace{\mu_{\mathrm{H_2O}(l)}}_{\text{reactant component}} \big)\Delta\xi. \tag{5.27}$$

The change in the structure of liquid water and water vapor is given in Fig 5.3, where the hydrogen bonding in liquid water is more extensive than that of water vapor. At a various temperature and pressure conditions, the different interactions that water molecules have with each other in the liquid and vapor phases have varying contributions to the chemical potential.

When the conditions under which the phase change occurs at a temperature and pressure condition along the vaporization curve (Fig 5.4), the chemical potential of liquid water and water vapor, $\mu_{\mathrm{H_2O}(l)}$ and $\mu_{\mathrm{H_2O}(g)}$, respectively are equal (i.e. $\mu_{\mathrm{H_2O}(l)} = \mu_{\mathrm{H_2O}(g)}$).

It follows that w_{chem} along the vaporization curve (Fig 5.4) would be

$$w_{\text{chem}} = \big(\overbrace{\mu_{\mathrm{H_2O(l)}}}^{\mu_{\mathrm{H_2O(g)}}} - \mu_{\mathrm{H_2O}(l)} \big)\Delta\xi = 0. \tag{5.28}$$

When the phase change occurs at any other temperature and pressure in the gas region (Fig

5.4), the phase change constitutes work done *by* the chemical system resulting in

$$w_{\text{chem}} < 0. \tag{5.29}$$

This example can be used to make the connection between reversibility in a chemical system can be made by explaining that the relevant phase change is reversible at a *given temperature and pressure* that exists along the lines of the phase diagram, where both phases coexist. A phase change is not reversible when it takes place at a *given temperature and pressure* that exists in the region of the phase diagram corresponding to the final state of the system.

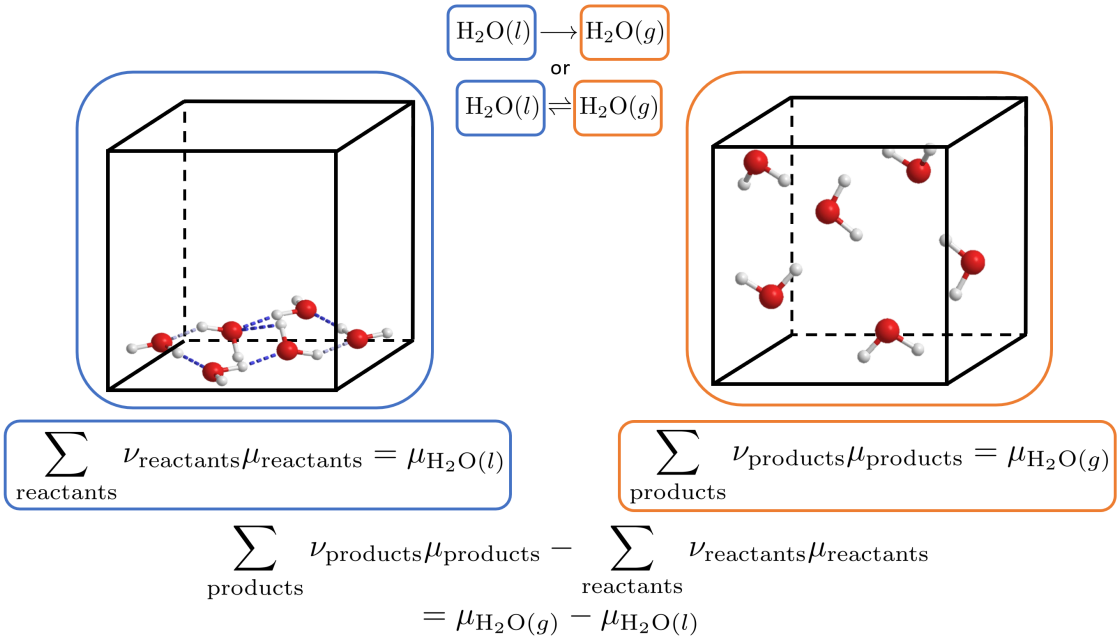

Figure 5.3: Liquid water $H_2O(l)$ (in blue) has more extensive hydrogen bonding between water molecules than water vapor $H_2O(g)$ (in orange). The chemical potential for the reactants side of the equations and the product side of the equation is $\mu_{H_2O(l)}$ and $\mu_{H_2O(g)}$, respectively. Depending on whether the phase change is reversible or spontaneous at the given temperature and pressure conditions, a double arrow or a single arrow is used to separate the reactant and product in the chemical equation.

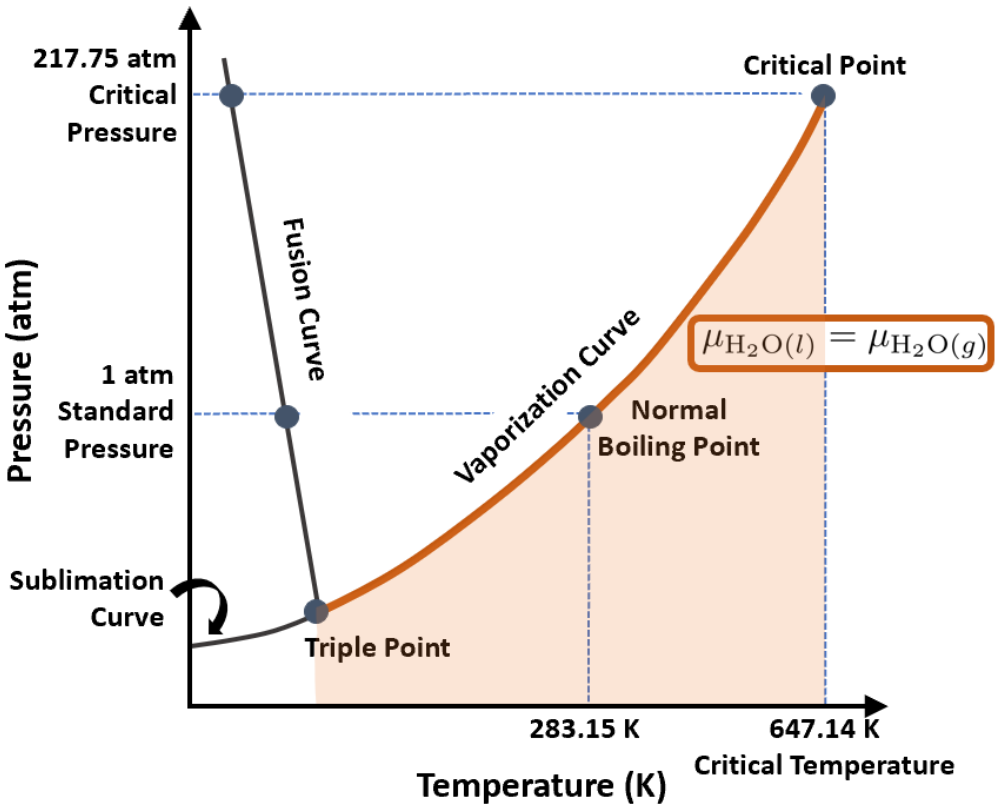

Figure 5.4: The vaporization of water occurs when liquid water $H_2O(l)$ is placed at a temperature and pressure that lies along the vaporization curve (orange line) or within the gas region (shaded orange region). When along the vaporization curve, the chemical potential of liquid water and water vapour are equal.

5.4 Connecting Spontaneity and Sign Conventions for Work in Chemistry

The definition of a spontaneous process as one that has a natural tendency to occur [96, 98, 100, 101], without the need for work to be done on the system [95, 96], or without the need for an external force to be applied [100] sufficiently introduces the idea of spontaneity.

Restating the definition of spontaneity in terms of chemical systems, we can make the following statements. When no chemical work is done by a chemical system, the system is at equilibrium since work is not done *by* or *on* the system. When chemical work is done *by* a chemical system, the reaction is spontaneous since no external force is required to drive the

chemical reaction.

Combining this with the sign conventions for work in Chemistry where work done is *positive* when work is done by the surroundings *on* the system, and *negative* when work is done *by* the system on the surroundings, we can restate the above statements about spontaneity in terms of the maximum chemical work w_{chem}, as

$$w_{\text{chem}} = 0 \tag{5.30}$$

for chemical equilibrium, and

$$w_{\text{chem}} < 0 \tag{5.31}$$

for spontaneous chemical reactions.

Combining the definition of ΔG at constant T and P in terms of chemical work (Equation 5.14) with the the criteria for equilibrium (Equation 5.30) and spontaneity (Equation 5.31) in terms of w_{chem}, the criteria for equilibrium (Equation 5.2) and spontaneity (Equation 5.3) in terms of ΔG are recovered.

This helps students connect the capacity for a forward chemical reaction or phase change to drive work, as a result of changes in the potential energy of the chemical system, with spontaneity, the basis for the study of electrochemistry, and reaction coupling in Biology.

5.5 Chemical Potential and the Standard Molar Gibbs Free Energy

The relationship between the chemical potential of a chemical species under standard conditions i, μ_i° and the standard molar Gibbs free energy of a chemical species i,

$$G_{\mathrm{m},i}^\circ = \mu_i^\circ, \tag{5.32}$$

can also be shown to students by simple comparison.

Combining equation 5.14 with equation 5.22, under standard constant T and P conditions, we obtain the standard Gibbs free energy change of reaction $\Delta G_{\mathrm{rxn}}^\circ$ when $\Delta\xi = 1$,

$$\Delta G_{\mathrm{rxn}}^\circ = \sum_{\text{products}} \nu_{\text{products}} \mu_{\text{products}}^\circ - \sum_{\text{reactants}} \nu_{\text{reactants}} \mu_{\text{reactants}}^\circ. \tag{5.33}$$

In current General Chemistry [97–101] and Physical Chemistry textbooks [95, 96], the standard Gibbs free energy change of reaction $\Delta G_{\mathrm{rxn}}^\circ$ is often given in terms of the standard molar Gibbs free energies of formation G_{m}° as

$$\Delta G_{\mathrm{rxn}}^\circ = \sum_{\text{products}} \nu_{\text{products}} G_{\mathrm{m,products}}^\circ - \sum_{\text{reactants}} \nu_{\text{reactants}} G_{\mathrm{m,reactants}}^\circ. \tag{5.34}$$

Comparing equations 5.33 and 5.34, it follows that the relation in equation 5.32 holds.

5.6 Conclusions

Presenting a molecular mechanics perspective of chemical potential provides students with a diagrammatic view and qualitative understanding of how the chemical potential arises from molecular motion and intermolecular interactions. This helps them appreciate how the changes in chemical composition that arise from chemical reactions or phase changes would contribute to a change in the total chemical potential energy, and as a result the maximum amount of 'useful' work or chemical work that can be extracted from the chemical system at constant temperature and pressure. This prompts students to think about what occurs on a molecular level, while sidestepping the need for multivariate calculus and statistical mechanics.

Since Gibbs free energy change is the maximum 'useful' work [93] or chemical work [85] at constant temperature and pressure, combined with the conventions for work in chemistry allows an intuitive understanding of the criteria of spontaneity as the chemical system doing 'useful' non-expansion work, and the criteria of equilibrium as the chemical system not doing any 'useful' non-expansion work. This emphasizes the idea that a chemical reaction or phase change can drive work, one that would aid in their understanding of electrochemistry or coupled reactions in Biology.

The relation of the standard molar Gibbs free energy to the standard chemical potential of a species can also be explained to students.

Bibliography

[1] John C Tully. Molecular dynamics with electronic transitions. *The Journal of Chemical Physics*, 93(2):1061–1071, 1990. ISSN 0021-9606. doi: 10.1063/1.459170.

[2] Lea M. Ibele and Basile F. E. Curchod. A molecular perspective on Tully models for nonadiabatic dynamics. *Physical Chemistry Chemical Physics*, 22(27):15183–15196, 2020. ISSN 1463-9076. doi: 10.1039/d0cp01353f.

[3] John C Tully. Perspective: Nonadiabatic dynamics theory. *The Journal of Chemical Physics*, 137(22):22A301, 2012. ISSN 0021-9606. doi: 10.1063/1.4757762.

[4] Tammie R. Nelson, Alexander J. White, Josiah A. Bjorgaard, Andrew E. Sifain, Yu Zhang, Benjamin Nebgen, Sebastian Fernandez-Alberti, Dmitry Mozyrsky, Adrian E. Roitberg, and Sergei Tretiak. Non-adiabatic Excited-State Molecular Dynamics: Theory and Applications for Modeling Photophysics in Extended Molecular Materials. *Chemical Reviews*, 120(4):2215–2287, 2020. ISSN 0009-2665. doi: 10.1021/acs.chemrev.9b00447.

[5] M. Born and R. Oppenheimer. Zur Quantentheorie der Molekeln. *Annalen der Physik*, 389(20):457–484, 1927. ISSN 0003-3804. doi: 10.1002/andp.19273892002.

[6] John C. Tully. Perspective on "Zur Quantentheorie der Molekeln". *Theoretical Chemistry Accounts*, 103(3-4):173–176, 2000. ISSN 1432-881X. doi: 10.1007/s002149900049.

[7] Joseph E Subotnik, Ethan C Alguire, Qi Ou, Brian R Landry, and Shervin Fatehi. The Requisite Electronic Structure Theory To Describe Photoexcited Nonadiabatic Dynamics: Nonadiabatic Derivative Couplings and Diabatic Electronic Couplings. *Accounts of Chemical Research*, 48(5):1340–1350, 2015. ISSN 0001-4842. doi: 10.1021/acs.accounts.5b00026.

[8] Alexander J. White, Vyacheslav N. Gorshkov, Sergei Tretiak, and Dmitry Mozyrsky. Non-adiabatic molecular dynamics by accelerated semiclassical Monte Carlo. *The Journal of Chemical Physics*, 143(1):014115, 2015. ISSN 0021-9606. doi: 10.1063/1.4923473.

[9] Michael Baer. *Beyond Born-Oppenheimer: Conical Intersections and Electronic Nonadiabatic Coupling Terms*. Wiley-Interscience, Hoboken, NJ, 2006. ISBN 9780471780083. doi: 10.1002/0471780081.ch1.

[10] Ignacio Franco and Sergei Tretiak. Electron-Vibrational Dynamics of Photoexcited Polyfluorenes. *Journal of the American Chemical Society*, 126(38):12130–12140, 2004. ISSN 0002-7863. doi: 10.1021/ja0489285.

[11] Gloria L. Silva, Volkan Ediz, David Yaron, and Bruce A. Armitage. Experimental and Computational Investigation of Unsymmetrical Cyanine Dyes: Understanding Torsionally Responsive Fluorogenic Dyes. *Journal of the American Chemical Society*, 129(17): 5710–5718, 2007. ISSN 0002-7863. doi: 10.1021/ja070025z.

[12] Avishek Saha, Brendan J. Gifford, Xiaowei He, Geyou Ao, Ming Zheng, Hiromichi Kataura, Han Htoon, Svetlana Kilina, Sergei Tretiak, and Stephen K. Doorn. Narrowband single-photon emission through selective aryl functionalization of zigzag carbon nanotubes. *Nature Chemistry*, 10(11):1089–1095, 2018. ISSN 1755-4330. doi: 10.1038/s41557-018-0126-4.

[13] Yasuhiro Shirasaki, Geoffrey J. Supran, Moungi G. Bawendi, and Vladimir Bulović. Emergence of colloidal quantum-dot light-emitting technologies. *Nature Photonics*, 7 (1):13–23, 2013. ISSN 1749-4885. doi: 10.1038/nphoton.2012.328.

[14] Achim Hartschuh, Hermeneglido N. Pedrosa, Lukas Novotny, and Todd D. Krauss. Simultaneous Fluorescence and Raman Scattering from Single Carbon Nanotubes. *Science*, 301(5638):1354–1356, 2003. ISSN 0036-8075. doi: 10.1126/science.1087118.

[15] Joshua Leveillee, Claudine Katan, Liujiang Zhou, Aditya D. Mohite, Jacky Even, Sergei Tretiak, André Schleife, and Amanda J. Neukirch. Influence of -conjugated cations and halogen substitution on the optoelectronic and excitonic properties of layered hybrid perovskites. *Physical Review Materials*, 2(10):105406, 2018. doi: 10.1103/physrevmaterials.2.105406.

[16] Françoise Provencher, Nicolas Bérubé, Anthony W. Parker, Gregory M. Greetham, Michael Towrie, Christoph Hellmann, Michel Côté, Natalie Stingelin, Carlos Silva, and Sophia C. Hayes. Direct observation of ultrafast long-range charge separation at polymer–fullerene heterojunctions. *Nature Communications*, 5(1):4288, 2014. doi: 10.1038/ncomms5288.

[17] Carlito S. Ponseca, Pavel Chabera, Jens Uhlig, Petter Persson, and Villy Sundstrom. Ultrafast Electron Dynamics in Solar Energy Conversion. *Chemical Reviews*, 117(16): 10940–11024, 2017. ISSN 0009-2665. doi: 10.1021/acs.chemrev.6b00807.

[18] Francesca Fassioli, Rayomond Dinshaw, Paul C. Arpin, and Gregory D. Scholes. Photosynthetic light harvesting: excitons and coherence. *Journal of The Royal Society Interface*, 11(92):20130901, 2014. ISSN 1742-5689. doi: 10.1098/rsif.2013.0901.

[19] Jonas M. Hostettler, Andreas Bach, and Peter Chen. Adiabatic and nonadiabatic dissociation of ethyl radical. *The Journal of Chemical Physics*, 130(3):034303, 2009. ISSN 0021-9606. doi: 10.1063/1.3058588.

[20] Akira Matsugi. Roaming Dissociation of Ethyl Radicals. *The Journal of Physical Chemistry Letters*, 4(24):4237–4240, 2013. ISSN 1948-7185. doi: 10.1021/jz4024018.

[21] Myung Hwa Kim, Lei Shen, Hongli Tao, Todd J. Martinez, and Arthur G. Suits. Conformationally Controlled Chemistry: Excited-State Dynamics Dictate Ground-State Reaction. *Science*, 315(5818):1561–1565, 2007. ISSN 0036-8075. doi: 10.1126/science.1136453.

[22] Hohjai Lee, Yuan-Chung Cheng, and Graham R. Fleming. Coherence Dynamics in Photosynthesis: Protein Protection of Excitonic Coherence. *Science*, 316(5830):1462–1465, 2007. ISSN 0036-8075. doi: 10.1126/science.1142188.

[23] Martin Reufer, Manfred J. Walter, Pavlos G. Lagoudakis, Anne Beate Hummel, Johanna S. Kolb, Hartmut G. Roskos, Ullrich Scherf, and John M. Lupton. Spin-conserving carrier recombination in conjugated polymers. *Nature Materials*, 4(4):340–346, 2005. ISSN 1476-1122. doi: 10.1038/nmat1354.

[24] Sebastian Mai, Philipp Marquetand, and Leticia González. Non-adiabatic and intersystem crossing dynamics in SO2. II. The role of triplet states in the bound state dynamics studied by surface-hopping simulations. *The Journal of Chemical Physics*, 140(20):204302, 05 2014. ISSN 0021-9606. doi: 10.1063/1.4875036.

[25] Richard A. Mathies, C. H. Brito Cruz, Walter T. Pollard, and Charles V. Shank. Direct observation of the femtosecond excited-state *cis-trans* isomerization in bacteriorhodopsin. *Science*, 240(4853):777–779, 1988. doi: 10.1126/science.3363359.

[26] Andranik Kazaryan, Zhenggang Lan, Lars V. Schafer, Walter Thiel, and Michael Filatov. Surface Hopping Excited-State Dynamics Study of the Photoisomerization of a Light-Driven Fluorene Molecular Rotary Motor. *Journal of Chemical Theory and Computation*, 7(7):2189–2199, 2011. ISSN 1549-9618. doi: 10.1021/ct200199w.

[27] Amanda J. Neukirch, Logan C. Shamberger, Enrique Abad, Barry J. Haycock, Hong Wang, Jose Ortega, Oleg V. Prezhdo, and James P. Lewis. Nonadiabatic Ensemble Simulations of cis-Stilbene and cis-Azobenzene Photoisomerization. *Journal of Chemical Theory and Computation*, 10(1):14–23, 2014. ISSN 1549-9618. doi: 10.1021/ct4009816.

[28] J. Clark, T. Nelson, S. Tretiak, G. Cirmi, and G. Lanzani. Femtosecond torsional relaxation. *Nature Physics*, 8(3):225–231, 2012. ISSN 1745-2473. doi: 10.1038/nphys2210.

[29] Joseph E. Subotnik, Amber Jain, Brian Landry, Andrew Petit, Wenjun Ouyang, and Nicole Bellonzi. Understanding the Surface Hopping View of Electronic Transitions and Decoherence. *Annual Review of Physical Chemistry*, 67(1):387–417, 2016. ISSN 0066-426X. doi: 10.1146/annurev-physchem-040215-112245.

[30] Linjun Wang, Alexey Akimov, and Oleg V. Prezhdo. Recent Progress in Surface Hopping: 2011–2015. *The Journal of Physical Chemistry Letters*, 7(11):2100–2112, 2016. ISSN 1948-7185. doi: 10.1021/acs.jpclett.6b00710.

[31] S. Bonella and D. F. Coker. A semiclassical limit for the mapping Hamiltonian approach to electronically nonadiabatic dynamics. *The Journal of Chemical Physics*, 114 (18):7778–7789, 2001. ISSN 0021-9606. doi: 10.1063/1.1366331.

[32] Ali Nassimi, Sara Bonella, and Raymond Kapral. Analysis of the quantum-classical Liouville equation in the mapping basis. *The Journal of Chemical Physics*, 133(13): 134115, 2010. ISSN 0021-9606. doi: 10.1063/1.3480018.

[33] Ali Nassimi and Raymond Kapral. Mapping approach for quantum-classical time correlation functions1. *Canadian Journal of Chemistry*, 87(7):880–890, 2009. ISSN 0008-4042. doi: 10.1139/v09-041.

[34] Jonathan R. Mannouch and Jeremy O. Richardson. A mapping approach to surface hopping. *The Journal of Chemical Physics*, 158(10):104111, 2023. ISSN 0021-9606. doi: 10.1063/5.0139734.

[35] Nandini Ananth. Mapping variable ring polymer molecular dynamics: A path-integral based method for nonadiabatic processes. *The Journal of Chemical Physics*, 139(12): 124102, 2013. ISSN 0021-9606. doi: 10.1063/1.4821590.

[36] Stephen J. Cotton and William H. Miller. Symmetrical windowing for quantum states in quasi-classical trajectory simulations: Application to electronically non-adiabatic processes. *The Journal of Chemical Physics*, 139(23):234112, 2013. ISSN 0021-9606. doi: 10.1063/1.4845235.

[37] Stephen J. Cotton, Ruibin Liang, and William H. Miller. On the adiabatic representation of Meyer-Miller electronic-nuclear dynamics. *The Journal of Chemical Physics*, 147(6):064112, 2017. ISSN 0021-9606. doi: 10.1063/1.4995301.

[38] Craig C Martens and Jian-Yun Fang. Semiclassical-limit molecular dynamics on multiple electronic surfaces. *The Journal of Chemical Physics*, 106(12):4918–4930, 1997. ISSN 0021-9606. doi: 10.1063/1.473541.

[39] Arnaldo Donoso and Craig C. Martens. Simulation of Coherent Nonadiabatic Dynamics Using Classical Trajectories. *The Journal of Physical Chemistry A*, 102(23): 4291–4300, 1998. ISSN 1089-5639. doi: 10.1021/jp980219o.

[40] Arnaldo Donoso and Craig C. Martens. Semiclassical multistate Liouville dynamics in the adiabatic representation. *The Journal of Chemical Physics*, 112(9):3980–3989, 2000. ISSN 0021-9606. doi: 10.1063/1.480948.

[41] Arnaldo Donoso, Daniela Kohen, and Craig C Martens. Simulation of nonadiabatic wave packet interferometry using classical trajectories. *The Journal of Chemical Physics*, 112(17):7345–7354, 2000. ISSN 0021-9606. doi: 10.1063/1.481333.

[42] Aaron Kelly and Raymond Kapral. Quantum-classical description of environmental effects on electronic dynamics at conical intersections. *The Journal of Chemical Physics*, 133(8):084502, 2010. ISSN 0021-9606. doi: 10.1063/1.3475773.

[43] Sara Bonella, Giovanni Ciccotti, and Raymond Kapral. Linearization approximations and Liouville quantum–classical dynamics. *Chemical Physics Letters*, 484(4-6):399–404, 2010. ISSN 0009-2614. doi: 10.1016/j.cplett.2009.11.056.

[44] Chun-Cheng Wan and Jeremy Schofield. Exact and asymptotic solutions of the mixed quantum-classical Liouville equation. *The Journal of Chemical Physics*, 112(10):4447–4459, 2000. ISSN 0021-9606. doi: 10.1063/1.481007.

[45] Chun-Cheng Wan and Jeremy Schofield. Solutions of mixed quantum-classical dynamics in multiple dimensions using classical trajectories. *The Journal of Chemical Physics*, 116(2):494–506, 2002. ISSN 0021-9606. doi: 10.1063/1.1425835.

[46] Koji Ando. Non-adiabatic couplings in Liouville description of mixed quantum-classical dynamics. *Chemical Physics Letters*, 360(3-4):240–242, 2002. ISSN 0009-2614. doi: 10.1016/s0009-2614(02)00848-5.

[47] Koji Ando and Mark Santer. Mixed quantum-classical Liouville molecular dynamics without momentum jump. *The Journal of Chemical Physics*, 118(23):10399–10406, 2003. ISSN 0021-9606. doi: 10.1063/1.1574015.

[48] Rachel Crespo-Otero and Mario Barbatti. Recent Advances and Perspectives on Nonadiabatic Mixed Quantum–Classical Dynamics. *Chemical Reviews*, 118(15): acs.chemrev.7b00577 43, 05 2018. ISSN 0009-2665. doi: 10.1021/acs.chemrev.7b00577.

[49] John C Tully and Richard K Preston. Trajectory Surface Hopping Approach to Nonadiabatic Molecular Collisions: The Reaction of H + with D 2. *The Journal of Chemical Physics*, 55(2):562–572, 1971. ISSN 0021-9606. doi: 10.1063/1.1675788.

[50] Mario Barbatti. Nonadiabatic dynamics with trajectory surface hopping method. *Wiley Interdisciplinary Reviews: Computational Molecular Science*, 1(4):620–633, 2011. ISSN 1759-0884. doi: 10.1002/wcms.64.

[51] Philip Pechukas. Time-Dependent Semiclassical Scattering Theory. II. Atomic Collisions. *Physical Review*, 181(1):174–185, 1969. ISSN 0031-899X. doi: 10.1103/physrev.181.174.

[52] Arnaldo Donoso and Craig C. Martens. Classical trajectory-based approaches to solving the quantum Liouville equation. *International Journal of Quantum Chemistry*, 90 (4-5):1348–1360, 2002. ISSN 0020-7608. doi: 10.1002/qua.10377.

[53] Jeanne M Riga and Craig C Martens. Simulation of environmental effects on coherent quantum dynamics in many-body systems. *The Journal of Chemical Physics*, 120(15): 6863–6873, 04 2004. ISSN 0021-9606. doi: 10.1063/1.1651472.

[54] Jeanne M. Riga, Erick Fredj, and Craig C. Martens. Simulation of vibrational dephasing of I2 in solid Kr using the semiclassical Liouville method. *The Journal of Chemical Physics*, 124(6):064506, 2006. ISSN 0021-9606. doi: 10.1063/1.2162878.

[55] Eduardo Roman and Craig C Martens. Semiclassical Liouville method for the simulation of electronic transitions: Single ensemble formulation. *The Journal of Chemical Physics*, 121(23):11572–11580, 12 2004. ISSN 0021-9606. doi: 10.1063/1.1818122.

[56] Eduardo Roman and Craig C Martens. Independent Trajectory Implementation of the Semiclassical Liouville Method: Application to Multidimensional Reaction Dynamics†. *The Journal of Physical Chemistry A*, 111(41):10256–10262, 10 2007. ISSN 1089-5639. doi: 10.1021/jp072629v.

[57] Arnaldo Donoso and Craig C. Martens. Quantum Tunneling Using Entangled Classical Trajectories. *Physical Review Letters*, 87(22):223202, 2001. ISSN 0031-9007. doi: 10.1103/physrevlett.87.223202.

[58] Arnaldo Donoso, Yujun Zheng, and Craig C Martens. Simulation of quantum processes using entangled trajectory molecular dynamics. *The Journal of Chemical Physics*, 119 (10):5010–5020, 2003. ISSN 0021-9606. doi: 10.1063/1.1597496.

[59] Giovanni Granucci and Maurizio Persico. Critical appraisal of the fewest switches algorithm for surface hopping. *The Journal of Chemical Physics*, 126(13):134114, 2007. ISSN 0021-9606. doi: 10.1063/1.2715585.

[60] Weiwei Xie, Shuming Bai, Lili Zhu, and Qiang Shi. Calculation of Electron Transfer Rates Using Mixed Quantum Classical Approaches: Nonadiabatic Limit and Beyond. *The Journal of Physical Chemistry A*, 117(29):6196–6204, 2013. ISSN 1089-5639. doi: 10.1021/jp400462f.

[61] Uwe Müller and Gerhard Stock. Surface-hopping modeling of photoinduced relaxation dynamics on coupled potential-energy surfaces. *The Journal of Chemical Physics*, 107 (16):6230–6245, 1997. ISSN 0021-9606. doi: 10.1063/1.474288.

[62] Craig C Martens. Surface Hopping without Momentum Jumps: A Quantum-Trajectory-Based Approach to Nonadiabatic Dynamics. *The Journal of Physical Chemistry A*, 123(5):1110–1128, 2019. ISSN 1089-5639. doi: 10.1021/acs.jpca.8b10487.

[63] Craig C. Martens. Classical and nonclassical effects in surface hopping methodology for simulating coupled electronic-nuclear dynamics. *Faraday Discussions*, 221(0):449–477, 2019. ISSN 1359-6640. doi: 10.1039/c9fd00042a.

[64] Raymond Kapral and Giovanni Ciccotti. Mixed quantum-classical dynamics. *The Journal of Chemical Physics*, 110(18):8919–8929, 1999. ISSN 0021-9606. doi: 10.1063/1.478811.

[65] G. Granucci, M. Persico, and A. Toniolo. Direct semiclassical simulation of photochemical processes with semiempirical wave functions. *The Journal of Chemical Physics*, 114(24):10608–10615, 06 2001. ISSN 0021-9606. doi: 10.1063/1.1376633. URL `https://doi.org/10.1063/1.1376633`.

[66] C Alden Mead and Donald G Truhlar. Conditions for the definition of a strictly diabatic electronic basis for molecular systems. *The Journal of Chemical Physics*, 77 (12):6090–6098, 1982. ISSN 0021-9606. doi: 10.1063/1.443853.

[67] Tijs Karman, Matthieu Besemer, Ad van der Avoird, and Gerrit C. Groenenboom. Diabatic states, nonadiabatic coupling, and the counterpoise procedure for weakly interacting open-shell molecules. *The Journal of Chemical Physics*, 148(9):094105, 03 2018. ISSN 0021-9606. doi: 10.1063/1.5013091.

[68] Paul Adrien Maurice Dirac. *The Principles of Quantum Mechanics*. Clarendon Press, Oxford,, 1930.

[69] U. Fano. Description of States in Quantum Mechanics by Density Matrix and Operator Techniques. *Rev. Mod. Phys.*, 29:74–93, 1957. doi: 10.1103/RevModPhys.29.74.

[70] C. Cohen-Tannoudji, B. Diu, and F. Laloë. *Quantum Mechanics*. Number v. 1 in A Wiley - Interscience publication. Wiley, 1977. ISBN 9780471164333.

[71] H. Weyl. Quantenmechanik und Gruppentheorie. *Zeitschrift für Physik*, 46(1-2):1–46, 1927. ISSN 0044-3328. doi: 10.1007/bf02055756.

[72] H. Weyl. *The Theory of Groups and Quantum Mechanics*. Dover Books on Mathematics. Dover Publications, 1950. ISBN 9780486602691.

[73] Kin'ya Takahashi. Distribution Functions in Classical and Quantum Mechanics. *Progress of Theoretical Physics Supplement*, (98):109–156, 1989.

[74] E. Wigner. On the Quantum Correction For Thermodynamic Equilibrium. *Physical Review*, 40(5):749–759, 1932. ISSN 0031-899X. doi: 10.1103/physrev.40.749.

[75] M. Hillery, R.F. O'Connell, M.O. Scully, and E.P. Wigner. Distribution functions in physics: Fundamentals. *Physics Reports*, 106(3):121–167, 1984. ISSN 0370-1573. doi: 10.1016/0370-1573(84)90160-1.

[76] Craig C. Martens. Nonadiabatic dynamics in the semiclassical Liouville representation: Locality, transformation theory, and the energy budget. *Chemical Physics*, 481:60–68, 2016. ISSN 0301-0104. doi: 10.1016/j.chemphys.2016.06.013.

[77] Cosmas K Zachos, David B Fairlie, and Thomas L Curtright. *Quantum Mechanics in Phase Space*. WORLD SCIENTIFIC. doi: 10.1142/5287.

[78] Austin T. Green and Craig C. Martens. Zombie cats on the quantum–classical frontier: Wigner–Moyal and semiclassical limit dynamics of quantum coherence in molecules. *The Journal of Chemical Physics*, 159(20):204102, 2023. ISSN 0021-9606. doi: 10.1063/5.0177421.

[79] Craig C Martens. Surface Hopping by Consensus. *The Journal of Physical Chemistry Letters*, 7(13):2610–2615, 2016. ISSN 1948-7185. doi: 10.1021/acs.jpclett.6b01186.

[80] Donald A. McQuarrie. *Statistical Mechanics*. Harper's chemistry series. Harper Collins, New York, 1976.

[81] Dorothy Miaoyu Huang, Austin T. Green, and Craig C. Martens. A first principles derivation of energy-conserving momentum jumps in surface hopping simulations. *The Journal of Chemical Physics*, 159(21):214108, 12 2023. ISSN 0021-9606. doi: 10.1063/5.0178534.

[82] R. P. Feynman. Forces in Molecules. *Physical Review*, 56(4):340–343, 1939. ISSN 0031-899X. doi: 10.1103/physrev.56.340.

[83] D J Klein and Paul L DeVries. Satisfying certain matrix element formulas. *The Journal of Chemical Physics*, 68(1):160–162, 1978. ISSN 0021-9606. doi: 10.1063/1.435506.

[84] Sandra Gómez, Eryn Spinlove, and Graham Worth. Benchmarking non-adiabatic quantum dynamics using the molecular Tully models. *Physical Chemistry Chemical Physics*, 26(3):1829–1844, 2023. ISSN 1463-9076. doi: 10.1039/d3cp03964a.

[85] Herbert B. Callen. *Thermodynamics and an Introduction to Thermostatistics*. John Wiley & Sons, Boston, MA, 2 edition, 1991. ISBN 9780471862567.

[86] Linjun Wang, Dhara Trivedi, and Oleg V. Prezhdo. Global Flux Surface Hopping Approach for Mixed Quantum-Classical Dynamics. *Journal of Chemical Theory and Computation*, 10(9):3598–3605, 2014. ISSN 1549-9618. doi: 10.1021/ct5003835.

[87] H. Goldstein, C.P. Poole, and J.L. Safko. *Classical Mechanics*. Addison Wesley, 2002. ISBN 9780201657029.

[88] C Leforestier, R.H Bisseling, C Cerjan, M.D Feit, R Friesner, A Guldberg, A Hammerich, G Jolicard, W Karrlein, H.-D Meyer, N Lipkin, O Roncero, and R Kosloff. A comparison of different propagation schemes for the time dependent Schrödinger equation. *Journal of Computational Physics*, 94(1):59–80, 1991. ISSN 0021-9991. doi: 10.1016/0021-9991(91)90137-a.

[89] D Kosloff and R Kosloff. A fourier method solution for the time dependent Schrödinger equation as a tool in molecular dynamics. *Journal of Computational Physics*, 52(1): 35–53, 1983. ISSN 0021-9991. doi: 10.1016/0021-9991(83)90015-3.

[90] J. S. Bell and Alain Aspect. *Speakable and Unspeakable in Quantum Mechanics: Collected Papers on Quantum Philosophy*. Cambridge University Press, 2 edition, 2004.

[91] J. E. Moyal. Quantum mechanics as a statistical theory. *Mathematical Proceedings of the Cambridge Philosophical Society*, 45(1):99–124, 1949. ISSN 0305-0041. doi: 10.1017/s0305004100000487.

[92] Craig C. Martens. On the independent trajectory representation of nonadiabatic quantum-classical dynamics. *Unpublished*, 2024.

[93] Steven S. Zumdahl and Donald J. DeCoste. *Chemical Principles*. Cengage Learning, Boston, MA, 8 edition, 2017. ISBN 9781305581982.

[94] P. Atkins, J. de Paula, and J. Keeler. *Atkins' Physical Chemistry Volume 2: Quantum Chemistry, Spectroscopy, and Statistical Thermodynamics*. Atkins' Physical Chemistry. Oxford University Press, Hoboken, NJ, 12 edition, 2023. ISBN 9780198851318.

[95] Thomas Engel and Philip Reid. *Thermodynamics, Statistical Thermodynamics, and Kinetics*. Pearson Education, Inc., New York, NY, 4 edition, 2019. ISBN 9780134804583.

[96] P. Atkins, J. de Paula, and J. Keeler. *Atkins' Physical Chemistry Volume 1: Thermodynamics and Kinetics*. Atkins' Physical Chemistry. Oxford University Press, Hoboken, NJ, 12 edition, 2023. ISBN 9780198851301.

[97] Peter Atkins, Loretta Jones, and Leroy Laverman. *Chemical Principles: The Quest for Insight*. W.H. Freeman and Company, New York, NY, 6 edition, 2013. ISBN 9781429288972.

[98] Raymond Chang and Kenneth A. Goldsby. *General Chemistry: The Essential Concepts*. McGraw-Hill Education, New York, NY, 7 edition, 2013. ISBN 9781259060427.

[99] Martin S. Siberberg. *Chemistry: The Molecular Nature of Matter and Change*. McGraw-Hill Higher Education, New York, NY, 3 edition, 2003. ISBN 0072396814.

[100] Nivaldo J. Tro. *Chemistry : Structure and Properties*. Pearson, Hoboken, NJ, 2 edition, 2018.

[101] Steven S. Zumdahl, Susan A. Zumdahl, and Donald J. DeCoste. *Chemistry*. Cengage Learning, Boston, MA, 10 edition, 2017. ISBN 9781305957404.

Appendix A

Approximate Diabatic Density Matrix for Dual Avoided Crossing Model

We consider a two state model of two localized nonadiabatic transitions, assuming that the transitions occur in a localized region where the population transfer is complete. We analyze the case where the system starts on the lower adiabatic surface and experiences an electronic transition to the upper adiabatic surface that is accompanied by nuclear dynamics. The system then continues on the upper adiabatic surface before experiencing a second electronic transition to the lower adiabatic surface.

In one-dimension, the Dual Avoided Crossing model depicted by Figure 2.8 is a simple example of this.

The initial adiabatic density matrix for the process depicted by Figure 2.8 is of the form

$$\rho_{\mathrm{A}}(t_0) = \begin{pmatrix} 0 & 0 \\ 0 & \rho(t_0) \end{pmatrix}, \tag{A.1}$$

with all probability on the lower state $V_{-}(\boldsymbol{q})$ until the first electronic transition takes place

at $t = t_1^*$, and the intermediate density matrix is

$$\rho^{\mathrm{A}}(\tau) = \begin{pmatrix} \rho(\tau) & 0 \\ 0 & 0 \end{pmatrix}, \tag{A.2}$$

with complete population transfer to the upper state $V_+(\boldsymbol{q})$ where the population remains for $\tau \in (t_1^*, t_2^*)$. A second electronic transfer takes place at $t = t_2^*$, giving the final density matrix

$$\rho^{\mathrm{A}}(t_{\mathrm{f}}) = \begin{pmatrix} 0 & 0 \\ 0 & \rho(t_{\mathrm{f}}) \end{pmatrix}, \tag{A.3}$$

with complete population transfer to the lower state $V_-(\boldsymbol{q})$.

In the diabatic representation, $\rho^{\mathrm{D}}(t)$ can be written throughout the process as

$$\rho^{\mathrm{D}}(t) = \begin{pmatrix} 0 & 0 \\ 0 & \rho(t) \end{pmatrix}, \tag{A.4}$$

allowing us to write the approximate adiabatic density matrix

$$\rho^{\mathrm{adia}}(t_{\mathrm{f}}) = \begin{pmatrix} \frac{1}{2}\big(1 - \cos\phi(t)\big) & \frac{1}{2}\sin\phi(t) \\ \frac{1}{2}\sin\phi(t) & \frac{1}{2}\big(1 + \cos\phi(t)\big) \end{pmatrix} \rho(t). \tag{A.5}$$

In the diabatic representation, $\rho^{\mathrm{D}}(t)$ can be written throughout the process as

$$\rho^{\mathrm{D}}(t) = \begin{pmatrix} 0 & 0 \\ 0 & \rho(t) \end{pmatrix}, \tag{A.6}$$

allowing us to write the approximate adiabatic density matrix

$$\rho^{\mathrm{A}}(t_{\mathrm{f}}) = \begin{pmatrix} \frac{1}{2}\big(1-\cos\phi(t)\big) & \frac{1}{2}\sin\phi(t) \\ \frac{1}{2}\sin\phi(t) & \frac{1}{2}\big(1+\cos\phi(t)\big) \end{pmatrix} \rho(t). \tag{A.7}$$

Appendix B

Details of the Wigner-Moyal Transformation

B.1 Wigner Distribution

For the two-state system as described in Equation 1.20, in terms of the star product as given in Equation 3.1, the elements of the Wigner distribution in the adiabatic representation $\rho^{\mathrm{A}}(\boldsymbol{q},\boldsymbol{p},t)$ in terms of elements of $\rho^{\mathrm{D}}(\boldsymbol{q},\boldsymbol{p},t)$ are given by

$$\begin{aligned}\rho^{\mathrm{A}}_{++}(\boldsymbol{q},\boldsymbol{p},t) &= \cos\frac{\phi(\boldsymbol{q})}{2}\star\rho^{\mathrm{D}}_{11}(\boldsymbol{q},\boldsymbol{p},t)\star\cos\frac{\phi(\boldsymbol{q})}{2}+\sin\frac{\phi(\boldsymbol{q})}{2}\star\rho^{\mathrm{D}}_{22}(\boldsymbol{q},\boldsymbol{p},t)\star\sin\frac{\phi(\boldsymbol{q})}{2}\\ &\quad+\cos\frac{\phi(\boldsymbol{q})}{2}\star\alpha^{\mathrm{D}}(\boldsymbol{q},\boldsymbol{p},t)\star\sin\frac{\phi(\boldsymbol{q})}{2}+\sin\frac{\phi(\boldsymbol{q})}{2}\star\alpha^{\mathrm{D}}(\boldsymbol{q},\boldsymbol{p},t)\star\cos\frac{\phi(\boldsymbol{q})}{2}\\ &\quad+i\cos\frac{\phi(\boldsymbol{q})}{2}\star\beta^{\mathrm{D}}(\boldsymbol{q},\boldsymbol{p},t)\star\sin\frac{\phi(\boldsymbol{q})}{2}-i\sin\frac{\phi(\boldsymbol{q})}{2}\star\beta^{\mathrm{D}}(\boldsymbol{q},\boldsymbol{p},t)\star\cos\frac{\phi(\boldsymbol{q})}{2},\end{aligned}\tag{B.1}$$

$$\begin{aligned}\rho^{\mathrm{A}}_{+-}(\boldsymbol{q},\boldsymbol{p},t) &= -\cos\frac{\phi(\boldsymbol{q})}{2}\star\rho^{\mathrm{D}}_{11}(\boldsymbol{q},\boldsymbol{p},t)\star\sin\frac{\phi(\boldsymbol{q})}{2}+\sin\frac{\phi(\boldsymbol{q})}{2}\star\rho^{\mathrm{D}}_{22}(\boldsymbol{q},\boldsymbol{p},t)\star\cos\frac{\phi(\boldsymbol{q})}{2}\\ &\quad+\cos\frac{\phi(\boldsymbol{q})}{2}\star\alpha^{\mathrm{D}}(\boldsymbol{q},\boldsymbol{p},t)\star\cos\frac{\phi(\boldsymbol{q})}{2}-\sin\frac{\phi(\boldsymbol{q})}{2}\star\alpha^{\mathrm{D}}(\boldsymbol{q},\boldsymbol{p},t)\star\sin\frac{\phi(\boldsymbol{q})}{2}\\ &\quad+i\cos\frac{\phi(\boldsymbol{q})}{2}\star\beta^{\mathrm{D}}(\boldsymbol{q},\boldsymbol{p},t)\star\cos\frac{\phi(\boldsymbol{q})}{2}+i\sin\frac{\phi(\boldsymbol{q})}{2}\star\beta^{\mathrm{D}}(\boldsymbol{q},\boldsymbol{p},t)\star\sin\frac{\phi(\boldsymbol{q})}{2},\end{aligned}\tag{B.2}$$

$$\begin{aligned}\rho^{\mathrm{A}}_{-+}(\boldsymbol{q},\boldsymbol{p},t) &= -\sin\frac{\phi(\boldsymbol{q})}{2}\star\rho^{\mathrm{D}}_{11}(\boldsymbol{q},\boldsymbol{p},t)\star\cos\frac{\phi(\boldsymbol{q})}{2}+\cos\frac{\phi(\boldsymbol{q})}{2}\star\rho^{\mathrm{D}}_{22}(\boldsymbol{q},\boldsymbol{p},t)\star\sin\frac{\phi(\boldsymbol{q})}{2}\\ &\quad-\sin\frac{\phi(\boldsymbol{q})}{2}\star\alpha^{\mathrm{D}}(\boldsymbol{q},\boldsymbol{p},t)\star\sin\frac{\phi(\boldsymbol{q})}{2}+\cos\frac{\phi(\boldsymbol{q})}{2}\star\alpha^{\mathrm{D}}(\boldsymbol{q},\boldsymbol{p},t)\star\cos\frac{\phi(\boldsymbol{q})}{2}\\ &\quad-i\sin\frac{\phi(\boldsymbol{q})}{2}\star\beta^{\mathrm{D}}(\boldsymbol{q},\boldsymbol{p},t)\star\sin\frac{\phi(\boldsymbol{q})}{2}-i\cos\frac{\phi(\boldsymbol{q})}{2}\star\beta^{\mathrm{D}}(\boldsymbol{q},\boldsymbol{p},t)\star\cos\frac{\phi(\boldsymbol{q})}{2},\end{aligned}\tag{B.3}$$

$$\begin{aligned}\rho^{\mathrm{A}}_{--}(\boldsymbol{q},\boldsymbol{p},t) &= \sin\frac{\phi(\boldsymbol{q})}{2}\star\rho^{\mathrm{D}}_{11}(\boldsymbol{q},\boldsymbol{p},t)\star\sin\frac{\phi(\boldsymbol{q})}{2}+\cos\frac{\phi(\boldsymbol{q})}{2}\star\rho^{\mathrm{D}}_{22}(\boldsymbol{q},\boldsymbol{p},t)\star\cos\frac{\phi(\boldsymbol{q})}{2}\\ &\quad-\sin\frac{\phi(\boldsymbol{q})}{2}\star\alpha^{\mathrm{D}}(\boldsymbol{q},\boldsymbol{p},t)\star\cos\frac{\phi(\boldsymbol{q})}{2}-\cos\frac{\phi(\boldsymbol{q})}{2}\star\alpha^{\mathrm{D}}(\boldsymbol{q},\boldsymbol{p},t)\star\sin\frac{\phi(\boldsymbol{q})}{2}\\ &\quad-i\sin\frac{\phi(\boldsymbol{q})}{2}\star\beta^{\mathrm{D}}(\boldsymbol{q},\boldsymbol{p},t)\star\cos\frac{\phi(\boldsymbol{q})}{2}+i\cos\frac{\phi(\boldsymbol{q})}{2}\star\beta^{\mathrm{D}}(\boldsymbol{q},\boldsymbol{p},t)\star\sin\frac{\phi(\boldsymbol{q})}{2}.\end{aligned}\tag{B.4}$$

B.1.1 Star Products with Sines and Cosines

In this section we present the star products of the elements of the Wigner distribution [74, 75], represented as $\rho_{ij}(\boldsymbol{q},\boldsymbol{p},t)$, with sines and cosines of half the transformation angle $\frac{\phi(\boldsymbol{q})}{2}$.

The corresponding functions are given by

$$\begin{aligned}\cos\frac{\phi(\boldsymbol{q})}{2}\star\rho_{ij}(\boldsymbol{q},\boldsymbol{p},t)\star\cos\frac{\phi(\boldsymbol{q})}{2} &= \left(\frac{1+\cos\phi(\boldsymbol{q})}{2}\right)\rho_{ij}(\boldsymbol{q},\boldsymbol{p},t)\\ &\quad-\frac{\hbar^2}{8}\nabla_{\boldsymbol{q}}\boldsymbol{d}(\boldsymbol{q})\sin\phi(\boldsymbol{q})\nabla^2_{\boldsymbol{p}}\rho_{ij}(\boldsymbol{q},\boldsymbol{p},t)\\ &\quad+\frac{\hbar^2}{4}\boldsymbol{d}^2(\boldsymbol{q})\nabla^2_{\boldsymbol{p}}\rho_{ij}(\boldsymbol{q},\boldsymbol{p},t)+\mathcal{O}(\hbar^3),\end{aligned}\tag{B.5}$$

$$\sin\frac{\phi(\boldsymbol{q})}{2}\star\rho_{ij}(\boldsymbol{q},\boldsymbol{p},t)\star\cos\frac{\phi(\boldsymbol{q})}{2} = \frac{\sin\phi(\boldsymbol{q})}{2}\rho_{ij}(\boldsymbol{q},\boldsymbol{p},t) + \frac{\hbar^2}{8}\nabla_{\boldsymbol{q}}\boldsymbol{d}(\boldsymbol{q})\cos\phi(\boldsymbol{q})\nabla^2_{\boldsymbol{p}}\rho_{ij}(\boldsymbol{q},\boldsymbol{p},t) - i\frac{\hbar}{2}\boldsymbol{d}(\boldsymbol{q})\nabla_{\boldsymbol{p}}\rho_{ij}(\boldsymbol{q},\boldsymbol{p},t) + \mathcal{O}(\hbar^3), \tag{B.6}$$

$$\cos\frac{\phi(\boldsymbol{q})}{2}\star\rho_{ij}(\boldsymbol{q},\boldsymbol{p},t)\star\sin\frac{\phi(\boldsymbol{q})}{2} = \frac{\sin\phi(\boldsymbol{q})}{2}\rho_{ij}(\boldsymbol{q},\boldsymbol{p},t) + \frac{\hbar^2}{8}\nabla_{\boldsymbol{q}}\boldsymbol{d}(\boldsymbol{q})\cos\phi(\boldsymbol{q})\nabla^2_{\boldsymbol{p}}\rho_{ij}(\boldsymbol{q},\boldsymbol{p},t) + i\frac{\hbar}{2}\boldsymbol{d}(\boldsymbol{q})\nabla_{\boldsymbol{p}}\rho_{ij}(\boldsymbol{q},\boldsymbol{p},t) + \mathcal{O}(\hbar^3), \tag{B.7}$$

$$\sin\frac{\phi(\boldsymbol{q})}{2}\star\rho_{ij}(\boldsymbol{q},\boldsymbol{p},t)\star\sin\frac{\phi(\boldsymbol{q})}{2} = \left(\frac{1-\cos\phi(\boldsymbol{q})}{2}\right)\rho_{ij}(\boldsymbol{q},\boldsymbol{p},t) + \frac{\hbar^2}{8}\nabla_{\boldsymbol{q}}\boldsymbol{d}(\boldsymbol{q})\sin\phi(\boldsymbol{q})\nabla^2_{\boldsymbol{p}}\rho_{ij}(\boldsymbol{q},\boldsymbol{p},t) + \frac{\hbar^2}{4}\boldsymbol{d}^2(\boldsymbol{q})\nabla^2_{\boldsymbol{p}}\rho_{ij}(\boldsymbol{q},\boldsymbol{p},t) + \mathcal{O}(\hbar^3). \tag{B.8}$$

Working out the star products of each element of the adiabatic Wigner distribution, and substituting Eqns B.5-B.8 into Eqns B.1-B.4, gives the diabatic-to-adiabatic transformed equations for the Wigner distribution given by Eqns 3.4-3.6 reported in Section 3.2.1 of Chapter 3.

Appendix C

Adiabatic Forces on Trajectory in Dual Avoided Crossing System

We now present a simple derivation of the adiabatic forces - both the quantum and classical - in terms of the diabatic potentials at five timepoints, the time of the first instantaneous electronic transition $t = t_1^*$, the instant ϵ before the first electronic transition $t = t_1^* - \epsilon$, and the instant ϵ after the first electronic transition $t = t_1^* + \epsilon$, the time of the second instantaneous electronic transition $t = t_2^*$, the time between the instant after the first electronic transition and before the second electronic transition $t = \tau$, and the instant after the second electronic transition $t = t_2^* + \epsilon$.

Similar to the process depicted in Fig 2.4, the process outlined above for the dual avoided crossing system in the diabatic representation only involves dynamics only on the diabatic state $V_2(\boldsymbol{q})$.

This resulted in the generalized expression for $\alpha^{\mathrm{A}}(t)$ and $\boldsymbol{F}^{\mathrm{A}}_{\mathrm{quant}}(t)$ being the same as Eqn 4.12 and Eqn 4.13, respectively.

For the process depicted in Fig 2.8, in generalized coordinates $\boldsymbol{q}(t)$, the first population transfer taking place is localized and complete at the nuclear coordinate $\boldsymbol{q}(t_1^*) = -1.57$, where $\boldsymbol{q}_1^* \equiv \boldsymbol{q}(t_1^*)$. This corresponds to the first vertical step in Fig 4.3. We took $\phi(\boldsymbol{q}_1^*) = \frac{\pi}{2}$ to be the midpoint of the step at $\boldsymbol{q}_1^*$. The second population transfer is also complete and localized at the nuclear coordinate $\boldsymbol{q}(t_2^*) = 1.57$, where $\boldsymbol{q}_2^* \equiv \boldsymbol{q}(t_2^*)$. This corresponds to the second vertical step in Fig 4.3.

At the instant ϵ before the first transition, the time between the instant after the first transition and before the second transition, and the instant after the second transition in the adiabatic representation, the coordinates were $\boldsymbol{q}(t_1^* - \epsilon)$, $\boldsymbol{q}(\tau)$, and $\boldsymbol{q}(t_2^* + \epsilon)$, respectively. The corresponding non-adiabatic mixing angles were $\phi\big(\boldsymbol{q}(t_1^* - \epsilon)\big) = 0$, $\phi\big(\boldsymbol{q}(\tau)\big) = \pi$, and $\phi\big(\boldsymbol{q}(t_2^* + \epsilon)\big) = 0$, respectively.

The total force $\boldsymbol{F}^{\mathrm{A}}_{\mathrm{total}}(t)$ in the adiabatic representation consists of the sum of a classical component $\boldsymbol{F}^{\mathrm{A}}_{\mathrm{class}}(t)$ and a quantum component $\boldsymbol{F}^{\mathrm{A}}_{\mathrm{quant}}(t)$ as given in Eqn 4.13.

We proceed to compute $\boldsymbol{F}^{\mathrm{A}}_{\mathrm{class}}(t)$ and quantum forces $\boldsymbol{F}^{\mathrm{A}}_{\mathrm{quant}}(t)$, in the limit $C \to 0$ for the five timepoints.

At the instant before the first electronic transition, where $t = t_1^* - \epsilon$, the classical force involves only one adiabatic state, the lower adiabatic state $V_-(\boldsymbol{q})$.

Given that $\phi\left(\boldsymbol{q}(t_1^* - \epsilon)\right) = 0$,

$$\cos\phi\left(\boldsymbol{q}(t_1^* - \epsilon)\right) = 1, \tag{C.1}$$

and

$$\sin\phi\left(\boldsymbol{q}(t_1^* - \epsilon)\right) = 0. \tag{C.2}$$

Substituting Eqns C.1-C.2 into the expression for the classical force in the adiabatic representation (Eqn 4.2), the classical force was found to be

$$\boldsymbol{F}^{\mathrm{A}}_{\mathrm{class}}(t_1^* - \epsilon) = \boldsymbol{F}^{\mathrm{A}}_{-}(t_1^* - \epsilon) = -\nabla_{\boldsymbol{q}} V_2\big(\boldsymbol{q}(t_1^* - \epsilon)\big). \tag{C.3}$$

Performing the same procedure for the quantum force, given by Eqn 4.13 for the process occurring in the dual avoided crossing system [1] in the adiabatic representation (Fig 2.8), the quantum force at the instant before the first electronic transition in the adiabatic representation $\boldsymbol{F}^{\mathrm{A}}_{\mathrm{quant}}(t_1^* - \epsilon)$ was found to be

$$\boldsymbol{F}^{\mathrm{A}}_{\mathrm{quant}}(t_1^* - \epsilon) = 0. \tag{C.4}$$

The classical force for each system at $t = t_1^* - \epsilon$ given by Eqn C.3 combines with the corresponding quantum force (Eqn C.4) to give the total force in the adiabatic representation for the process occuring in the dual avoided crossing system [1].

The total force was found to be

$$\boldsymbol{F}^{\mathrm{A}}_{\mathrm{total}}(t_1^* - \epsilon) = -\nabla_{\boldsymbol{q}} V_2\big(\boldsymbol{q}(t_1^* - \epsilon)\big) = \boldsymbol{F}^{\mathrm{D}}_{\mathrm{class},2}(t_1^* - \epsilon), . \tag{C.5}$$

At an instant before the first transition $t = t^* - \epsilon$, the corresponding process in the diabatic representation (Fig 2.9) involves the evolution of the localized wavepacket/trajectory along diabatic surface $V_2(\boldsymbol{q})$. The classical force acting to evolve the localized wavepacket/trajectory

was $\boldsymbol{F}^{\mathrm{D}}_{\mathrm{class},2}(t_1^* - \epsilon)$.

In deriving Eqn C.5, we found that the total force in the adiabatic representation $\boldsymbol{F}^{\mathrm{A}}_{\mathrm{total}}(t_1^* - \epsilon)$ is equivalent to $\boldsymbol{F}^{\mathrm{D}}_{\mathrm{class},2}(t_1^* - \epsilon)$, accurately portraying the evolution of the localized wavepacket/trajectory along diabatic surface $V_2(\boldsymbol{q})$ before the first electronic transition takes place in the adiabatic representation.

We derived the forces during the first *instantaneous* electronic transition at $t = t_1^*$, where the nuclear coordinate is $q_1^* = -1.57$.

Given that $\phi(t_1^*) = \frac{\pi}{2}$,

$$\cos\phi(t_1^*) = 0, \tag{C.6}$$

and

$$\sin\phi(t_1^*) = 1. \tag{C.7}$$

The localized wavepacket/trajectory experiences both the upper and lower adiabatic potentials $V_+(\boldsymbol{q}_1^*)$ and $V_-(\boldsymbol{q}_1^*)$ equally at the instant of the first transition t_1^*. The classical adiabatic force was found to be given by the expression

$$\begin{aligned} \boldsymbol{F}^{\mathrm{A}}_{\mathrm{class}}(t_1^*) &= -\frac{\nabla_{\boldsymbol{q}} V_+(\boldsymbol{q}_1^*) + \nabla_{\boldsymbol{q}} V_-(\boldsymbol{q}_1^*)}{2} \\ &= -\frac{\nabla_{\boldsymbol{q}} V_1(\boldsymbol{q}_1^*) + \nabla_{\boldsymbol{q}} V_2(\boldsymbol{q}_1^*)}{2}. \end{aligned} \tag{C.8}$$

Substituting Eqns C.6-C.7 into the expression of the quantum force given by Eqn 4.13 for the process (Fig 2.8), the quantum force at the instant of first $- \rightarrow +$ transition t_1^* in the

adiabatic representation $\boldsymbol{F}^{\mathrm{A}}_{\mathrm{quant}}(\boldsymbol{q}^*)$ was found to be

$$\boldsymbol{F}^{\mathrm{A}}_{\mathrm{quant}}(t_1^*) = \frac{\nabla_{\boldsymbol{q}} V_1(\boldsymbol{q}_1^*) - \nabla_{\boldsymbol{q}} V_2(\boldsymbol{q}_1^*)}{2}. \tag{C.9}$$

Combining $\boldsymbol{F}^{\mathrm{A}}_{\mathrm{quant}}(t_1^*)$ (Eqn C.9) with $\boldsymbol{F}^{\mathrm{A}}_{\mathrm{class}}(t_1^*)$ (Eqn C.8), the total force in the adiabatic representation at the instant of first transition t_1^* was found to be

$$\boldsymbol{F}^{\mathrm{A}}_{\mathrm{total}}(t_1^*) = -\nabla_{\boldsymbol{q}} V_2(\boldsymbol{q}_1^*) = \boldsymbol{F}^{\mathrm{D}}_{\mathrm{class},2}(t_1^*), \tag{C.10}$$

the classical force acting to evolve the localized wavepacket/trajectory on the diabatic potential energy surface $V_2(\boldsymbol{q}_1^*) = 0$, as depicted in Fig 2.9.

We now derive the forces at the time interval between the instant after the first transition and before the second transition $t = \tau$, where $\tau \in [t_1^* + \epsilon, t_2^* - \epsilon]$.

Given that $\phi\left(\boldsymbol{q}(\tau)\right) = \pi$,

$$\cos\phi\left(\boldsymbol{q}(\tau)\right) = -1, \tag{C.11}$$

and

$$\sin\phi\left(\boldsymbol{q}(\tau)\right) = 0. \tag{C.12}$$

Substituting Eqns C.11-C.12 into Eqn 4.2, the expression for the classical force (Eqn 4.2) was found to be

$$\boldsymbol{F}^{\mathrm{A}}_{\mathrm{class}}(\tau) = \boldsymbol{F}^{\mathrm{A}}_{+}(\tau) = -\nabla_{\boldsymbol{q}} V_2\big(\boldsymbol{q}(\tau)\big). \tag{C.13}$$

Substituting Eqns C.11-C.12 into the expression of the quantum force, Eqn 4.13 for the system (Fig 2.8), the quantum force at during the time interval between instant after the first electronic transition and the instant before the second electronic transition in the adiabatic representation $\boldsymbol{F}^{\mathrm{A}}_{\mathrm{quant}}(\tau)$ was found to be

$$\boldsymbol{F}^{\mathrm{A}}_{\mathrm{quant}}(\tau) = 0. \tag{C.14}$$

The classical force at $t = \tau$ represented by Eqn C.13 for the system, combines with the corresponding quantum force (Eqn C.14) to give the total force for each system in the adiabatic representation.

The total force in the adiabatic representation at τ is

$$\boldsymbol{F}^{\mathrm{A}}_{\mathrm{total}}(\tau) = -\nabla_{\boldsymbol{q}} V_1\big(\boldsymbol{q}(\tau)\big) = \boldsymbol{F}^{\mathrm{D}}_{\mathrm{class},2}(\tau), \tag{C.15}$$

the classical force acting on the localized wavepacket/trajectory on the diabatic potential energy surface $V_2(\boldsymbol{q}^*) = 0$, as depicted by Fig 2.9 in the diabatic representation.

Since $\phi(t_1^*) = \phi(t_2^*) = \frac{\pi}{2}$, at the time of the second *instantaneous* localized $+ \rightarrow -$ transition in the adiabatic representation $t = t_2^*$, the expressions for $\sin\phi(t_2^*)$ and $\cos\phi(t_2^*)$ are equivalent to that for the first *instantaneous* localized $- \rightarrow +$ transition given by Eqns C.6-C.7, giving an expression for the classical force in the adiabatic representation that is similar to Eqn C.8,

$$\begin{aligned} \boldsymbol{F}^{\mathrm{A}}_{\mathrm{class}}(t_2^*) &= -\frac{\nabla_{\boldsymbol{q}} V_+(\boldsymbol{q}_2^*) + \nabla_{\boldsymbol{q}} V_-(\boldsymbol{q}_2^*)}{2} \\ &= -\frac{\nabla_{\boldsymbol{q}} V_1(\boldsymbol{q}_2^*) + \nabla_{\boldsymbol{q}} V_2(\boldsymbol{q}_2^*)}{2}. \end{aligned} \tag{C.16}$$

The quantum force in the adiabatic representation when the second electronic transition takes place takes the same form as that for the first electronic transition given by Eqn C.9,

$$\boldsymbol{F}^{\mathrm{A}}_{\mathrm{quant}}(t_2^*) = \frac{\nabla_{\boldsymbol{q}} V_1(\boldsymbol{q}_2^*) - \nabla_{\boldsymbol{q}} V_2(\boldsymbol{q}_2^*)}{2}. \tag{C.17}$$

Combining $\boldsymbol{F}^{\mathrm{A}}_{\mathrm{quant}}(t_2^*)$ (Eqn C.17) with $\boldsymbol{F}^{\mathrm{A}}_{\mathrm{class}}(t_2^*)$ (Eqn C.16), the total force in the adiabatic representation at the instant of second transition t_2^* was found to be

$$\boldsymbol{F}^{\mathrm{A}}_{\mathrm{total}}(t_2^*) = -\nabla_{\boldsymbol{q}} V_2(\boldsymbol{q}_2^*) = \boldsymbol{F}^{\mathrm{D}}_{\mathrm{class},2}(\boldsymbol{q}_1^*), \tag{C.18}$$

the classical force acting on the localized wavepacket/trajectory evolving along the diabatic potential energy surface $V_2(\boldsymbol{q}_2^*)$, as depicted in Fig 2.9.

At the instant of the second $+ \rightarrow -$ transition, $t = t_2^*$ in the adiabatic representation (Fig 2.8), the localized wavepacket/trajectory evolving along the diabatic surface $V_2(\boldsymbol{q})$ is driven by the classical force $\boldsymbol{F}^{\mathrm{D}}_{\mathrm{class},2}\big(t_2^*\big)$ in the corresponding process in the diabatic representation (Fig 2.9).

In deriving Eqn C.18, we found that the total force in the adiabatic representation $\boldsymbol{F}^{\mathrm{A}}_{\mathrm{total}}\big(t_2^*\big)$ is equivalent to the classical force experienced along the diabatic surface $V_2(\boldsymbol{q})$ $\boldsymbol{F}^{\mathrm{D}}_{\mathrm{class},2}(t_2^*)$, accurately portraying the evolution of the localized wavepacket/trajectory along diabatic surface $V_2(\boldsymbol{q})$ while the second electronic transition takes place in the adiabatic representation.

Finally, we derive the forces at the instant after the second transition $t = t_2^* + \epsilon$.

Given that $\phi\left(\boldsymbol{q}(t_2^* + \epsilon)\right) = 0$,

$$\cos\phi\left(\boldsymbol{q}(t_2^* + \epsilon)\right) = 1, \tag{C.19}$$

and

$$\sin\phi\left(\boldsymbol{q}(t_2^*+\epsilon)\right)=0. \tag{C.20}$$

Substituting Eqns C.19-C.20 into Eqn 4.2, the expression for the classical force was found to be

$$\boldsymbol{F}^{\mathrm{A}}_{\mathrm{class}}(t_2^*+\epsilon)=\boldsymbol{F}^{\mathrm{A}}_{-}(t_2^*+\epsilon)=-\nabla_{\boldsymbol{q}}V_2\big(\boldsymbol{q}(t_2^*+\epsilon)\big). \tag{C.21}$$

Substituting Eqns C.19-C.20 into the expression of the quantum force, Eqn 4.13 for the system, the quantum force at the instant after the second electronic transition in the adiabatic representation $\boldsymbol{F}^{\mathrm{A}}_{\mathrm{quant}}(t_2^*+\epsilon)$ was found to be

$$\boldsymbol{F}^{\mathrm{A}}_{\mathrm{quant}}(t_2^*+\epsilon)=0. \tag{C.22}$$

The classical force for the process at $t=t_2^*+\epsilon$ (Eqn C.21) for the system, combines with the corresponding quantum force (Eqn C.22) to give the total force for each system in the adiabatic representation.

The total force in the adiabatic representation at $t_2^*+\epsilon$ is

$$\boldsymbol{F}^{\mathrm{A}}_{\mathrm{total}}(t_2^*+\epsilon)=-\nabla_{\boldsymbol{q}}V_2\big(\boldsymbol{q}(t_2^*+\epsilon)\big)=\boldsymbol{F}^{\mathrm{D}}_{\mathrm{class},2}(t_2^*+\epsilon), \tag{C.23}$$

the classical force acting on the localized wavepacket/trajectory along the diabatic potential energy surface $V_2(\boldsymbol{q}_2^*)$, as depicted in Fig 2.9.